DOT/FAA/TC-21/29

Federal Aviation Administration
William J. Hughes Technical Center
Aviation Research Division
Atlantic City International Airport
New Jersey 08405

The In-Cloud Icing and Large-Drop Experiment (ICICLE) Science and Operations Plans

November 2021

Final report

U.S. Department of Transportation
Federal Aviation Administration

NOTICE

This document is disseminated under the sponsorship of the U.S. Department of Transportation in the interest of information exchange. The U.S. Government assumes no liability for the contents or use thereof. The U.S. Government does not endorse products or manufacturers. Trade or manufacturers' names appear herein solely because they are considered essential to the objective of this report. The findings and conclusions in this report are those of the author(s) and do not necessarily represent the views of the funding agency. This document does not constitute FAA policy. Consult the FAA sponsoring organization listed on the Technical Documentation page as to its use.

This report is available at the Federal Aviation Administration William J. Hughes Technical Center's Full-Text Technical Reports page: actlibrary.tc.faa.gov in Adobe Acrobat portable document format (PDF).

Technical Report Documentation Page

Form DOT F 1700.7 (8-72) Reproduction of completed page authorized

1. Report No.	2. Government Accession No.	3. Recipient's Catalog No.
DOT/FAA/TC-21/29		

4. Title and Subtitle	5. Report Date
The In-Cloud Icing and Large-Drop Experiment Science and Operations Plan	November 2021
	6. Performing Organization Code

7. Author(s)	8. Performing Organization Report No.
Ben Bernstein, Stephanie DiVito, James T. Riley, Scott Landolt, Julie Haggerty, Gregory Thompson, Dan Adriaansen, David Serke, Cathy Kessinger, Sarah Tessendorf, Mengistu Wolde, Alexei Korolev, Anthony Brown, Leonid Nichman, Danny Sims, and Chris Dumont	

9. Performing Organization Name and Address	10. Work Unit No. (TRAIS)
Leading Edge Atmospherics, LLC 2125 Ridgeview Way Longmont, Colorado 80504	11. Contract or Grant No.

12. Sponsoring Agency Name and Address	13. Type of Report and Period Covered
U.S. Department of Transportation Federal Aviation Administration William J. Hughes Technical Center Aviation Research Division Atlantic City International Airport, NJ 08405	Final Report
	14. Sponsoring Agency Code

15. Supplementary Notes

The Federal Aviation Administration William J. Hughes Technical Center Aviation Research Division COR was James Riley.

16. Abstract

This document provides an in-depth description of the scientific and technical objectives of, and the operations planning for "ICICLE" (the In-Cloud Icing and Large-drop Experiment). ICICLE was conducted between late January and early March of 2019 in an effort to:

1) further advance the understanding of meteorological processes related to the production and depletion of supercooled liquid water, with an emphasis on supercooled large drops (SLD), and;
2) evaluate and refine icing tools that can be used to diagnose, forecast and differentiate between icing and non-icing conditions.

Such tools are either currently operational in the en-route domain or being considered as part of a new capability under development for the terminal area domain. Both will allow users to make informed, icing-relevant decisions for flight operations. To accomplish these goals, data from icing tools will be compared to research-quality data collected both in flight and on the ground. The National Research Council of Canada's heavily-instrumented Convair-580 research aircraft captured essential observations in icing and adjacent non-icing conditions across Michigan, Indiana, Illinois, Iowa, Wisconsin, and the adjacent Great Lakes over more than 110 hours of flight. Simultaneously, data from operational sources such as National Weather Service surface stations, radars and satellites were collected and supplemented by data from five ground-based suites of instruments and four weather balloon sites across the ICICLE domain. In-depth analysis and rigorous statistical verification are planned, which will result in the development and refinement of those tools and their application for operations, providing enhanced icing information to the aviation community for years to come.

17. Key Words	18. Distribution Statement
Aircraft Icing, Terminal Area Icing, In-Flight Icing, Supercooled Liquid Water, Supercooled Large Drops, Appendix O, Appendix C	This document is available to the U.S. public through the National Technical Information Service (NTIS), Springfield, Virginia 22161. This document is also available from the Federal Aviation Administration William J. Hughes Technical Center at actlibrary.tc.faa.gov.

19. Security Classif. (of this report)	20. Security Classif. (of this page)	21. No. of Pages	22. Price
Unclassified	Unclassified	174	

Acknowledgements

The authors would like to extend their sincere thanks to the many people who made the ICICLE program possible. These include, but are certainly not limited to our friends and partners at Meteo France, Deutscher Wetterdienst, the U.K. Met. Office (the French, German and U.K. Weather Services), SAFIRE, the National Air and Space Agency (NASA) Langley Research Center, the Desert Research Institute (DRI), Valparaiso University, Northern Illinois University, the University of Illinois at Urbana-Champaign, Iowa State University, Emery Air, personnel from the Rockford and Sterling (IL), Kalamazoo and South Haven (MI), Cedar Rapids and Decorah (IA) airports, and the many additional contributions from engineers, scientists, students and support staff from the Federal Aviation Administration, National Center for Atmospheric Research, and National Oceanographic and Atmospheric Administration.

We would also like to acknowledge the icing flight researchers that have worked tirelessly on this topic for decades. These include scientists, engineers, pilots, crew members and ground support teams from the U.S. Military, the National Advisory Committee on Aeronautics (NACA), NASA, the Federal Aviation Administration (FAA), the National Center for Atmospheric Research (NCAR), the National Research Council of Canada (NRC), Environment and Climate Change Canada (ECCC), universities and research organizations such as the University of Wyoming and DRI, aircraft manufacturers who have shared their experience, and private companies that work on communications, instrumentation, data collection and processing that makes icing research a practical reality. It is thanks to *their* dedication, pioneering work, shared knowledge, and sacrifices that the ICICLE team had the foundation upon which to build and execute this program.

Finally, we would like to thank Tom Bond (FAA and NASA, retired), without whose leadership and determination this program would not have become a reality.

Contents

Figures

Tables

Acronyms

Acronym	Definition
2DC	Optical array two-dimensional cloud imaging probe
2DP	Optical array two-dimensional precipitation imaging probe
2DS	Optical array two-dimensional stereo imaging probe
ABI	Advanced Baseline Imager
ACARS	Aircraft Communication Addressing and Reporting System
AECL	Airborne Elastic Cloud Lidar
ADDS	Aviation Digital Data Service
ADP	Air Data Probe
AGL	Above Ground Level
AIMMS	Aircraft-Integrated Meteorological Measurement System
AIRMET	Airmen's Meteorological information
AMDAR	Aircraft Meteorological Data Relay
App C	FAA FAR 1419 Part 25 Appendix C icing regulations
App O	FAA FAR 1420 Part 25 Appendix O icing regulations
ARD	Aviation Research Division
ASOS	Automated Surface Observing System
ATC	Air Traffic Control
ATR	Avions de Transport Regional
AVHRR	Advanced Very High Resolution Radiometer
AWC	Aviation Weather Center
AWD	Aviation Weather Division
AWOS	Automated Weather Observing System
AWRP	Aviation Weather Research Program
BLSN	Blowing Snow
CCN	Cloud Condensation Nuclei
CCZ	Combined CIP CTZ (cloud top height)
CDP	Cloud Droplet Probe
CEP	Cloud Extinction Probe
CG	Cloud-to-Ground lightning
CIP	Current Icing Product
CoCoRAHS	Community Collaborative Rain, Hail and Snow Network

Acronym	Definition
CONUS	Contiguous United States
CoSPA	Consolidated Storm Prediction for Aviation
CPC	Condensation Particle Counter
CPI	Cloud Particle Imager
CSU-CHILL	Colorado State University - Chicago Illinois radar
CTREC	Cartesian Tracking Radar Echoes by Correlation
CTT	Cloud Top Temperature
CTZ	Cloud Top Height
CW	Coastal Waters
CWO	Contract Weather Observer
D_{max}	Maximum Drop Diameter
DMT	Droplet Measurement Technologies
DAQ	Data Acquisition
DRI	Desert Research Institute
DWD	Deuthscher Wetterdienst
DZ	Drizzle
ECCC	Environment and Climate Change Canada
EMB	Embraer
EOL	Earth Observing Laboratory
ESRL	Earth Systems Research Laboratory
FAA	Federal Aviation Administration
FAR	Federal Aviation Regulation
FC	Field Catalog
FCDP	Fast Cloud Droplet Probe
FDDA	Freezing Drizzle Derivation Algorithm
FG	Fog
FIP	Forecast Icing Product
FIRE-ACE	First ISCCP Regional Experiment Arctic Cloud Experiment
FSS	Fractions Skill Score
FSSP	Forward Scattering Spectrometer Probe
FWHM	Full Width Half Maximum
FZDZ	Freezing Drizzle
FZRA	Freezing Rain
GA	General Aviation

Acronym	Definition
G-AIRMET	Graphical AIRMET
GFS	Global Forecast System
GIS	Geographic Information System
GOES	Geostationary Operational Environmental Satellite
GSD	Global Systems Division
GVR	G-band (water) Vapor Radiometer
HES	Hyperspectral Environmental Suite
HG	Honeywell
HiRA	High-Resolution Assessment
HRRR	High-Resolution Rapid Refresh
HVPS	High Volume Precipitation Spectrometer
ICICLE	In-Cloud Icing and Large-drop Experiment
IFI	In-Flight Icing
IFR	Instrument Flight Rules
IIDA	Integrated Icing Diagnostic Algorithm
IIFA	Integrated Icing Forecast Algorithm
ILS	Instrument Landing System
IMU	Inertial Measuring Unit
IN	Ice Nuclei
IR	Infrared
ISCCP	International Satellite Cloud Climatology Project
ISU	Iowa State University
IWC	Ice Water Content
JPSS	Joint Polar Satellite System
KPR	Ka-band Precipitation Radar
KRFD	Rockford, Illinois airport – the primary operations base for ICICLE.
KVH	KVH Industries, Inc.
LaRC	(NASA) Langley Research Center
LAWRS	Limited Aviation Weather Reporting Stations
LCREF	Layer Composite Reflectivity
LEA	Leading Edge Atmospherics
LWC	Liquid Water Content
LWE	Liquid Water Equivalent
LWP	Liquid Water Path

Acronym	Definition
M300	M300 data recording system
MAS	MODIS Airborne Simulator
MEA	Minimum En-route Altitude
METAR	Meteorological Aerodrome Report
MF	Meteo France
MMD	Median Mass Diameter
MODE	Method for Object-based Diagnostic Evaluation
MODIS	Moderate Resolution Imaging Spectroradiometer
mPING	Meteorological Phenomena Identification Near the Ground
MRMS	Multi-Radar/Multi-Sensor
MSL	Mean Sea Level
MVD	Median Volumetric Diameter
NAM	North American Model
NAS	National Airspace System
NASA	National Aeronautics and Space Administration
NAV	Navigation
NAX	NRC Airborne X-band radar
NAW	NRC Airborne W-band radar
NCAR	National Center for Atmospheric Research
NCEP	National Centers for Environmental Prediction
NEXRAD	Next Generation Radar
NextGen	Next Generation Air Transportation System
NIU	Northern Illinois University
NLDN	National Lightning Data Network
NOAA	National Oceanographic and Atmospheric Administration
NRC	National Research Council of Canada
NSSL	National Severe Storms Laboratory
NTSB	National Transportation Safety Board
NWP	Numerical Weather Prediction
NWS	National Weather Service
OAT	Outside Air Temperature
PADS	Particle Analysis and Display System
PARSIVEL	Particle Size and Velocity
PCASP	Passive Capacity Aerosol Spectrometer Probe

Acronym	Definition
PC	Partial cloudiness (a.k.a. cloud underproduction) scheme
PIP	Precipitation Imaging Probe
PIREP	Pilot Report
PIU	Port Inboard Upper
PL	Ice Pellets
POC	Point Of Contact
POD	Probability Of Detection
POLA	Port Outboard Lower Aft
POU	Port Output Upper
PSB	Port Scalar Boom
PUW	Port Under Wing
PWTA	Port Wing Tip Aft
PWTF	Port Wing Tip Forward
PWV	Precipitable Water Vapor
QC	Quality Control
RA	Rain
RadIA	Radar Icing Algorithm
RAP	Rapid Refresh model
RH	Relative Humidity
RMNT	Rosemount
RQI	Radar Quality Index
RUC	Rapid Update Cycle
SEA	Science Engineering Associates
SIGMET	Significant Meteorological information
SLD	Supercooled Large Drops
SLW	Supercooled Liquid Water
SN	Snow
SND	Sounder
SNOWIE	Seeded and Natural Orographic Wintertime clouds: the Idaho Experiment
SP2	Single Particle Soot Photometer
SPECI	Aviation Selected Special Weather Report
SIL	Starboard Inboard Lower
SIU	Starboard Inboard Upper
SOL	Starboard Outboard Lower

Acronym	Definition
SOU	Starboard Outboard Upper
SSB	Starboard Scalar Boom
SSP	Starboard Single Pylon/Probe
SWTA	Starboard Wing Tip Aft
SWTF	Starboard Wing Tip Forward
SUW	Starboard Under Wing
T	Temperature
TAF	Terminal Area Forecast
TAS	Terminal Airspace
TAT	Total Air Temperature
TAIWIN	Terminal Area Icing Weather Information for NextGen
Tb	Brightness Temperature
TBD	To Be Determined
Td	Dew point Temperature
TLE	Time-Lagged Ensemble
TWC	Total Water Content
UCAR	University Corporation for Atmospheric Research
UHSAS	Ultra-High Sensitivity Aerosol Spectrometer
UIUC	University of Illinois at Urbana-Champaign
UKMO	United Kingdom Met Office
UTC	Universal Time (same as Z)
V	Aircraft speed (velocity)
V1-V6	Vertical sampling strategies 1 through 6
Valpo	Valparaiso University
VCP	Volume Coverage Pattern
VFR	Visual Flight Rules
VIIRS	Visible Infrared Imaging Radiometer Suite
VOR	Very High Frequency (VHF) Omni-Directional Range
WCM	Water Content Measurement probe
WFO	Weather Forecast Office
WRF	Weather Research and Forecasting
WSR	Weather Service Radar
Wx	Weather
ZDR	Differential Reflectivity

Executive summary

This document provides an in-depth description of the scientific and technical objectives and numerous elements of the operations planning for “ICICLE,” the In-Cloud Icing and Large-drop Experiment. ICICLE was conducted during January-March 2019 in an effort to: 1) further advance the understanding of meteorological processes related to the production and depletion supercooled liquid water (SLW), with an emphasis on supercooled large drops (SLD); and 2) evaluate, develop, and refine icing tools that can be used to diagnose, forecast, and differentiate between icing and non-icing conditions. Data from those tools were collected and are being compared to research-quality flight data from the National Research Council of Canada’s heavily-instrumented Convair-580 research aircraft and several suites of ground-based instrumentation across Michigan, Indiana, Illinois, Iowa, Wisconsin, and the adjacent Great Lakes. Through analysis of these data, scientists and developers will be able to develop and advance icing tools to properly capture and distribute information on icing conditions within the terminal area and en-route portions of the National Airspace System (NAS). Beyond the objectives of ICICLE, this document provides extensive detail on the operational and test datasets and tools being used (and considered for use) to diagnose and predict icing, as well as the reasoning behind the design of ICICLE. Considering the variety and importance of the environments that were sampled, and the data collected during this campaign, ICICLE provides outstanding opportunities for icing research and development for many years to come.

1 Introduction

Aircraft icing presents a significant hazard to the flying community, affecting both revenue service and general aviation. It has been cited as a contributing factor in numerous incidents and accidents, which continue to this day (Green 2006, 2015; Petty and Floyd 2004). The crash of an ATR-72 on 31 October 1994 that killed 68 people brought one particular aspect of icing to the forefront; supercooled large drops or "SLD" (e.g. Politovich 1989; Marwitz et al. 1997; Weener 2011a, 2011b). SLD is a form of supercooled liquid water (SLW) where drop sizes are relatively large (diameter > 100 microns). This includes freezing drizzle (FZDZ) and freezing rain (FZRA). SLD can adhere to sub-freezing surfaces and cause particularly hazardous ice to form and accumulate on aircraft and other objects, both aloft and on the ground. In its final report on the ATR-72 accident, the National Transportation Safety Board (NTSB) concluded that a prolonged hold in SLD was a contributing factor (NTSB 1996). They provided a suite of recommendations, including the need to revisit the aircraft icing certification envelopes to better address SLD conditions, and to develop and provide improved icing tools and information to pilots.

The Federal Aviation Administration (FAA) has provided long-standing support for icing research, with the goal of reducing the rate of and preventing aircraft icing-related accidents and fatalities in the National Airspace System (NAS). In the wake of the ATR-72 accident and others associated with SLD, the FAA and other agencies expanded and re-focused the scope of their icing work to address these conditions. One major milestone was the adoption of new FAA regulations, enacted in January 2015, introducing an icing certification rule (§25.1420) and a new engineering standard (Part 25, Appendix O) that defines SLD environments for certification. Affected aircraft include those that have a maximum takeoff weight of less than 60,000 pounds and/or reversible flight controls. Appendix O supplements the Appendix C icing certification envelopes that have been in place for decades, expanding upon these "small drop" envelopes that cover median volumetric diameters (MVDs) up to 40-50 microns to include "large drop" or SLD envelopes (FAA 1999, 2015).

With the advent of these recent additions to the icing regulations, the levels of certification now must address flight into the following icing environments: (1) Appendix C only, (2) Appendix C plus a portion of Appendix O (FZDZ or FZRA), and (3) all icing. Aircraft certifications based on these classifications require users have sufficient information for decision-making that distinguishes between each of them, as well as icing-free areas, which would serve as possible escape routes (Korolev et al. 2006). Rule §25.1420 applies to all phases of flight, including operations in the terminal-area (including take-off and landing) and en-route. The FAA's Aviation Weather Research Program (AWRP) sponsors aircraft icing research and development

to support NAS operations for those domains through the Terminal Area Icing Weather Information for NextGen (TAIWIN) (DiVito and Riley 2017) and In-Flight Icing (IFI) (Politovich and Bernstein 2006) projects. These projects strive to meet these critical needs for aviation.

Appendix O was developed using research flight data gathered during several icing research flight programs, including the Canadian Freezing Drizzle Experiment (1995-2000; Isaac et al. 2001b; Cober et al. 2001), the Supercooled Large Drop Research Program (1997-1998; Miller et al. 1998), the Alliance Icing Research Study (1999-2003; Isaac et al. 2001a, 2001b, 2005) and the First International Satellite Cloud Climatology Project (ISCCP) Regional Experiment Arctic Cloud Experiment (FIRE-ACE; 1998; Curry et al. 2000). Much of this work culminated in the FAA's release of in-depth descriptions of the data used and analysis performed to develop Appendix O (Cober et al. 2009, Cober and Isaac 2012) and, ultimately, the new regulations (FAA 2015). Through these and other flight programs, plus experience from research, certification testing and flight operations, it has become abundantly clear that icing environments can be highly complex and pose significant challenges requiring meteorologists to thoroughly understand nuances of icing clouds, and to develop, enhance, test, and apply tools that diagnose and forecast them effectively.

There has been a great deal of progress on these fronts in the 15 years since the most recent major icing research flight programs. New observational and forecast icing tools have been developed with two of them becoming operational products serving the NAS (Bernstein et al. 2005; McDonough et al. 2004). Expansions to the icing certification envelopes, advances in icing-relevant technologies, and the need to thoroughly validate and verify tools and techniques has driven the necessity to compile a new, high-quality set of in-situ measurements covering a broad spectrum of icing conditions (FZDZ, FZRA, "small-drop" icing, and mixed phase) as well as non-icing conditions (glaciated environments and clear air). To that end, the FAA planned and executed "ICICLE" (the In-Cloud Icing and Large drop Experiment; DiVito et al. 2019). During ICICLE, the FAA and other agencies worked with the National Research Council of Canada (NRC) and Environment and Climate Change Canada (ECCC) to fly the heavily-instrumented NRC Convair-580 research aircraft into the conditions described above. ICICLE was conducted during a six-week window from 27 January to 8 March 2019, with samples taken within clouds and precipitation around the western Great Lakes region, plus bordering parts of the Midwest (see Figure 1, where nm is nautical miles). This area was ideal for the program, with a proven history of frequent SLW, SLD and glaciated conditions during the winter months (Bennett 1959; Strapp et al. 1996; Cortinas et al 2004; Bernstein et al. 2007; Landolt et al. 2017, 2019).

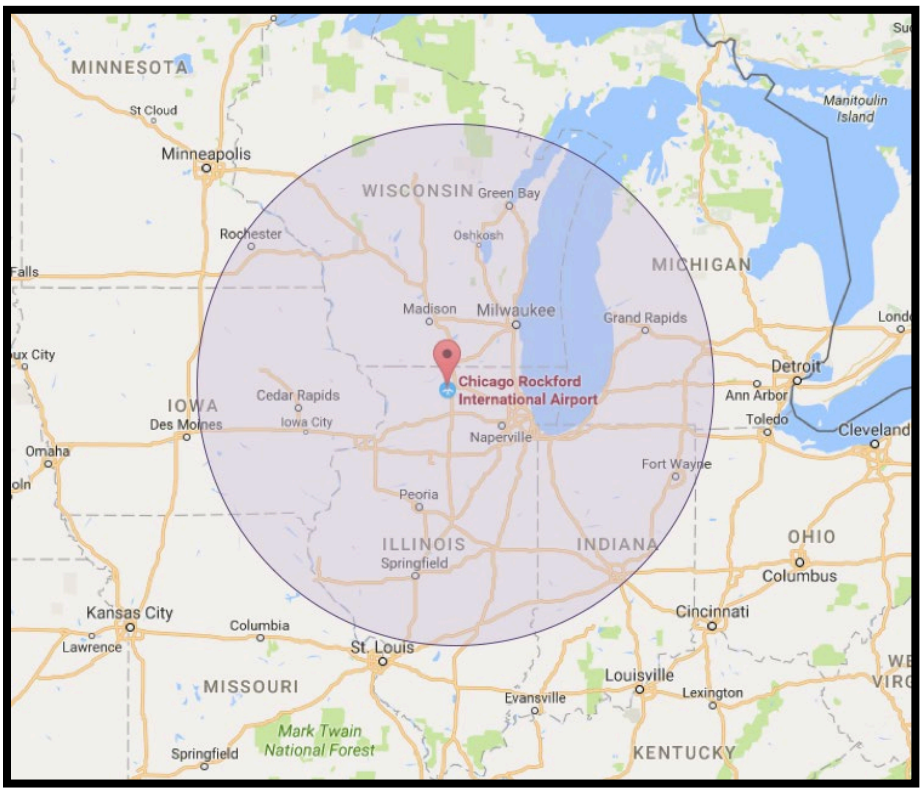

Figure 1. Primary ICICLE domain for areas within ~200 nm of Rockford, Illinois (KRFD)

The primary goals of ICICLE included the collection of a dataset to:

1. Further advance the understanding of meteorological processes related to the production and depletion of SLW, with an emphasis on SLD, and;
2. Evaluate and refine candidate and operational icing tools to diagnose, forecast and differentiate between the icing and non-icing conditions described above on critical space and time scales for flight operations.

Following the successful collection of high-quality aircraft observations and corresponding data from operational satellites, radars, surface stations, and output from numerical models and automated icing algorithms, these goals and others are being achieved through in-depth analysis, validation, and statistical verification.

2 Scientific background

2.1 Supercooled liquid water and supercooled large drops

SLW is liquid water that exists at sub-freezing temperatures, a phenomenon which commonly occurs in the atmosphere (Bigg 1953). It is observed at all times of the year within cloud types ranging from stratiform to cumuliform and encompasses drop diameters ranging from a few micrometers (microns) to a few millimeters.

There are numerous mechanisms responsible for the production and depletion of SLW in the atmosphere. SLW production typically begins with the activation of hygroscopic aerosols to form cloud drops via lifting and/or cooling. This is most often associated with forcing from frontal zones, topographic lift, convection, and moisture/temperature advection. These factors can vary in strength and often work in concert. Depending on the background environmental conditions, including temperature, moisture content, amount and types of cloud condensation nuclei (CCN) and ice nuclei (IN), and the intensity of lift, the resulting clouds and precipitation will be comprised of liquid water drops, ice crystals, or a mixture thereof.

If the mechanisms that form SLW exist in a favorable environment, the amount of liquid water present can increase via the creation of more droplets and/or the growth of existing droplets. The amount of SLW and drop size can vary dramatically within a given event. Once SLW develops, its survival is dependent on the balance between production and depletion. Typical depletion mechanisms include evaporation, precipitation, phase change from water to ice, or the collection of droplets by ice crystals (riming). Mixed-phase icing (co-existence of SLW and ice crystals) is common (Miller et al. 1998; Fleishauer et al. 2002; Korolev et al. 2003; Cober and Isaac 2012). Its longevity and the ratio of liquid to ice depends on the balance between the production and depletion mechanisms described above, as well as their evolution during a given event.

The character of icing environments covers a broad spectrum in terms of temperature, liquid water content (LWC), drop size, layer depth, areal coverage, duration, consistency, etc. Some examples include:

- Deep cumuliform clouds where intense icing can develop and dissipate rapidly (e.g., Jones and Lewis 1949).
- Shallow, sometimes long-lived freezing fog events (Beckwith 1965; Bernstein 2000a; Harbaugh 2007).
- Widespread stratiform layers that can track with an advancing front for several days (Jeck 2008).

- Streaks and swaths of stratocumulus clouds that can extend horizontally from a few miles to hundreds of miles (Kristovich and Steve 1995).
- Localized FZDZ events that may begin during the night and cease soon after sunrise (Cortinas et al. 2004).
- FZRA/FZDZ events that can extend over large areas and/or persist for days (Martner et al. 1992; Sanders et al. 2013; McCray et al. 2019).

One example of a long-lived, widespread SLD event is the disastrous ice storm that struck Quebec and Ontario in 1998 (Regan 1998; Gyakum and Roebber 2001). On the other end of the spectrum, small-scale icing events can also be quite dangerous. Examples include the EMB-120 accidents near Detroit in 1997 and West Palm Beach in 2001, the Cessna Citation and Saab 340 accidents near Pueblo in 2005 and San Luis Obispo in 2006, a short-lived FZDZ event that forced the cancellation of hundreds of flights at Denver, and the infamous ATR-72 accident near Chicago in 1994 (NTSB 1996, 1998, 2001, 2006, 2007; Politovich et al. 2002).

While "small-drop" icing clouds can easily form in a wide variety of meteorological situations, "large-drop" icing represents a small percentage of all icing environments and their forcing can be unique. For example, the 1998 Canadian ice storm and others that have struck the United States are typically formed via the "classical" FZRA mechanism and deep overrunning (Martner et al. 1992; Rauber et al. 1994). Classical FZRA occurs when snow falls through a layer of above-freezing air ("warm nose"), melts to form rain-sized drops (diameter > 500 μ) that subsequently fall into a sub-freezing layer below to become supercooled rain (see Figure 2 a) (Bennett 1959; Bocchieri 1980; Czys et al. 1996). When snowflakes only partially melt in the warm nose, they can subsequently refreeze into ice pellets (PL) in the lower sub-freezing layer (Hanesiak and Stewart 1995). In contrast, the "non-classical" mechanism, which forms most FZDZ, occurs in the absence of melting. Instead, water drops reach drizzle sizes (100-500 μ) (Cober and Isaac 2012) via the collision-coalescence process (see Figure 2 b) (Ohtake 1963; Huffman and Norman 1988; Rauber et al. 2000). It is possible, but relatively uncommon, for FZDZ to form via the classical mechanism and for FZRA to form via the non-classical mechanism (Bernstein 2000b). Note that drizzle (DZ) and rain (RA) can form at sub-freezing or above-freezing temperatures and subsequently reach areas with subfreezing temperatures to become FZDZ and FZRA. In addition, FZDZ and FZRA that form aloft can reach the surface as DZ and RA at above-freezing temperatures or not reach the surface at all (Hudson and Yum 2001).

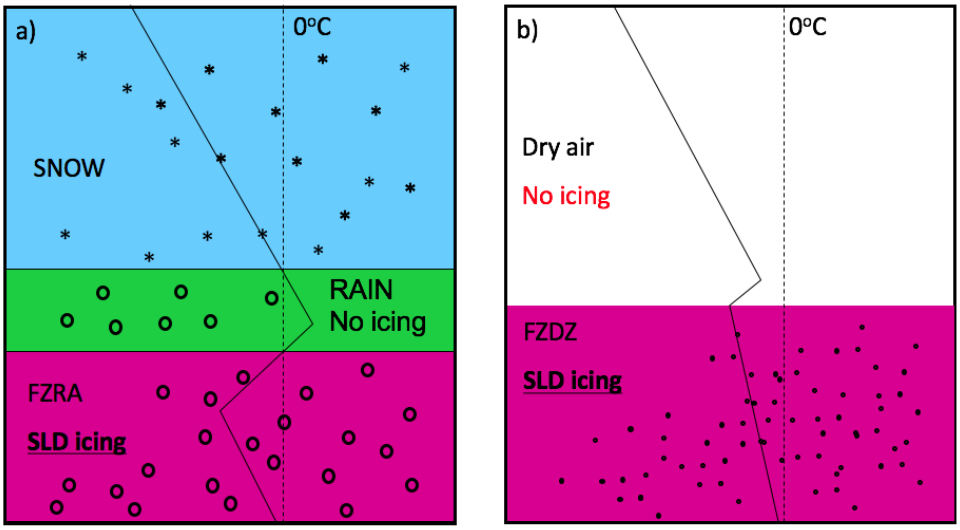

Figure 2. Conceptual diagrams of a) "classical" FZRA and b) "non-classical" FZDZ

Research on the production of non-classical FZDZ has identified several features that have been associated with its occurrence. These include presence of significant moisture, clean source air (low CCN and IN concentrations), inefficient ice phase (few and/or small ice crystals that result in minimal liquid depletion), relatively warm cloud top temperatures (often > -15°C), cloud top radiative cooling, isobaric mixing, vertical velocity fluctuations, embedded convection, and wind shear (Cober et al. 1996; Politovich 1989; Pobanz et al. 1994; Rasmussen et al. 1995, 2002; Korolev and Isaac 2000; Hauf and Schroeder 2006; Ikeda et al. 2007; Bernstein et al. 2019; Majewski and French 2019). Not all of these conditions appear to be necessary and/or sufficient for FZDZ to develop. For example, although Rasmussen et al. (2002) concluded that two necessary conditions are low ice crystal concentrations (< 0.08 L^{-1}) in the region of FZDZ formation and ice nuclei depletion, FZDZ has been observed in clouds with relatively cool cloud tops and an active ice phase (Ikeda et al. 2007; McDonough et al. 2017; Tessendorf et al. 2017a, 2017b). This suggests that mixed-phase FZDZ can persist when FZDZ production exceeds depletion, similar to the balance between SLW and ice crystals described above (Politovich and Bernstein 1995). Given that FZDZ has been observed in clouds with significant ice, including fall streaks from ice generating cells (see Figure 3), and is commonly reported simultaneously with snow at the surface (Cortinas et al. 2004), the efficiency of SLD depletion by ice crystals, including from generating cells, is not yet clear (Rauber et al. 2015).

With the inherent complexity of the production and depletion of SLW, the broad ranges of water contents and particle spectra that can be present, as well as their spatial structures and temporal evolution, the diagnosis and prediction of icing can be daunting. Even if the meteorological conditions present are diagnosed or predicted *perfectly*, the effects of that icing on the spectrum

of aircraft in service may vary widely, considering aircraft size, shape, speed, configuration, history of flight, and the presence and use of ice protection. When these layers of meteorological and aircraft complexity are combined with human factors—such as pilot workload, experience (with icing, overall and with a given aircraft type), time of day, and the ability to see the ice-affected parts of the aircraft (Sand and Biter 1997; Ryerson et al. 2006; Ratvasky et al. 2010; Brown 2011)—it is incredibly difficult for even a perfect icing diagnosis or forecast to correlate with any single pilot report at a given point in space and time.

That said, when a large number of diagnoses and forecasts are compared to thousands of pilot reports or in-situ measurements, tools and products that are of good quality should be able to demonstrate significant skill. This should include the ability to differentiate between the presence and absence of icing, its relative intensity, and the expected drop-size, including the presence of SLD and its sub-categories, FZDZ and FZRA. Through real-time evaluations made during the ICICLE program and extensive post-analysis that will follow, the ability of icing tools and forecasters to achieve this goal will continue to be tested thoroughly.

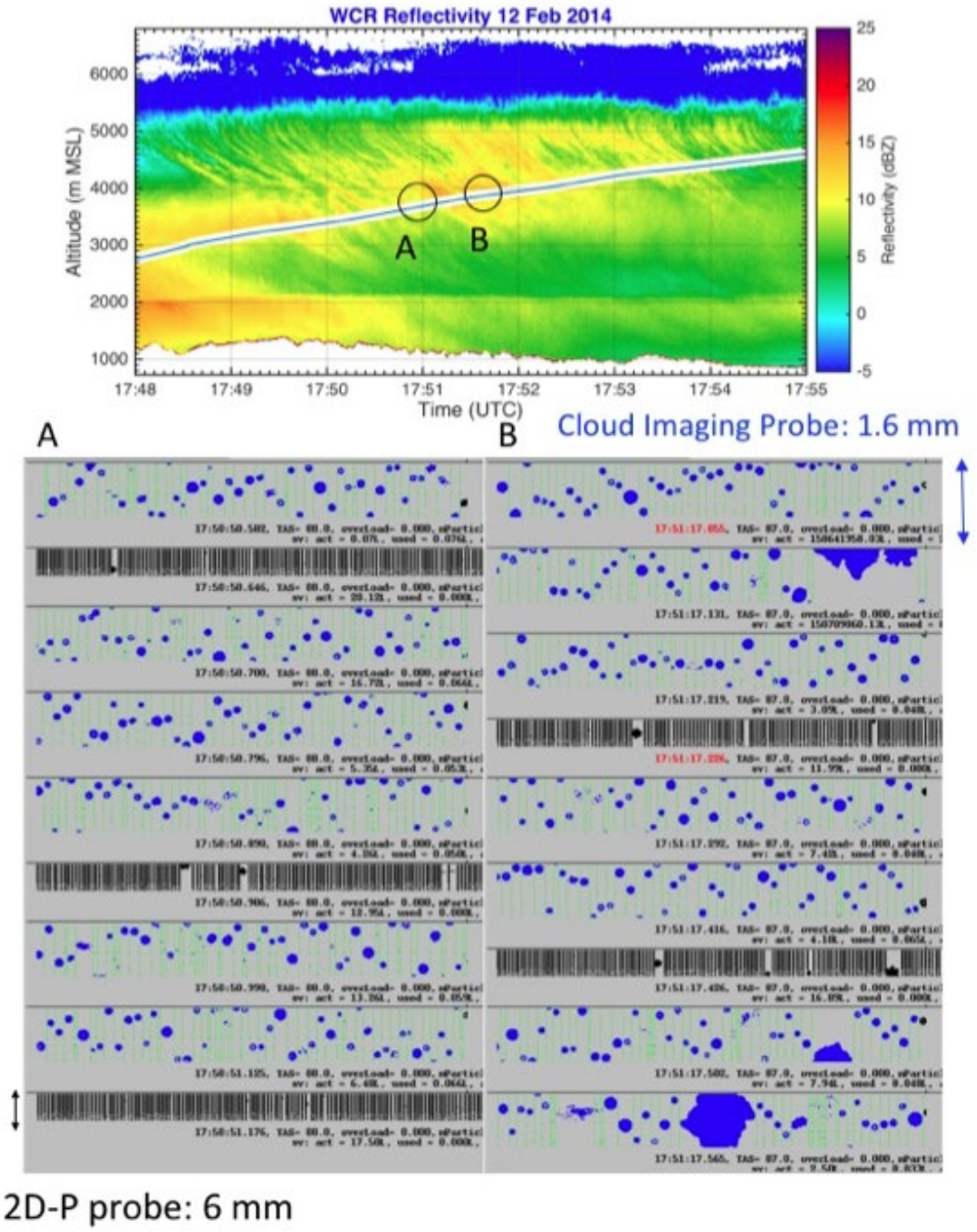

Figure 3. W-band Cloud Radar reflectivity through a cloud with FZDZ and ice particles (top) with associated images from the Cloud Imaging Probe (blue) and 2DP probe (black images in narrow rows) in fall streaks (Tessendorf et al. 2017c)

2.2 Climatology of icing conditions, including SLD

Seasonal and regional distributions of icing and SLD across North America have been assessed several times over the last 60 years and are reasonably well known (Katz 1967; Heath and Cantrell 1972; Roach et al. 1984; USAF 1986; Ryerson 1988; Grelson 1997; Young et al. 2002;

Fowler et al. 2002; Le Bot and Lassegues 2004; see Bernstein et al. 2007 for a summary and recent results). In these studies, historical assessments of data from weather balloons, surface observations, pilot reports, and automated icing algorithms have consistently indicated that the Great Lakes region has a relatively high frequency of icing at the surface and aloft, including conditions sought for the ICICLE program. During the period of interest, icing is most commonly found in two primary parts of the contiguous United States (CONUS): the Pacific Northwest and the corridor from the Midwest and Great Lakes to New England (see Figure 4). Maxima are particularly evident in January and they persist, but weaken, by April. SLD frequency charts show fairly similar results, though the eastern SLD maximum is focused to the south of the icing maximum in January.

A climatology of freezing precipitation surface observations, from before automated surface observations were common, also indicates that the maximum for surface FZDZ is somewhat displaced from the SLD-aloft maximum, with a broad swath of FZDZ running from the Texas Panhandle to Minnesota and Wisconsin, and an extension eastward across the Great Lakes to New England (see Figure 5) (Cortinas et al. 2004). Other than localized anomalies, CONUS FZDZ was generally maximized across Iowa, Minnesota, Wisconsin and the Upper Peninsula of Michigan. While FZRA occurs within this same area, its focus is shifted east, from Michigan and Indiana to New England, with peak frequencies from New York to Maine. Overall, FZDZ is more frequent than FZRA at the surface. Both are relatively *infrequent* at the surface in the Pacific Northwest, except in areas like the Columbia Basin and Snake River Valley. Landolt et al. (2019, 2020) found similar patterns in their analysis of modern surface observations alongside output from their ASOS-based FZDZ algorithm. It is important to note that the relative lack of surface FZDZ and FZRA in the Pacific Northwest is not reflective of a lack of SLD aloft, which has been observed at altitude there on numerous occasions (Ikeda et al. 2007; Horn et al. 2007; Rosenfeld et al. 2013; Serke et al. 2017; Tessendorf et al. 2019a; Bernstein et al. 2019).

Overall, icing and SLD frequencies peak between early December and late March in the western Great Lakes and adjacent parts of the Midwest. Thus, the ICICLE window of late January to early March was ideal for capturing desired icing environments within the target domain. Past experience has indicated that December can be a challenging month to conduct flight programs because of staff and resource availability. While January tends to have icing on the cold side of the spectrum in the Great Lakes and Midwest, due to the main storm track often being somewhat to the south, icing still occurs frequently in the target domain, and there are typically many opportunities to capture data of interest for the program (see Figure 1 and Figure 4). Historical surface observations at stations in the ICICLE domain indicate a relative minimum in SLD frequency in January compared to other winter months, but SLD still occurs there and the SLD

frequency maximum aloft is located within the Convair-580's range toward the southeast. The SLD aloft maximum moves back toward Rockford in late winter, as evidenced by the plots for April (see Figure 4). The period of planned operations was expected to be quite favorable in the ICICLE domain.

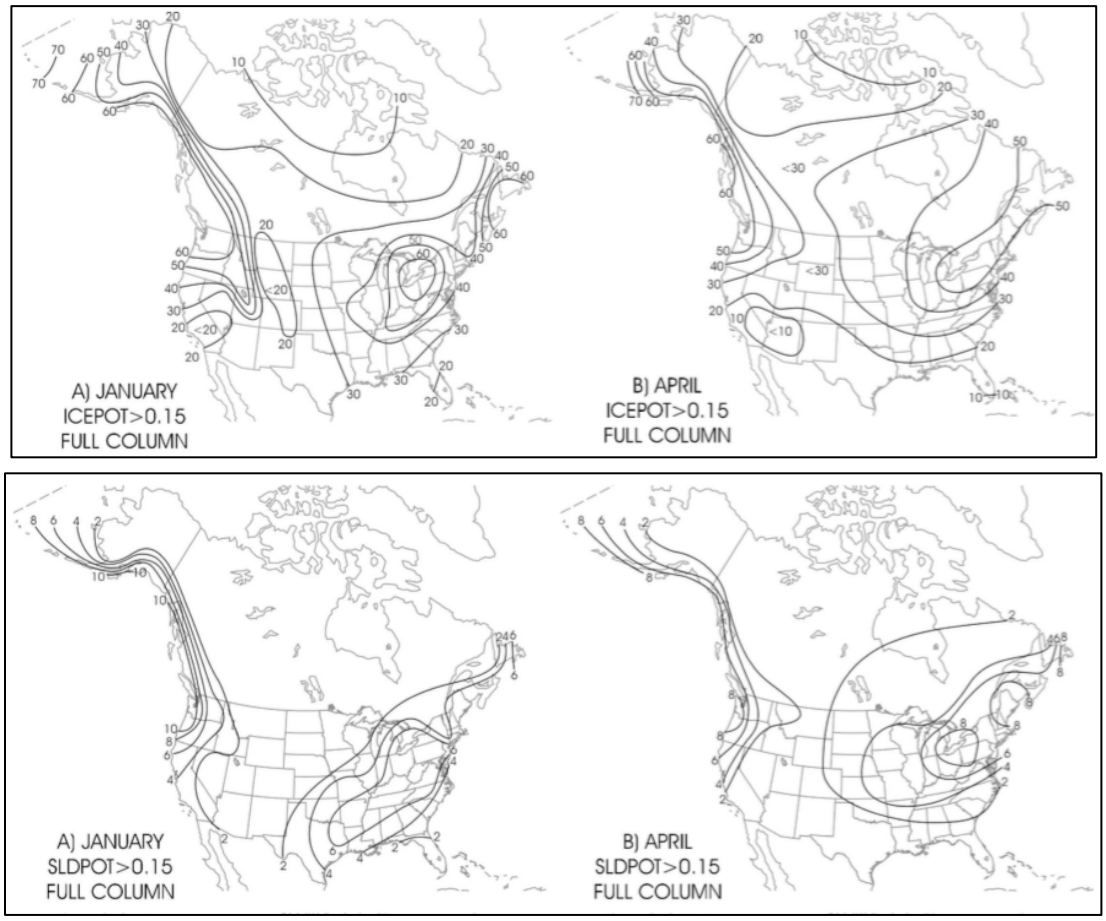

Figure 4. Icing and SLD frequencies (top and bottom, respectively) inferred from 15 years of soundings and surface observations for January and April (Bernstein et al. 2007)

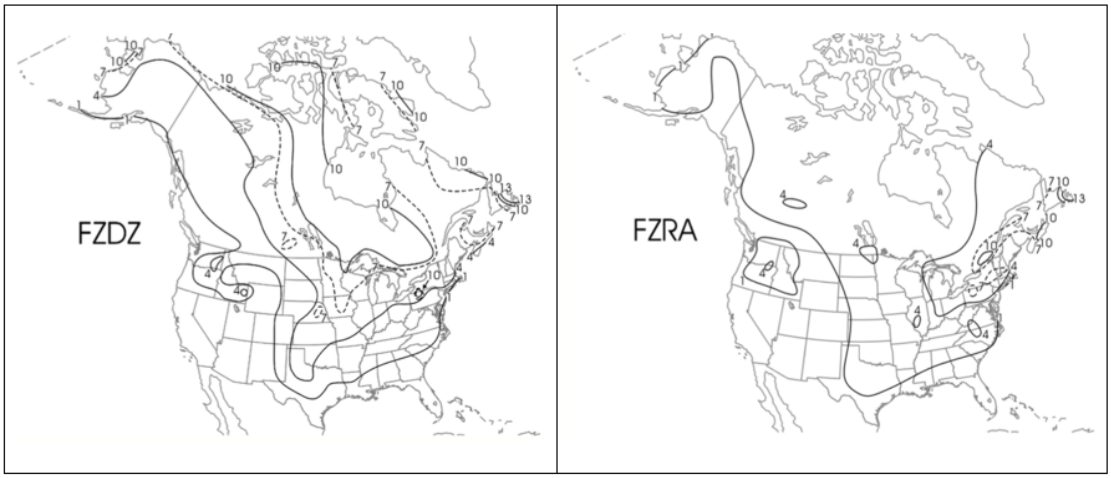

Figure 5. Median annual days of FZDZ, FZRA from 1976 to 1990 (Cortinas et al. 2004)

2.3 Diurnal tendencies

Surface FZDZ and FZRA climatologies have indicated that peak frequencies occur in the pre-dawn and early morning hours (see Figure 6) (Strapp et al. 1996; Cortinas et al. 2004; Landolt et al. 2020). For FZDZ, the driving forces behind these trends appear to include: a) the combination of cloud top cooling and isolation of liquid layers from boundary layer sources during the night; b) the reversal of those factors in the morning; and/or c) diurnal heating at the surface, causing changes in precipitation type (Cortinas et al. 2004; Rasmussen et al. 2002; Bernstein et al. 2019). It was notable that FZDZ events most commonly ended with precipitation ceasing or changing to snow. FZRA events also frequently ended with precipitation ceasing, but when precipitation did continue, various types were reported, with rain being the most common.

With the exception of the pilot report (PIREP) climatology presented by Schultz and Politovich (1992) and subsequent confirmation in verification studies by Brown et al. (1997) (see Figure 7), all of which were affected by diurnal air traffic patterns, the authors were not aware of a large-scale, diurnal climatology of icing conditions aloft. However, anecdotal evidence from the lead author's support of hundreds of icing flights indicates that diurnal icing tendencies do exist. They seem to be most pronounced when other forcing, such as frontal lift or lake-effect, is relatively weak. In these circumstances, icing conditions tend to be strongest (highest LWC and/or MVD) during the pre-dawn and early-morning hours, decrease to a relative minimum in the late morning, re-invigorate (in terms of LWC) in the early afternoon, then weaken again in the evening. This tendency seems to be most pronounced during the icing "shoulder season" in the region: roughly October-November and March-April (Bernstein et al. 2011). Relatively few icing test flights have occurred in the hours following local sunset, so clear trends for that time window have not been well established. However, the presence of relatively strong icing in the

early morning indicates that conditions of particular interest for ICICLE tend to re-invigorate during the night. While the trends above appear to be driven by diurnal cycles in boundary layer stability, cloud top heating/cooling, and the development/erosion of thin cloud layers, these cycles remain a topic for further investigation.

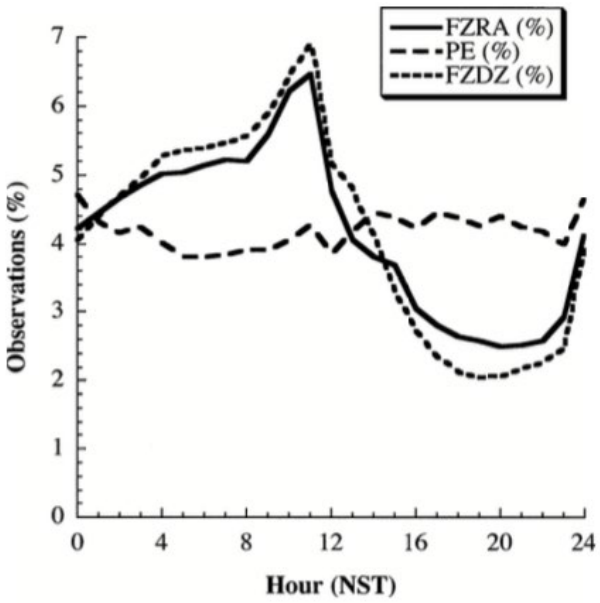

Figure 6. Diurnal distribution of FZRA, PL (formerly PE) and FZDZ surface observations. Normalized solar time (NST), where sunset = 0 NST, sunrise = 12 NST (Cortinas et al 2004)

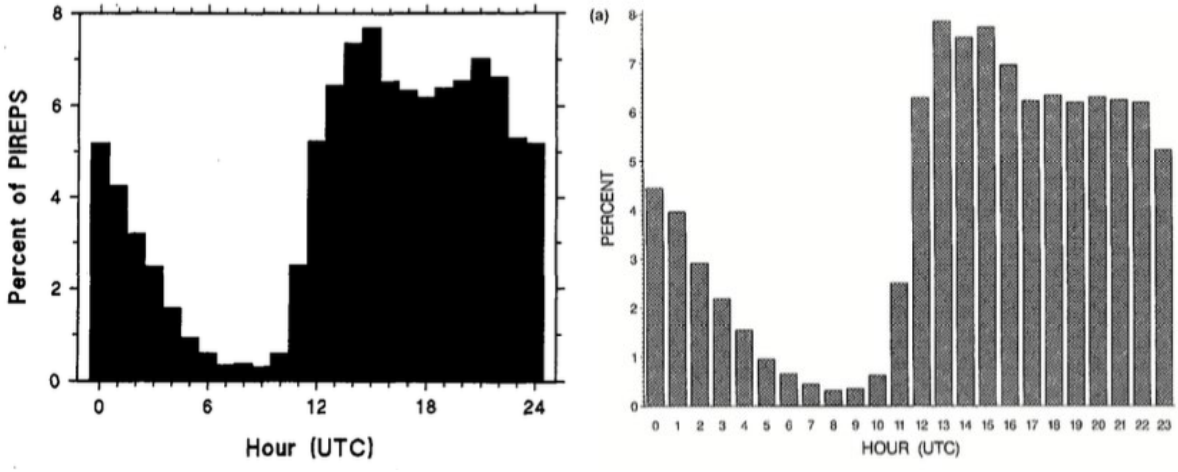

Figure 7. Percentage of icing PIREPs by time of day (Schultz and Politovich 1992 [left] and Brown et al. 1997 [right])

Long-term radiometric studies of integrated SLW in the column above Bern, Switzerland have indicated similar patterns (Hocke et al. 2017). During much of the cool season, integrated SLW was maximized in the hours around and before sunrise, followed by marked decreases in the morning. Though there are hints of recovery in the afternoon, especially in October-November, increases appear to be more universal during the hours between midnight and sunrise. This matches not only experience from flight programs described above, but also notions of cloud top SLW increasing at night due to nocturnal cooling (Rasmussen et al 2002) as a potential contributing factor in diurnal patterns in FZDZ (Bernstein et al. 2019; Landolt et al. 2020).

Evaluations of radiometer data collected in hilly terrain near Boise, Idaho during the Seeded and Natural Orographic Wintertime clouds: the Idaho Experiment (SNOWIE) field program also held some insight into diurnal trends. Results indicate that the January-March average distribution of the *starting time* for periods with liquid water occur most frequently just after midnight (0100-0300 local time, MST), with a hint of a secondary maximum in the morning (0600-1000 MST) (Tessendorf et al. 2017d, 2019a). Liquid water initiation is evident at all hours of the day. Though the Switzerland and Idaho regions are markedly different from the Great Lakes, some commonalities in diurnal trends appear to be present.

There has been considerable interest in sampling SLW and SLD throughout their diurnal cycle during ICICLE, both to capture data at different times of day and to help determine whether candidate tools may have signal and ability differences associated with diurnal changes in icing characteristics. Whether and how those differences could affect the ability for icing tools to differentiate between small-drop, large-drop, and non-icing conditions is also of interest. Examples are provided in Section 3.

3 Technical background

As described in the Introduction, the FAA's AWRP has sponsored aircraft icing weather research to support NAS operations for many years. Icing information for en-route operations is managed by the IFI program, primarily focusing on the Current and Forecast Icing Products (CIP and FIP). Since 2002, these operational products have provided real-time, hourly diagnoses and forecasts of icing probability, SLD potential and, since 2006, icing severity across the CONUS. Versions of these products that cover Alaska are also being pursued (e.g. Icing Product Alaska or IPA). The TAIWIN program manages icing for terminal area operations. Operational decisions made within the terminal area require information on the presence or absence of icing (including FZDZ and FZRA) at very-high spatial and temporal resolutions. Development of a capability to support takeoff and landing operations is ongoing. The specific needs of the TAIWIN and IFI

programs drive the need for the assessment and enhancement of icing-related technologies, which are described below.

3.1 Icing-related technology enhancements

As noted in the Introduction, a great deal has been learned about the production and depletion of SLW and SLD. Much of this knowledge has been gained through field programs focused on cloud microphysics, including those that contributed to the development of Appendix O (Rasmussen et al. 1992; Miller et al. 1998; Isaac et al. 2001a, 2001b, 2005; Stoelinga et al. 2003, Tessendorf et al. 2019a), and through commercial icing certification programs (Bernstein et al. 2006a, 2011; van 't Hoff et al. 2020). During this period of increasing depth of experience and applied research, there have been significant upgrades to observational and forecast weather tools, as well as products that combine their data to provide icing information to the flying public (McDonough and Bernstein 1999; McDonough et al. 2004; Tafferner et al. 2003; Le Bot 2003; Bernstein et al. 2005; Adriaansen et al. 2015, 2019). Each has shown the potential to enhance the ability to observe, diagnose, and predict icing with greater precision, accuracy, and at finer spatial and temporal scales.

Upgrades to operational instruments covering the NAS include the launch of the GOES-R generation satellites (GOES-16, -17), the addition of dual-polarization capability to NEXRADs, enhancements to the processing of automated surface observations, and the development of higher-resolution, more sophisticated numerical models with advanced microphysics packages (Adriaansen et al. 2015, 2019; Benjamin et al. 2016a,b; Guan et al. 2002; Ikeda et al. 2007, 2013; Landolt et al. 2017, 2019, 2020; Mecikalski et al. 2007; Milbrandt et al. 2016; Plummer et al. 2010; Reeves et al. 2014, 2016; Reeves and Howard 2017; Rugg et al. 2019; Ryerson and Ramsay 2007; Serke et al. 2008, 2012, 2015; Sims et al. 2019; Spangenberg et al. 2011; Smith et al. 2015, 2019; Tessendorf et al. 2017a, 2019b; Thompson and Eidhammer 2014; Thompson et al. 1997a, 1997b, 2004, 2008, 2017; Wade 2003; Weygandt et al. 2016, 2017; Williams et al. 2015a, 2015b; Xu et al. 2019). While all of these platforms and tools show significant potential, there is a lack of recent, research-quality, icing-focused flight data to thoroughly evaluate their ability, especially in the context of the new FAA icing regulations that incorporate SLD. The most recent major icing flight program occurred more than ten years ago, before many of these advancements were fully operational. Also, despite extensive research on icing and SLD, there are still uncertainties and limitations in the understanding and ability to predict these phenomena (McDonough et al. 2008b, 2017; Thompson et al. 2017).

To advance the SLW & SLD diagnosis and forecast capabilities to meet user needs, it is critical to compile a new, high-quality set of in-situ measurements. This dataset has to cover a broad range of icing conditions, including FZDZ, FZRA, "small drop" icing and mixed phase, as well as adjacent non-icing conditions (glaciated and clear air). To achieve this, the ICICLE test aircraft must sample these conditions thoroughly, on multiple occasions and in a variety of locations. When practical and safe to do, this should include capturing the full vertical extent of the clouds and precipitation, as well as horizontal variability. This has been accomplished using a suite of high-quality instruments to fully document these conditions in-situ in terms of temperature, liquid- and ice-water content, particle size and shape, remotely using lidar and radar, and indirectly by characterizing source air using aerosol sensors (Wolde and Marcotte 2008; Wolde et al. 2012, 2020; Korolev and Heckman 2019; DiVito et al. 2019).

3.2 Icing weather tools

As described above, icing weather tools and data sources have evolved significantly since the last major aircraft-icing focused flight programs. Each tool brings value to assessing the icing situation, and each has limitations. Summarizing relevant recent history and the state of the current operational tools as well as those that are under development provides helpful context.

3.2.1 Surface observations

Automated Surface Observing Systems (ASOS) and Automated Weather Observing Systems (AWOS) are stationed across the country, providing meteorological information for airports through Meteorological Aerodrome Reports (METARs) and Aviation Selected Special Weather Reports (SPECIs) (NOAA 1998). Each ASOS station is assigned a Service Level, on an alphabetic scale from A to D, which indicates the level of meteorological data that it provides (see Table 1a, where "X" indicates the station has that capability at all times, "O" indicates the station has limited capabilities at certain times of day, and "-" indicates the station does not have that capability).

Table 1a. ASOS Service Levels at airports

ASOS Service Level	Number of Airports	Automated	Manual Augmentation Available	FZRA Sensor	DZ/FZDZ/PL Reporting Capability
A	73	X	X	X	X
B	55	X	X	X	X
C	296	X	O	X	O
D	428	X	-	X	-

Research has shown that surface observations of FZDZ, FZRA, and ice pellets (PL) have been among the strongest indicators of the presence of SLD at the surface and aloft, and reports of drizzle (DZ) and rain (RA) have also proven useful for identifying SLD aloft under certain circumstances (Bernstein et al. 1997, 2005). Currently, automated detection and reporting of some critical conditions for icing at the surface and aloft are either inadequate or nonexistent. These include the detection and reporting of DZ, FZDZ, and PL (Landolt et al. 2017, 2019). ASOS Service Level A and B stations have the capability to report these precipitation types through human augmentation of the automated reports by Contract Weather Observers (CWOs). Service Level C stations have limited capability for human augmentation by air traffic control personnel. These Limited Aviation Weather Reporting Stations (LAWRS) observers are trained to take weather observations during their regular duties. However, Service Level C reports are typically only augmented by LAWRS observers when they have time to make observations. Furthermore, LAWRS observers are not allowed to leave the control tower, creating additional difficulties in observing and reporting certain weather conditions. Service Level D stations do not have human observers, thus their reports are never augmented. This results in the inability of ASOS-D sites to report DZ, FZDZ, PL, and mixed-phase precipitation (Landolt et al. 2019). Unfortunately, airports with Service Level C and D ASOSs are commonly used by aircraft that are affected by the new SLD certification rules (§25.1420).

AWOS also has a variety of station types, indicated by a roman numeral from I to IV, with additional characters appended to indicate its capabilities (FAA 2017). AWOS I stations provide wind, temperature, dew point, altimeter, and density altitude. AWOS II adds visibility. AWOS III adds sky condition, ceiling height, visibility and liquid precipitation accumulation. AWOS IIIP (P for precipitation) adds limited measurements of precipitation type and intensity, AWOS IIIT (T for thunder) adds indications of thunderstorms, and AWOS IIIP/T adds both. AWOS IV provide everything from AWOS IIIP/T, plus freezing rain (AWOS IV Z), runway surface conditions (AWOS IV R), or both (AWOS IV Z/R). Table 1b provides a summary of these, where an “X” indicates the station has this capability at all times and a “-” indicates the station does not have this capability. Most AWOS do not have an observer and many do not have a FZRA sensor. None of the AWOS stations within the ICICLE domain had FZRA sensors, though personnel at those sites had the ability to augment the METARs and SPECIs with reports of freezing precipitation. Almost 2,000 AWOS stations are in use today and more are added each year. Overall, the known shortcomings of ASOS and AWOS have resulted in a need for additional weather capabilities at many airports across the country.

Table 1b. AWOS Service Levels at airports. Note: Current counts for each AWOS station type are not readily available.

AWOS Service Level	Automated	Pressure	T, Td, wind, altimeter, density alt.	Visibility	Sky condition, ceiling height	Liquid precipitation accumulation. Precipitation type.	Thunder	FZRA, RWY VIS
I	X	X	X	-	-	-	-	-
II	X	X	X	X	-	-	-	-
III	X	X	X	X	X	X, P	T, P/T	-
IV	X	X	X	X	X	X	X	Z, R, Z/R

Scientists at the National Center for Atmospheric Research (NCAR) have evaluated and modified present weather algorithms (Ramsay 1999; Wade 2003; Ryerson and Ramsay 2007; Landolt et al. 2017, 2019, 2020) that can be used in conjunction with freezing rain sensors on ASOS stations (see Figure 8). The most recent modified present weather algorithm, known as the Freezing Drizzle Derivation Algorithm (FDDA), enables the automatic reporting of FZDZ.

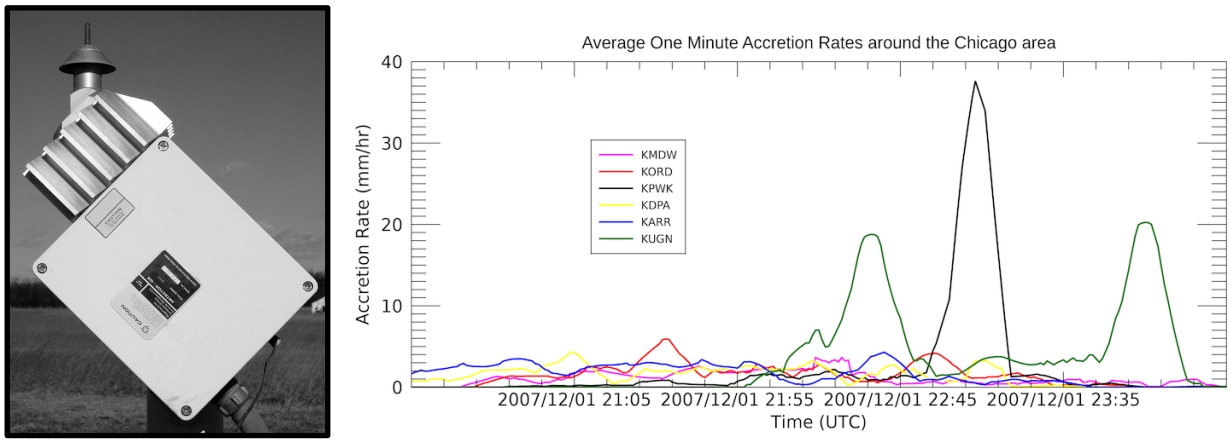

Figure 8. ASOS FZRA sensor (left) and time-series plots of ice accretion rates indicated by these sensors at sites around Chicago during a FZDZ event on 1-2 Dec 2007 (right).

Output from ASOS sensors has been used in verification studies (Benjamin et al. 2016a; Wolff et al. 2017) and this is expected to continue. However, a new present weather sensor with the capability to automatically detect and report DZ, FZDZ, PL, and mixtures of precipitation types is ultimately necessary to support future operations by aircraft with certifications under §25.1420.

All ASOS and some AWOS report cloud coverage and height through the use of a ceilometer, which uses an infrared laser (lidar) to detect clouds and measure cloud base height. Because this

sensor acts similarly to a radar and provides raw reflectivity, these data may prove to be a useful part of the suite of tools used to diagnose icing conditions aloft. For example, the backscatter coefficient, ß(z), which represents the portion of light reflected back toward the ceilometer from a distance z (for example, from water droplets), can be used to see more detail regarding the clouds and precipitation (see Figure 9). At this time, raw reflectivity data from these operational ceilometers are neither readily available nor archived, so research ceilometers are required for testing the ability of these sensors in icing environments.

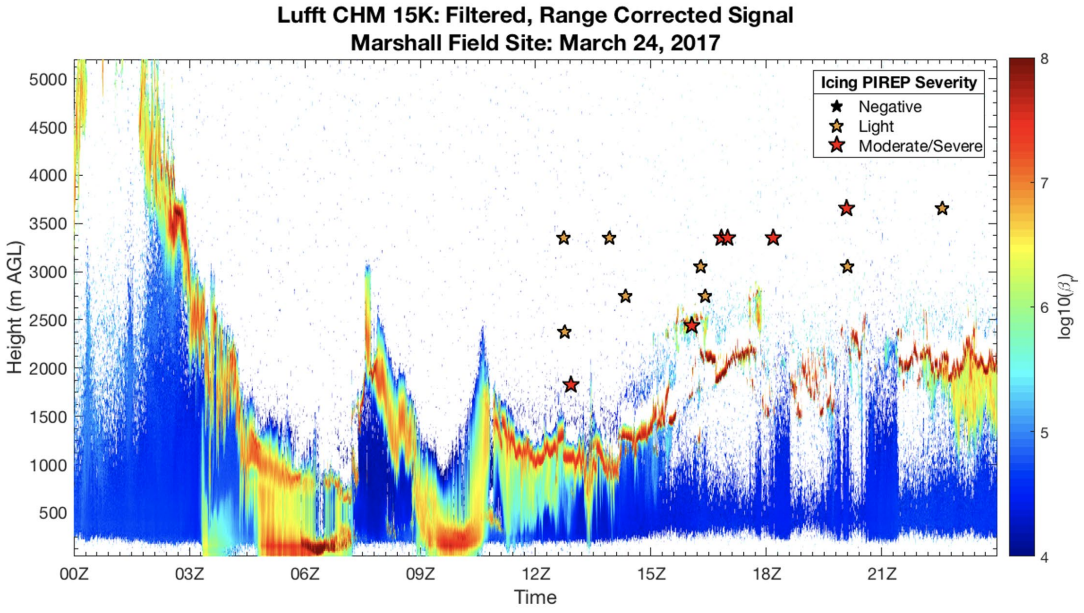

Figure 9. Example ceilometer backscatter profile from an icing event northwest of Denver, CO. Pilot reports made within a 60x60km box surrounding the site are indicated with stars.

Another observation of interest is Liquid Water Equivalent (LWE). Scientists at NCAR have examined snowfall variability and freezing precipitation variability across representative terminal areas. For snowfall variability, an LWE system was developed and used by NCAR to measure precipitation amounts and intensities during various types of precipitation events. These LWE systems include present weather sensors, precipitation gauges, and icing sensors. For freezing precipitation, ice accretion rates have been determined using a Rosemount ice detector identical to those used on ASOS (Lentz et al. 2019; Schwartz et al. 2017). This continues to be an area of interest and such sensor suites allow for additional analysis of LWE and ice accretion rates.

Because the new icing certification rule (§25.1420) is based on drop size, it is important to measure drop-size distributions at the surface to ensure that surface-based tools employed during ICICLE correctly identify the precipitation type. ASOS and AWOS infer particle size rather than measuring it directly. Particle Size and Velocity (PARSIVEL) disdrometer sensors, which measure the size distribution and fall velocities of hydrometeors from 300 μm (perhaps as small as 100 μm) to 30 mm at the surface (Löffler-Mang and Joss 2000; Yuter et al. 2006; Battaglia et al. 2010), are used in research for direct comparison with output from ASOS and AWOS sensors.

3.2.2 Soundings

Balloon-borne instruments provide vertical profiles of pressure, temperature, dew point, wind velocity and direction, which are valuable for the assessment of icing conditions aloft (Appleman 1954; Air Weather Service 1980; Huffman and Norman 1988; Rauber et al. 2000). Using a network of sites across the United States (see Figure 10), the National Weather Service (NWS) routinely launches regularly-scheduled soundings at 0000 and 1200 UTC, with occasional launches at times like 1800 UTC when particularly interesting weather is occurring. The NWS network includes three sites within the primary ICICLE domain (KILX, KDVN, and KGRB) and four others just outside the domain (KMSP, KAPX, KDTX, and KILN) (see Figure 10). Supplemental soundings are launched by request from four sites across the domain and they are discussed in Section 6.7. Soundings provide highly valuable indications of the presence and depth of cloud layers, intervening dry layers, cloud top and cloud base temperatures, 0ºC level(s), and stability, all of which have been shown to be important for assessing likely phase, moisture content, rough estimations of LWC and drop size, and the potential for SLD (see examples in Figure 11).

Regarding cloud phase, the depth and strength of the cloud layers and any dry layers that may exist between them reveal a sense of the potential for higher clouds to seed lower clouds with precipitation (often snow) from above. Such seeding could result in mixed phase and partial, if not complete, glaciation of cloud layers with potential for icing. Of course, drizzle, rain and other forms of precipitation can also seed lower layers and/or reach the ground (McDonough and Bernstein 2004). Regarding stability, vertical temperature structure provides valuable information about the connection of a given layer to air mass sources, including the boundary layer and potential for mixing at cloud top. As noted earlier, certain structures have been related to SLD production at the surface and aloft, such as FZRA from the “classical” melting mechanism, and FZDZ from collision-coalescence, including the isolation of continental air masses from ground-based sources of CCN and IN (Bocchieri 1980; Huffman and Norman 1988; Rauber et al. 2000; Bernstein et al. 2019).

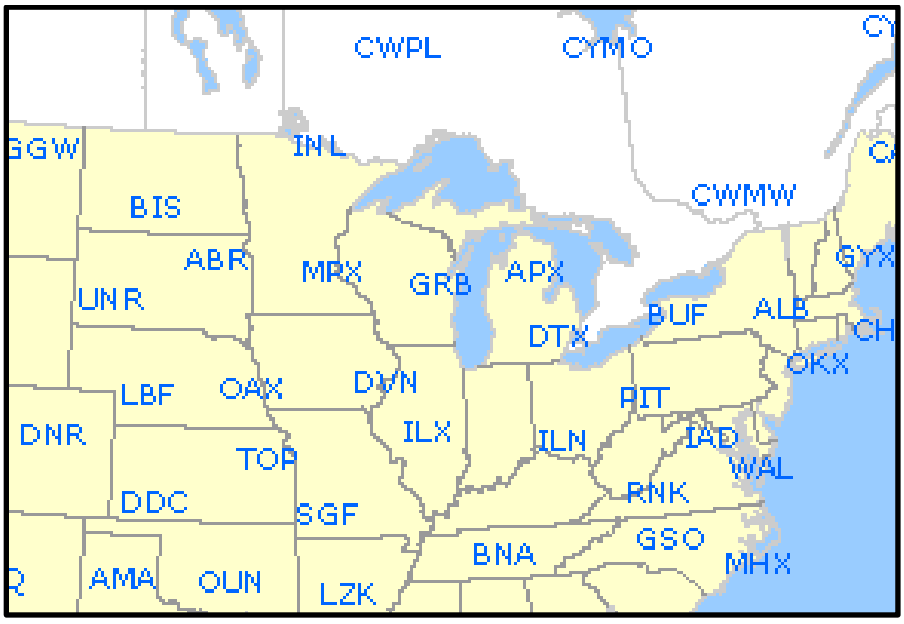

Figure 10. U.S. and Canadian sounding sites across the ICICLE domain and surrounding area, marked with 3-letter station IDs.

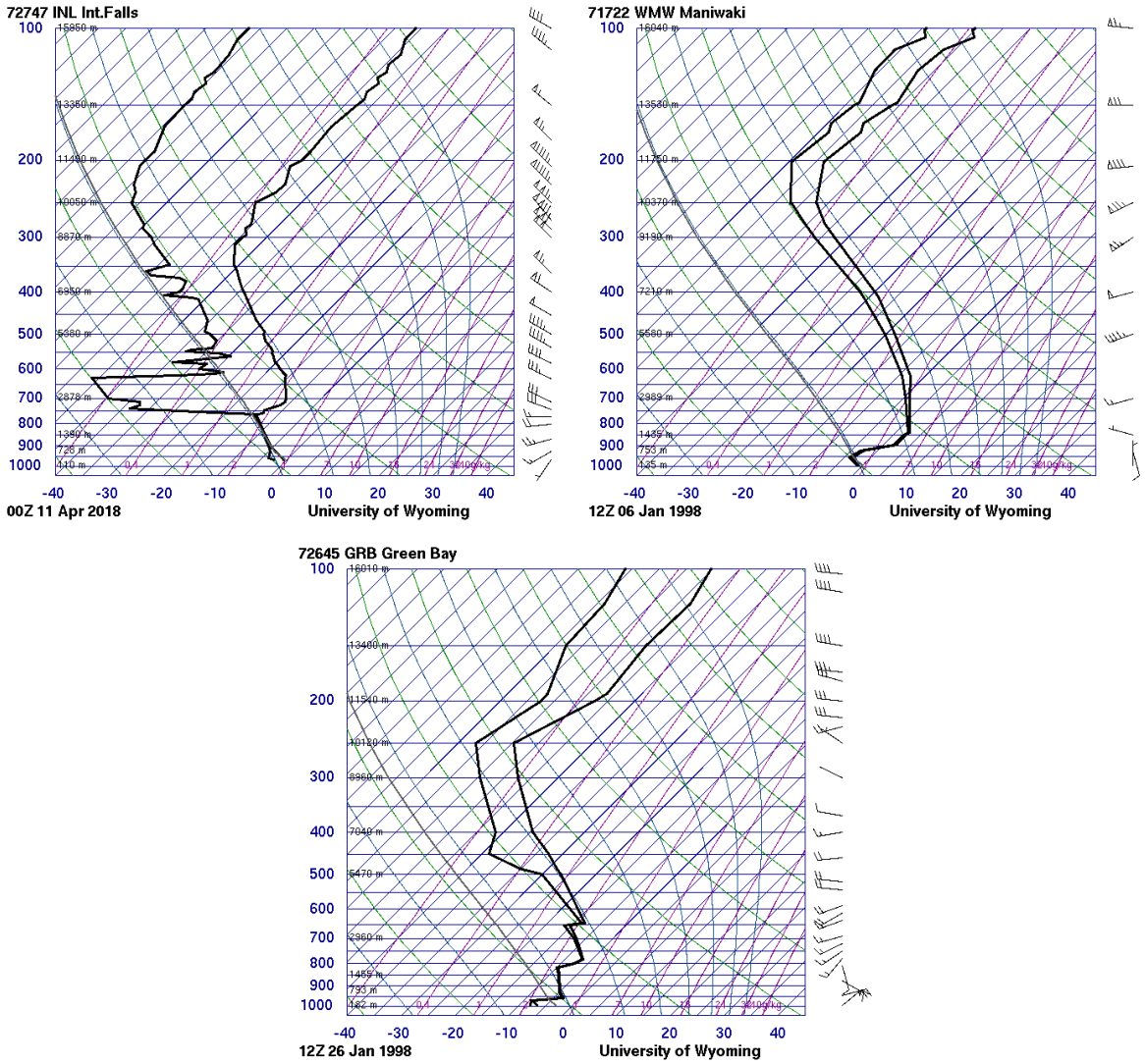

Figure 11. Example soundings for single-layer icing cloud (top left), classical FZRA (top right), and multi-layered mixed-phase FZDZ (bottom) situations.

3.2.3 Satellite

Researchers at NCAR, U.S. Naval Research Lab, NASA, NOAA, and other institutions have found that multiple wavelengths (channels) of satellite data have been highly useful in locating and characterizing clouds. This includes the identification of clouds containing liquid water and ice crystals, and assessment of particle size (Curry and Liu 1992; Lee et al. 1997; Thompson et al. 1997b; Minnis et al. 2003; Mecikalski et al. 2007; Ellrod and Bailey 2007; McDonough et al. 2008a; Spangenberg et al. 2011; Smith et al. 2015, 2019).

Starting with basic satellite channels, the visible channel (~0.6 μm) is of course highly useful for indicating the presence of clouds during the daytime. Visible albedo (the measure of the diffuse

reflection of solar radiation) can also help with the assessment of water content in the upper portion of clouds. To be most valuable for icing diagnosis, and to avoid misidentification of things like snow cover as "clouds," the visible channel must be combined with other channels. When a cloud is identified as being comprised of mostly liquid water, the visible albedo can provide an indication of the integrated liquid water content. In combination with stability profiles, this information can be used to assess the vertical distribution of liquid water content.

Infrared (IR) channels supply additional crucial information. Longwave IR (~11 μm) is essential for the assessment of cloud top temperature (CTT), which is helpful in the determination of cloud phase. Since SLW can only exist at temperatures between 0ºC and -40ºC, the first step is to differentiate between cloud tops that are ice-dominated, those that are comprised of above-freezing water, and those that are likely to contain SLW. Liquid droplets and ice crystals emit and reflect energy differently in the shortwave IR (~3.9 μm) and simple subtraction of the longwave- and shortwave-IR channels during nighttime hours is highly useful for identifying liquid water clouds. IR differences can also be used during daytime hours, but their application can be more challenging because water drops and ice crystals both emit radiation in all IR wavelengths and also reflect solar energy. Shortwave-IR reflectance can also be quite valuable for the assessment of particle size during the daytime. The solar terminator can complicate the use of both the infrared-difference and shortwave-reflectance fields because the "daytime" character of the shortwave-IR field changes markedly with sun angle (see Figure 12). An additional challenge of using shortwave IR data in the diagnosis of cloud phase is that the largest water drops reflect and emit radiation similarly to ice crystals. Thus, the use of this signal to differentiate between SLD clouds and ice clouds can be challenging. This is an area of active research.

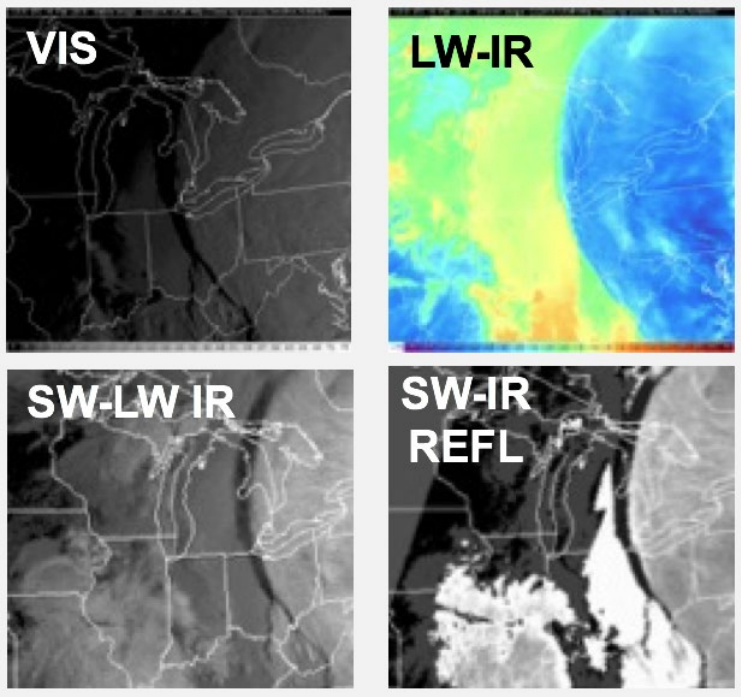

Figure 12. Example GOES satellite images from an icing event near dawn, showing visible (top-left), long-wave infrared (top-right), shortwave-minus-longwave infrared (bottom-left) and shortwave infrared reflectance (bottom-right) fields.

Despite these limitations, satellite products have been used for decades to successfully guide aircraft into conditions desired during some recent icing flight research and certification programs mentioned earlier. This experience has revealed that clouds comprised of very small cloud droplets were often significantly brighter than regions of larger drops in the IR-difference and shortwave-IR reflectance fields, which is also strongly supported by radiative transfer theory (Pilewskie and Twomey, 1987) and prior studies (Nakajima et al. 1991).

One example set for daytime satellite imagery is provided in Figure 13. The standard visible and longwave IR images are shown in the top row and shortwave-reflectance is shown in the lower left. A multi-spectral analysis was used to determine the highest likelihood of SLW, which is highlighted in blue in the lower-right image. The shortwave-reflectance image indicates that some of the clouds were highly reflective and may have been dominated by small drops. Some embedded areas had lower reflectance and may have been composed of larger drops (see arrow). A much larger area of markedly lower reflectance and relatively low CTT was present over Canada and was likely to have been composed of ice crystals at cloud top.

With the advent of the GOES-16/17 series satellites, several new, high-resolution channels became available on the Advanced Baseline Imager (ABI). A summary of wavelengths and imager products can be found in Table 2a and 2b, where the columns labeled HES

(Hyperspectral Environmental Suite) in Table 2b reflect products that can be improved with high spectral infrared data from the SND (sounder) or CW (coastal waters) instruments. For icing, the new 1.6 μm wavelength channel has strong potential to discriminate water drops from ice and perhaps provide information on the size of the water drops. Several of the new derived products may also have relevance to icing and should be evaluated in the context of icing. NASA-Langley and the University of Wisconsin have used radiative transfer models to create potential new GOES-16 (a.k.a. GOES-East) icing products (Smith et al. 2015). Since their research has focused on SLW determination, a dedicated effort is required to assess the value of these products for differentiation of Appendix C and O conditions.

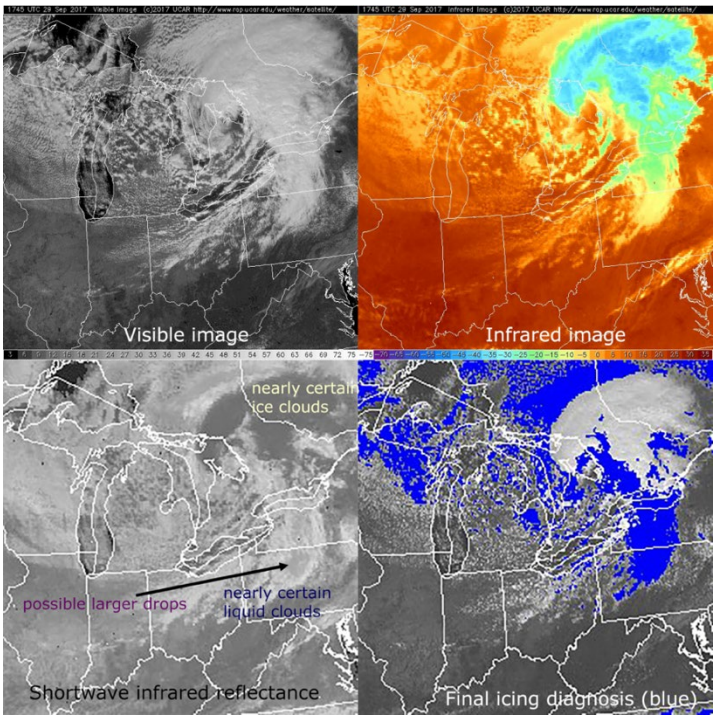

Figure 13. Example visible, infrared, shortwave infrared reflectance, and icing diagnosis imagery.

Table 2a. Summary of GOES-16 ABI bands. The minimum and maximum wavelength range represent the full width half maximum (FWHM; or 50%) points (Schmit et al. 2005).

Future GOES imager (ABI) band	Wavelength range (μm)	Central wavelength (μm)	Nominal subsatellite IGFOV (km)	Sample use	Heritage instrument(s)
1	0.45–0.49	0.47	1	Daytime aerosol over land, coastal water mapping	MODIS
2	0.59–0.69	0.64	0.5	Daytime clouds fog, insolation, winds	Current GOES imager/ sounder
3	0.846–0.885	0.865	1	Daytime vegetation/burn scar and aerosol over water, winds	VIIRS, spectrally modified AVHRR
4	1.371–1.386	1.378	2	Daytime cirrus cloud	VIIRS, MODIS
5	1.58–1.64	1.61	1	Daytime cloud-top phase and particle size, snow	VIIRS, spectrally modified AVHRR
6	2.225–2.275	2.25	2	Daytime land/cloud properties, particle size, vegetation, snow	VIIRS, similar to MODIS
7	3.80–4.00	3.90	2	Surface and cloud, fog at night, fire, winds	Current GOES imager
8	5.77–6.6	6.19	2	High-level atmospheric water vapor, winds, rainfall	Current GOES imager
9	6.75–7.15	6.95	2	Midlevel atmospheric water vapor, winds, rainfall	Current GOES sounder
10	7.24–7.44	7.34	2	Lower-level water vapor, winds, and SO_2	Spectrally modified current GOES sounder
11	8.3–8.7	8.5	2	Total water for stability, cloud phase, dust, SO_2 rainfall	MAS
12	9.42–9.8	9.61	2	Total ozone, turbulence, and winds	Spectrally modified current sounder
13	10.1–10.6	10.35	2	Surface and cloud	MAS
14	10.8–11.6	11.2	2	Imagery, SST, clouds, rainfall	Current GOES sounder
15	11.8–12.8	12.3	2	Total water, ash, and SST	Current GOES sounder
16	13.0–13.6	13.3	2	Air temperature, cloud heights and amounts	Current GOES sounder/ *GOES-12+* imager

Table 2b. Selected GOES-16 imager products and needed spectral coverage from the ABI (Schmit et al. 2005).

Sample product list	Primary ABI band(s) (μm)	Secondary ABI band(s) (μm)	HES SND	HES CW
Aerosols/dust/smoke	0.47, 2.2, 8.5, 12.3	0.64, 0.865, 1.6, 10.3, 11.2	Yes	Yes
Clear-sky masks	0.64, 1.38, 8.5, 11.2, 12.3	0.47, 0.865, 1.6, 8.5, 13.3		
Cloud imagery	0.64, 1.38, 3.9, 11.2, 13.3	0.865, 8.5, 10.35	Yes	
Cloud-top: . . . Microphysics	0.64, 1.6, 3.9, 10.35, 11.2	0.865, 2.2, 8.5	Yes	
. . . Phase	1.6, 8.5, 11.2, 13.3	0.6, 1.38, 2.2	Yes	
. . . Pressure/temperature	8.5, 11.2, 13.3	3.9, 6.15, 7, 10.3	Yes	
Fires/hot spots	3.9, 11.2	0.64, 2.2, 12.3, 13.3		Yes
Fire burn scars	0.865	0.64, 10.3		Yes
Hurricane intensity	11.2	0.64, 3.9, 6.15, 8.5, 13.3	Yes	
Insolation	0.47, 0.64	0.865, 1.6		
Land skin temperature	3.9, 11.2, 12.3	7.3, 8.5, 10.3	Yes	
Low cloud and fog	3.9, 11.2	0.64, 1.61, 10.3, 12.3	Yes	
Rainfall rate/QPE	8.5, 11.2, 12.3, 13.3	0.64, 6.15, 7.3, 10.3	Yes	
Derived motion	0.64, 3.9, 6.19, 7, 7.3, 11.2	0.865, 1.38, 9.6, 10.3, 12.3, 13.3	Yes	
Sea ice products	0.64, 1.6	2.2, 3.9, 11.2, 12.3		
Sea surface temperature	3.9, 11.2, 12.3	8.5, 10.35	Yes	
Snow detection (cover)	1.61	0.64, 0.865, 2.2, 3.9, 11.2		Yes
SO_2 (upper level)	8.5, 7.34	9.6, 11.2, 13.3	Yes	
Surface properties	8.5, 10.35	11.2	Yes	
Suspended sediment	0.64, 0.865	0.47		Yes
Total ozone	9.6	11.2, 13.3	Yes	
Turbulence	6.15, 7, 9.6	7.3, 11.2, 13.3		
Vegetation index	0.64, 0.865	2.2		Yes
Volcanic ash product	0.64, 3.9, 8.5, 12.3	7.3, 11.2, 13.3	Yes	

3.2.4 Radar

The ground-based national network of 10-cm wavelength WSR-88D precipitation radars, known as NEXRADs (Next generation radars) (Leone et al. 1989), plays a vital role in icing hazard detection. The network consists of over 150 installations that each sample an airspace volume to a range of >200 km every ~6 min, measuring reflectivity, Doppler velocity, spectrum width, and dual-polarization moments. With the addition of dual-polarization in 2013, two orthogonal pulses are transmitted with the returns received nearly instantaneously, allowing for particle shape characterization, among other things (Zrnic et al. 1993; Reeves et al. 2016; Serke et al. 2019; Zhang et al. 2019).

Extensive research has been conducted over the years to develop algorithms that use dual-polarization moments for in-flight icing detection (Vivekanandan et al. 1999, 2001; Reinking et al. 1997; Schneider et al. 2002; Serke et al. 2005, 2008, 2012, 2016; Reehorst et al. 2009; Ikeda et al. 2009, Plummer et al. 2010; Williams et al. 2011, 2015b; Ellis et al. 2012; Reeves et al. 2016; Van Den Broeke et al. 2016). One such algorithm is the Radar Icing Algorithm (RadIA) (Serke et al. 2017). RadIA begins by ingesting both the Level-2 polar coordinate format radar data and the closest associated Numerical Weather Prediction (NWP) model temperature profile, which can be adjusted based on the radar-derived melting level altitude. The data are then run through a particle identification process to remove clutter, non-meteorological targets and particle types that exist at T>0ºC. Fuzzy logic membership functions are applied to the remaining data, based on findings from icing research flight campaigns. The results are normalized interest values for the presence of each of the following particle types: small drop, large drop, mixed-phase and plate-shaped crystals on a 0-1 scale (see Figure 14). When the interest level of a particular particle type is well above 0.5, it is presumed to exist in the atmosphere for that specific location and time. When the interest level is well below 0.5, it is presumed not to exist. If this assertion can be consistently proven to be true, then gridded output from each of the internal algorithms could be used as an ingredient in integrated icing products (Sims et al. 2019).

In 2010, the first RadIA prototype was conceived and tested on data from the research-quality CSU-CHILL Radar (Ellis et al. 2012; Serke et al. 2012). Between 2012 and 2015, RadIA was tested in real-time mode using Cleveland, Ohio NEXRAD data and compared to other icing detection instruments (Serke et al. 2016). In early 2017, RadIA was run again in real-time on Boise, Idaho NEXRAD data in support of the SNOWIE Field Campaign (see Figure 14) for the detection of large-drop, small-drop, and mixed-phase conditions (Serke et al. 2017; Tessendorf et al. 2017b). Current research focuses on extending RadIA's application from output from a single radar to 3-D gridded radar data from the Multi-Radar/Multi-Sensor (MRMS) System (Zhang et al. 2011).

RadIA is being considered for use in the operational version of CIP, which currently uses the maximum reflectivity in the MRMS mosaic of the lowest 4 km of the column, known as Layer Composite Reflectivity (LCREF). LCREF is used to spatially quantify the location and intensity of precipitation. CIP uses this information as part of assessing the icing "scenario" and runs the reflectivity values through interest maps to adjust the icing probability, icing severity, and SLD potential fields. Though the 3-dimensional radar volumetric data and dual-polarization moment characterizations have proven useful in case studies, CIP does not yet take advantage of these data (Serke et al. 2019). This is an area of active research.

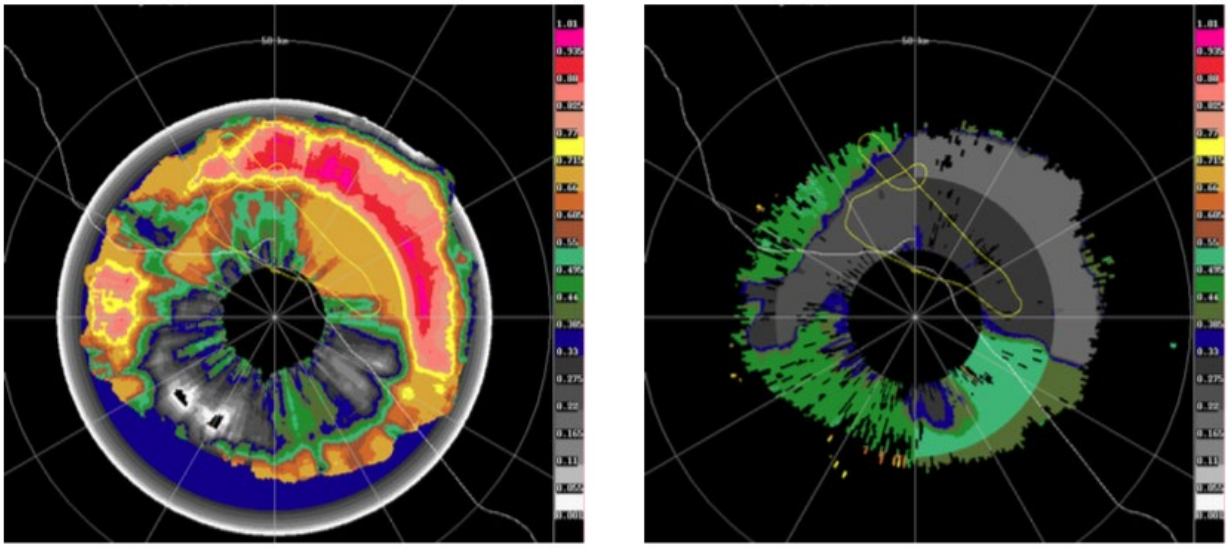

Figure 14. Example plot of RadIA Interest (0-1 scale) in mixed-phase (left) and FZDZ (right). A research aircraft flight track (solid yellow line) is also shown (Tessendorf et al. 2017a).

It is important to note that radar-based signatures can be affected by meteorological features, such as low-level temperature inversions, which are common during icing events (Reeves and Waters 2019). By definition, classical FZRA events must have inversions, and these can be quite strong and/or deep. Recent evidence has shown that stable layers, such as low-level inversions, can be a factor in the development of non-classical FZDZ events aloft, which can proliferate downward to the surface. These factors could have implications for the use of radar-based icing tools. Reeves and Waters (2019) demonstrated that shallow SLD icing events might only be captured in close proximity to radars due to the lowest beams rising to the point of overshooting the tops of the clouds and precipitation. This issue is particularly evident for relatively weak clouds and worsens with increasing distance from the radar. The Volume Coverage Pattern (VCP) mode of the radar can also contribute to what is detectable (see Table 3, where VCP modes retired as of January 2018 are indicated with an asterisk). Closest to the radar, the lack of sampling at very high beam angles can cause precipitation overhead to be missed in what is known as the "cone of silence." Beam width expansion with distance also causes increased airspace volume sampling, sometimes making it more difficult to resolve important features (see Figure 15 and Figure 16).

Table 3. Attributes of NEXRAD VCP modes (Reeves and Waters 2019).

VCP	Scan time (min)	No. of tilts	Elevation angles (°)	Recommended usage
215	6	15	0.5, 0.9, 1.3, 1.8, 2.4, 3.1, 4, 5.1, 6.4, 8, 10, 12, 14, 16.7, 19.5	General-purpose precipitation, including tropical systems capable of producing tornadoes
12	4.15	14	0.5, 0.9, 1.3, 1.8, 2.4, 3.1, 4, 5.1, 6.4, 8, 10, 12.5, 15.6, 19.5	Severe weather, including tornadoes
35	7	9	0.5, 0.9, 1.3, 1.8, 2.4, 3.1, 4, 5.1, 6.4	Scattered to widespread light to moderate stratiform precipitation
121	6	9	0.5, 1.5, 2.4, 3.4, 4.3, 6, 9.9, 14.6, 19.5	Large number of rotating storms or tropical systems or when better velocity data are needed
31/32	9.75	5	0.5, 1.5, 2.4, 3.4, 4.3	Clear air, light rain, and/or wintry precipitation
11*	5	14	0.5, 1.5, 2.4, 3.4, 4.3, 5.3, 6.2 7.5, 8.7, 10, 14 16.7, 19.5	Convection, especially close to radar
21*	6	9	0.5, 1.5, 2.4, 3.4, 4.3, 6, 9.9, 14.6, 19.5	Shallow precipitation with embedded convection

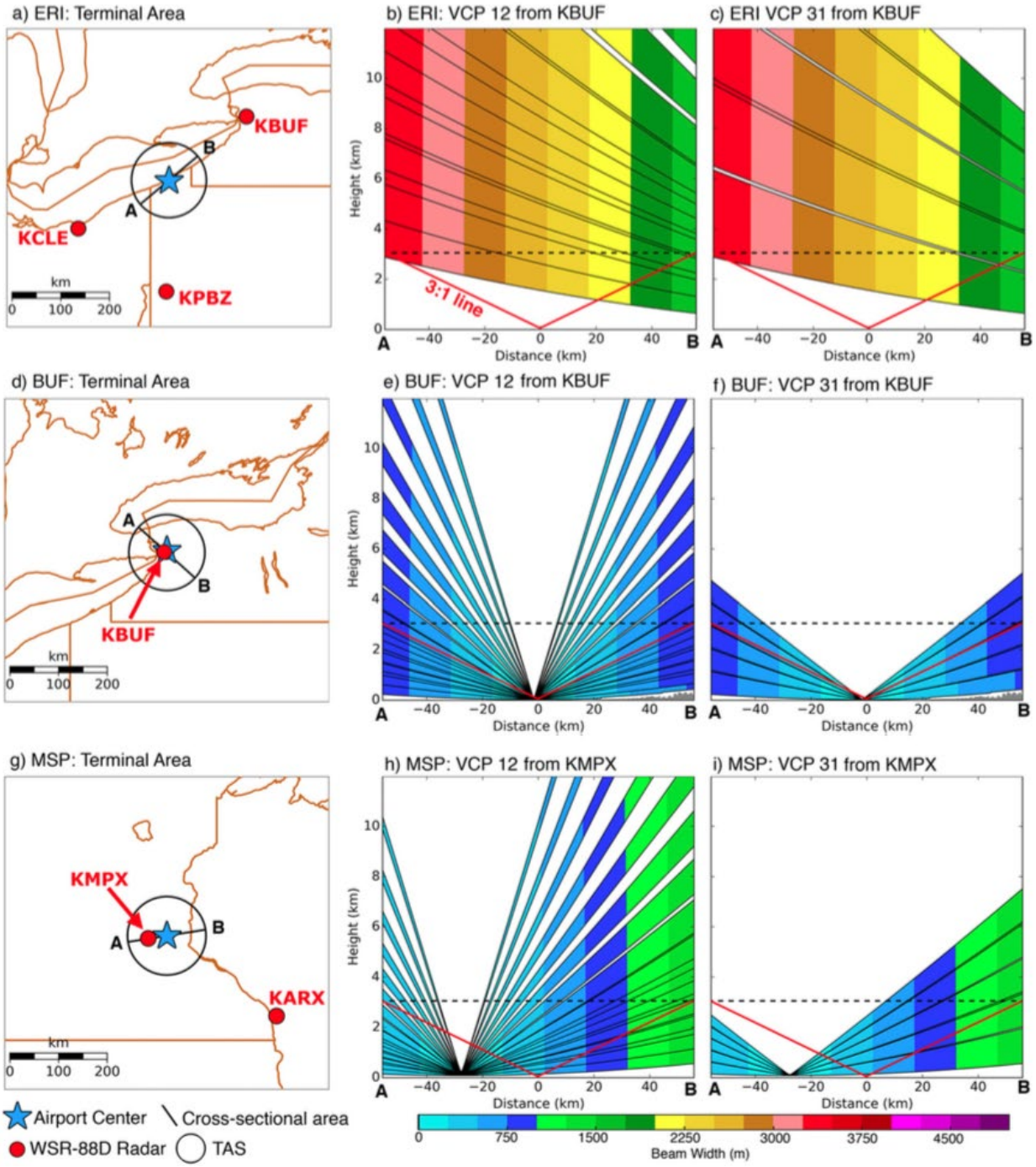

Figure 15. Maps showing terminal airspaces (TASs), nearby radars and vertical cross sections of beam width for VCP 12 (b, e, h), and VCP 31 (c, f, i) at KERI (top), KBUF (middle), and KMSP (bottom). The top of the TAS is given by the dashed line (Reeves and Waters 2019).

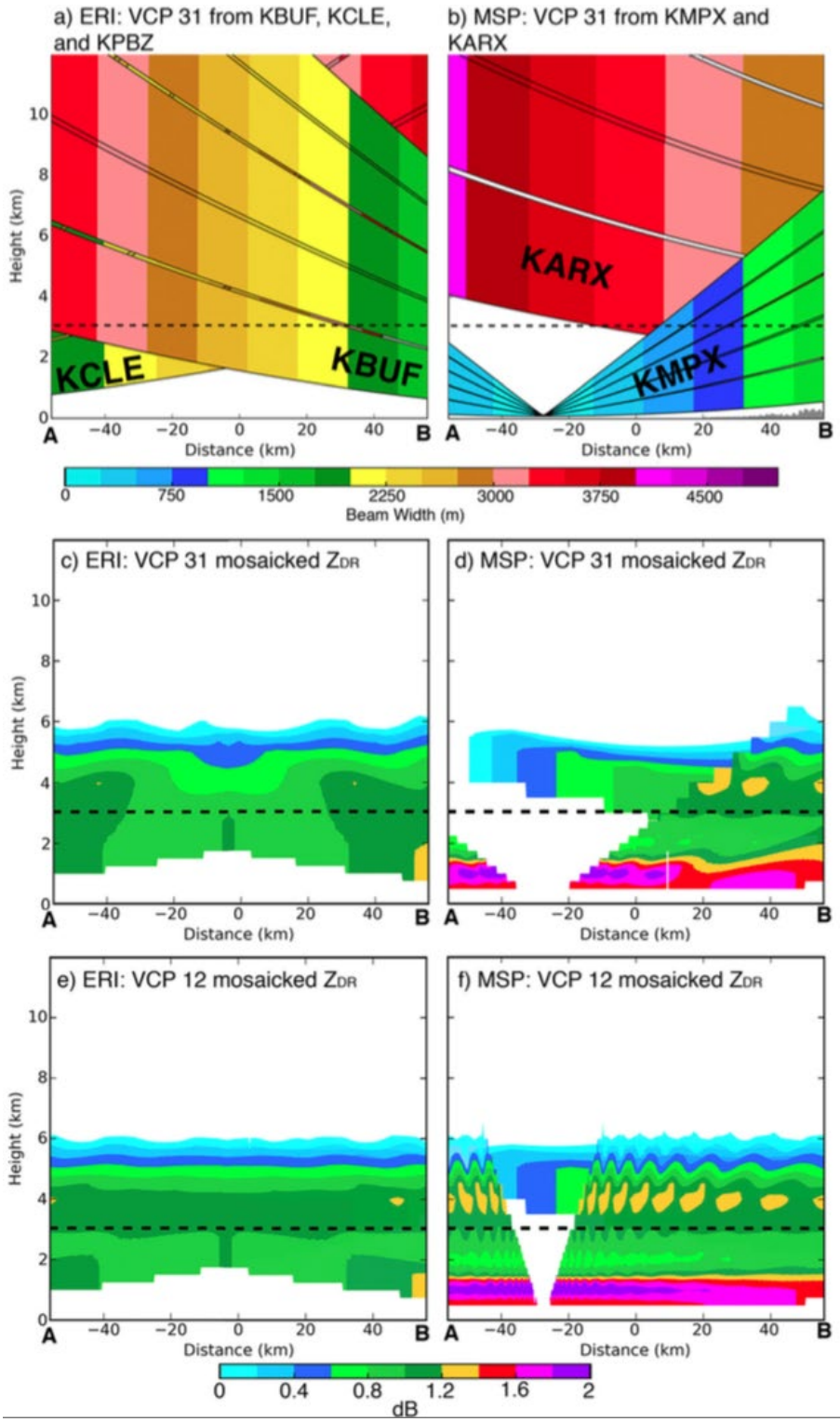

Figure 16. As in Figure 15, but showing all radars with coverage in the KERI and KMSP TASs assuming VCP 31 and vertical cross sections of mosaicked ZDR for VCPs 31 (c, d) and VCPs 12 (e, f) at KERI (left) and KMSP (right). Images c-f demonstrate potential signal issues for a classical FZRA situation mosaicked data (Reeves and Waters 2019).

3.2.5 Feature tracking and advection

The extrapolation and advection of features evident in satellite and radar data can be a valuable tool for forecasting. Over time, clouds and precipitation areas can maintain many of their features if they move and/or evolve in a predictable manner. Humans are quite good at identifying, tracking and forecasting such features and attempts to automate this have met with success, particularly for convective weather phenomena (Wilson et al. 1998; Mueller et al. 2003). The concept has also worked well for some winter weather features, such as snow bands, and it has been used in real-time ground de-icing forecast products (Rasmussen et al. 2001). It has long been theorized that these techniques might prove useful for the extrapolation and advection of icing-relevant features (Bernstein et al. 2000).

Recently, the Cartesian Tracking Radar Echoes by Correlation (CTREC) algorithm (Tuttle and Foote 1990) has been applied to GOES-16 satellite data, with emphasis on the nighttime "fog" product (short- and long-wave IR subtraction; see Section 3.2.3). Preliminary results from case studies have indicated that some icing cloud features are highly trackable, especially for single-layer clouds (see Figure 17). As expected, complex cases with multiple cloud layers have proven to be more challenging, but concepts for addressing these situations are under consideration.

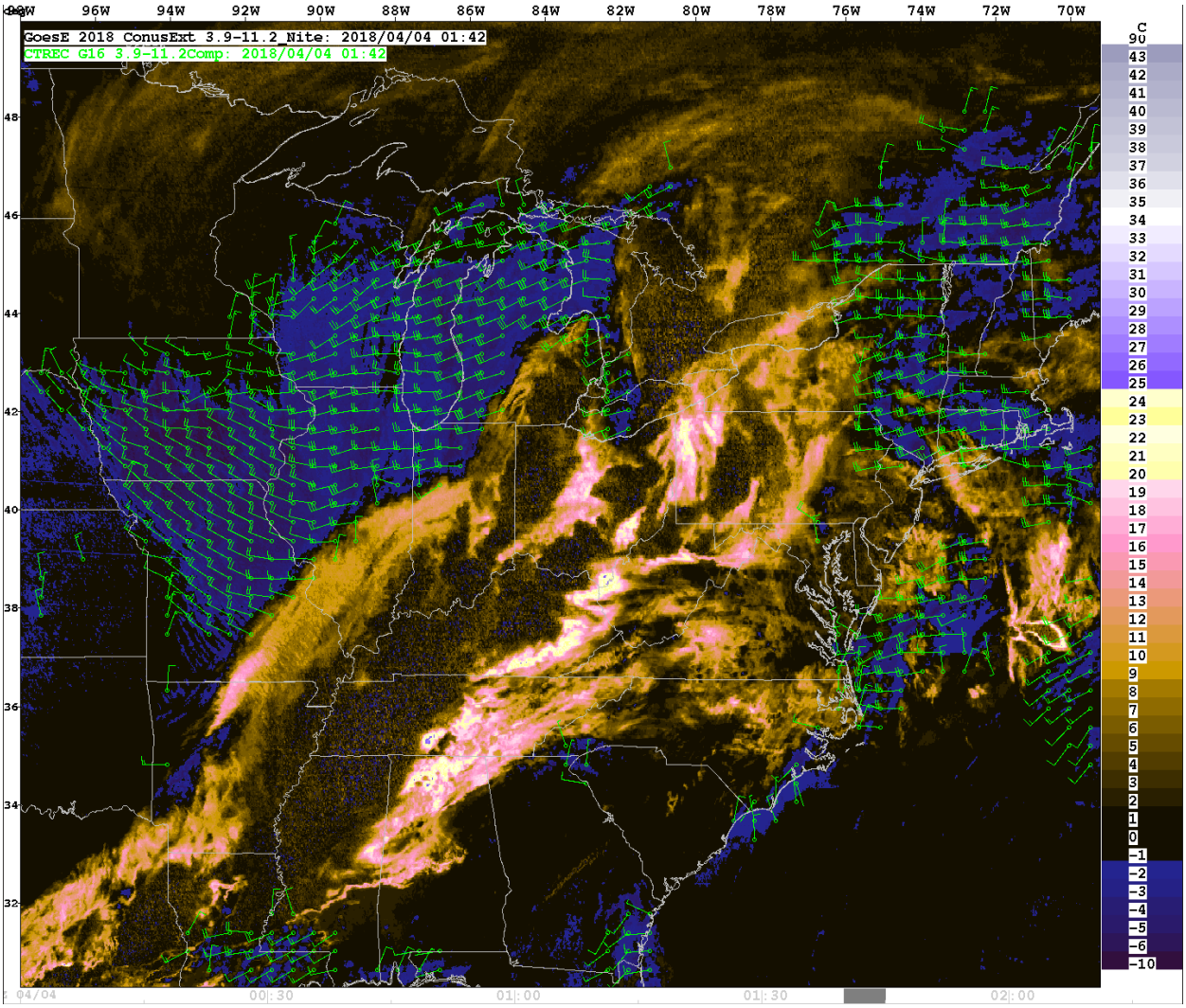

Figure 17. Example CTREC winds showing the motion of low clouds identified using the GOES "fog" product (blue areas with green wind barbs) and high clouds (tan and brown shading).

3.2.6 NWP models

NWP models supply essential meteorological information for the diagnosis and forecasting of icing over the CONUS, including temperature, humidity, liquid- and ice-water contents and the spectra of particle sizes that comprise them (Benjamin et al. 1998, 2004, 2016a, 2016b; Thompson et al. 1997a, 2004, 2008, 2017; Manning and Davis 1997; Reisner et al. 1998; Geresdi et al. 2005). With the recent availability of higher-resolution models, such as the High-Resolution Rapid Refresh (HRRR) and updates to existing models, an evaluation of the current capabilities of NWP models is required to better understand the abilities, shortcomings and applicability of individual models, ensembles and model "blends" with respect to icing environments. Further, methods to address areas in the models known to need improvement are being explored, such as how the models assimilate data during initialization, how aerosol

particles nucleate into water drops and ice crystals, and the under-prediction of clouds at common icing temperatures.

As an example of current and preliminary FAA-supported research into the use of NWP models and ensembles of models to predict icing conditions, Thompson et al (2017) analyzed 60 cool-season months of Weather Research and Forecasting (WRF) model forecasts. For practical considerations, the HRRR model is a specific configuration of the WRF model, so the two should be considered synonymous. The model showed excellent correspondence to measured values of liquid water content, temperature and median volume diameter in the FAA icing database (Jeck 2008, 2010) (see Figure 18).

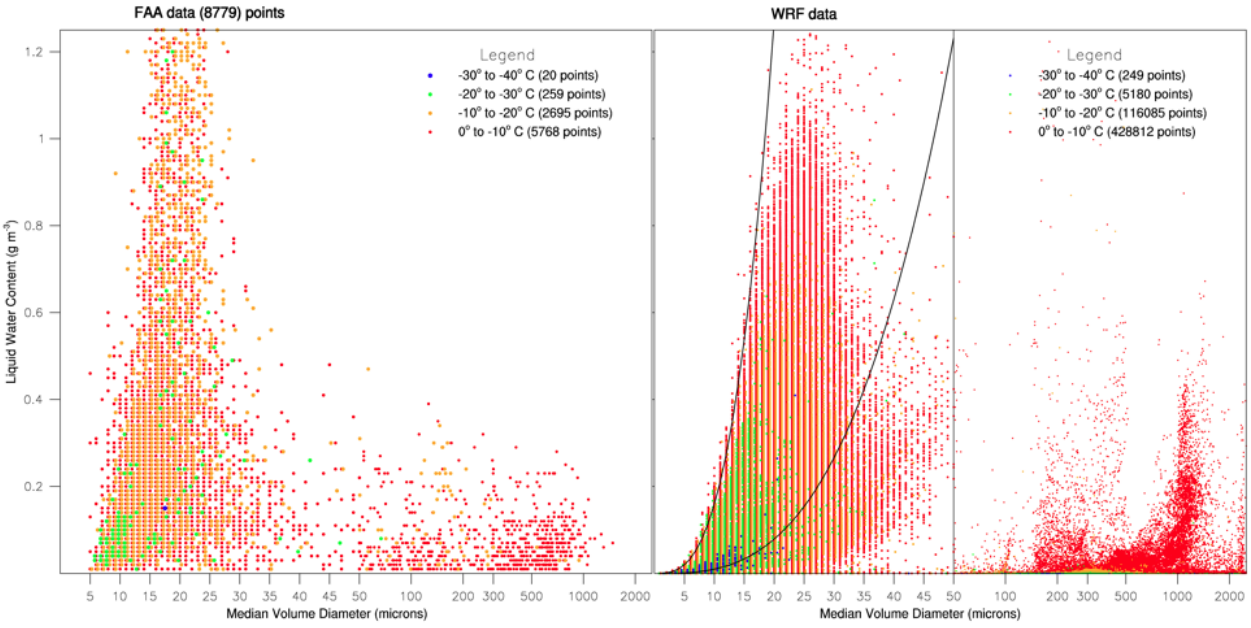

Figure 18. Scatterplots of FAA observations (left) and WRF model results (right) of MVD vs. LWC color coded by temperature. The left and right parts of each panel represent Appendix C and Appendix O conditions, respectively (Thompson et al 2017)

One drawback noted in the conclusions of Thompson et al (2017) relates to connections between aerosols and cloud physics. Number concentration of aerosols is highly important in clouds because more aerosols result in more droplets of overall smaller size for the same LWC. The model results shown in Figure 18 reveal the possibility of too few cloud droplets predicted and corresponding MVD tending to be slightly larger in the model than in the observations.

In addition to the LWC and MVD analysis, the WRF model correctly forecast SLW within one hour of ~50-60% of icing pilot reports when considering the 24 x 24 km^2 area surrounding the report. Only a decade earlier, the Rapid Update Cycle (RUC) model correctly captured only

about half as many PIREPs using both a larger box and a larger time window for PIREP matching (Wolff and McDonough, 2010). Furthermore, the Thompson et al (2017) WRF study showed that the number of correctly matched *negative*-icing reports was roughly 83% (see Figure 19) and the amount of airspace warned by the model's explicit prediction of SLW/icing was less than one-fifth of that warned by the operational FIP at the 0.05 probability threshold. Although FIP's positive PIREP capture rate at this threshold is far higher at nearly 90%, the airspace warned is much larger. Therefore, the possibility of using more information from higher-resolution NWP models for more direct icing prediction together with aspects of both FIP and CIP could be an avenue toward maintaining a high capture rate of icing reports while warning for less airspace.

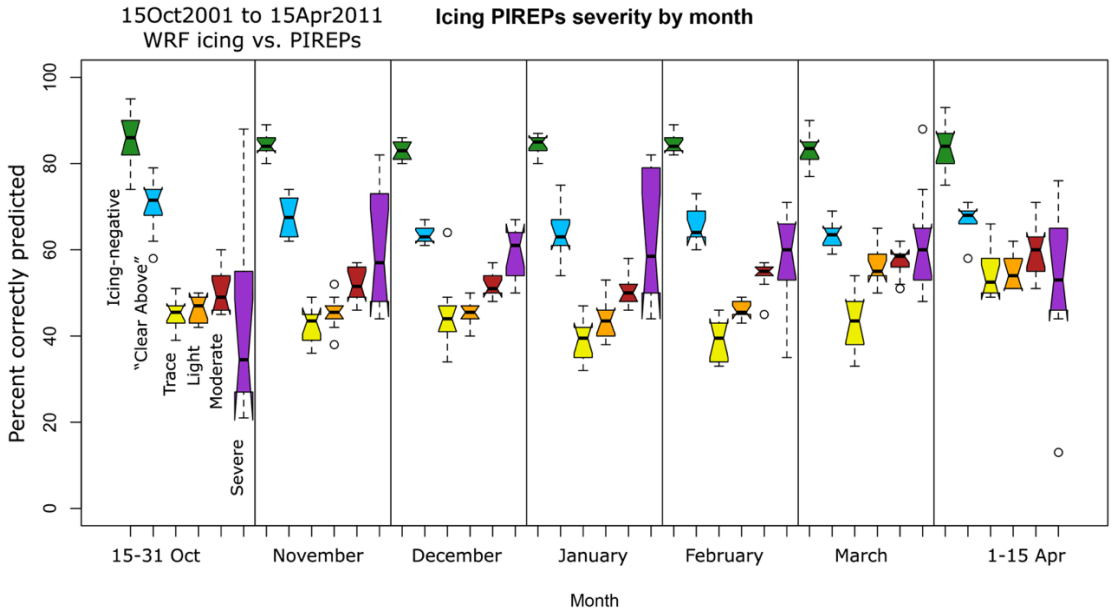

Figure 19. Box plots of the percentage of correctly predicted positive and negative icing PIREPs of specific types for 60 cool-season months of WRF forecasts (Thompson 2019).

Complementing the analysis of Thompson et al (2017), Xu et al. (2019) analyzed icing PIREPs and surface weather conditions in comparison to the HRRR model during the 2017-18 winter season. They again found that ~60% of positive icing PIREPs were captured by the HRRR SLW field, depending on HRRR forecast duration (see Figure 20). Furthermore, the capture rate of surface weather observations of FZDZ and FZRA was near 60% using the same time and space constraints mentioned above. If confirmed, this a significant advancement in NWP models over the models of only a decade earlier.

Besides the direct SLW prediction by NWP models, various techniques can be applied to post-process NWP data into subsequent icing products. One such capability the TAIWIN project is currently exploring is a time-lagged ensemble (TLE) approach, where a group of NWP model forecasts from successive model start times valid at the same time are mathematically combined (Xu et al. 2019). This technique has been used in other FAA-supported research (e.g., convective weather, CoSPA products) (DeLaura et al. 2011). A post-processed HRRR model TLE for icing conditions was created using simple weighted averages of various individual HRRR forecasts to obtain a final icing prediction that is a blend of the output from multiple forecast times. Figure 21 presents an example of the final forecasts that were validated against icing PIREPs in the same manner as for each individual forecast (see the right-most points in Figure 19). It is evident that the predictive skill of the TLE is far greater than that of any individual HRRR member, with the capture rate of positive icing reports improving from ~60% up to 83%. However, the blending of multiple HRRR forecasts also increases the volume of airspace warned by a factor of approximately 2.5. This volume of warned airspace is very similar to that from the operational FIP at an icing probability threshold of 0.35 (a mid-range value, since the icing probability scale maximizes well below 1.0) (Kucera et al. 2007). Thus, it is clear that the TLE method has significant potential as a post-processing technique to improve direct model prediction of icing conditions with consideration towards maintaining reasonable amount of airspace warned.

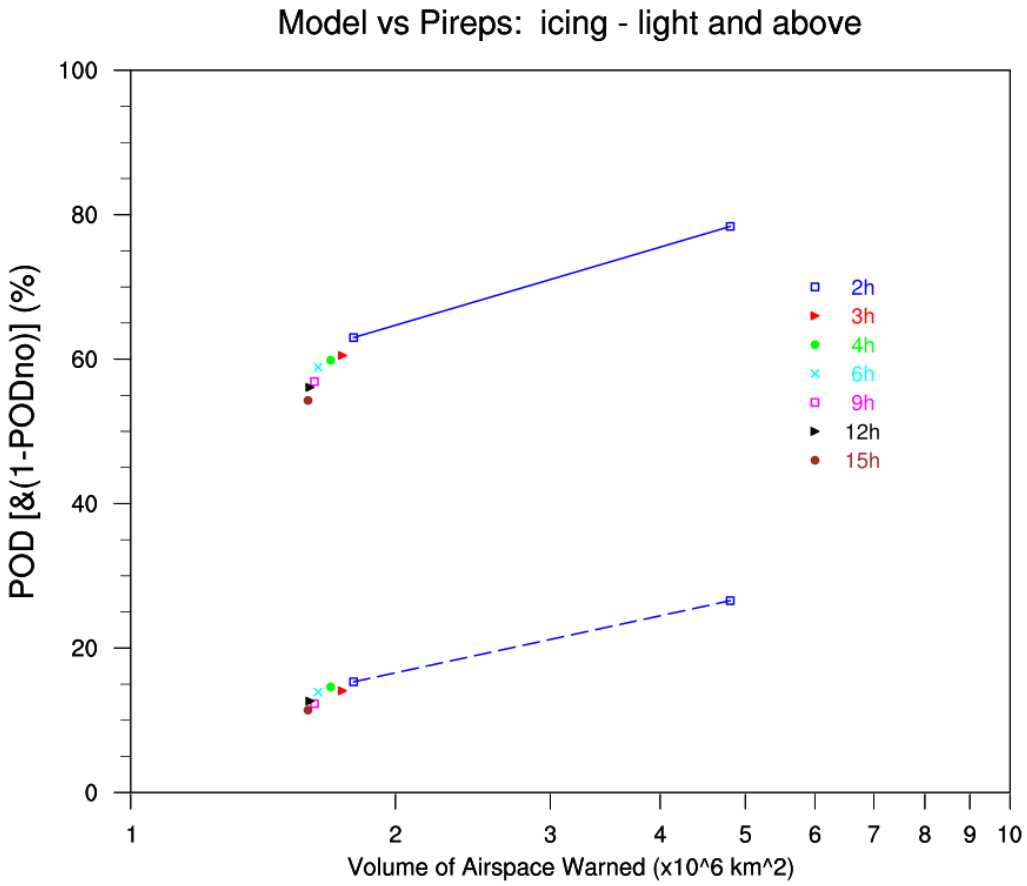

Figure 20. Probability of detection (POD; solid) and 1 - POD_{no} (dashed) vs. volume of airspace warned for seven individual HRRR forecasts (2, 3, 4, 6, 9, 12, 15-h) of icing conditions (left points) in addition to the TLE average icing prediction (right-most point) (Xu et al. 2019).

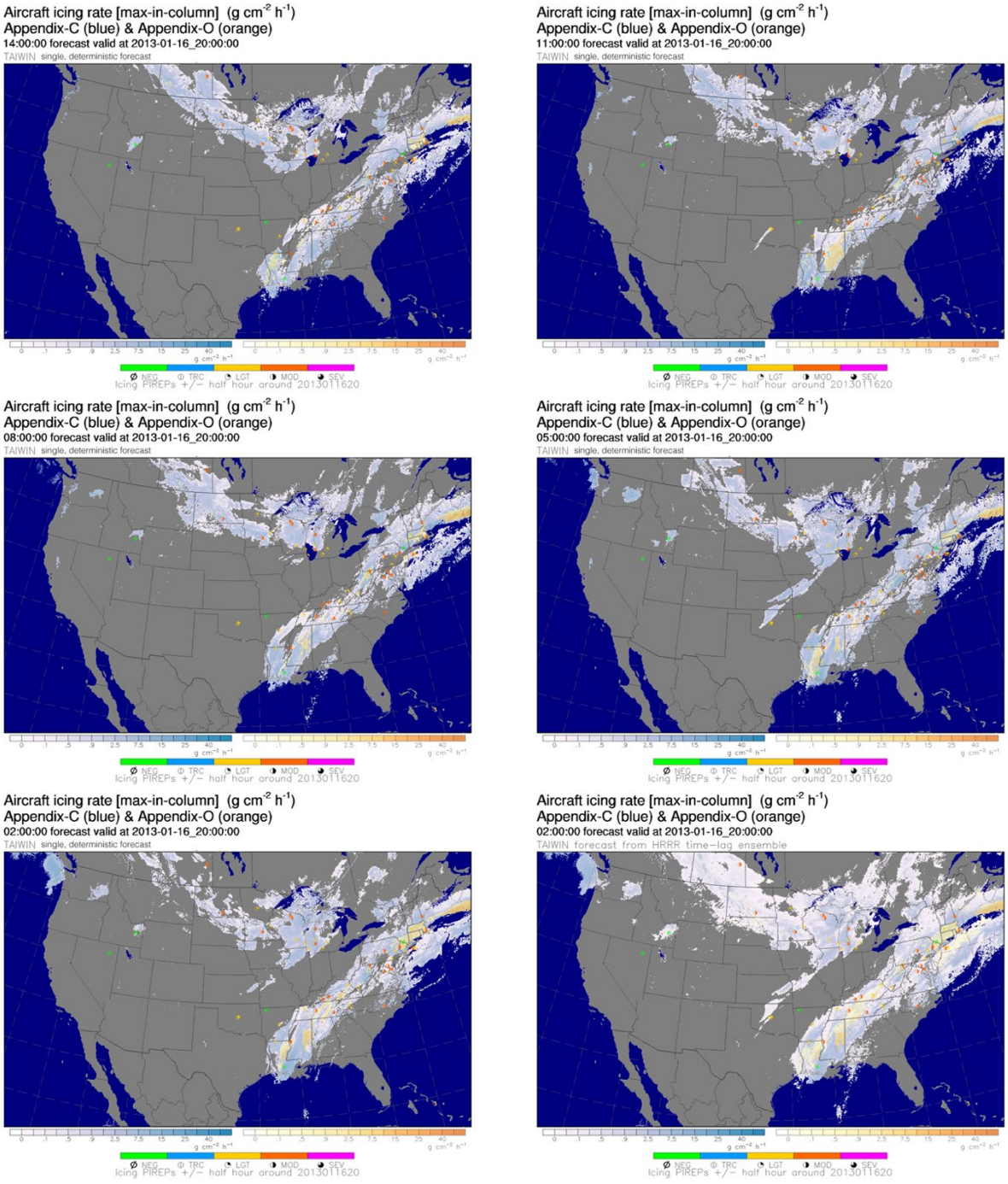

Figure 21. a) HRRR-model 14-h forecast of icing conditions (max-in-column; color shading) valid at 2000 UTC 16 Jan 2013 with overlay of icing PIREPS using colored icons; b – e) same as in (a) except from 11, 8, 5, and 2-h forecast, valid at the same time; f) combination of all five forecasts using time-lag-ensemble average technique.

Understanding the influence model initialization has on model forecasts is an important aspect of evaluating the models. Model initialization data tends to be weakest in the hours between ~7Z and ~11Z, when fewer Aircraft Communication Addressing and Reporting System (ACARS)

and Aircraft Meteorological Data Relay (AMDAR) profiles are available and the 12Z NWS operational soundings are not yet available for ingest. Anecdotal evidence suggests that icing-relevant forecast fields (relative humidity, LWC, temperature) from the RAP model seems to improve across the 12Z initialization window during the cold season. The importance of high-frequency vertical profiles collecting such data for improving model initialization has been demonstrated by Moninger et al. (2008) and Benjamin et al. (2016b). For this reason, and many others, model initialization is an ongoing area of research, and implies value for conducting Convair-580 flights at all times of day during ICICLE.

As computers become faster and more powerful, it has become increasingly practical to run NWP models at higher resolution. This progression has been evident as the Rapid Update Cycle (RUC) and Rapid Refresh (RAP) models improved from 60- to 40-, 20- and eventually 13-km horizontal grid spacing over the last ~20 years, and the HRRR is now running operationally with 3-km spacing (Benjamin et al. 2016a, 2016b; Weygandt et al. 2017). Further increases in resolution continue to be tested to see whether higher resoultion models will increase the ability to predict and resolve icing-relavent fields and features. Non-trivial errors relevant to icing diagnosis and prediction exist in both the RAP and HRRR, such as temperature errors on the order of 1-4ºC in icing-prone environments. It is essential to understand these errors, their spatial and temporal tendencies, and their implications as icing products that depend on numerical models begin to depend upon models with high resolution (Fenton et al. 2017).

3.2.7 CIP and FIP

Automated, gridded icing products have been under development since the 1990s and have advanced markedly in the decades since, both in the U.S. and abroad (Schultz and Politovich 1992; Forbes et al. 1993; Bernstein 1996; Carriere et al. 1997; McDonough et al. 2004; Wolff et al. 2007, 2009; Adriaansen et al. 2014, 2015, 2019; Tafferner et al. 2003; Kalinka et al. 2017; Le Bot 2003; Le Bot et al. 2008; Morcrette et al. 2019; Olofsson et al. 2003). The current suite of gridded operational icing products, CIP and FIP, were first developed in the late 1990s as IIDA and IIFA (Integrated Icing Diagnostic and Forecast Algorithms) and began providing graphical icing information to the aviation community soon thereafter (McDonough and Bernstein 1999, McDonough et al. 2004; Bernstein et al. 2005; Sims and Carty 2000). Initial products included icing and SLD “potential,” which were uncalibrated likelihoods of icing and SLD. The icing potential field was later calibrated and converted to probability (Brown and Bernstein 2006; Kucera et al. 2007; Wolff et al. 2009) and an icing severity field was also developed (Politovich et al. 2006; Bernstein et al. 2006b; Wolff et al. 2007).

The SLD field has proven difficult to calibrate, due to a relative lack of independent SLD observations, and thus it retains the "SLD potential" (rather than probability) moniker. It is currently provided to aviation users as a hatched overlay on icing severity charts on the Aviation Digital Data Service (ADDS), plotted where the SLD potential exceeds 0.05 on a 0.0 to 1.0 scale (see Figure 22). Gridded maps and vertical cross-sections of the full spectrum of SLD potential were provided via the Experimental ADDS sites and in test-user demonstrations during product development (Sims and Carty 2000; Politovich et al. 2002, 2006), but are not provided as a stand-alone graphic operationally. Since first debuting as the experimental IIDA with 60-km grid spacing, the operational CIP and FIP have gradually improved to 40, 20 and their current 13 km spacing, matching the evolution of the RUC and RAP models (Wolff and McDonough 2010; Adriaansen et al. 2015). Both CIP and FIP are moving toward 3-km horizontal grid spacing, with 500 ft vertical spacing, based off the HRRR model (Adriaansen et al. 2019). The concept of high-resolution, gridded icing algorithms was tested in the late 1990s and mid-2000s, as versions of IIDA and CIP were run on satellite grids, rather than coarser model grids during the Mount Washington Icing Sensors Program (Ryerson et al. 2000) and NASA-Glenn Research Center flight programs (see Figure 23) (Politovich and Bernstein 2006; Reehorst et al. 2009).

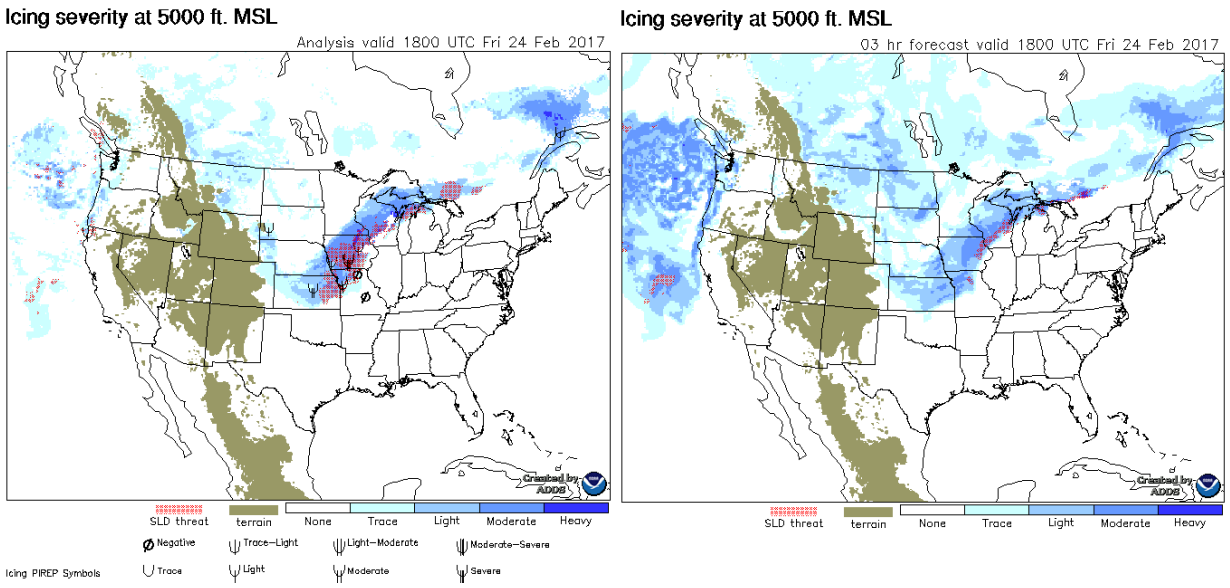

Figure 22. Examples of icing severity and SLD fields from the operational CIP and (3-hr) FIP.

Despite the long-running development and operational distribution of CIP and FIP products, they have some limitations regarding their application to the new SLD regulations. In particular, the operational SLD fields do not differentiate between the FZDZ and FZRA sub-categories of Appendix O. That said, code within CIP and FIP does include indications of the mechanisms

associated with FZDZ and FZRA (Bernstein et al. 2005). These internal fields and recent updates to the SLD algorithms and other upstream fields, such as cloud top and base height assessment (Wolff et al. 2009; Adriaansen et al. 2014, 2015) merit further examination.

FIP's icing and SLD algorithms attempt to mimic those in CIP, using only model output. The lack of observational data from satellite, radar and surface-based sources can make predicting SLD and its subcategories more challenging. For example, compare the red hatched areas on the left and right sides of Figure 22. In this case, non-classical SLD over central Iowa was captured by CIP via surface observations it employed, but the SLD was not indicated by FIP. Advancements in forecasts of microphysics fields from NWP models and their application may serve to improve FIP SLD fields. These same improvements—combined with enhanced use of satellite (e.g., infrared derivative fields), radar (e.g., FZDZ signatures, RadIA), and surface observations (e.g., enhancements to ASOS FZDZ, DZ and PL detection), etc.—also have the potential to enhance CIP's SLD fields (Sims et al. 2019).

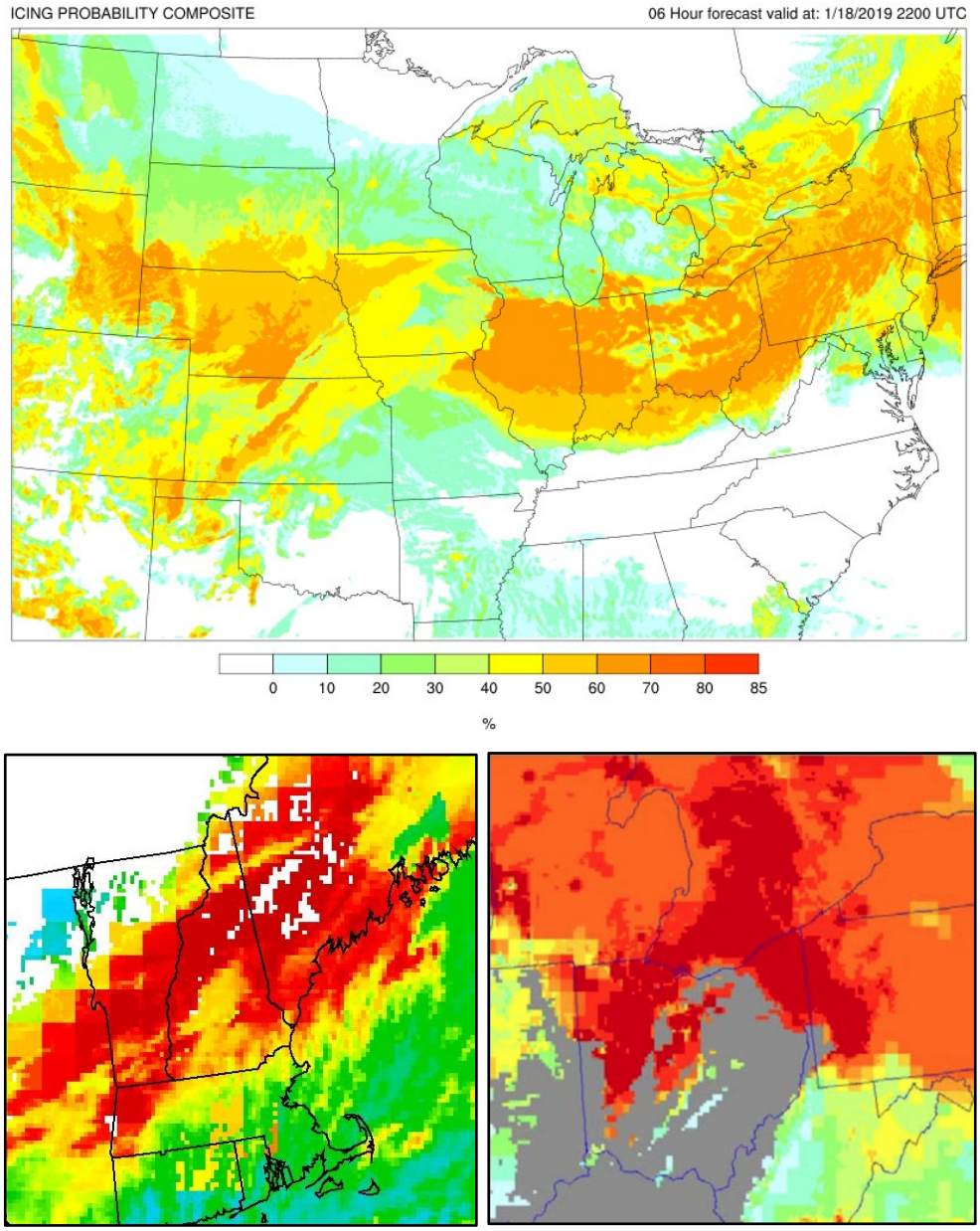

Figure 23. Examples of 3-km HRRR-based FIP icing probability composite (top) and high-resolution test output from IIDA and CIP from 1999 and 2004, respectively (bottom).

3.3 Identification of icing-free areas aloft

Beyond the detection of FZDZ and FZRA aloft, Appendix O regulations require that certain aircraft escape all icing after exposure to SLD. Thus, it will become increasingly important to identify areas aloft that are free of all icing. These typically occur in areas that a) have above-freezing temperatures, b) are completely free of clouds and precipitation, or c) are comprised entirely of ice crystals. While these situations may seem simple to identify using the tools described above, doing so with precision and accuracy can be quite challenging.

Among the icing-free situations, it is generally easiest to identify locations with above-freezing temperatures. Though operational model temperature forecasts are quite good, errors on the order of 1ºC or more are common in the lower troposphere, and can be several degrees larger in cold-season icing situations (Benjamin et al. 2016b; Fenton et al. 2017). Such errors may be relatively large in complex environments, dynamic situations, and along boundaries like fronts, terrain features and shorelines (Weygandt et al. 2017; Ikeda et al. 2013).

On the warm end of the icing temperature spectrum, errors in the height and location of the 0ºC line/level can impact the assessment of icing-free areas. On the cold end of the spectrum, it is reasonable to expect that clouds and precipitation at T < -40ºC will be free of SLW. However, simply applying a minimum temperature threshold of -40ºC is less than ideal for operations. While icing is uncommon at T < -25ºC and rare at T < -30ºC (see Figure 24) (Rauber and Tokay 1991; Korolev et al. 2003; Jeck 2008; Thompson et al. 2017), it has been observed at unusually cold temperatures in deep convection (Rosenfeld and Woodley 2000) and in very clean air masses, sometimes persisting for hours or even days (McDonough et al. 2017; Bernstein et al. 2019). NWP model forecasts can allow SLW to develop at temperatures anywhere between 0 and -40ºC, based on the microphysics package, but also rarely predict it at temperatures colder than -25ºC (Thompson et al. 2017) (see Figure 24). CIP and FIP employ lower limits of -25ºC and -30ºC for non-convective and convective situations, respectively. While these thresholds capture the vast majority of all icing and limit the volume of airspace warned, their application has resulted in very cold SLW icing environments sometimes being missed (Chapman et al. 2002, 2004; McDonough et al. 2017). To better capture such environments, cold temperature limits could be extended when observations (e.g., satellite indications of cold liquid water tops, PIREP clusters) and/or model forecasts provide strong evidence that anomalously cold icing may be present.

The second icing-free situation described above (cloud and precipitation free areas) is a bit more challenging to address. Cloud and precipitation presence can be assessed by satellites, radars and surface stations, and predicted by NWP models. CIP employs all of these tools to find cloud and precipitation presence in 3-D space. Its assessment was designed to be conservative to be sure to fully capture the depth of all clouds and precipitation present, extending vertically to altitudes slightly above cloud top and below cloud base. Icing clouds are identified most effectively when they are directly visible to satellite during the day and night, making it relatively easy to delineate their lateral extent, cloud top temperature and microphysical characteristics. Icing clouds, and indeed all clouds, are more difficult to discern a) near the solar terminator, due to deterioration of highly-valuable satellite fields and/or b) when they are obscured by higher cloud

layers. This can result in clouds being represented poorly or missed altogether (Adriaansen et al. 2015; Spangenberg et al. 2011).

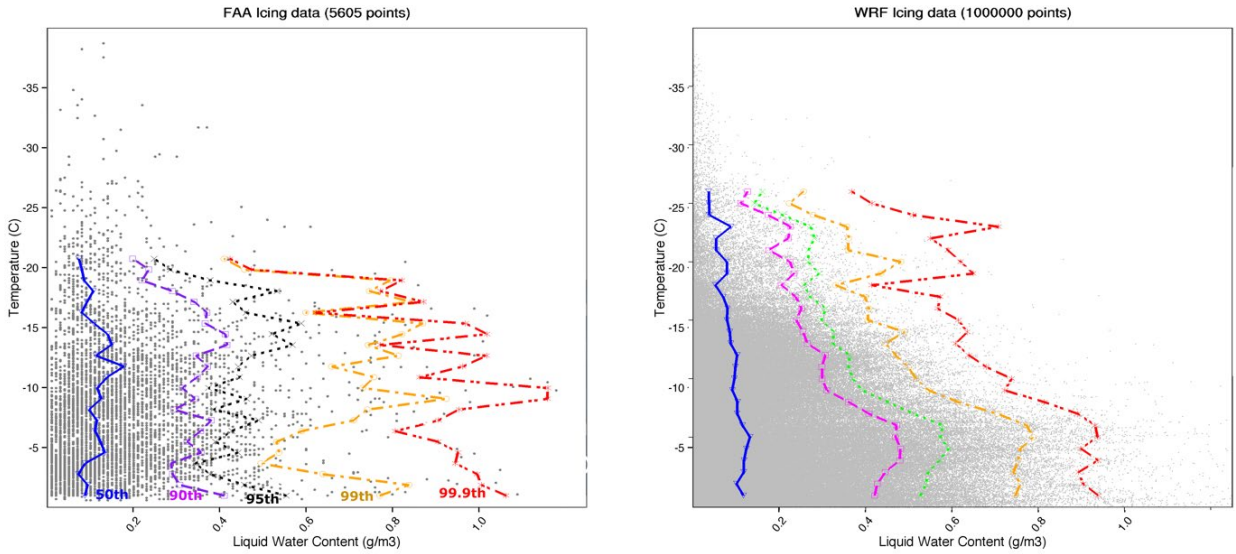

Figure 24. Scatterplot of 5605 aircraft icing observations of temperature (ºC) and LWC (gm^{-3}) with the 50th, 90th, 95th, 99th, and 99.9th percentiles for each degree (left) and a random sample of 1 million WRF Model points with corresponding percentiles (right) (Thompson et al. 2017).

Cloud base height sets a clear lower limit to icing altitudes when precipitation is absent, and surface-based ceilometers estimate this very well, especially when cloud bases are well defined. Such estimates are particularly valuable directly above the site, but their value drops off with horizontal distance and age. Greater observation density and frequency can help ameliorate this issue. In data-sparse areas of the United States (e.g., parts of Maine, the Appalachians, the Intermountain West, Alaska, and offshore), the relative dearth of observations can be problematic (Adriaansen et al. 2015) and its effect on icing assessment can be exacerbated near shorelines, mountain ranges, and around meteorological transitions zones, such as fronts. Observation age can also be quite important as icing relevant features move through, especially when ceilings are changing and/or precipitation transitions are occurring (Adriaansen et al. 2012). Such temporal variations are common in icing situations (NTSB 1998). Several methods have been tested to improve the mapping of METAR data over the years, including mathematical blending of reported ceilings with a surrogate ceiling field based on numerical model microphysics (Adriaansen et al. 2015) (see Figure 25).

While cloud base is the vertical lower limit of icing within a non-precipitating cloud layer, cloud top is often the upper limit, especially when cloud tops are relatively warm (> -15ºC or so). The

upper portion of cloud layers are often particularly important, since relatively strong icing conditions commonly occur near cloud top (Hardy 1944; Korolev et al. 2006). Satellite data generally needs to be matched with sources of vertical profiles of temperature, such as from NWP models, to assess cloud top height (Spangenberg et al. 2011; Smith et al. 2015). Cloud tops commonly fall between NWP model levels, which can be separated by hundreds of meters. To fully encompass the important cloud top region, CIP's cloud top height is set to the model level immediately above the altitude where cloud tops are expected. This approach can result in overestimation of cloud (and icing) top height, which can be large when model temperature profiles have inversions near cloud top.

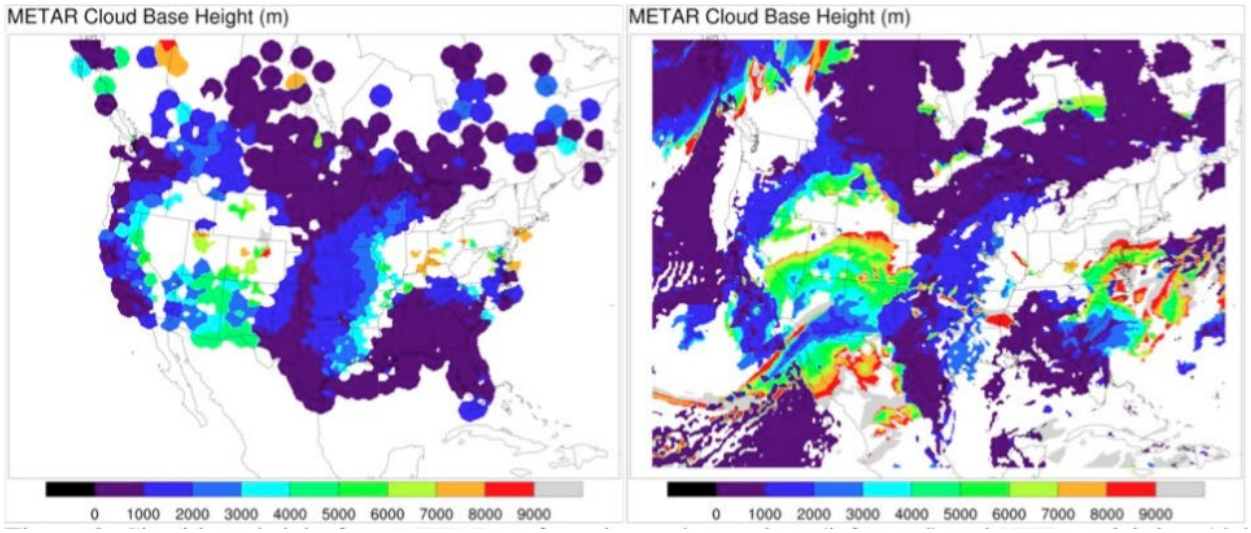

Figure 25. Example ceiling heights from actual (left) and synthetic (right) METARs (Adriaansen et al. 2014).

Potential improvements to CIP's (and FIP's) cloud top height algorithm have been tested, supplementing the original technique with analysis of model profiles of relative humidity, equivalent potential temperature, total condensate, and vertical velocity (Haggerty et al. 2008; Wolff et al. 2009). In one test of a hybrid cloud top height algorithm that employed the model profiles described above, roughly half of cloud top estimates improved significantly, with the 50th percentile found to be 500 m too high, compared to 1500 m in the standard version. This resulted in a marked reduction in the volume of airspace warned for icing. However, there are often tradeoffs with such changes to icing algorithms. In this case, there were indications that the more than a quarter of the new cloud tops were too low, implying that more cloud top icing situations could be missed (see Figure 26). Subsequent versions of the CIP and FIP cloud top algorithms may yield further improvement.

Between the highest cloud top and lowest cloud base, there can be breaks between cloud layers. Icing conditions can change dramatically from one layer to another, so it is important to identify multi-layered situations, treat each cloud layer independently and identify icing-free altitudes between layers. Both CIP and FIP use a fairly simple assessment of relative humidity (RH) profiles to try to identify breaks between cloud layers. Identification of icing embedded within multi-layered clouds, and determination of their critical elements (3-D location, phase, LWC, drop size, etc.) is one of the most challenging elements of both manual and automated icing diagnosis and forecasting.

The third icing-free category, glaciated environments, can also be challenging to identify. Even with all observed and forecast datasets in hand, when signals appear to indicate that ice crystals are present if not dominant, pockets or layers of pure and mixed-phase SLW and SLD can still exist. They are sometimes not evident in observations and can be miscategorized or missed altogether by models. Examples include liquid clouds that are obscured from satellite view, mixed-phase clouds with radar reflectivity dominated by large ice crystals, and liquid clouds aloft (often near the top of layers) that are coincident with snow at the surface. Satellite, radar, NWP models, CIP, and FIP already employ techniques to find such hidden icing and icing-free regions, and more techniques are under development. ICICLE will provide an excellent opportunity to test their efficacy.

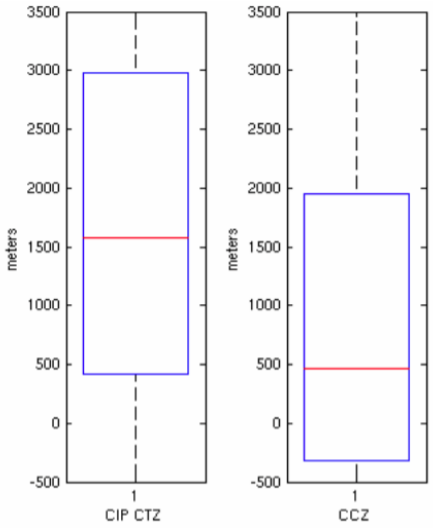

Figure 26. Differences between CIP-calculated and PIREP-indicated cloud top for 769 daytime PIREPs. CIP-CTZ (left) and CCZ (right) are the standard and test versions of CIP cloud top. The red line denotes the median error while the box encloses the 25th and 75th percentiles of the errors (Haggerty et al. 2008, adapted).

3.4 Verification

As previously discussed, icing tools, "truth" datasets, and verification approaches have evolved significantly since the last dedicated icing research field program. High-quality data gathered during ICICLE will provide the opportunity for in-depth comparisons between numerous in-situ and remotely-sensed observational datasets to the icing tools described above to assess their quality and determine their meaning in various icing situations and scales. Researchers will use these results to identify gaps in the capabilities of the tools examined and potential areas for improvement for terminal-area and en-route flight operations. With the opportunity to compare high-resolution icing tools to high-resolution "truth data," determining the best methods for comparing those data may depend heavily on how the icing tools are to be presented to, and used by, the flying public. For example, if a tool is touted as providing information at highly specific locations in time and space (e.g., every 5 minutes with 1-km horizontal spacing), then that tool should be tested to determine how meaningful the information provided is on those scales.

Traditional verification methods used to evaluate diagnoses and forecasts from icing algorithms or NWP models have primarily relied upon PIREPs aloft and present weather type observations at the surface. While these observations are important sources of information with wide spatial coverage, they have notable limitations. Many of the limitations associated with PIREPs have been discussed in Brown et al. (1993, 1997), Brown (1996), Kelsch and Wharton (1996), and reiterated in subsequent publications. Briefly, PIREPs often contain less precise or less accurate spatial and temporal information than observations from automated sources such as ice detectors (Braid et al. 2006, 2011). Aircraft location is typically recorded at the time of the report, which could be displaced from the location where icing was encountered. This can be problematic because icing events can have significant variability in space and time, and it is very difficult to quantify the representativeness of PIREPs to the conditions present at one location and point in time. In addition, the severity of reported icing is influenced by a variety of factors beyond the meteorological condition present, such as the aircraft type, and is ultimately based on the subjective judgment of the pilot (Sand and Biter 1997). This was demonstrated in a study comparing measurements from a research aircraft to PIREPs made nearby, including from the test aircraft, as it flew through areas with significant meteorological variability. Results showed instances of both good and poor agreement between the datasets (Wolff and Bernstein, 2004).

In early studies using PIREPs to verify icing products, Brown et al. (1997) noted substantial bias in the reporting of positive versus negative icing. Pilots are much more likely to report icing when it is encountered, and are encouraged to do so, but there is little encouragement or incentive to report a lack of icing conditions (see example plot; Figure 27). Icing conditions

cover a relatively small proportion of airspace compared to icing-free conditions, yet positive icing reports are far more common than negative/null reports. Thus, PIREPs are not representative of the actual distribution of the presence or absence of icing, limiting the choice of appropriate verification measures that can be applied for icing aloft. Due to these reporting biases, false alarm ratio (FAR) cannot be estimated and even statistics such as probability of detection of an event (POD_Y) or non-event (POD_N) must be interpreted carefully, with close attention paid to methodology, including spatial and temporal data matching (Brown et al. 1997; Brown and Young 2000). See Table 4 for a description of FAR, POD_Y, and POD_N, where the "f" and "x" values indicate the forecast and observed values and where 1=yes and 0=no for icing. Probability of detection (POD) of yes and no observations, PODy and PODn, are the proportion of all yes and no observations that were forecast correctly, respectively. False Alarm Ratio (FAR) is the proportion of yes forecasts that were met with no observations.

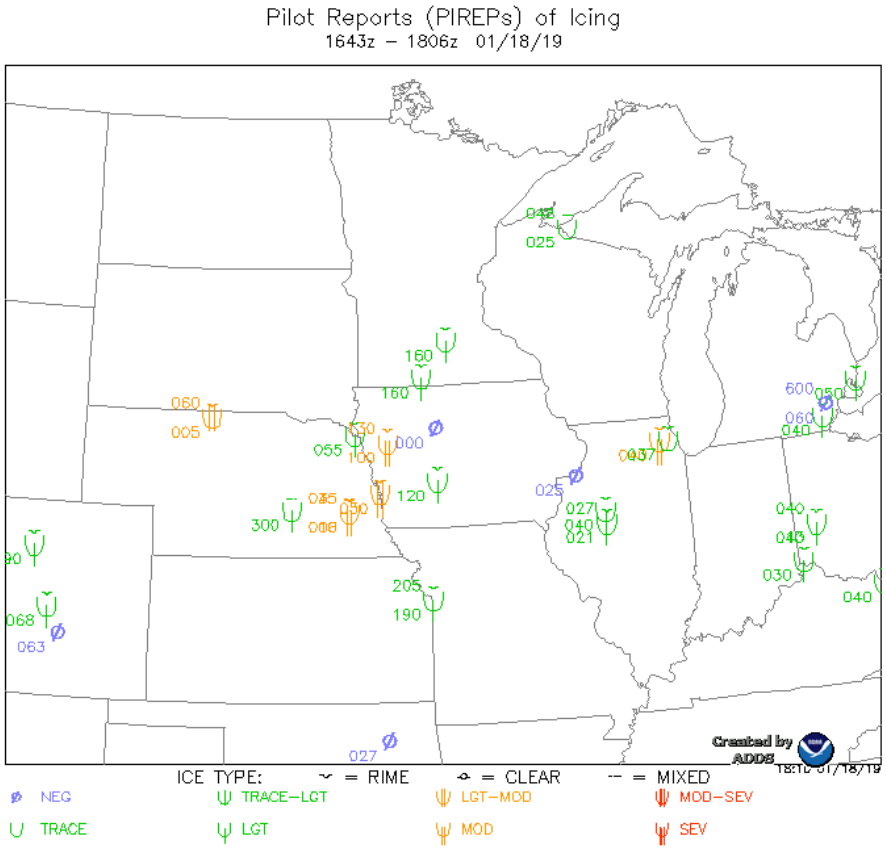

Figure 27. Example plot of PIREPs of icing. Severity is indicated by the icon color and shape.

Table 4. Standard 2x2 contingency table illustrating the counts used in verification statistics for dichotomous (e.g., yes/no) forecasts and observations (Brown et al. 1997).

	Observation (x)		
Forecast (f)	Yes ($x = 1$)	No ($x = 0$)	Total
Yes ($f = 1$)	$p(f = 1, x = 1)$	$p(f = 1, x = 0)$	$p(f = 1)$
No ($f = 0$)	$p(f = 0, x = 1)$	$p(f = 0, x = 0)$	$p(f = 0)$
Total	$p(x = 1)$	$p(x = 0)$	1

At the surface, METARs can provide information regarding surface precipitation type at regular time intervals at airport locations. SPECIs can add valuable information at non-standard METAR reporting times, including changes in precipitation type. As noted in Section 3.2.1, there are known deficiencies in precipitation type reports from the ASOS and AWOS network. Elmore et al. (2015) demonstrated this for precipitation type verification, and Landolt et al. (2017, 2019, 2020) demonstrated the inability of automated stations to report DZ, FZDZ and PL. The FDDA described earlier offers additional value for verification work, especially for Appendix O, but it also has limitations in inferring precipitation type. For example, the algorithm assumes the present weather sensor is always correct. Analysis by Landolt et al. (2019) showed that human observers disagreed with the output from the sensor nearly 30% of the time. Errors in observations from the present weather sensor can have significant impacts on the eventual output of the FDDA. The inability of many METARs and SPECIs to report multiple precipitation types at unmanned sites is also a limiting factor.

The Meteorological Phenomena Identification Near the Ground (mPING) (Elmore et al. 2014) project was established to help mitigate some deficiencies in automated reports, including discrimination between important winter surface precipitation types that the automated sites struggle with, and the ability to report mixed-phase precipitation. Through the use of a mobile app, numerous categories of surface precipitation types are reported, including: DZ, FZDZ, RA, FZRA, PL, SN, some mixtures thereof, and a lack of precipitation (none) (see Figure 28). Because the reports are primarily generated by the public, there is inherent spatial bias toward more populated areas and major roadways, and for more reports to occur during normal waking hours.

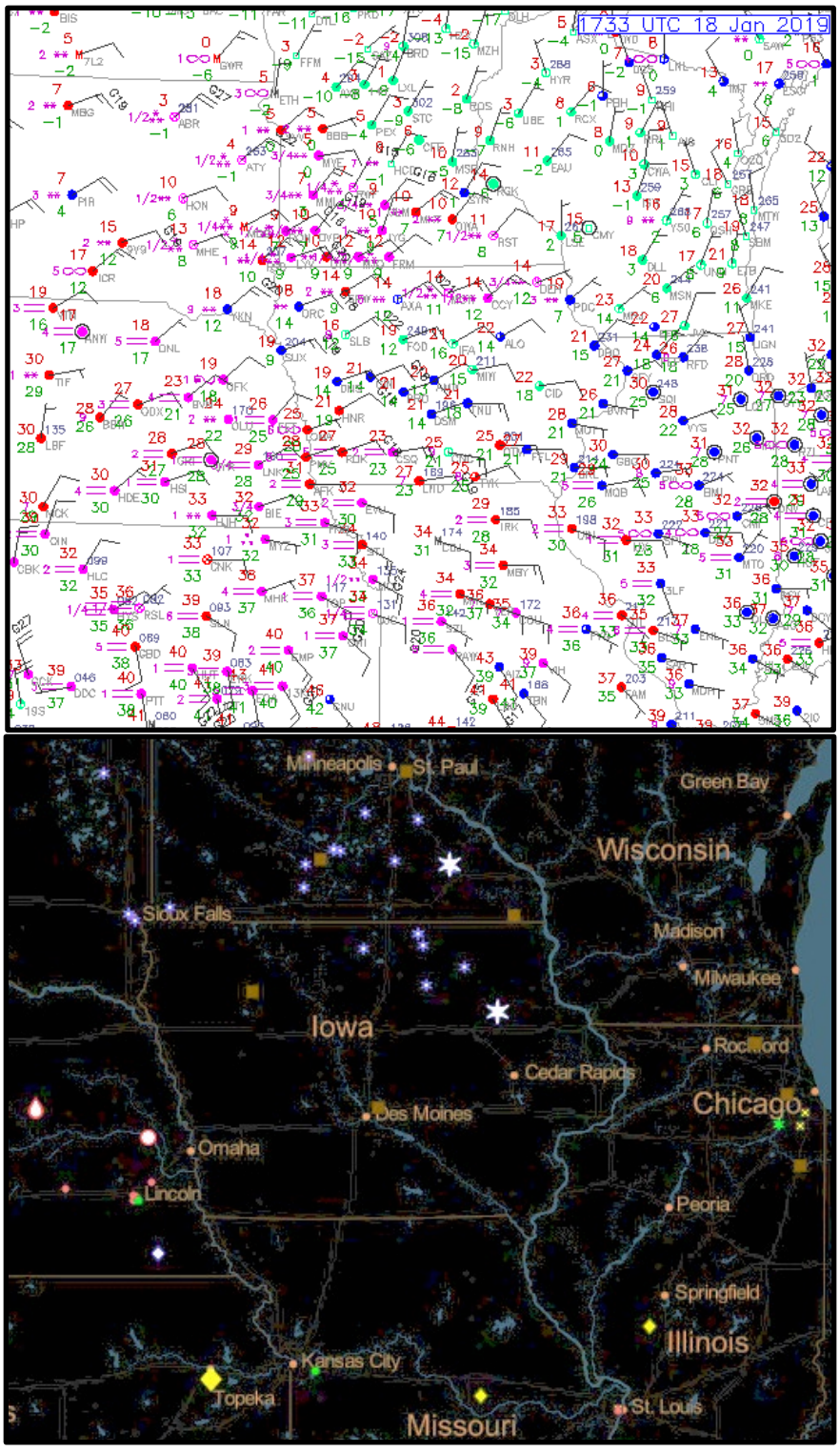

Figure 28. Example plots of METARs (top) and mPING surface observations (bottom): SN (blue stars), RA (green dots), FZRA (pink dots), FZDZ (pink drops), FG (yellow diamonds) and no precipitation (brown squares). Larger icons in (b) indicate more recent reports.

As noted above, surface precipitation type verification has traditionally been conducted using METARs (Benjamin et al. 2016a, Ikeda et al. 2013), and more recently mPING reports (Reeves et al. 2014, 2016, Elmore et al. 2015). The availability of gridded surface precipitation type analyses within the MRMS dataset offers an additional tool that may prove beneficial, especially for null or non-events, which are typically under-reported. This gridded analysis product may also allow for object-based (e.g., Method for Object-based Diagnostic Evaluation [MODE]) (Davis et al. 2009) and neighborhood (e.g., Fractions Skill Score [FSS]) (Roberts and Lean 2008) verification techniques to be employed.

Balloon-borne soundings can also serve as a verification data source. In the past, they have been used successfully in comparisons with NWP model output, such as from the RUC, RAP and HRRR. Such comparisons have proven quite useful when calculating error and bias statistics for fields like temperature, relative humidity and winds (Benjamin et al. 2016b). Recent results comparing soundings to RAP and HRRR model output for icing situations provided insights on relative error, and geographic tendencies between the two models (Fenton et al. 2017). The operational and supplemental soundings made during ICICLE may prove useful for comparison with models and other icing tools that were available during the program.

Regardless of the type of observation used, it is important to bear in mind the limitations with each dataset when applying verification methods and interpreting the results. When using surface observations, traditional statistics computed from a 2x2 contingency table (see Table 4) can be used to compute POD_Y, POD_N and FAR. In an effort to accommodate some uncertainty in the observations, a spatial neighborhood and/or temporal window is often applied in these types of evaluations (Etherton et al. 2014; Fowler et al. 2017; Fenton et al. 2017).

More recently, new spatial verification techniques have been applied to assess icing-relevant conditions in NWP models. For example, Fowler et al. (2017) applied the high-resolution assessment (HiRA) framework (Mittermaier 2014) when comparing PIREPs to forecast conditions aloft. At its simplest, the HiRA strategy takes a deterministic forecast and creates a probabilistic forecast from it, by treating the forecast grid points in the neighborhood of (i.e. surrounding) a point observation as members of an ensemble. HiRA was developed using surface observation stations so that the neighborhood lies completely within the horizontal plane. With PIREPs, the vertical neighborhood must also be defined. It is typical to select all levels included in the PIREP, including those just above and below the reported icing level(s). While the HiRA provides information about the likelihood of an event occurring within a neighborhood, using something more traditional like a maximum value in the neighborhood provides information about the severity of events predicted in that neighborhood. Beyond PIREPs, it may be

interesting to apply these techniques to other "truth" datasets collected during ICICLE, such as data from the research aircraft (as in Chapman et al. 2006) and ground suites.

Regardless of the approach used, choices regarding neighborhoods and time windows must be considered carefully, especially when assessing the accuracy and meaning of icing diagnoses and forecasts made at fine time and space scales.

4 ICICLE objectives

While the previous sections provide detailed descriptions and background of the science and technical aspects around which the ICICLE flight program was designed, it is valuable to clearly state the scientific, technical, and sampling objectives of the program. This information highlights the objectives of greatest priority and provides ICICLE operations decision-makers critical information to help determine whether to fly and which objectives to prioritize on any given day or mission.

The overarching objective of the field program is described first, followed by scientific, technical and sampling objectives. Technical objectives are grouped based on the specific technology they address (e.g., satellite), while Scientific and Sampling objectives tend to be more general in nature. Other than the overarching program objective, each objective is marked as either "primary" or "secondary." Primary objectives include a sub-rating of 1 through 5 (most to least important) to indicate their level of priority within ICICLE.

4.1 Overarching field program objective

Observe, document and further characterize the atmospheric environments associated with a variety of in-flight and surface-level icing conditions to evaluate and improve candidate icing tools and operational products, specifically as they pertain to the detection, prediction and differentiation of icing environments, their subcategories and non-icing environments.

4.2 Scientific objectives

Primary (1) – Observe, document, and further characterize environmental parameters and particle size distributions (hydrometeors, as well as aerosols) associated with FZDZ and FZRA events.

Primary (2) – Observe, document, and further characterize environmental parameters and particle size distributions associated with "small-drop" icing events, including Appendix C and "LWC exceedance" conditions (where LWC values are greater than those at the top of the

Appendix C continuous-maximum icing envelope), which are sometimes associated with shallow/young convection.

Primary (2) – Observe, document, and further characterize spatial and temporal (including diurnal) transitions both within and between Appendix C and Appendix O icing environments.

Primary (3) – Document the occurrence and progression of specific precipitation processes, such as vapor deposition and riming growth of snow, and collision-coalescence SLD formation.

Primary (5) – Observe, document and further characterize synoptic, mesoscale and local effects on icing and non-icing environments and transitions between them.

Secondary – Document precursor atmospheric conditions in advance of and surrounding Appendix O and Appendix C icing events, particularly in the context of aerosols that could become CCN or IN.

4.3 Technical objectives

Use field program data to assess the current ability and potential contributions of operational and candidate tools for the diagnosis and prediction of icing conditions (including temperature, LWC, drop size distribution [DSD] and maximum drop diameter [D_{max}]) with emphasis on differentiation between Appendix C, Appendix O, its subcategories, and other icing and non-icing conditions.

Objectives related to specific tools are described below:

<u>Surface observations</u>

- Primary (1) – Test the relationship between operational and experimental ASOS algorithm-indicated precipitation type (especially FZDZ and FZRA) and aircraft data taken above stations.
- Primary (3) – Assess the spatial and temporal variability of icing-relevant precipitation types and their reporting.
- Primary (4) – Investigate the use of ASOS ceilometers to identify icing layers in non-precipitating and lightly precipitating clouds.

<u>Radar</u>

- Primary (1) – Evaluate the ability of dual-polarization radar algorithms to identify Appendix O conditions, their essential characteristics (e.g., D_{max}), and differentiate them from other icing and non-icing conditions.

- Primary (5) – Using low-cost k-band radars, expand upon operational NEXRAD ability to detect low-reflectivity SLD conditions during operations and post-campaign analysis.
- Secondary – Identify areas and effects of blocking by terrain and poor sampling due to distance and scanning strategies, including their effects on data in terminal areas.

Satellite

- Primary (1) – Assess the ability of GOES-16 channels and combinations thereof to discriminate phase (water, ice and mixed) and provide particle size information for the upper portions of clouds.
- Primary (2) – Evaluate automated feature advection tools for icing.
- Primary (3) – Investigate potential relationships from published scientific literature pertaining to visible cloud albedo, LWC, and effective diameter as it relates to the diagnosis of Appendix O & Appendix C icing conditions.
- Secondary – Evaluate existing satellite-based icing diagnostic tools.

Numerical Models

- Evaluate the ability of operational and experimental models to predict and differentiate between Appendix O and Appendix C icing conditions (including LWC, DSD, and D_{max}) and non-icing conditions, such as clear sky and glaciated clouds. Candidates include:
    - Primary (1) – HRRR, WRF, RAP.
    - Primary (1) – Time-lagged ensembles (TLE).
    - Primary (2) – Partial cloudiness schemes.
    - Secondary – Ultra-high resolution WRF-600m, HRRR-1km, NAM, GFS.

Icing Products

- Evaluate operational and developmental icing products ability to diagnose, predict and differentiate between Appendix O and Appendix C icing conditions (including their LWC, DSD, and D_{max}) and non-icing conditions, such as clear sky and glaciated clouds. Candidates include:
    - Primary (1) – Operational CIP and FIP.
    - Primary (1) – Products under development.
    - Secondary – AIRMETs and SIGMETs.

Verification

- Analyze the wide array of high-quality research data from ICICLE (e.g., aircraft and ground suite data) and compare it with output from icing tools. Consider the use of traditional and more advanced verification techniques, such as random forests, machine learning, or other statistical models (Cai et al. 2009, Williams 2014).

4.4 Sampling objectives

To gather data needed to meet the scientific and technical objectives described above, the aircraft must sample and document the meteorological conditions in specific, appropriate ways. Data from the aircraft must be processed and archived properly, along with corresponding data from sources being tested for icing diagnosis and forecasting, as well as supporting data necessary to document each case fully. Because these "sampling objectives" straddle the scientific, technical and operational aspects of ICICLE, they are listed separately. Specific sampling approaches and the purposes behind them are fully described in Section 7.

- Primary (1) – For the targeted spectrum of icing and non-icing conditions, aircraft measurements must include aircraft 3-D location, aircraft speed, static and total temperature, LWC, drop size (MVD, DSD, D_{max}, etc.) and particle type/habit, as well as documentation of ice accretions on the aircraft. Observations from aerosol probes, 3-D wind probes, on-board radars, lidars, and radiometers should be taken to augment these data. Quantify CCN and IN concentrations, if possible.
- Primary (1) – Ensure the full vertical extent of cloud and precipitation is sampled when possible, including the sub-cloud layer, cloud top and clear air immediately above.
- Primary (1) – Attempt to collect a statistically significant population of null icing environments, including clear-air, glaciated and above-freezing environments. It is especially important to capture these environments in close proximity to areas of icing. Null data may also be captured during ferry flights and when flying to/from target areas.
- Primary (3) – Collect photography and video of ice accretions and cloud characteristics (e.g., cloud top structure) during and after sampling.
- Primary (1) – Collect data from operational sources, including, but not limited to surface observations (ASOS, AWOS, etc.), NEXRAD (individual, mosaics, dual-pol fields and products), GOES-16 satellite, radiosondes, pilot reports, lightning networks, and synoptic charts, as well as operational and experimental numerical forecast models (HRRR, WRF, RAP, NAM, GFS) and icing products (CIP, FIP, AIRMETs, SIGMETs).
- Primary (2) – Collect supplemental temperature, moisture and wind profiles from supplemental sounding sites to augment the operational radiosonde network.

During the campaign, it is necessary to capture a broad spectrum of winter weather conditions that are commonly found within and adjacent to Appendix O icing conditions aloft. For the purpose of guiding the data collection effort to achieve the objectives, it is instructive to describe the basic meteorological environments that need to be sampled to meet these objectives. Table 5 presents each environment, a rough percentage of total flight hours planned for targeting it, the expected frequency and difficulty in finding and sampling it, and features commonly associated with it. These include temperature, LWC, layer depth, event duration and timing, surface signatures, typical synoptic setup (see Figure 29), and key aspects of sampling. Sampling challenges are primarily caused by difficulty in diagnosis/forecasting (e.g., embedded high MVD layers) and particularly high degrees of 4-D variability (e.g., high LWC pockets in convection).

Table 5. Description of ICICLE targeted environments

Event type (across) Parameter (down)	*FZDZ aloft down to sfc*	*FZDZ aloft only*	*FZDZ Seeder-Feeder*	*FZRA*	*Classical PL*	*Shallow StCu*	*High LWC / MVD 30-40*	*Typical App C*	*Deep Glaciated*	*Clear Air*
Condition #	**1**	**2**	**3**	**4**	**5**	**6**	**7**	**8**	**9**	**10**
Priority level	High	High	High	High	Medium	High	Med / High	Low	Low	Low
% flight hr	15	10-15	10	15	5	10-15	5-10	5-10	5	5
Frequency (1-10)	5	5	4	3	2	6	3/1	9	9	10
Sampling Diff. (1-10)	5	5	6	8 (Z vs MEA)	9 (narrow)	3 (Z vs MEA)	8*	2	1	1
T range (°C)	-1 to -20	-1 to -20	-1 to -20	-1 to -13	-1 to -13	-2 to -20	-2 to -20	-2 to -20	0 to -30	0 to -30
Dominated by	Liquid	Liquid	Liquid/SN mix	Varies	Mixed PCP	Liquid	Liquid	Liquid/Mix	Snow	None
LWC (gm^{-3})	0.1-0.4	0.1-0.4	0.1-0.4	0.1-0.3	0.1-0.2 (FZRA)	0.2-0.8	>1.0 / 0.1-0.4	0.1-0.4	0-0.2	0
MVD (mic)	20-**250**	20-**250**	20-**250**	20-2500	20-2500	10-25	12-20 / 30-40	15-25	10-20	N/A
Dmax (mic) Liquid	200-500	200-500	200-500	>500	>500	15-30	15-25 / 35-60	20-30	20-30	N/A
Depth (kft)	1-5	1-5	1-5	0.2-1.0	0.3-1.5 (FZRA)	1-3	2-6 / 1-5	1-5	3-40	N/A
Length (nm)	10-200	10-200	10-200	10-100	5-250	20-200	5-25 / 10-100	20-500	20-100+	5-100+
Width (nm)	10-200	10-200	10-200	50-250	50-250	20-200	5-50 / 10-100	20-500	20-100+	5-100+
Duration (h)	1-10+	1-10+	1-10+	1-24+	1-24+	2-24+	0.5-3 / 2-24+	4-24+	2-24+	2-24+
Surface Wx Type	FZDZ	DZ/-SN/None	FZDZ/-SN	FZRA, PL, RA	FZRA, PL, RA	None/-SN	SHRA / Varies	None	SN, RA	None
Possible precip mix	-SN/-SG	Varies	Varies	SN + all above	SN + all above	-SG/-RA	Varies	-SN/-SG	SG	N/A
Cloud Cover	OVC	OVC	OVC	BKN-OVC	BKN-OVC	BKN-OVC	SCT-BKN/BKN-	BKN-OVC	BKN-OVC	Varies
Ceiling Height (ft)	200-600	200-600	200-600	200-1000	200-1000	300-800	500-1000	200-1000	200-2000	Varies
Visisbility (mi)	0.25-5	0.25-5	0.25-5	0.5-3	0.5-3	3-10	1-10	2-10	0.25-10	Varies
CTT (°C)	-4 to -12	-4 to -12	-4 to -20	-15 to -60	-15 to -60	-5 to -20	-4 to -13	-5 to -20	-15 to -60	Varies
CTZ (kft)	3-6	3-10	3-6/4+	10-30	10-30	2-4	5-15	3-8	10-30	Varies
Clear above sample	Often	Often	Sometimes	Rarely	Rarely	Often	Often	Often	Rarely	Yes
Layers	Occasional	Sometimes	Often	Occasional	Occasional	Sometimes	Sometimes	Sometimes	Sometimes	Sometimes
Warm nose depth	N/A	N/A	N/A	500-3000	200-2000	N/A	N/A	N/A	N/A	N/A
Stability	Semi-stable	Semi-stable	Semi-stable	Stable to FZLVL	Stable to FZLVL	Well mixed	Unstable/Semi-	Varies	Varies	Varies
Start time Z	03-12	03-12	03-12	03-12	Any	Any	16-20 / Any	Any	Any	Any
End time Z	12-16	12-16	12-16	12-16	Any	Any	20-02 / Any	Any	Any	Any
Missed App.	Y	Y	Y	Y	Y	Y	Unlikely / Y	Y	Maybe	Unlikely
Flt. leg length (nm)	30-60	30-60	30-60	50-100	50-100	30-100	10-25 / 20-100	30-60	20-100	10-100+
Bow tie length (nm)	20-40	20-40	20-40	50-100	50-100	50-100	Unlikely / 20-60	20-40	20-100	Unlikely
Sample Every x ft	500-1000	500-1000	500-1000	1000	1000	500	500-1000	500-1000	1000-2000	1000-2000+
Sample Dendritic Zone	N	N	Possibly	YES	YES	Occasional	N	Occasional	YES	N/A
Sample Melt Layer	N	Possibly	N	YES	YES	Possibly	Possibly	Possibly	Possibly	N/A
Sub-cld VFR sample	Difficult	Y w/No PCP	Possibly	N	N	YES	YES	YES	Unlikely	Unlikely
Best Month (Jan-Mar)	Jan-Feb	Feb-Mar	Jan-Feb	Jan-Feb	Mar	Any	Feb-Mar	Any	Any	Any
Typical Synoptics	7-8, 47-48, 52	7-8, 47-48, 52	7-8, 47-48, 52	6-8, 46-48	7-8, 47-48	11,15,12,19	1,4,17/seeFZDZ	Several	Several	Any

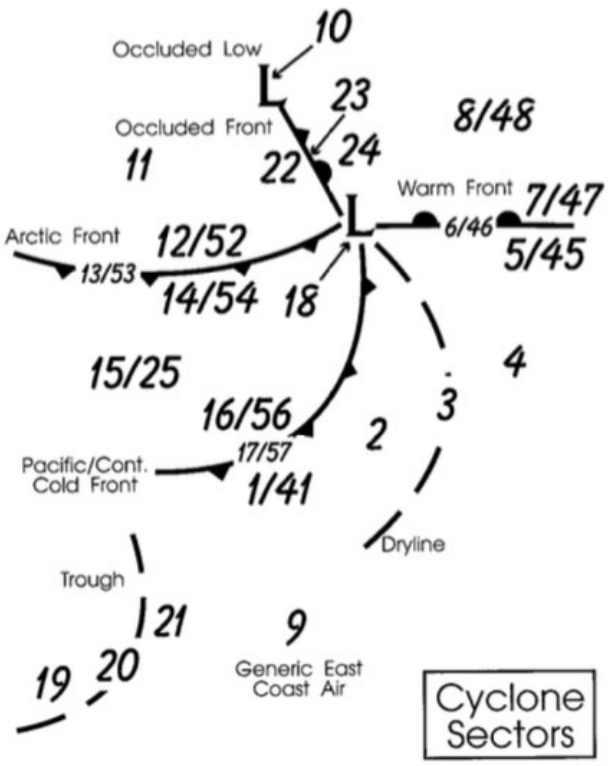

Figure 29. Locations of cyclone sectors for an idealized storm (Bernstein et al. 1997).

5 ICICLE flight operations factors

Several important factors are considered for ICICLE flight operations. These include, but are not limited to, mission safety, presence of environmental conditions needed to meet the ICICLE objectives (see Table 5), their prioritization with respect to one another, availability and coverage of operational data sources, locations of supplemental ground-based sensors, air traffic and alternate landing locations within the domain, and alternative operating bases in the event the target conditions are not within the primary domain. Several of these topics are addressed below. Though only called out in specific instances within this Section, safety of the crew and the aircraft are always paramount and inherent in all aspects of the ICICLE program.

5.1 Low-altitude sampling

The ability to sample at low altitudes is a high priority for ICICLE for multiple reasons, as follows:

1. Icing, including SLD, is often found at low altitudes in the northern CONUS, especially during the months when it most frequently occurs. Time-height estimates of historical

icing and SLD frequency based upon balloon and surface observations taken near Flint, Michigan highlight this (see Figure 30).

2. Classical FZRA layer depths are typically less than ~0.6 km, while non-classical FZDZ layer depths are typically less than ~1.5 km (see Figure 31).
3. Terminal areas, which are the focus of TAIWIN, are currently defined as covering altitudes from the surface up to ~3.65 km (12,000 ft) above ground level (AGL).
4. To fully document the vertical structure of icing events, including full profiles of clouds and precipitation, it is important to sample from above cloud top through cloud base and the sub-cloud region, including near the surface, when safe and practical to do so. This is addressed through deep vertical profiles, with near surface altitudes sampled via missed approaches and low-level flight legs. Note that cloud bases less than ~0.3 km (1,000 ft) are common during icing events, especially when FZDZ is present (see Figure 32) (Landolt et al. 2020; Green 2006).

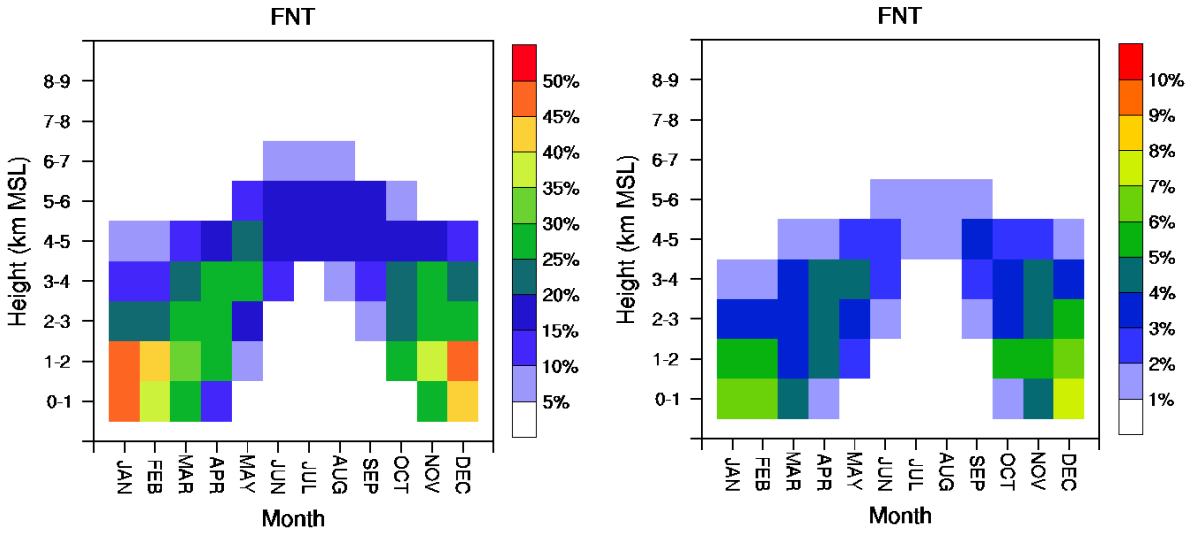

Figure 30. Monthly vertical distribution of inferred icing frequencies and SLD frequencies (%) over Flint MI (FNT)) using a threshold of 0.15 for icing and SLD potential. Images are from the study by Bernstein, et al. 2007, but the right image was not previously published.

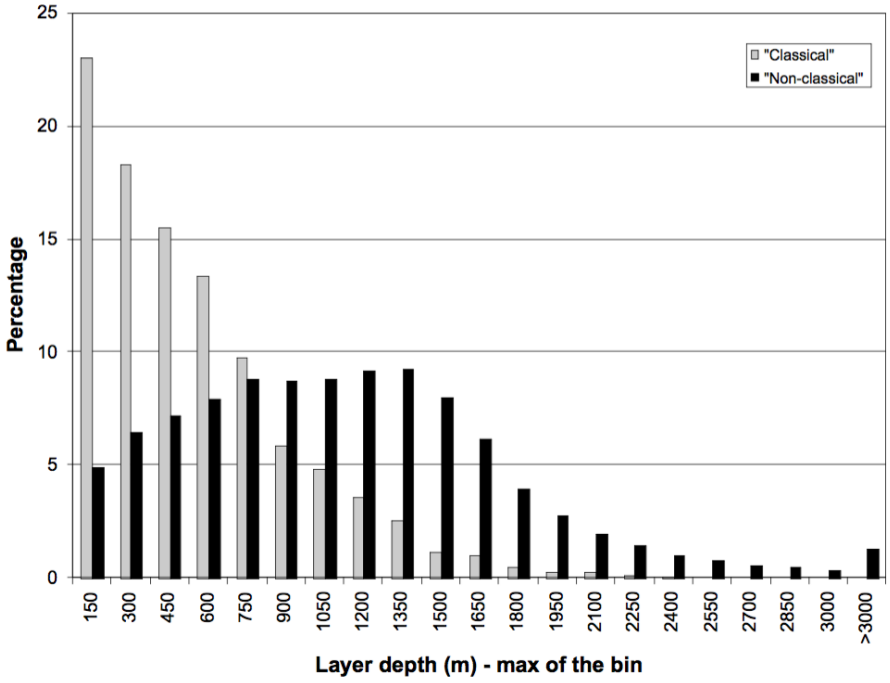

Figure 31. Distribution of SLD layer depth for the classical (grey) and non-classical (black) mechanisms (Bernstein et al. 2007).

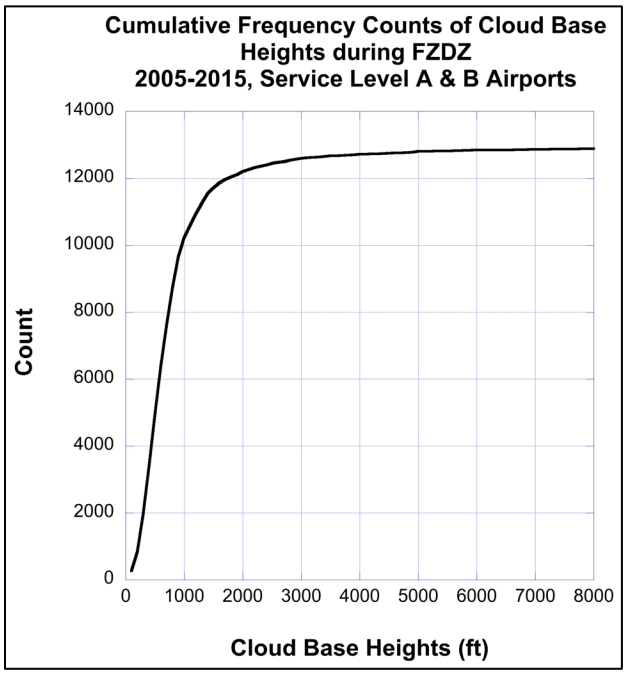

Figure 32. Cumulative frequency of 11 years of cloud-base heights during FZDZ events from ASOS Service Level A and B airports (Landolt et al. 2020).

Flight safety is always important when flying in icing, especially SLD. The low-altitude sampling desired for ICICLE is most easily and safely performed in areas of flat terrain. The risks associated with flying an iced-up aircraft, which could have significant performance degradation (Sand et al. 1984; Cooper et al. 1984; Politovich 1989, 1996; Ratvasky et al. 2010; Brown 2011), can be somewhat lessened by sampling over flat terrain rather than in steep terrain. The ICICLE domain provided an excellent environment for such sampling. There are vast swaths of relatively flat terrain (see Figure 33) while minimum en-route altitudes (MEAs) are commonly on the order of 2,500-3,000 ft (800-1000 m) mean sea level (MSL) (see Figure 34, where MEAs (ft MSL) are indicated above black rectangles that indicate the airway), allowing for flight legs to be made at low altitudes in IFR (Instrument Flight Rules) conditions, when they are deemed safe. Relatively flat terrain and low MEAs were also available in other relatively-high-frequency icing and SLD areas outside of the ICICLE domain, such as parts of Upstate New York and New England. However, sampling in such areas could be limited to small corridors and could be affected by significant traffic, making it challenging to sample events thoroughly. In some cases, relatively poor radar data coverage is also an issue (Reeves and Waters 2019), limiting the opportunity to compare flight data with some icing tools.

If the primary ICICLE domain surrounding Rockford was not experiencing the targeted environmental conditions (i.e., there is an icing “dry spell”), alternative domains have been identified for consideration. Dry spell contingency plans are discussed in Section 5.4.

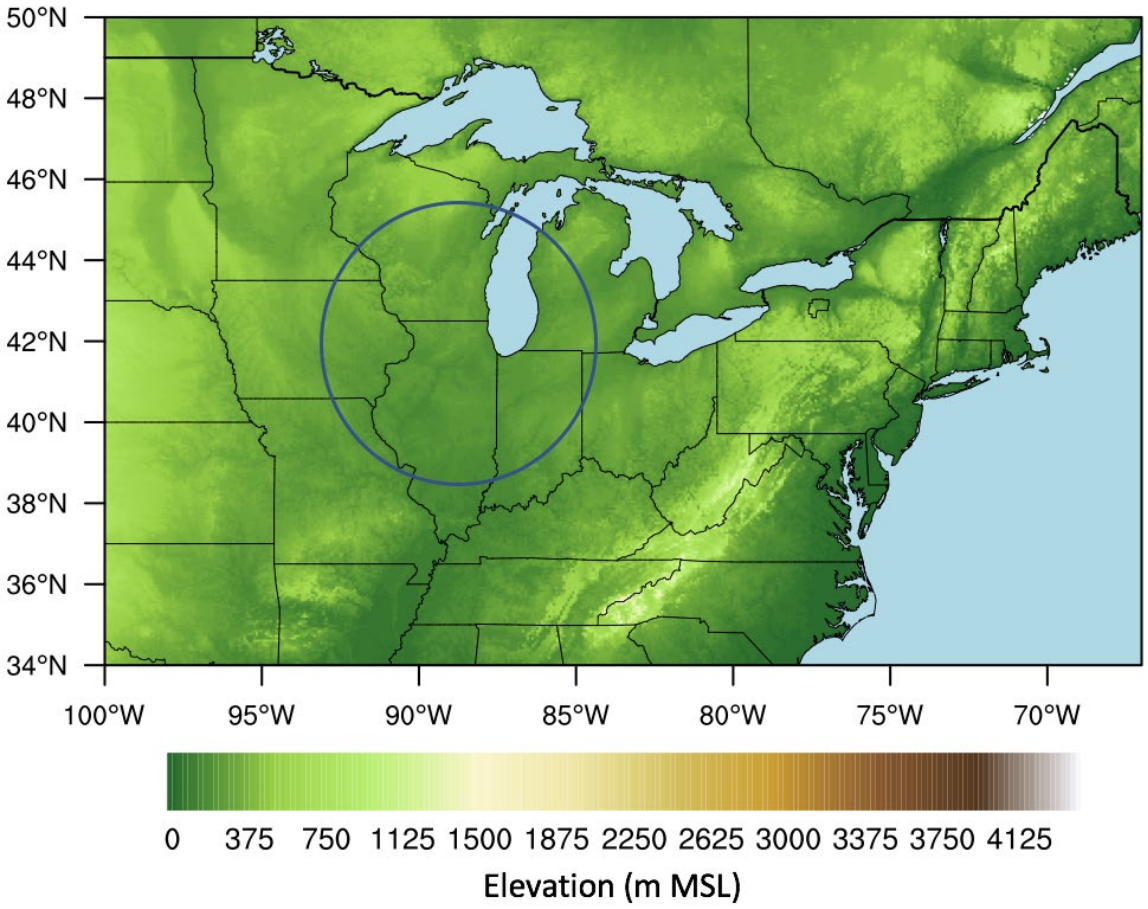

Figure 33. Terrain map, where the blue circle indicates the primary ICICLE domain.

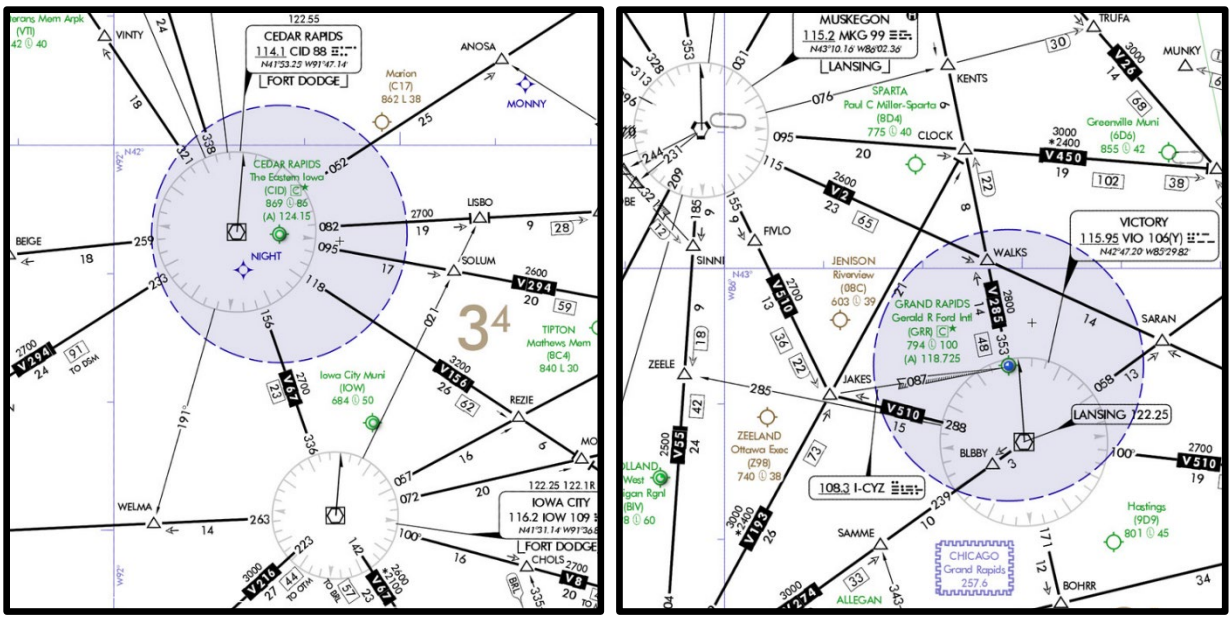

Figure 34. Example low IFR charts showing low MEAs around Cedar Rapids, Iowa (KCID; left) and Grand Rapids, MI (KGRR; right).

5.2 Air traffic

There are a number of airports within the ICICLE domain, some of which are large in size (e.g., Chicago O'Hare), so pockets of significant traffic can be expected. Icing sampling tends to occur below 15,000 ft altitude and Figure 35 shows an example of air traffic at these altitudes for a typical winter morning icing event. While there was little traffic over most of the ICICLE domain at this snapshot in time, traffic varies from day to day and over the course of the day, with early morning and evening rushes around the largest airports (Schultz and Politovich 1992; Brown et al. 1997) (see Figure 7). Traffic patterns can also change dramatically with time, as changes in local weather cause changes in runway use, resulting in changes in traffic within the approach and departure corridors. While test flights are not normally made in close proximity to major airports like Chicago, changes in the pattern may provide opportunity to operate in corridors fairly close to such airports. In Figure 35, for example, traffic is quiet near South Bend, IN ("SBN," to the east of Chicago), so sampling near there can be practical. On other days, traffic can be heavier near SBN, especially between 10,000 and 20,000 ft, making it difficult to sample there at those altitudes. Thus, air traffic influences ICICLE flight operations, especially near busy airports.

Figure 35 includes a 200-nm range ring around KRFD, considered to be the nominal range for a 4-hour mission with the NRC Convair-580 in and out of KRFD, with ~2 hours dedicated to

sampling. It is important to note that the use of remote landing sites between flights can extend sampling time and allow the aircraft to operate in additional areas outside of the 200-nm ring.

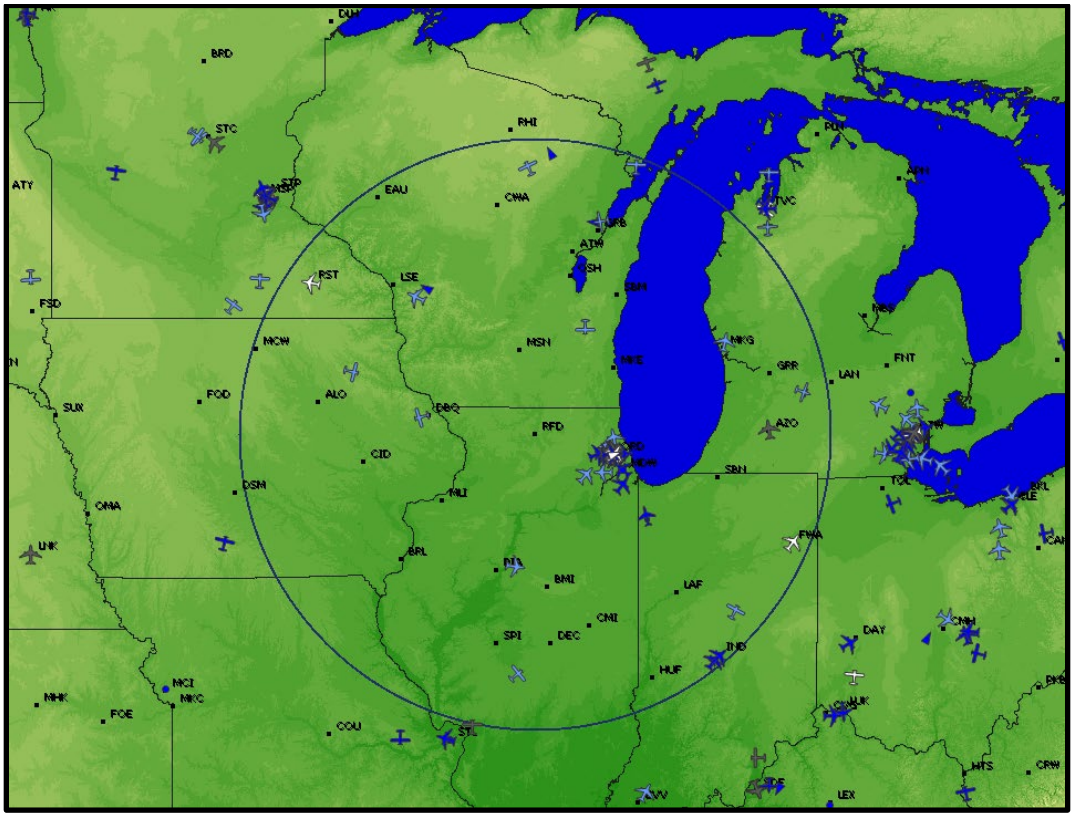

Figure 35. Example map of aircraft flying at altitudes of < 5,000 ft (dark blue), 5,000-10,000 ft (medium blue) and 10,000-15,000 ft (light blue). Altitude varied for grey aircraft. The primary ICICLE domain is shown as a black circle.

5.3 Availability of alternates

For strategic planning, acceptable alternate landing sites ("alternates") can be mission critical when ceilings and visibilities (C & V) are low at the operations base or the planned remote landing location. Without suitable alternates, some missions would have to be canceled. Fortunately, the western Great Lakes and Midwest have many airports with runways that are at least 6,000 ft in length (requested length by the Convair-580 crew; see Figure 36). Many of those have navigation systems that allow for low-altitude approaches and landings when C & V are low, as they sometimes are during wintertime icing events. This is especially true early in the day, when SLD tends to be more common.

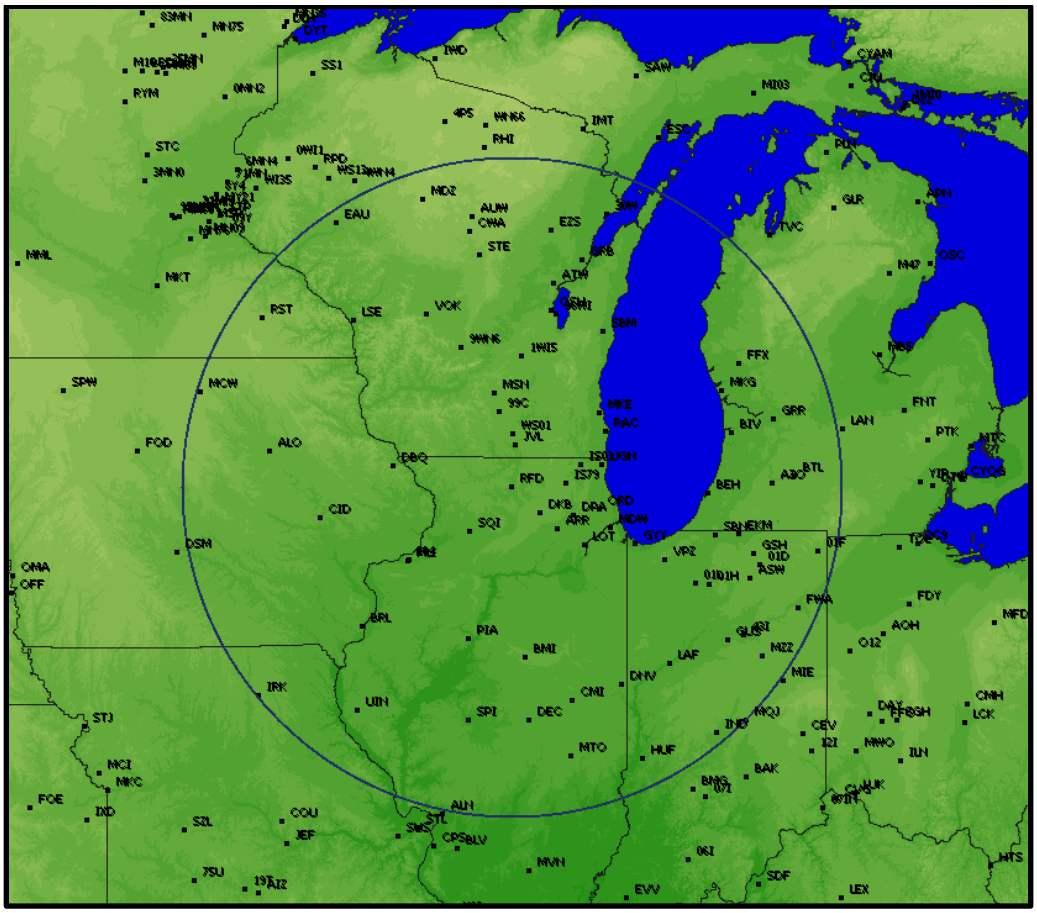

Figure 36. Map showing airports with at least one 6000 ft or longer runway.

5.4 Icing “dry spells” - alternative operations bases

The high frequency and variety of wintertime cloud and precipitation types in the flight domain are associated with a myriad of characteristics as storms follow their typical wintertime tracks. These include storms that lift from the Texas Panhandle to the western Great Lakes and others that drop southeast from Canada (Zishka and Smith 1980). These common storm tracks draw warm air into the region from the south, and/or cold air from the northwest, including across the Great Lakes. Of course, other synoptic and mesoscale features can also lead to significant icing in the project domain.

Although icing and SLD climatological frequencies in the primary project domain are favorable for the 6-week period of flight from late January through early March (see Figure 4, Figure 5 and Figure 30), it is well-understood that storm tracks shift from time to time, and it is necessary to plan for the possibility of extended periods with relatively little icing within reach from Rockford. For instance, January-to-March icing frequencies in icing-prone Flint, MI (northwest of Detroit) have been shown to vary between 40% and 80%, with some periods having had

relatively little icing (e.g., February 1982) (see Figure 37). Peoria, Illinois (KPIA, south of Rockford) tends to have lower frequencies than Flint, and there have been some particularly weak icing periods there. Notice that periods of infrequent icing may or may not be coincident between two sites, even in the same region. For example, while Flint had less icing than normal during February 1979, Peoria had above-average activity during this same period.

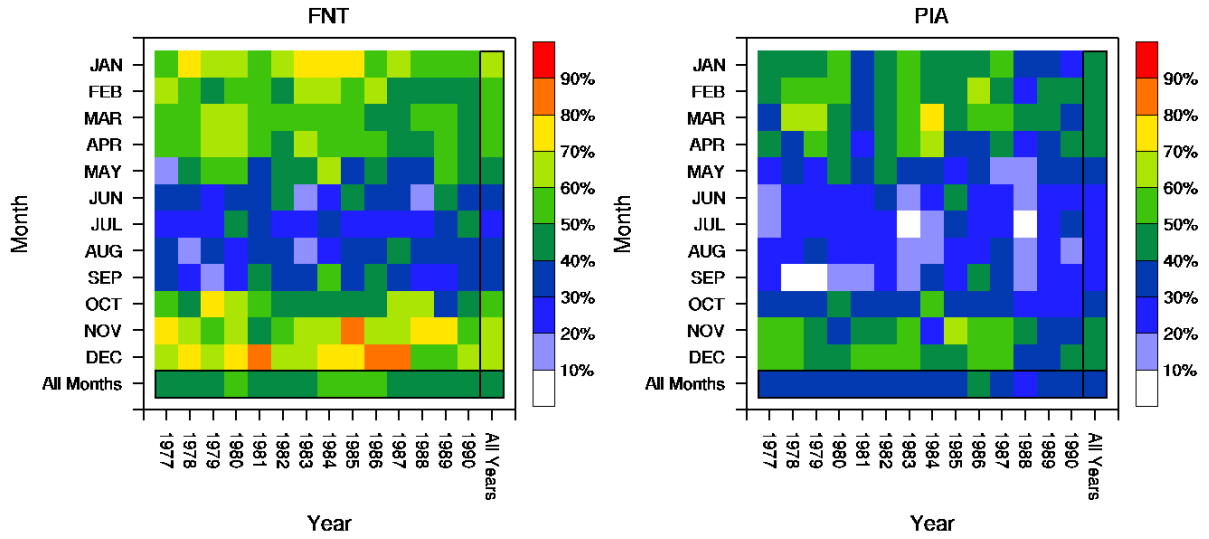

Figure 37. Inferred icing frequencies for each month-year combination, for all months of a given year (bottom row), and for all years of a given month (right column) above Flint MI and Peoria IL. Images from Bernstein, et al. 2007 study; the right image was not previously published.

Experience from icing certification programs over 15+ years has demonstrated such variability, with locations that are normally very active during certain months becoming inactive for days and even weeks at a time when the storm tracks are displaced, causing relatively cloud- and precipitation-free weather to dominate. Such periods are referred to here as icing "dry spells."

The period for ICICLE was chosen to be late January to early March 2019, due to the relatively short season for low-altitude and surface SLD in the CONUS and to avoid challenges associated with flight operations near the holiday season. However, to account for the possibility of icing "dry spells" around Rockford, it was imperative to identify secondary domains that could meet program, aircraft and crew needs. These areas had to be reasonably favorable for icing, including SLD, and for sampling, with a large portion of the domain having relatively flat terrain, light traffic, and good-quality data from candidate icing tools. There also had to also be at least one airfield that met all requirements for an operations base; a sufficiently large hangar for the Convair-580 (with potential availability), sufficient runways and approach systems, Jet-A fuel, de-icing capability, regular METARs and Terminal Area Forecasts (TAFs), and a manned

control tower. Such airfields were considered to be options if a) extended “dry spells” occurred or b) interesting, more remote events were worthy of investigation and resource use.

Eight (8) “alternative icing regions” with suitable bases were identified. They include Rapid City SD (KRAP), Topeka KS (KFOE), Fayetteville AR (KXNA), Smyrna TN (KMQY), Columbus OH (KCMH), Richmond VA (KRIC), Ottawa Ontario (CYOW), Brunswick ME (KBXM) (see Figure 38). Potential target airports for each region are listed in Table 6. Ottawa (CYOW) was included because it is the home base for the Convair-580 and areas of interest in the United States are accessible from there.

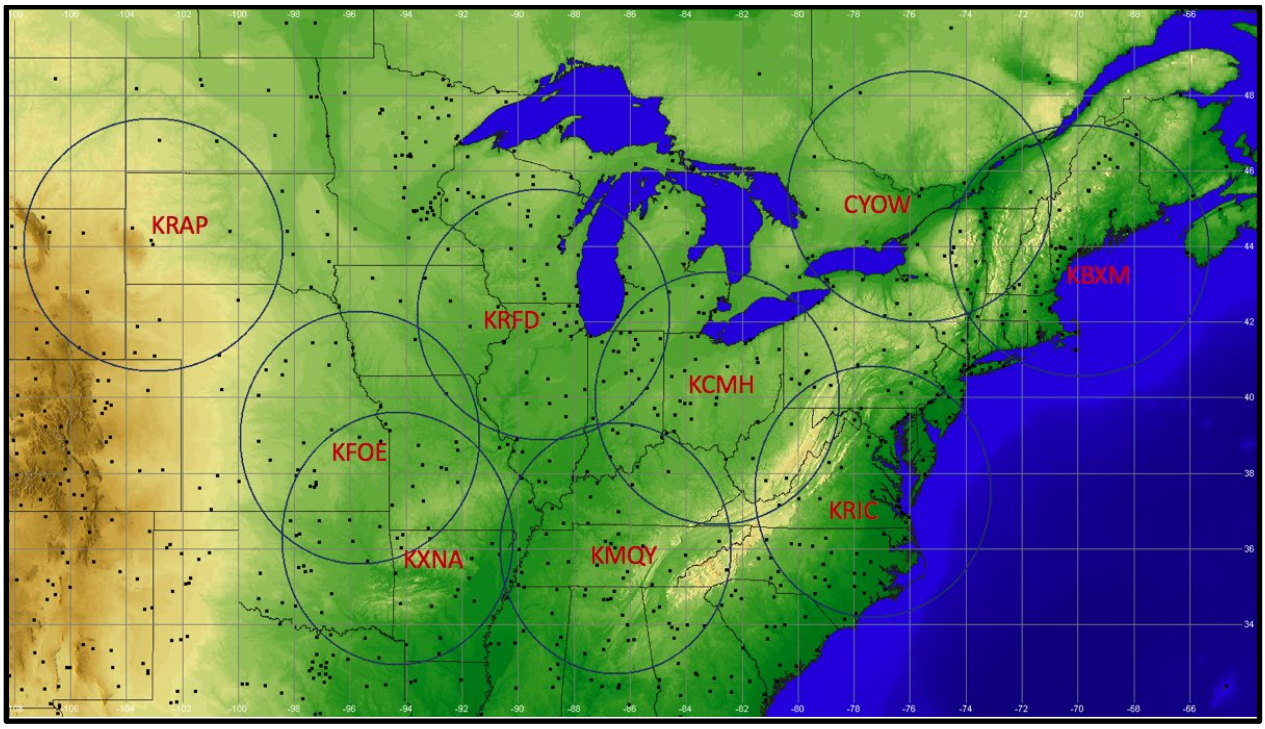

Figure 38. Map showing KRFD and the eight alternative bases with 200-nm range rings for each. Airports with at least one runway >6000 ft in length are indicated with black dots.

Table 6. Alternate airports for use in case of "icing dry spells" around KRFD. Airport Service Levels are indicated in colored text as follows: A and B (green), C (red), D (orange), other (AWOS or Canadian; grey)

Icing Shift	Airport IDs	Name(s)	Distance (nm) and direction from KRFD	Some potential workable targets within approximately 200 nm
None	KRFD	Rockford IL	0	MSN-AUW-GRB-MKE-MKG-AZO-FWA-SBN-IND-CMI-PIA-UIN-DVN-CID-DBQ-ALO-DSM-RST-EAU
East	KCMH KBXM KRIC CYOW	Columbus OH Brunswick ME Richmond VA Ottawa OT	310 ESE 820 ENE 610 ESE 610 ENE	CMH-CAK-CLE-ERI-UNV-CRW-HTS-LEX-DAY PWM-MHT-ORH-ALB-BTV-AUG-BGR-CAR-CON RIC-CHO-ROA-LYH-ORF-GSO-RDU-FAY-CLT-FLO YOW-ART-SYR-BGM-ROC-BUF-YOW-YYB-YQB-YXU
West	KFOE KRAP	Topeka KS (Forbes) Rapid City SD	360 SW 620 WNW	TOP-MCI-COU-SGF-FYV-TUL-ICT-SLN-GRI-OMA-SUX RAP-GCC-SHR-CPR-CYS-BFF-LBF-PIR-BIS-DIK
North	NONE	N/A – One-day sorties		TVC-SAW-DLH-BJI-INL-GFK-FAR-ATY-FSD
South	MQY XNA	Smyrna TN Fayetteville AR	390 SSE 440 SSW	HSV-BHM-TUP-MEM-PAH-EVV-LEX-TYS-GSP-CHA XNA-FYV-LIT-TXK-OKC-TUL-ICT-MCI-SGF-COU

For reference, icing frequency charts for sounding sites located within each of the alternative icing regions are given in Figure 39 and Figure 40. In these plots, it is evident that icing is generally less frequent at these locations. Only Dayton (near the alternative base at KCMH; Columbus, OH) has overall icing frequencies that approach those of Flint, MI. It is interesting to note that each of these areas have had occasional periods with relatively high icing frequencies. For example, January-March of 1983 was more active than usual at Topeka KS, Oklahoma City OK, Nashville TN, Greensboro NC and Portland ME. The winter of 1982-83 featured a strong El Niño, which can make the storm track more active in the southern part of the United States (Kunkel and Angel 1999). Note that January-March 1983 was still quite active at Flint and Dayton, so that particular El Niño year had good icing frequencies within both the primary ICICLE domain and some of the alternative domains. The phenomenon of El Niño was quite relevant as ICICLE approached, because several forecasts indicated the possibility of a significant "Modoki" El Niño developing during winter 2018-19. The implications of strong El Niño events on storm tracks, temperatures, precipitation and icing remains a topic of research (Montroy et al. 1998; Yu and Zou 2013; Bernstein et al. 2007; Austin et al. 2011).

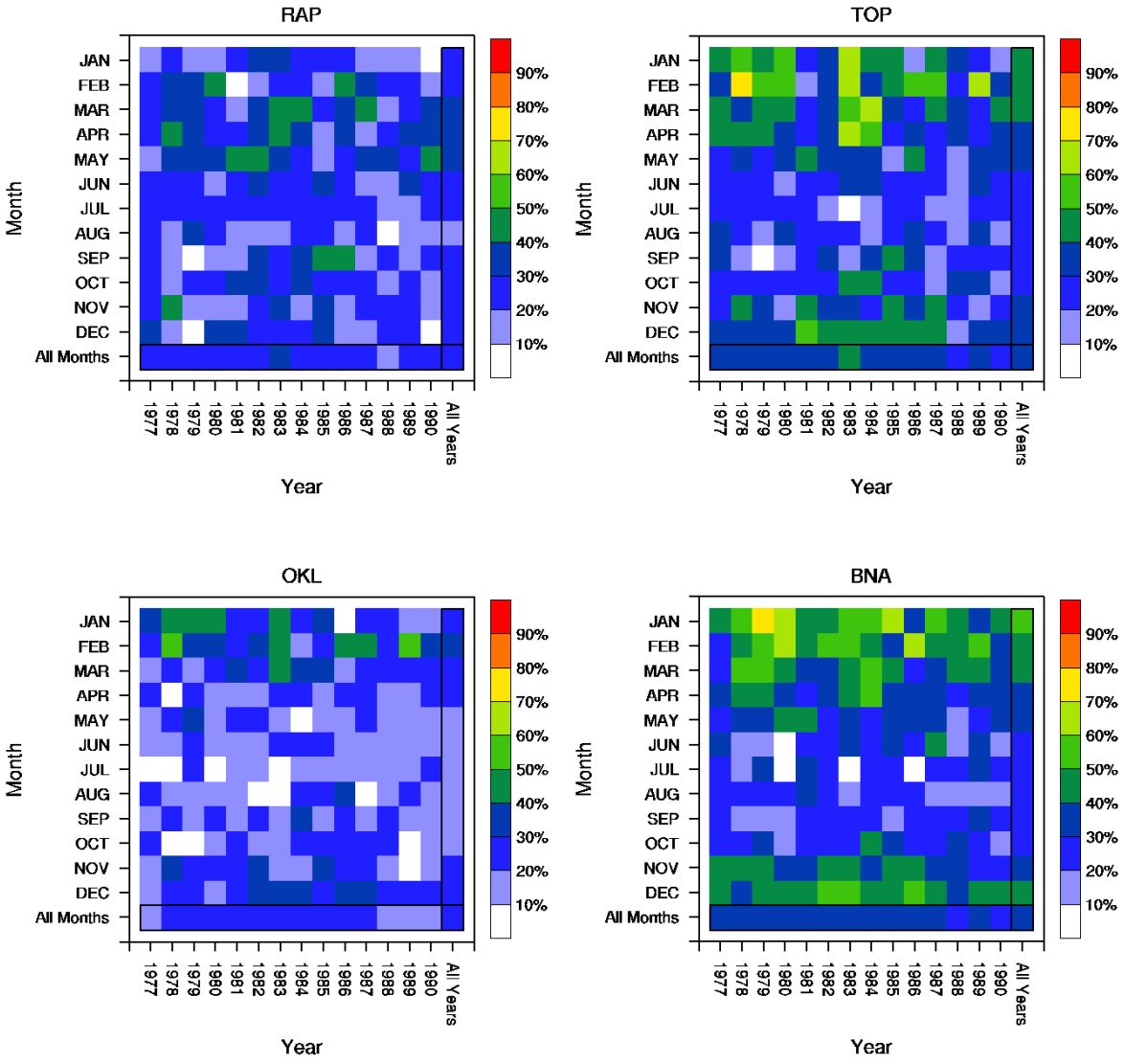

Figure 39. Same as Figure 37, but Rapid City SD (RAP), Topeka KS (TOP), Norman/Oklahoma City OK (OKL) and Nashville TN (BNA). Images were generated for the Bernstein et al. 2007 study, but not included in the publication.

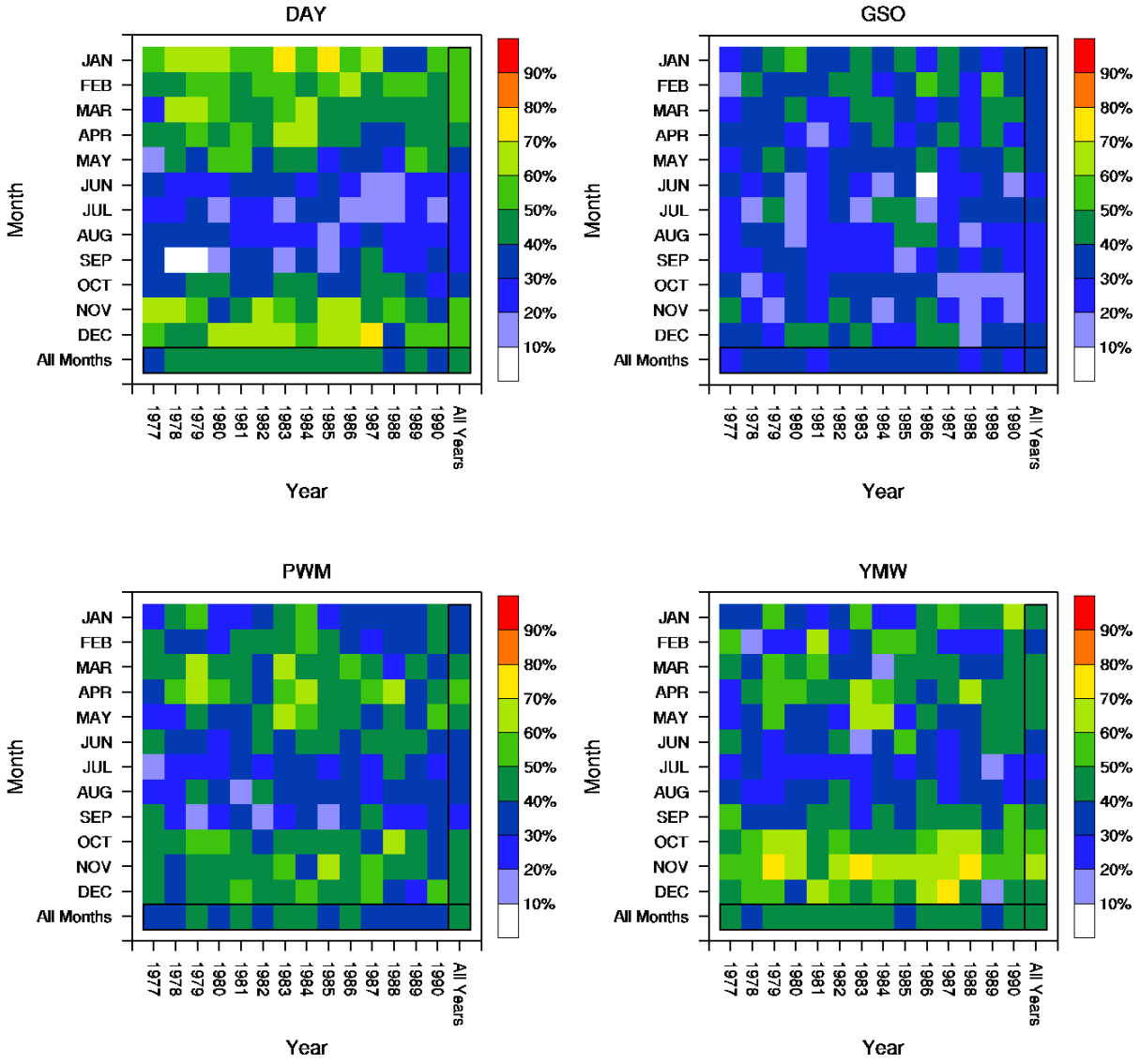

Figure 40. Same as Figures 37 and 39, but for Dayton OH (DAY), Greensboro NC (GSO), Portland ME (PWM) and Maniwaki ON (YMW).

6 Field program data sources

To document the environments described in Table 5 thoroughly, a rich dataset is needed from a variety of sources. These include the NRC Convair-580 research aircraft, as well as a wide array of "icing tools," including observational platforms and numerical weather prediction models. Together, they can be used to sample, document, diagnose and forecast the full spectrum of icing and non-icing conditions of interest. The icing tools include operational products and candidates for advancing the state of the art of icing diagnosis and forecasting, which are in the process of being tested to determine their ability to identify these conditions and transition zones between them. While a review of the icing-relevant science behind these tools is provided in Section 3.2, Section 6 considers them in terms of the data they provide for ICICLE operations and research. This includes a description of the aircraft, its sensors, and each icing tool, with a summary provided at the end of this section in Table 10.

6.1 Aircraft

The NRC Convair-580 served as the test aircraft for the program. It is a twin-engine, pressurized aircraft that has performance characteristics that meet experimental requirements, including being capable of long-distance operation. It can carry up to a dozen research crewmembers and a wide array of robust instrumentation for cloud microphysics sampling (see Figure 41 and Figure 42). For ICICLE, NRC and ECCC equipped the NRC Convair-580 with extensive in-situ and remote sensing instruments, providing duplicate measurements in some cases (Wolde and Marcotte 2008; Wolde et al. 2012, 2020) (see Table 7). The NRC/ECCC list of on-board remote sensors and in-situ probes matches the ranked list of desired probes and other on-board measurements generated by the IFI and TAIWIN scientists (see Table 8).

The Convair-580's sensors are installed in various locations on the aircraft, including on underwing and wingtip pylons, on various sections of the fuselage, and inside the aircraft cabin (see Figure 41 and Figure 42). The crew has extensive, critical experience flying in icing conditions, including SLD (Isaac et al. 2001a, 2001b, 2005; Brown 2011; Smalley et al. 2017), and can document ice shapes and changes in aircraft performance.

Figure 41. NRC Convair-580 research aircraft showing the various instruments installed on underwing, wingtips and on fuselage location. The cabin rack and data system monitors are also shown.

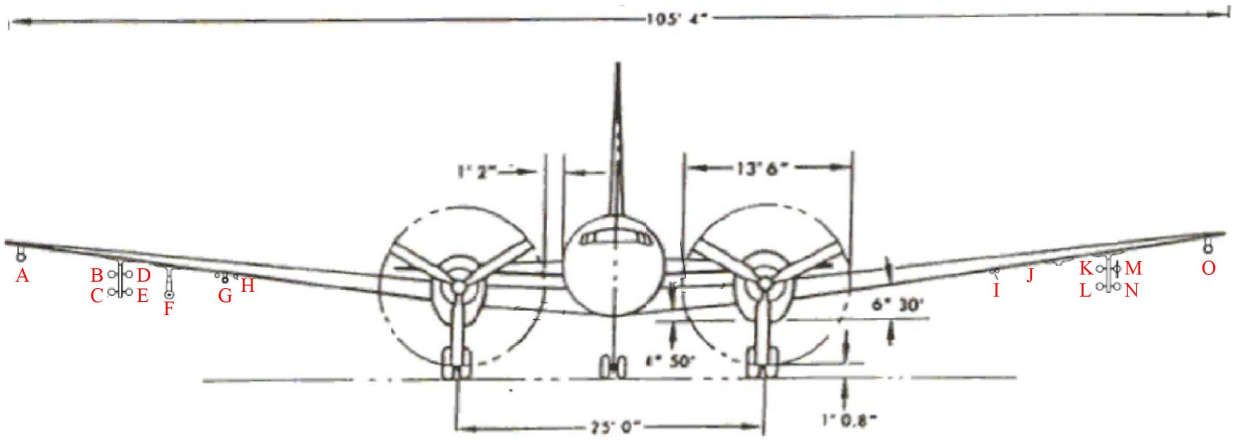

A	*Forward: AIMMS-20; Aft: G-band radiometer (GVR)*	**I**	*Rosemount TAT & Reverse Flow TAT*
B	*Forward Scattering Spectrometer Probe (FSSP)*	**J**	*Aero-probe, Rosemount TAT (x2) and Rosemount Icing Detector*
C	*Rosemount 858*	**K**	*2D Stereo Probe (2DS)*
D	*Cloud Droplet Probe (CDP)-2 & Rosemount Icing Detector*	**L**	*High Volume Precipitation Spectrometer (HVPS)*
E	*Top: 2D Stereo Probe (2DS); bottom: Fast CDP (FCDP)*	**M**	*Precipitation Imaging Probe (PIP)*
F	*Cloud Particle Imager (CPI)*	**N**	*2D Cloud Probe (OAP-2DC); Aft: Cloud Extinction Probe (CEP) retroreflector*
G	*Scalar boom (pitot), Rosemount TAT, Nevzorov, ECCC hot-wire probe*	**O**	*FORWARD: Ka-band Precipitation Radar (KPR)/Ultra-High Sensitivity Aerosol Spectrometer (UHSAS); Aft: Cloud Extinction Probe*
H	*Goodrich Icing Detector*		

Figure 42. NRC Convair-580 Wingstore configurations for ICICLE

Table 7. Convair-580 remote sensing instruments (top panel) and in-situ sensors (bottom panel) for ICICLE. Note the redundancy of measurements.

Meas. Type	Instrument	Parameters	Location	DAQ
Radar Reflectivity and Doppler Velocity	NRC Airborne X-band radar (NAX)	Reflectivity, Doppler Velocity, polarization in some channels	Fuselage and NAWX rack	NAX
	NRC Airborne W-band radar (NAW)	Reflectivity, Doppler Velocity, polarization in some channels		NAW
	Ka-band Precipitation Radar (KPR)	Reflectivity and Doppler	PWTF	KPR
Lidar backscattering and depolarization	355nm AECL Lidar_Zenith	Lidar backscatter and depolarization		AECL_Zenith
	355nm AECL Lidar_Nadir			AECL_Nadir
Liquid Water Path (LWP) and Precipitable Water Vapour (PWV)	G-band Radiometer	Tb, PWV, LWP	SWTA	GVR
Stormscope	Goodrich WX-500			

Meas. Type	Instrument	Parameters	Location	DAQ
Aircraft State	GPS_ProPack	Positions	NAV rack, antenna on roof	NRC
	GPS_FlexPAck	Positions	NAV rack, antenna on roof	NRC
	KVH 1750 IMU	Inertial state	Rack #5	KVH
	HG 1700 IMU	Inertial state	NAWX rack	HG
	Aventech IMU	Inertial state		Aventech
	KPR IMU	Inertial state	PWTF	KPR
	High altitude Radar Altimeter	AGL altitude		M300
Atmospheric State	RMNT Pressure Transducers	Static and dynamic pressure	SSB	NRC
			Fuselage	NRC
	RMNT TAT	Temperature	SSB	NRC
	RMNT TAT		PUW	NRC
	Reverse Flow TAT		PUW	NRC
	RMNT TAT		PSB	NRC
	RMNT TAT		PSB	NRC
	AIMMS-20 Air Data Probe (ADP)	Temperature, Pressures, Relative Humidity, incidence angles	SWTF	Aventech
	Aeroprobe (5-hole Pressure Sensors)	Differential pressures (Air Data)	PSB	NRC
	RMNT 858 ADP	Pressures, incidence angles	SOL	NRC
	Licor 840a	Water vapor concentration	Rack #5; roof inlet	NRC
	Licor 7000	Water vapor concentration	Rack #5; roof inlet	NRC
	Edgetech Hygrometer	Dew point (Td)	Fuselage	NRC

Meas. Type	Instrument	Parameters	Location	DAQ
Aerosol size and concentration	Cloud Condensation Nuclei Counter (CCNc) with CPI	CCN concentration 0.75 – 10 µm after super saturation	Rack #3 Roof heated aerosol inlet	CCN
	Ultra-High Sensitivity Aerosols Spectrometer (UHSAS)	Aerosol size & conc. (0.06 nm – 1 µm)		UHSAS
	Single Particle Soot Photometer (SP2)	Aerosol – soot (200 – 430 nm)		SP2
	Condensation Particle Counter (CPC)	Aerosol concentration >~ 7 nm		CPC
Icing	Goodrich Icing Detector (x2)	Rate of icing	SUW	NRC
			PSB	NRC
Attenuation of light	Cloud Extinction Probe	Extinction coefficient	POLA & PWTA	M300
Bulk Cloud Properties	Nevzorov hot-wire	Liquid and Total Water Content (LWC & TWC)	SSB	M300
	ECCC hot-wire		SSB	M300
	SEA WCM-2000		Starboard Window	M300
Forward scattering	Forward Scattering Spectrometer Probe (FSSP)	cloud droplet size (~1–50 µm) & concentrations	SOU	M300
	Cloud Droplet Probe (CDP-2)		SIU	PADS
	Fast CDP (FCDP)		SIL	FCDP
Cloud Particles (Images, size and concentrations)	2DS (Stereo) Probe	Particle imaging 10 µm x 128 pixels	SIL	2DS-NRC
			PIU	2DS-ECCC
	Optical Array Probe (OAP-2DC)	Particle imaging 50 µm x 32 pixels	SOL	M300
	Cloud Particle Imager (CPI)	High-resolution (2.3µm) particle imaging	SSP	CPI
Precipitation particles (images, size and concentrations)	High Volume Precipitation Spectrometer (HVPS)	Particle imaging 150 µm x 128pixels	PIU	HVPS
	Precipitation Imaging Probe (PIP)	Particle imaging, 100 µm x 64pixels	POU	PADS

Table 8. Ranked summary of desired instrumentation from TAIWIN/IFI scientists

Priority Level	Sensor	Reasoning
Highest	State parameters (pressure, temp, humidity, winds)	Absolutely critical to know where you are and what the base-level conditions are. Winds – valuable if they are available, but not pivotal.
	Rosemount ice detector	Need to know if you are in icing. Cloud phase verification.
	Multiple LWC hot-wire probes	Model and sensor verification.
	CCN counter	CCN concentration
	Small drop probe (e.g., CDP, FCDP or FSSP)	Needed for drop-size distribution, D_{max} and MVD.
	Cloud imaging probe (e.g., 2DC or 2DS)	Needed for drop-size distribution, D_{max} and MVD.
	Precipitation probe (e.g., PIP or HVPS)	Needed for drop-size distribution, D_{max} and MVD.
High	TWC hot-wire probes	Basic information on LWC, IWC for comparison with model and instrument data and derivatives thereof
	PCASP or UHSAS or other aerosol probe	Aerosol data
	Cloud radar (W-band, X-band, Ka-band), polarized?	Real-time assessment of microphysical environment beyond what operational instruments might provide.
Moderate	Cloud lidar	Same as above. Use with radar, helps discriminate between ice and mixed phase
	Microwave radiometer (183 GHz)	Time-history of integrated water content, water vapor, reflectivity (precip information), etc.

6.2 Satellites

The National Oceanographic and Atmospheric Administration's (NOAA's) geostationary satellites provide excellent coverage of the ICICLE domain (see Figure 43). GOES-East (GOES-16; centered at 75°W) was in an excellent position to provide high-quality imagery across the ICICLE domain, centered on Rockford (42.2°N, 89.1°W). This latest-generation satellite produced high-resolution imagery for numerous channels of interest, expanding upon the visible, short- and long-wave infrared channels traditionally used for icing (see Section 3.2.3) and improved resolution in both space and time compared to the previous generation of GOES satellites, including 0.5-kilometer (km) spacing for the visible channel and 1-km spacing for other channels. Channel combinations can be used to generate traditional and new icing-relevant fields, such as the "microphysics" field. Data are nominally provided every 5-min, but 1-min

rapid-scans with even finer spatial resolution was made available by request for some events (Schmit et al. 2005, NOAA 2018).

Located at 137.2°W, GOES-17 took over as GOES-West in January 2019. Though GOES-17 has similar capabilities to GOES-16, its position is not as ideal for the flight program, since the imagery is taken at steeper viewing angles over the ICICLE domain. These two satellites provide essentially coincident imagery, providing an opportunity to examine the importance of viewing angle for icing-relevant fields.

Polar orbiter satellites such as MODIS, VIIRS and JPSS (Minnis et al. 2011; Smith et al. 2019; Weinrich 2020) have the ability to provide additional information when passing overhead during periods of operations, but those satellites are not planned to be a focus of data analysis or forecasting for ICICLE.

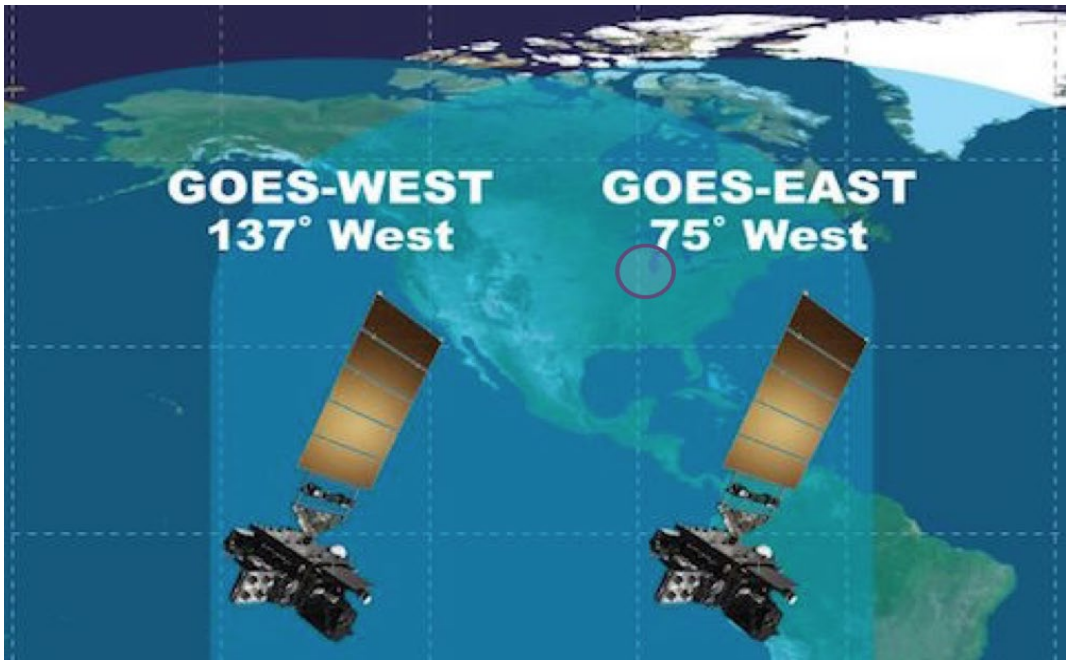

Figure 43. Map of GOES coverage for North America and surrounding areas, adapted from NOAA 2017. An approximation of the primary ICICLE domain is shown using the overlying circle. KRFD is located at 42.2°N, 89.1°W.

6.3 NEXRADs and radar mosaics

NOAA's NEXRAD network provides excellent coverage of the primary ICICLE domain, with some areas covered by multiple radars at varying distances (see Figure 44). This allows the testing of various radar characteristics and their impact on icing identification. Radars scanning areas of interest from different distances provide additional perspectives on events, and blends of

their data could be used in mosaics to maximize 3-D coverage above a given site and across the ICICLE domain. It is important to examine the signals from FZDZ, FZRA or SN events as they are viewed by NEXRADs at various distances above ICICLE ground suites (see Section 6.5), as well as in mosaicked data, such as the FZRA examples presented in Figure 16. Feature-tracking of radar reflectivity will also be explored during and following ICICLE.

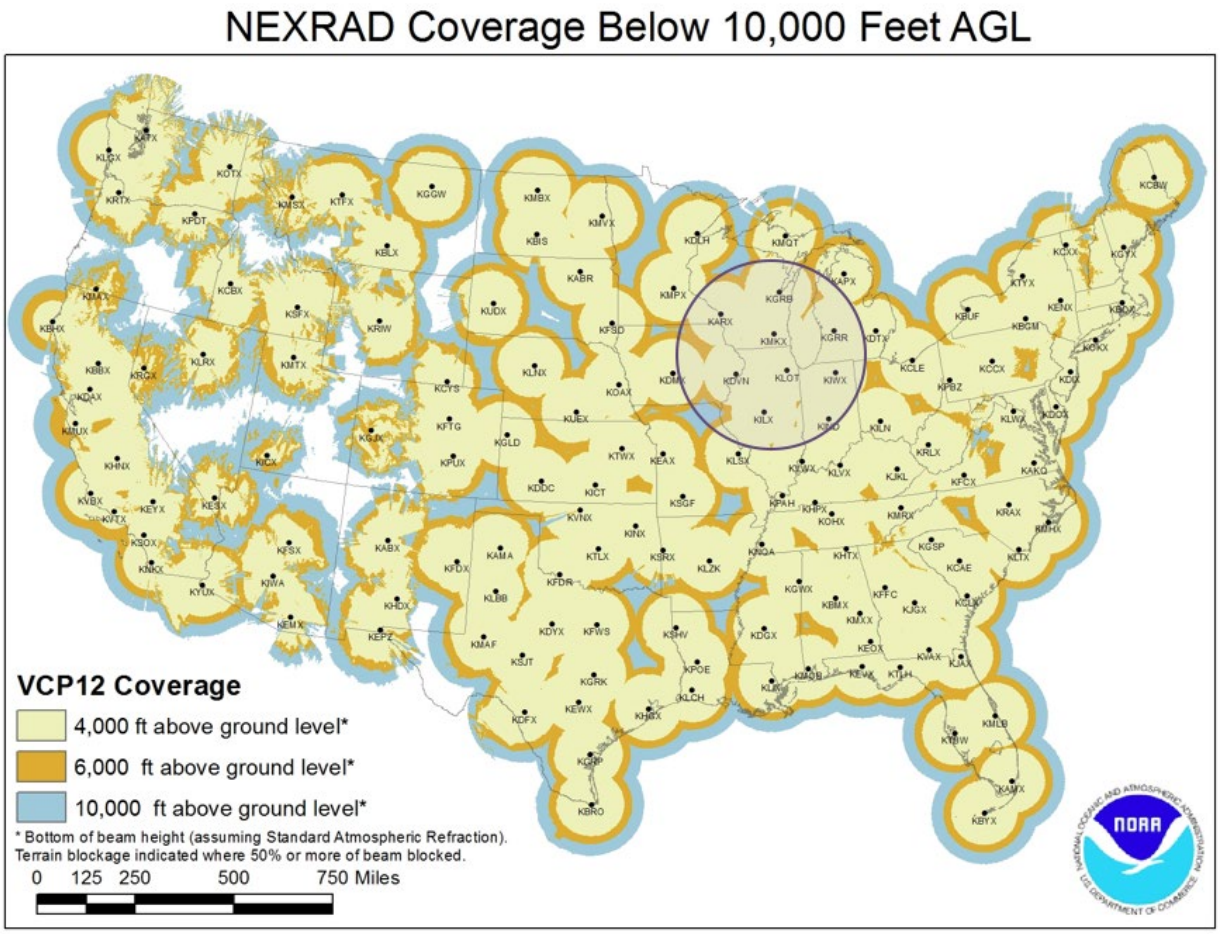

Figure 44. NEXRAD coverage, including the primary ICICLE domain (black circle; adapted from NOAA 2011).

6.4 Surface observations

Observations from surface stations are an integral part of icing-related operational decisions (Green 2015). As described in Section 3.2.1, the ASOS and AWOS can report rain (RA) and snow (SN), as well as FZRA if the system includes a FZRA sensor, which measures ice accretion.

Data from the ASOS are compiled and distributed in METARs and SPECIs. AWOS data are generally only distributed in METARs, although some AWOS sites can also produce SPECIs. Unless augmented, METARs provide only one precipitation type, where frozen precipitation (snow) is prioritized over freezing and non-freezing liquid types. This could result in the masking of precipitation types that are very important for icing, especially SLD.

Figure 45 shows the locations of ASOS and AWOS sites across the ICICLE domain and immediate surroundings, with the various Service Levels and configurations marked. It is important to note only sites indicated by brown, orange, and tan dots have a freezing rain sensor. Those indicated by yellow, green, and blue dots did not have that sensor as of the time of this writing. Also, only those sites marked with brown-dots on Figure 45 have CWOs (e.g., Rockford [KRFD] and Grand Rapids [KGRR]). Because of the limitations of ASOS and AWOS, as well as the varying levels of service across the ICICLE domain, supplemental surface sensors were deployed as part of several "ground suites." They are marked with large blue dots and large red dots on Figure 45 and discussed in the next section.

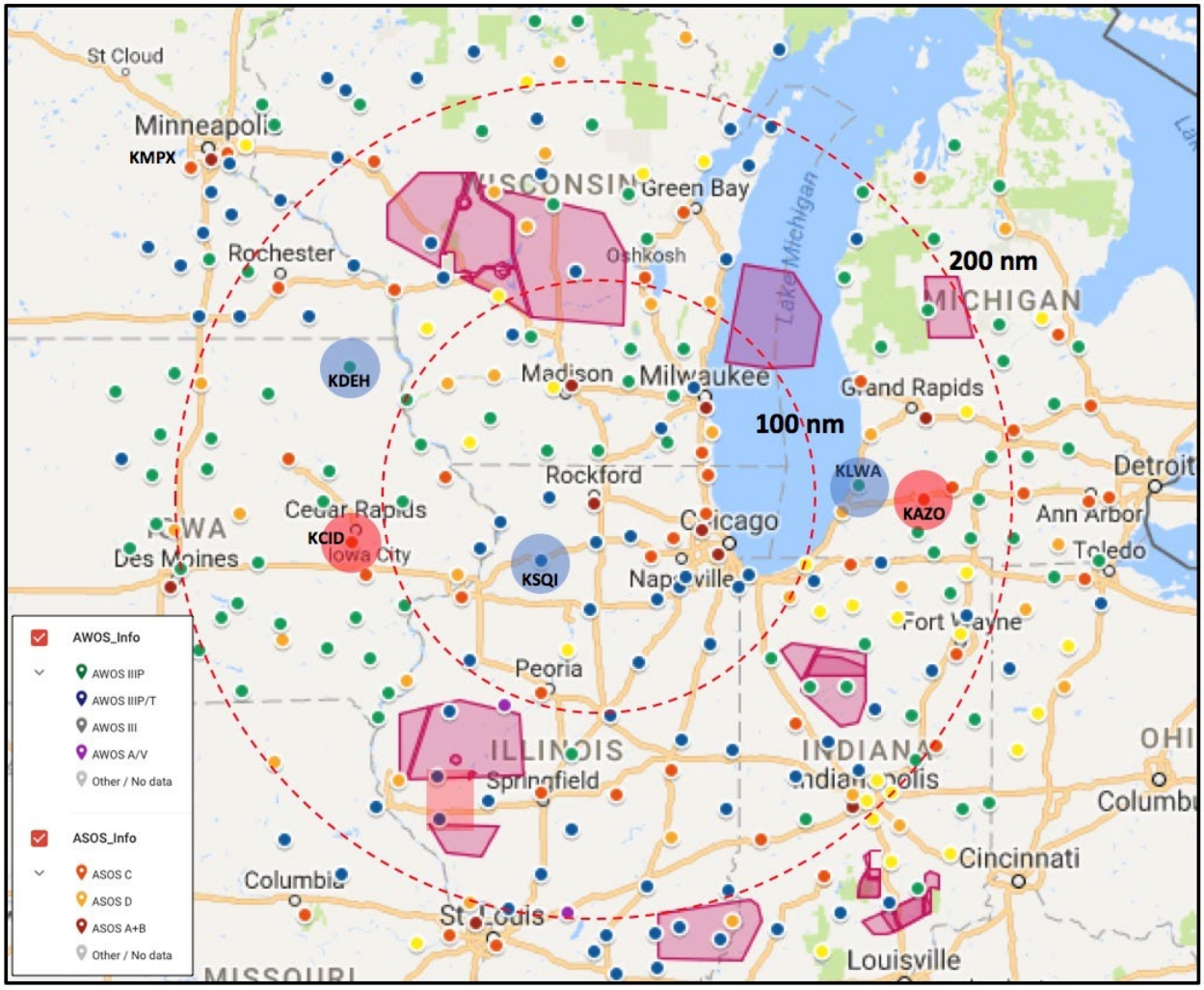

Figure 45. Surface stations, including ASOS (tan, red, brown dots), AWOS (green, blue, purple, grey dots) and RWIS (road weather information system; green dots) sites. 100-nm and 200-nm range rings centered around KRFD (dashed red circles) are shown. ICICLE ground suites are indicated with large blue dots and red dots. Military and restricted flight areas (red and purple shaded polygons) are also shown.

6.5 Supplemental surface-based instruments

Supplemental surface-based instruments ("ground suites") were placed at five sites across the primary ICICLE domain to provide additional icing-relevant observations and supplement operational ASOS and AWOS measurements. These sites included Kalamazoo MI (KAZO), Cedar Rapids IA (KCID), South Haven MI (KLWA), Decorah IA (KDEH), and Sterling IL (KSQI). A summary of the instrumentation at the ground suites is provided in Table 9, with more detailed information about each suite provided in the following sub-sections.

Between the ground suites and operational ASOS and AWOS sites, variability within the terminal area can be captured more readily while also addressing the need to fill gaps in the network. When multiple icing targets were available on a given day, emphasis was placed on operations near sites with ground suites to gather flight data above them when appropriate.

Table 9. Summary of supplemental ground-based sensors.

Sensor Type	**KAZO (ASOS)**	**KCID (ASOS)**	**KLWA (AWOS)**	**KDEH (AWOS)**	**KSQI (AWOS)**
Ceilometer	x				
Present Weather Sensor	x	x	x	x	x
FZRA sensor	x	x	x	x	x
Disdrometer	x	x	x	x	x
Precipitation Gauge	x	x	x	x	x
State parameter sensor	x	x	x	x	x

6.5.1 Ground suite #1 – Kalamazoo, MI

Kalamazoo, MI airport (KAZO) is located within the eastern portion of the ICICLE domain (~160 nm E of KRFD) (see Figure 1 and Figure 46), and has a Service Level "C" ASOS. Historically, KAZO has a high frequency of targeted environmental conditions due to its proximity to common wintertime storm tracks, and location downwind of Lake Michigan, where cold-season lake-effect icing commonly occurs in northwesterly flow.

KAZO's runway is 6,500 ft long (17/35) with an instrument landing system (ILS) approach on runway 35. Traffic is typically light (~111 operations/day) and even lighter when IFR winter weather is prevalent since ~80% of KAZO operations are from General Aviation (GA) aircraft. Within 50 nm, there are numerous alternate landing locations with at least one 6,000 ft+ runway with ILS (KBTL, KGRR, KJXN, KGSH, KEKM, KSBN, KBEH, and KBIV) (see Figure 36 and Figure 46). Others are within 75 nm (KLAN, KMKG, and KFWA). Located just beyond the southwest edge of the KAZO terminal area (as defined by TAIWIN – 30 nm radius), KSBN (South Bend, IN) has a hangar that could meet the needs of the Convair-580. Within the KAZO terminal area, there are two ASOS Service Level Cs and five AWOSs, including the KLWA site (~32 nm WNW) which has a ground suite. The Grand Rapids, MI (KGRR) ASOS-B is located just outside of the KAZO terminal area. Soundings are launched from the NWS site at Detroit (KDTX; ~90 nm E) and could be launched from a supplemental site at Valparaiso University (~80 nm SW) (see Section 6.7).

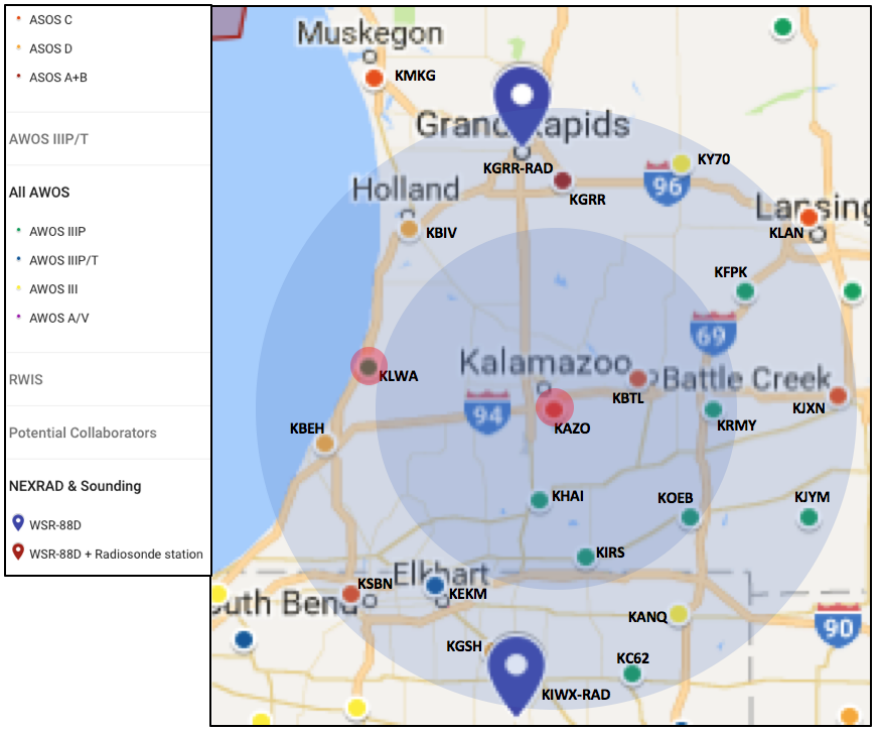

Figure 46. The area surrounding the ground suite at KAZO. The inner circle encompasses the 30-nm radius around KAZO, approximating its terminal area. The outer circle encompasses a 50-nm radius. The legend at the upper left describes the surface station types. The ground suite sites KAZO and KLWA are marked with large red dots.

KAZO is also located fairly close to two NEXRADs, with KGRR (Grand Rapids) ~38 nm to the north, and KIWX (Northern Indiana) ~55 nm to the south. These radars can view the airspace around KAZO from opposite directions and provide similar, but slightly different beam coverage, creating a complimentary radar dataset across the terminal area (see Figure 47). In addition, KAZO is ~90 nm west of the Detroit (KDTX) radar, providing a potential for comparison with data from the closer radars. The Milwaukee and Chicago area radars (KMKX, KLOT) are each located ~120 nm away. All of the factors described above were important when selecting KAZO as a site for a ground instrumentation suite.

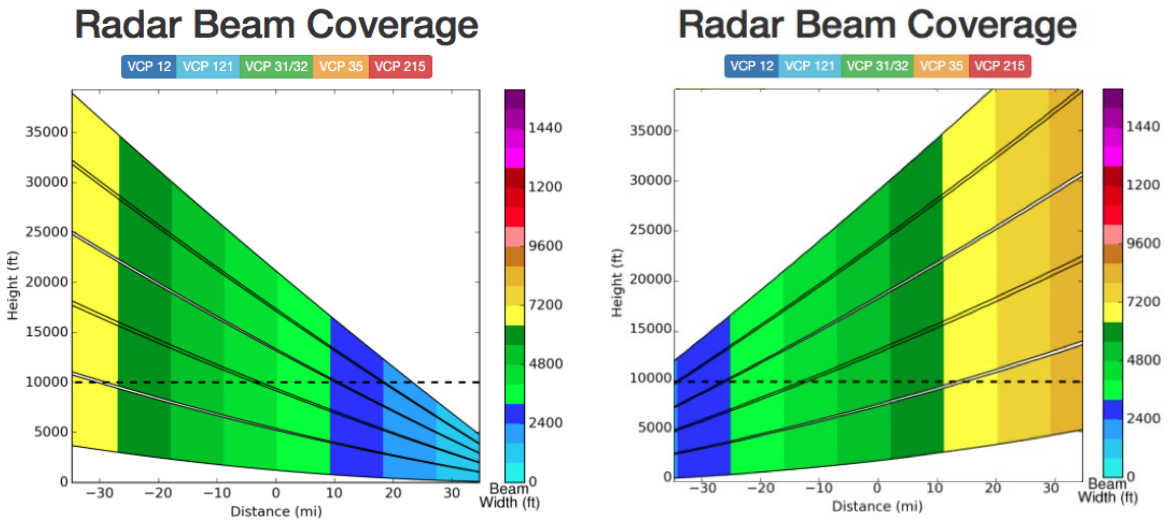

Figure 47. NEXRAD beam coverage from the National Severe Storms Laboratory's (NSSL's) TAIWIN RQI website for VCP31 over KAZO (located at zero (0) on the x-axis) from the KGRR (left) and KIWX (right) NEXRADs. The plot for KIWX/KAZO is an approximation plot using the KCID/KDVN pairing, which is at essentially the same distance. The KIWX beam direction plot has been flipped to provide a clearer view of its coverage of KAZO. Negative and positive distances at the bottom of the charts are roughly toward the south and north, respectively.

6.5.2 Ground suite #2 – Cedar Rapids, IA

Cedar Rapids, IA airport (KCID) is located within the western portion of the primary ICICLE domain (~120 nm WSW of KRFD) (see Figure 1 and Figure 48) and has a Service Level "C" ASOS. Like KAZO, KCID also has a historically high frequency of targeted environmental conditions due to its proximity to common wintertime storm tracks. It has a strong tendency to be on the northern and western side of the storm track that runs from the Texas Panhandle to Chicago.

KCID's main runway is 8,600 ft long, oriented east-west (090 and 270), and has ILS approaches in both directions. Its secondary runway is 6,200 ft long, oriented northwest-southeast (310 and 130) but does not have ILS. Traffic is typically light (~128 operations/day), with ~45% of that from GA aircraft. Within ~75 nm of KCID, there are several alternate landing locations with at least one 6,000+ ft runway with ILS (KDBQ, KMLI, KALO, and KOTM [5,885ft]) (see Figure 36 and Figure 48).

Operational surface stations within ~30 nm of KCID include two Service Level C ASOSs and two AWOSs. Soundings are launched from the NWS site at Davenport (KDVN; ~53 nm east-southeast) and could be launched from a supplemental site at Iowa State University (~85 nm west) (see Section 6.7). Two NEXRADs are located in the vicinity of KCID, with KDVN ~53

nm to the east-southeast, and KDMX (Des Moines) ~89 nm to the west-southwest. The more distant KARX (LaCrosse, WI) NEXRAD is ~118 nm to the northeast. These radars view the airspace around KCID from different directions and provide different beam coverages and widths. This provides an interesting radar dataset across the terminal area (see Figure 49), which is representative of numerous medium and smaller airports across the country that have limited radar coverage.

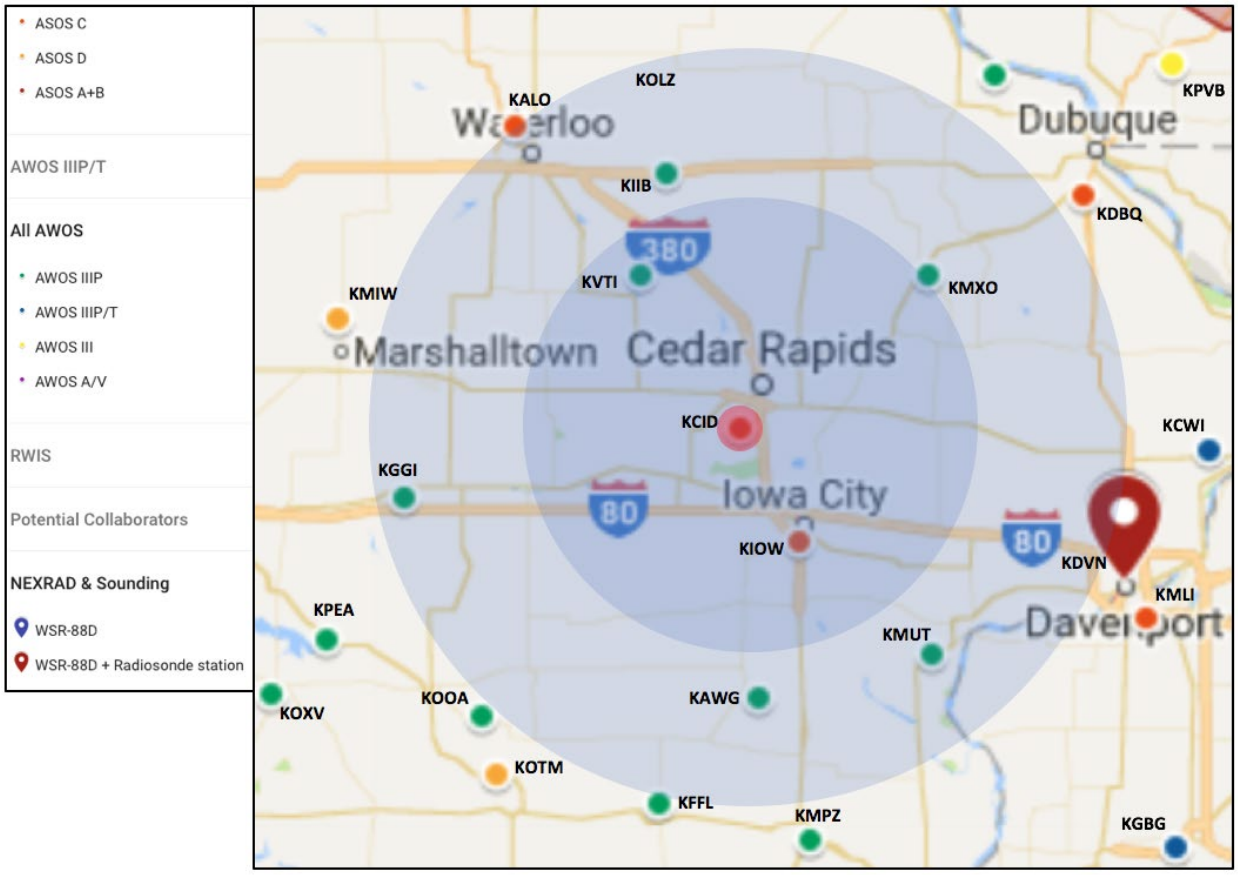

Figure 48. Same as Figure 46, but for the area surrounding the ground suite at KCID.

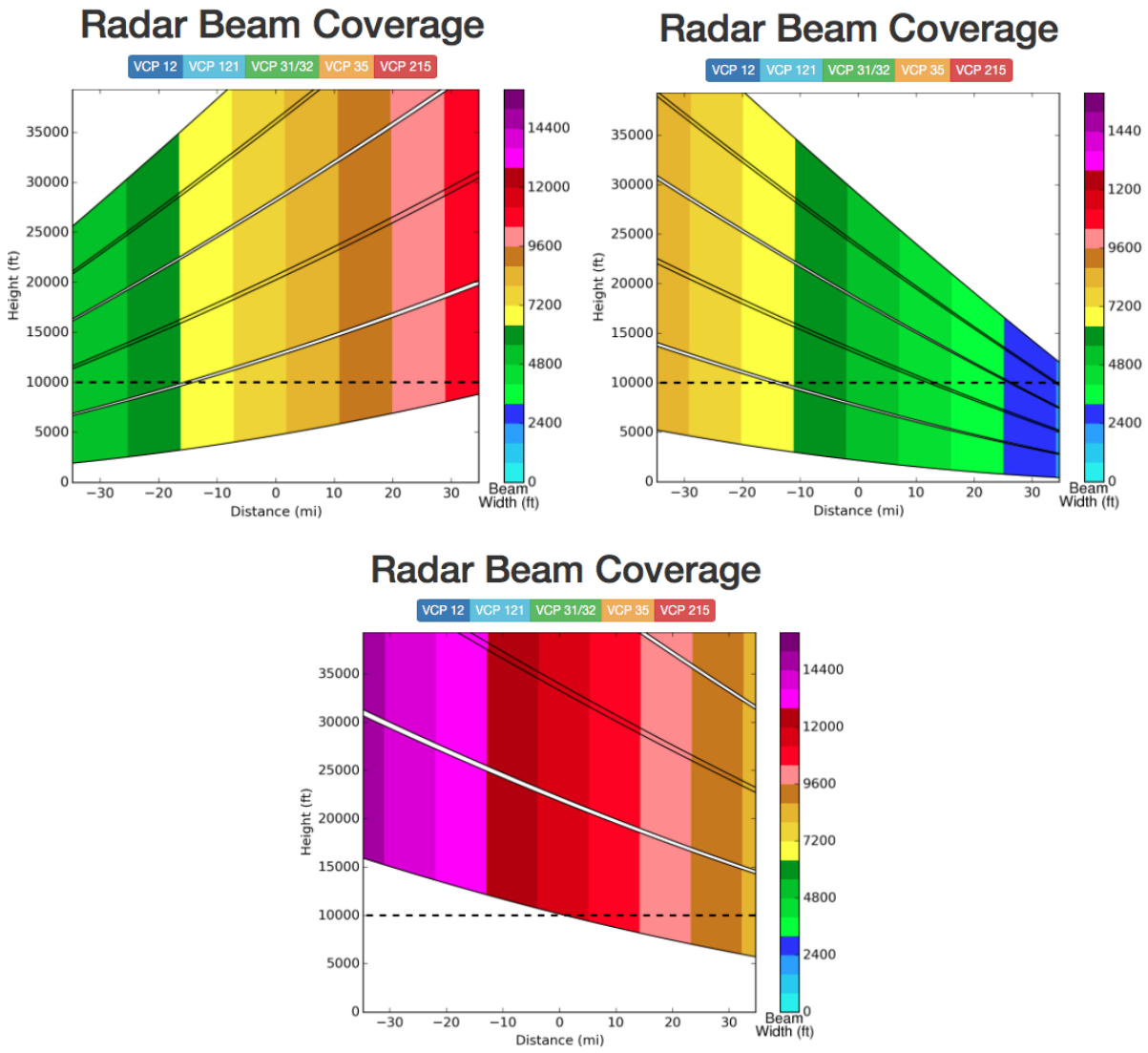

Figure 49. Same as Figure 47, but for KCID, and relative to the KDMX (left), KDVN (right) and KARX (bottom) NEXRADs. The plot for KDMX/KCID and KARX/KCID plots are approximations using other pairings at essentially the same distance within similar terrain.

6.5.3 Ground suites #3, #4, and #5

Three additional ground suites were deployed to address gaps in the ASOS/AWOS network with respect to icing-relevant reporting capabilities (see Table 9 and Figure 45). Instruments were installed at the following three AWOS sites:

- South Haven, MI (KLWA), ~127 nm E of KRFD and ~32 nm W of KAZO
- Sterling, IL (KSQI), ~38 nm SW of KRFD
- Decorah, IA (KDEH), ~134 nm NW of KRFD

None of the AWOS sites within the domain have a FZRA sensor. Meanwhile, all of the ASOS sites do have a freezing rain sensor, which allows them the ability to report FZRA automatically. As noted in Section 3.2.1, only ASOS sites at Service Level A and B airports, and sometimes Service Level C, can report FZDZ and PL (indicative of SLD aloft) due to the presence of CWOs or LAWRS observers, respectively. KSQI has an AWOS IIIP/T, while KDEH and KLWA each have an AWOS IIIP. These particular classes of stations have a present weather sensor with some reporting capability, but no freezing rain sensor. Icing-relevant gaps that exist in the network and locations of the sub-sites are shown in Figure 45.

6.6 Pilot reports

The primary ICICLE domain is a good area for pilot reports (see examples in Figure 50), because it contains a few major airports with heavy traffic (e.g., Chicago O'Hare) and numerous small-to-midsize airports with lighter traffic (e.g., Grand Rapids, South Bend, Green Bay, Des Moines). As noted earlier, the airspace with the heaviest air traffic needs to be avoided during ICICLE, but numerous, relatively quiet areas can be used for sampling because they allow for efficient sampling, while PIREPs are often still plentiful in nearby areas. A wide variety of aircraft types fly in this region, covering a range of speeds and carrying different ice protection systems. This can result in rather different perspectives for the same icing environment, sometimes resulting in different reported severity and type. Data are available as text and graphics.

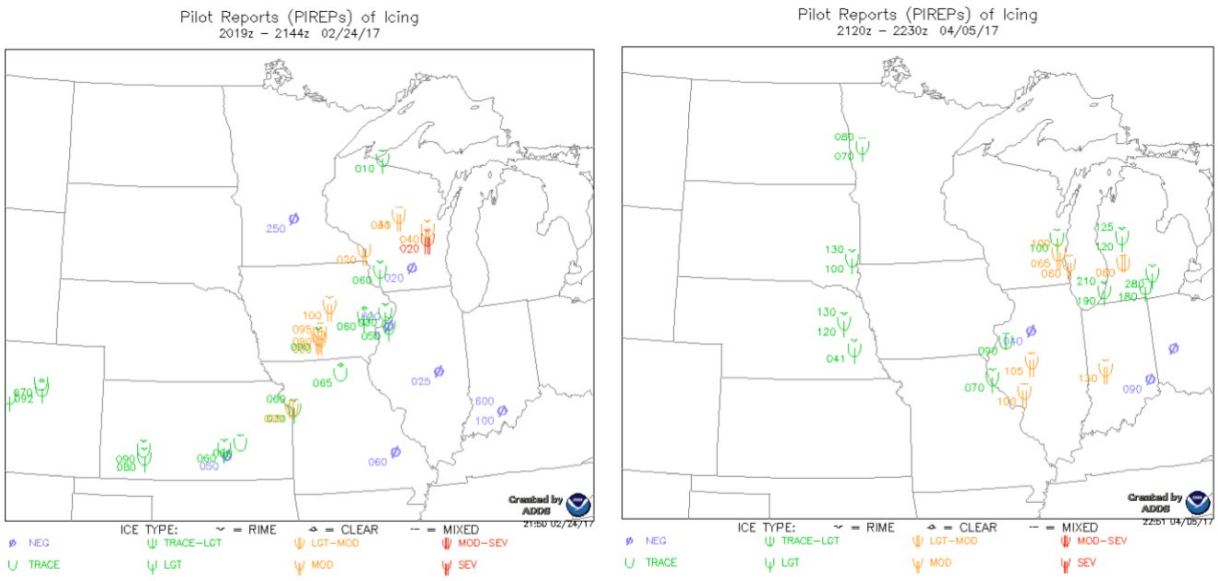

LSE UA /OV LSE180003/TM 2144/FLDURGD/TP CRJ2/SK BASES 020 OVC/TA BTWN -10 AND -2/IC MOD RIME ALL THE WAY DOWN
MLI UA /OV DVN/TM 2143/FL040/TP BE9L/SK OVCUNKN-TOP058/IC LGT RIME/RM DURC
MCI UA /OV MCI/TM 2140/FL070/TP C750/SK OVC050-TOP065/TA M10/IC LGT CLR 050-065
MIW UA /OV ALO225030/TM 2140/FL100/TP C208/TA M12/IC MOD RIME
RHI UA /OV RHI/TM 2138/FL070/TP CRJ2/SK BASES30-TOP90/TA M15/IC TRACE RIME
LSE UA /OV LSE/TM 2133/FL035/TP CRJ2/SK OVC020/TA M10/IC MOD RIME
MKC UA /OV 10 M SW/TM 2133/FL060/TP G150/TA -10/IC LGT-MOD MIXED
MCI UA /OV MCI130015/TM 2131/FL060/TP C25A/SK OVC030-TOP060/TA 01/IC LGT RIME 030-060
CWA UA /OV CWA/TM 2110/FL040/TP CRJ2/TA M08/IC MOD MX 040-BLO/RM DURD
KATW UA /OV 5 MI SW ATW/TM 2108/FL040/TP BE20/IC MDT RIME ICG/RM MDT RIME ICG ENCOUNTERED FROM 040-SFC
IRK UA /OV IRK/TM 2104/FL065/TP C402/SK TOP 065 BKN 016/TA 0/IC TRACE CLR/RM DURD ZKC FDC
DSM UA /OV DSM090015/TM 2101/FL090/TP BE40/TA -11//IC MODERATE MIXED ICING 090-SURFACE
KCID UA /OV CID110015/TM 2058/FL060/TP C208/SK OVC/TA M04/IC LGT CLR
CNC UA /OV DSM135020/TM 2055/FL095/TP CRJ9/SK OVC021-TOP095/TA M08/IC MOD MX 095-030/RM DURD
MLI UA /OV DVN360015/TM 2055/FL030/TP BE9L/TA M01/IC LGT RIME
IWD UA /OV IWD/TM 2050/FL010/TP C208/TA M08/IC LGT RIME 060 AND BLO/RM DURD
KDEC UA /OV DEC060010/TM 2050/FL025/TP FA7X/SK TOPS 37 BASES 27/TB NEG/IC NEG/RM ON APP TO KDEC
ORD UA /OV OVS/TM 2047/FL060/TP C208/TA M02/IC LGT RIME
MLI UA /OV MLI/TM 2040/FL050/TP C208/SK T046/TA M02/IC LGT RIME
MSN UA /OV MSN/TM 2040/FL020/TP CRJ9/SK OVC020-TOP068/IC NEG
KRFD UA /OV KRFD/TM 2035/FLDURGD/TP B738/SK OVC003-TOP040
KOSH UUA /OV KOSH/TM 2025/FL020/TP PAYI/6/TA M02/IC SEVER RIME 020
DSM UA /OV DSM130015/TM 2020/FL090/TP CRJ7/TA M11/IC LGT RIME 090-070 MOD MX 070-060 TRC MX BLW 060
MLI UA /OV MLI/TM 2019/FL055/TP C56X/SK B011/OVC/T050 CLR ABV/IC NEG ICE/RM DURC

Figure 50. Pilot Reports of icing from two example events. Indicators of reported severity and type are given beneath both charts. Text from select reports in the left panel are given in the bottom panel. Images and text generated from the NOAA Aviation Weather Center website.

6.7 Soundings

There are three operational NWS Weather Forecast Office (WFO) sounding sites within the primary ICICLE domain (see Figure 51), located at Green Bay WI (KGRB), Davenport IA (KDVN) and Springfield IL (KILX). There are four other NWS sites near the outer edge of the domain: Twin Cities/Chanhassen MN (KMPX), Gaylord MI (KAPX), Detroit/Pontiac MI (KDTX), and Wilmington OH (KILN). Vertical profiles of the environment are taken daily at these sites at approximately 00Z and 12Z. The NWS network is augmented by four universities launching on-demand soundings within the ICICLE domain that. Their aim was to capture

representative and/or relevant profiles in areas where flights were expected. Launches could be made during 1) the pre-dawn hours to provide information to forecasters working early-morning shifts, and/or 2) the hours during and surrounding flights to provide additional documentation of events. Participating universities included Iowa State University (ISU), Northern Illinois University (NIU), University of Illinois Urbana-Champaign (UIUC) and Valparaiso University (Valpo). ISU, NIU and UIUC soundings were all launched from fixed sites. Valparaiso University has the ability launch remotely if the weather situation dictates (e.g. "Valpo-KBEH," Benton Harbor MI). The sounding systems at each supplemental sounding location for ICICLE are as follows:

- Valpo – Intermet iMet-3050 and iMet-3200
- ISU – Metropolitan State University of Denver Qinetiq Tactical Sounding System
- NIU – Intermet iMet-3050A
- UIUC – Intermet iMet-3050

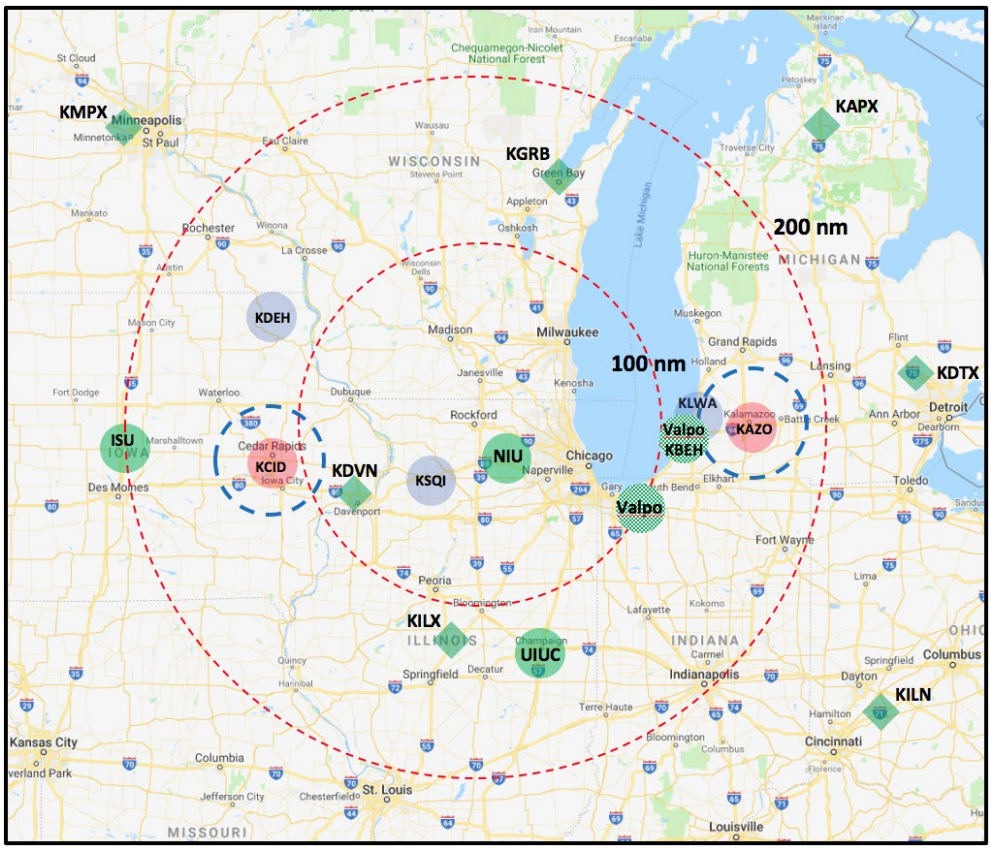

Figure 51. Locations of supplemental (green dots) and NWS (green diamonds) sounding sites. 100 nm and 250 nm range rings from KRFD (dashed red circles) and 30 nm rings around ground suites are shown: KAZO, KCID (large red dots), KLWA, KSQI and KDEH (large blue dots).

6.8 NWP models

As described in Section 3.2.6, NWP models provide 4-D forecast grids of icing-relevant fields such as temperature, humidity, microphysics, surface precipitation and winds across the NAS. Among the operational models run at National Centers for Environmental Prediction (NCEP), the HRRR and the RAP models have continued to be of particular interest to FAA icing projects. The RAP provides the background 3-D fields used by the operational CIP and FIP, while the HRRR is slated to supplant the RAP model in this role. Other operational models such as the NAM and GFS are useful for long-range planning. All of these models easily cover ICICLE's primary and alternative domains. The HRRR has the finest grid spacing among these four models (see Figure 52). Grid spacing, forecast length, underlying physics and available fields that are relevant for icing vary from model to model.

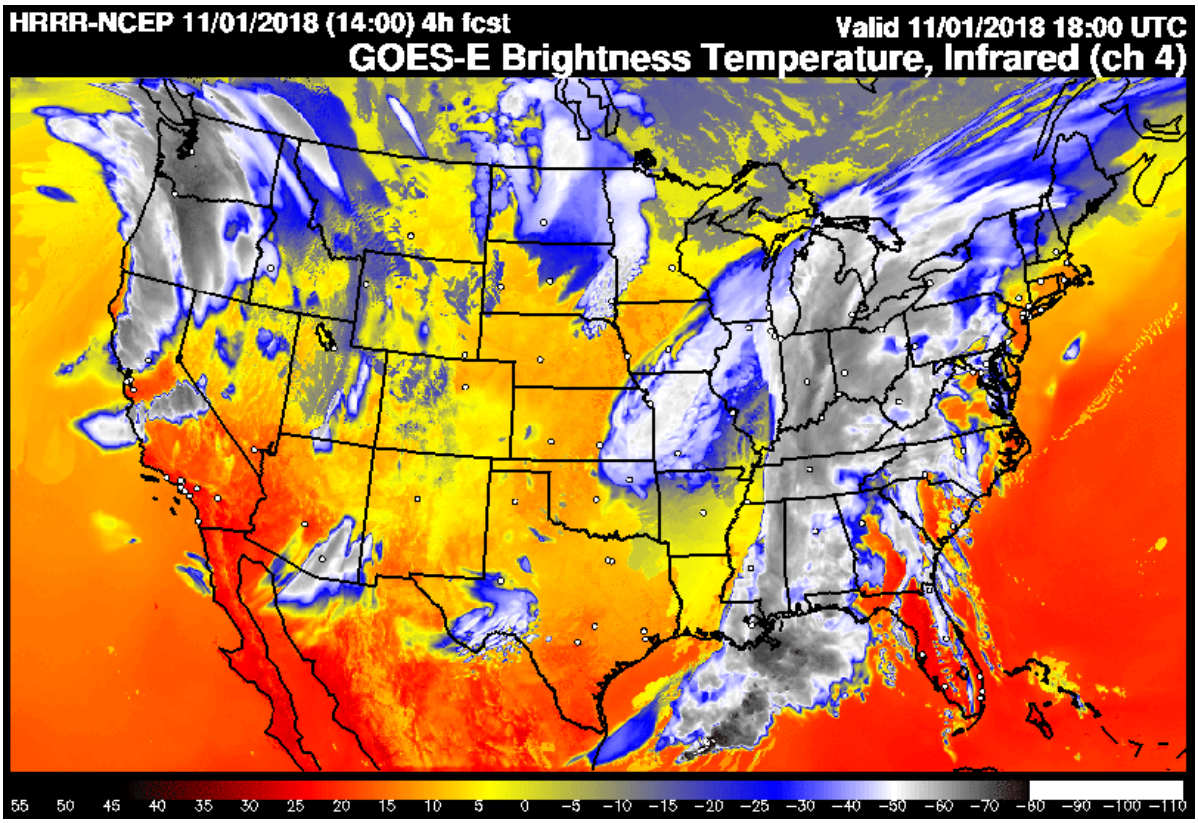

Figure 52. Example chart of operational HRRR model forecast infrared brightness temperature (synthetic, long-wave infrared satellite image). Image generated from NOAA HRRR website.

Some experimental derivatives of high-resolution model output will be made available during ICICLE. These include time-lagged ensembles of the operational 3-km HRRR microphysics output and an even higher resolution version of the HRRR with 1-km horizontal grid spacing and additional vertical levels, with the intent of better representing fine-scale icing features and low-

altitude icing environments (see Figure 53). A 0.6-km version of the WRF model running the Thompson and Eidhammer (2014) microphysics package was also available, further testing the limits of models to forecast very-high resolution icing features (see Figure 54). During ICICLE operations, real-time output and graphics will be available from all of the operational and experimental models described above, allowing for their use in program-related decisions and model assessments.

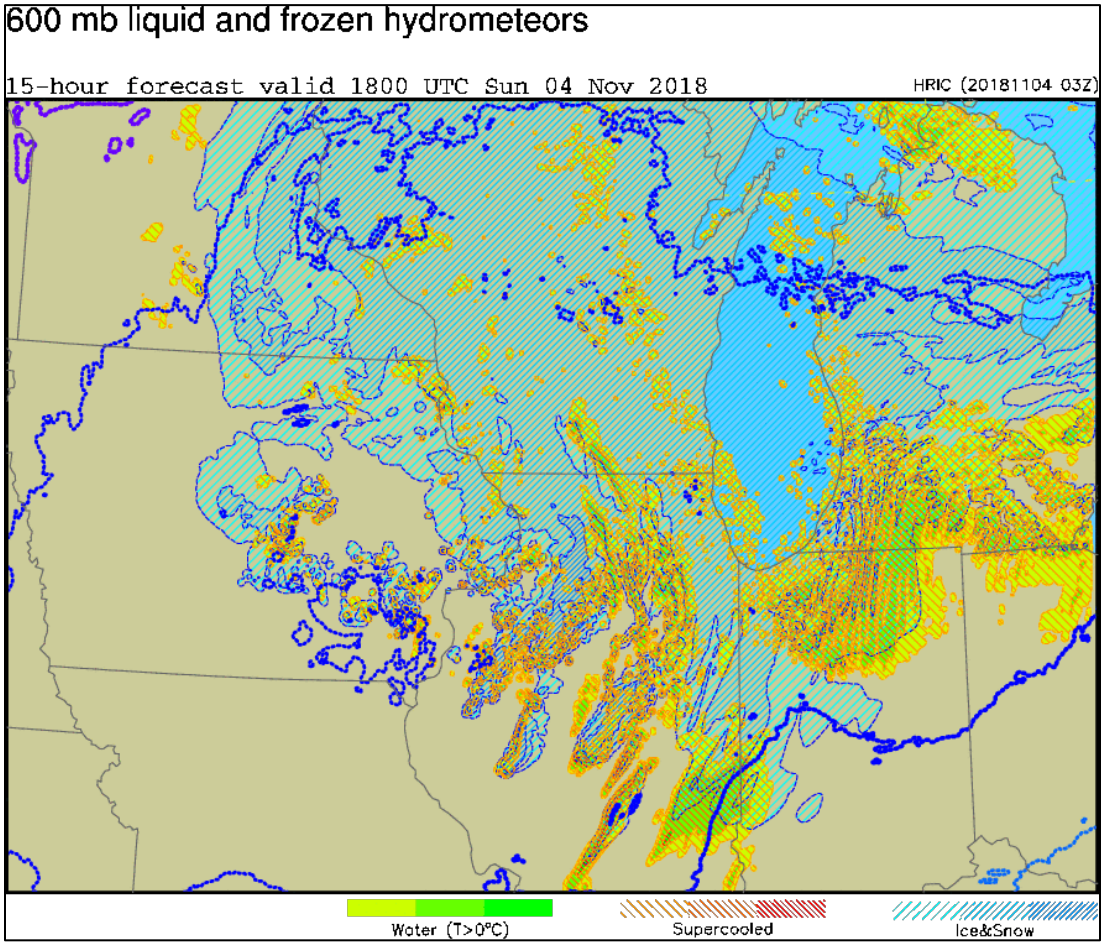

Figure 53. Column maximum plot of 1-km HRRR-model microphysics showing predicted locations of supercooled liquid water (green overlaid with red hatching).

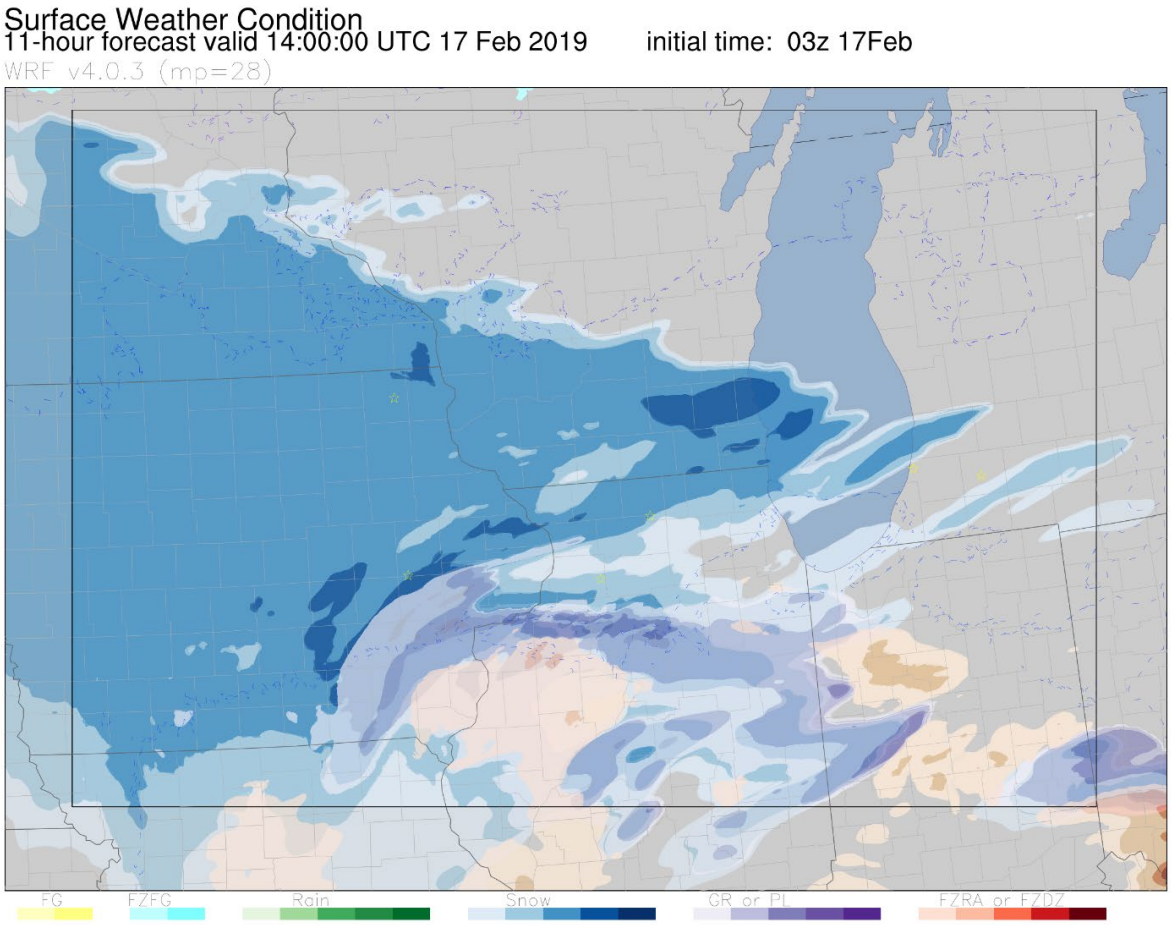

Figure 54. Plot of an 11-hr forecast of surface weather conditions from the 600-m version of WRF. Shading represents intensities of fog (yellow), freezing fog (cyan), rain (green), snow (blue), graupel/ice pellets (purple) and freezing precipitaiton (FZDZ and FZRA; red).

Observations made during ICICLE will help to assess the validity of fine-scale features depicted by these models, both at the surface and aloft. Highly variable icing features in space and time have been documented in observational flight data on numerous occasions (Sand et al. 1984; Rasmussen et al. 1995; Miller et al. 1998; Isaac et al. 2005). This analysis will provide highly-valuable feedback to model developers and downstream algorithm developers regarding how well the models are capturing and forecasting these features, including in the microphysics fields. The results may have a significant impact on how fine-scale model output will be applied in real-time icing products.

Additionally, in contrast to prior icing field projects, ICICLE will attempt to characterize the aerosol populations entering clouds. The purpose is to assist numerical model developers in making improvements associated with the modeling of the activation of aerosols as water drops as they relate to LWC and MVD and ice crystals as they relate to crystal concentrations. Both

can impact a model's ability to simulate the propensity for clouds to produce and maintain SLW and SLD.

6.9 Summary of platforms and data sources

It is essential for data from numerous sources to be reliably available in real-time for diagnosis, forecasting, operational decisions, and planned comparisons with aircraft data. Many of these datasets are described in Sections 3 and 6 above, and they are summarized in Table 10 below. The Convair-580 research aircraft is not included this table, because it is covered thoroughly in Table 7. European collaborator products are included in an effort to coordinate and leverage research and development of icing products and weather models internationally.

Table 10. Summary of data sources and whether they will be in the ICICLE Field Catalog ("FC") and data archive ("AR").

Dataset	Source	Location	Timing	Frequency	Fields	FC	AR	Notes
Satellite	GOES	75.2°W	24/7	5 min (1-min during requested periods)	Imager, derived fields, advection products, NASA-LaRC Cloud Product Suite	Y	Y	Primarily GOES-16. GOES-17 has steeper viewing angles. Polar orbiter scans also possible.
Radar S-band	NEXRAD, MRMS	Numerous	24/7	Variable	Reflectivity, velocity, dual-pol, derived fields, RadIA	Y	Y	~12 NEXRADs cover primary ICICLE domain.
Soundings	NWS	Numerous	Nominally 0Z, 12Z	Nominally 12-hourly	Profiles of P, T, Td, winds	Y	Y	KDTX, KGRB, KDVN, KILX within primary domain.
Soundings	Supplemental	TBD	On-demand	On-demand	Same as above	Y	Y	Launched by Valparaiso University, Northern Illinois University, University of Illinois Urbana-Champaign, Iowa State University.
Surface observations, METARs	ASOS, AWOS, other networks	Numerous	24/7	Variable	T, Td, P, winds, cloud coverage, ceiling, visibility, precipitation presence and type, obscurations, altimeter, etc.	Y	Y	Capability varies by station type, instrument suite and augmentation by human observers. FZDZ algorithm output.

Dataset	Source	Location	Timing	Frequency	Fields	FC	AR	Notes
Surface Observations	Supplemental sensors for Present Wx, FZRA. Disdrometers,	Super-sites and sub-sites	24/7	6 second, 1 minute	Presence of precipitation, precip type, icing, drop size	Y	Y	Instrument combinations for each of the five ground suites (KAZO, KCID, KLWA, KSQI, KDEH) are described in Section 6.5
Surface Observations	Volunteer Observers	Across ICICLE domain	Variable	TBD, likely variable	Presence of precipitation, precip type, accumulation.	Y	Y	mPING, CoCoRAHS (see Reges et al. 2016)
Pilot Reports	Pilots, ATC	N. America	24/7	Variable	Icing severity, type, altitude, T, clouds, turbulence, winds, remarks	Y	Y	Variable quality. Information varies by report. Density & frequency vary.
Lightning	NLDN	N. America	24/7	< 1 min	Lightning presence, polarity	Y	Y	CG from NLDN
Numerical Models	NCEP Operational: HRRR, RAP, NAM, GFS	CONUS +	24/7	Model dependent	State parameters, microphysics, precipitation amount & type, winds, etc.	Y	Y	Operational models. Maps and vertical profiles.
Numerical Models	NCAR, NOAA/ESRL: HRRR (3-km, 1-km, TLE), WRF	Varies	Varies	Varies. ESRL 1-km HRRR runs 1-2 times daily	State parameters, microphysics, precip amount & type, winds. Time-lagged ensemble, fractional-cloudiness.	Y	Y	Experimental runs. Maps, vertical profiles, vertical cross-sections.
Icing Products	CIP, FIP	CONUS +	24/7	Hourly	Icing probability, severity, SLD potential. Intermediate fields and test fields (experimental only)	Y	Y	Operational and experimental runs. Intermediate & test fields may include scenario, LWC, SLD sub-categories, D_{max}, etc.
Icing Products	AWC AIRMETs, SIGMETs	CONUS	24/7	G-AIRMETs (3-hourly), SIGMETs (as needed)	Advisories and warnings, icing severity and type, sometimes SLD	Y	Y	Operational, text and graphical
European Collaborator Products	Météo France, DWD, UKMO	Varies	24/7	NWP models and icing products	TBD	N	Y	Images and/or gridded data

7 Operational Planning and Sampling Strategies

This section provides a description of the basic sampling strategies, followed by a description of how these strategies could be applied to the ICICLE Priorities described in Section 4.

7.1 Flight hours

A total of 120 flight hours are planned for the ICICLE program, approximately 110 of which are for scientific missions. This is expected to be sufficient for accomplishing the objectives described in Sections 4-5 and Table 5. Sampling strategies and flight plans have been developed to meet these objectives in a safe, thorough, efficient and practical manner. The primary approaches are described below and related to the objectives they were intended to satisfy. For demonstration purposes, sampling strategies are provided for several events that occurred during the ICICLE "Dry Run," which occurred in late October and early November of 2018.

7.2 "Dry Run" exercises

Two "Dry Run" exercises were conducted in advance of ICICLE.

- Exercise 1 – February-March 2018: Three-week forecast exercise over the primary domain, coordinating with Operations Director. Purposes were: a) for forecasters to gain familiarity with weather, data, and operational issues in primary domain, b) to assess availability, quality and reliability of real-time data sources and plots thereof, determining their ability to meet forecaster needs, and c) to establish connection between forecasts and flight-related decisions via daily communication between forecaster and operations director. Daily assessments of the forecasts and actual events were logged. No flights occurred.
- Exercise 2 – October-November 2018: One-week mock flight program, with full interaction between forecasters, the operations director and NRC/ECCC. This included mock flight planning for the day (and days that followed), taking into account meteorological conditions available, location, timing, priorities for the program, mock flight hours used, aircraft and crew readiness, traffic and other sampling limitations, and, of course, safety. Sampling strategies were applied for mock missions, though no flights occurred. Daily assessments of the forecasts and actual events were logged and some data were archived in the Field Catalog.

7.3 Sampling strategies

To sample icing events properly, it is important to have basic sampling strategies in place. These can be adjusted to meet scientific and sampling needs in the context of events that could cover a broad range of scales and complexities. Adjustments should be made on a case-by-case basis, taking into account the meteorology of the event, the Convair-580's capabilities, the sampling area's flight constraints, and safety. As with all aspects of proposed flights, Air Traffic Control (ATC) permission is necessary for them to be executed.

7.3.1 Horizontal sampling strategies (H1-H3)

Three (3) horizontal sampling options are provided below. All patterns include flight leg distances, with approximate time estimates to complete them, using the Convair-580's "science speed" of 170 kt (see Figure 55).

The H1 "straight flight leg" pattern allows the aircraft to pass back and forth along the same line multiple times, within and/or across features of interest as they evolve.

The H2 "lawn mower" pattern allows the aircraft to cover a geographic area with a series of staggered, parallel, straight flight legs. This pattern can be used to capture variability across an area and validate fields from satellite, radar, models, etc. The "racetrack" pattern is a modification of the H2 pattern, shown using a semi-transparent, grey arrow at the lower-left portion of the pattern in the center panel of Figure 55.

The H3 "box" and "bow tie" patterns are provided to allow for geographic coverage using flight legs with a different orientation. When performing H3 patterns using a series of right-hand turns, overlap of flight data and on-board radar coverage can be maximized, because the sideward-looking radars point toward the right. The bow-tie pattern is provided as a sequence, numbered 1 through 6, as shown in the right panel of Figure 55.

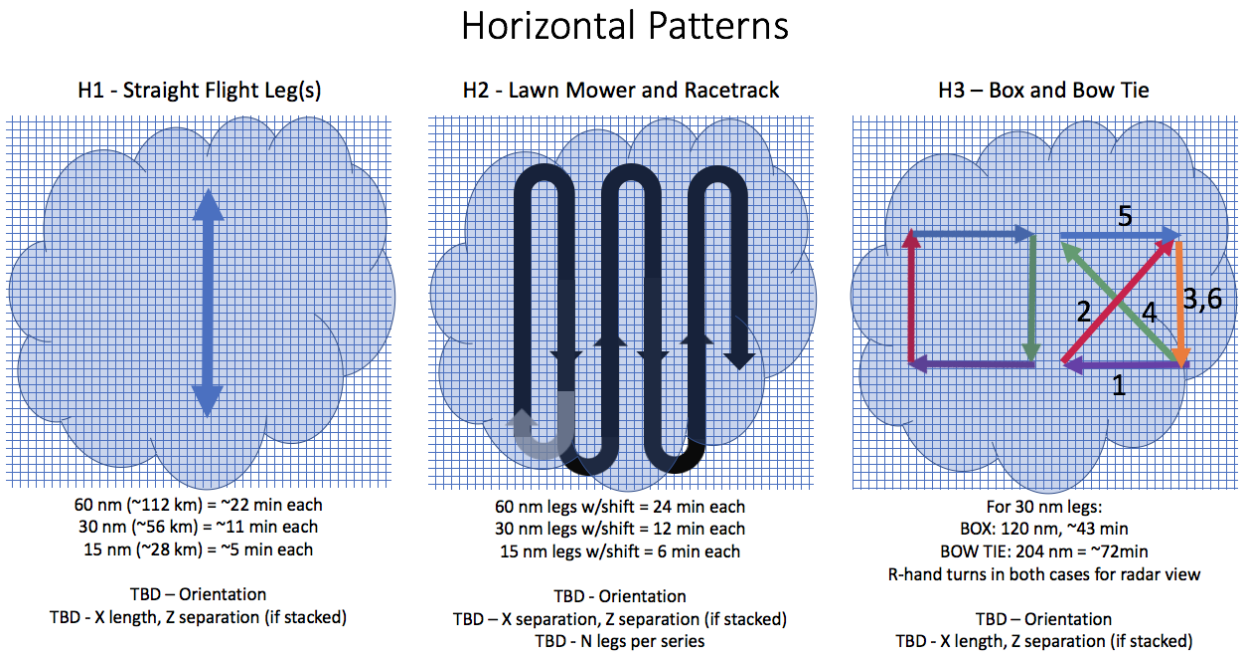

Figure 55. Basic, horizontal flight patterns H1, H2, and H3. Example flight leg lengths and approximate times needed to complete the flight legs and/or patterns are provided.

7.3.2 Vertical sampling strategies (V1-V6)

The six (6) vertical profile options developed are described below and illustrated in Figure 56.

The V1 profile is a stacked series of horizontal samples, like those described for H1 and H2 above. V1 can be performed from the top down or bottom up (reversing the arrows shown on the left in Figure 56). This pattern is sometimes referred to as a "shuttle descent."

The V2 profile is essentially a straight-line vertical profile. For example, approaching an airfield from the south on descent, completing it, and then climbing while flying away from the airfield toward the north (see Figure 56, center).

V3 is a banked, spiral descent over a given location, such as an airfield (see Figure 56, right). The oval at the bottom of V3 is a surface projection of the spiral pattern.

Vertical profiles can be preceded by a flight leg above cloud top (see dashed orange arrows) to first capture a top-down view of the clouds using on-board radar and lidar. Top-down profiles may include descent to altitudes below cloud base when desirable and practical. After completing top-down profiles, there is an option to perform a missed approach (Option A; see Figure 56), sampling altitudes very near the surface. Whether or not Option A is executed, the aircraft can either level off at a low altitude (below cloud base in some cases – Option B) or

ascend to higher altitudes (often above cloud top – Option C). Aerosol samples can be captured during level flight legs outside of cloud.

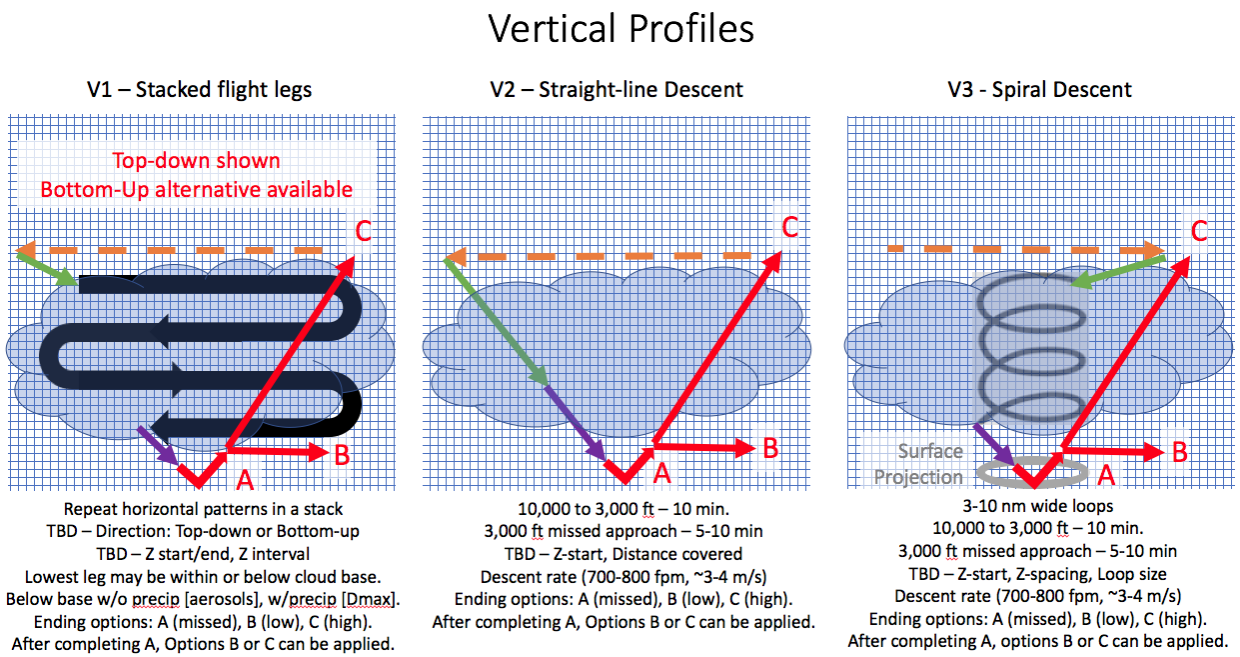

Figure 56. Standard vertical flight profiles V1, V2, and V3. Where possible, approximate times needed to complete the portions of the profiles are provided. Several items are TBD. Dashed orange lines are above-cloud leg designed to capture top-down view of cloud using radar.

The V4 profile is a (sideways) W-style descent, using a series of gradual, slanted descents along the same line. It can be employed when sampling relatively deep clouds as an alternative to V1 with large vertical spacing between level flight legs. Figure 57 (top left) shows the W-style descent followed by a missed approach pattern similar to V2.

The V5 profile is a "porpoise" pattern, typically employed for a) shallow clouds where the aircraft can quickly traverse the altitudes between cloud top and cloud base, or b) short profiles across one vertical portion of a cloud, often near cloud top (Figure 57, top right). The V5 profile is of particular interest when the clouds covered a large area. Short duration segments can sometimes be made above cloud top, like the dashed lines below cloud base in Figure 57 (top right). Sub-cloud and above-cloud aerosol sampling may be achieved via level flight legs that last several minutes (see black dotted lines in Figure 57, top right).

The V6 profile is one concept for sampling aerosols at stacked altitudes in clear air, such as upstream of cloudy areas of interest (Figure 57, bottom). Due to time constraints, only one vertical series and sampling at fewer vertical levels than indicated may be necessary.

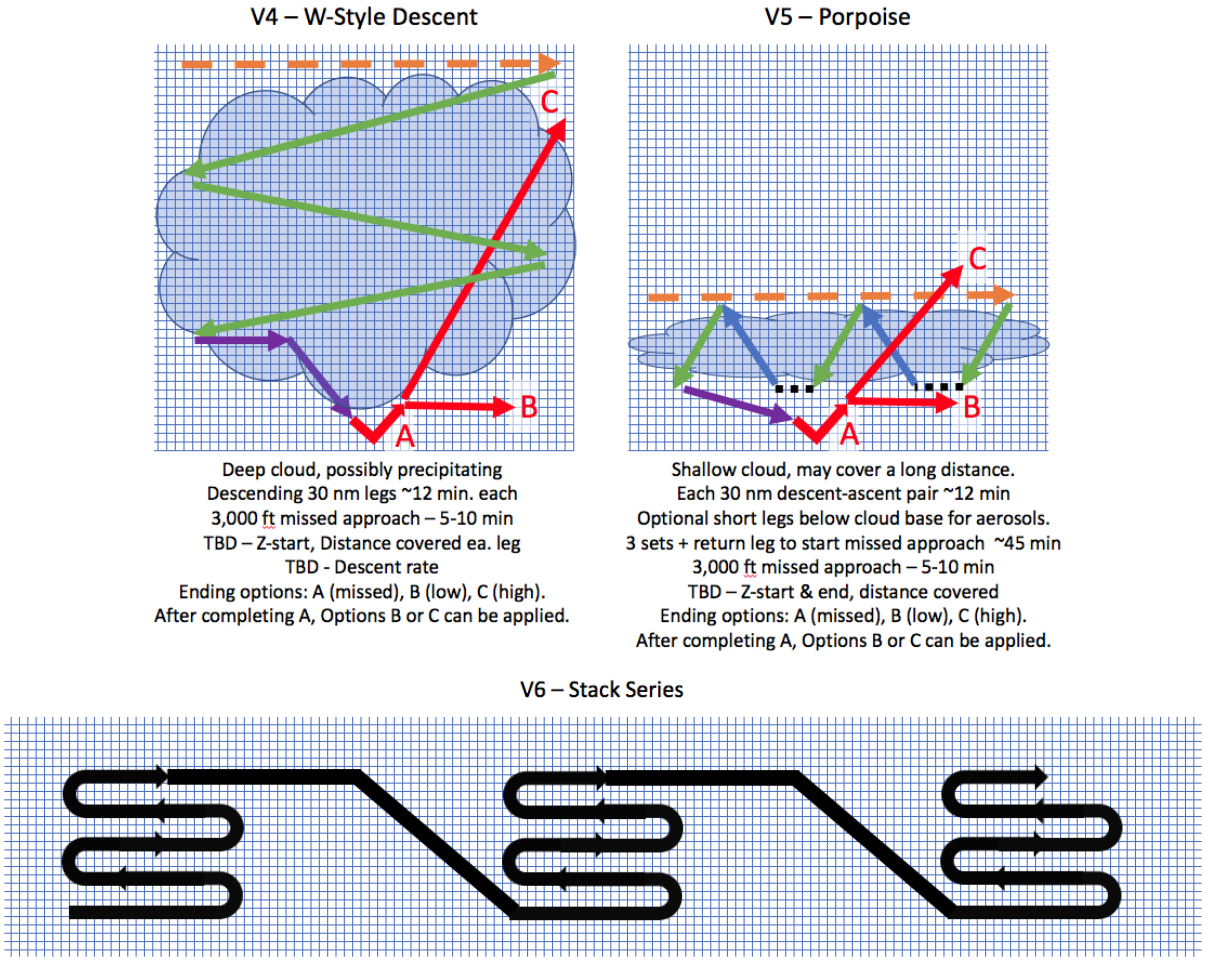

Figure 57. Same as Figure 56, but for V4, V5, and V6 profiles.

7.4 Examples of the application of horizontal and vertical patterns

Using ICICLE Dry Run cases from Exercise 2, the following examples demonstrate how the horizontal patterns and vertical profiles could have been used to sample conditions of interest. No actual flights were made during the Dry Run Exercises. The events are presented based on the relative complexity of the sampling methods considered, rather than chronologically.

7.4.1 November 2, 2018

Before dawn, a shallow layer of drizzling, supercooled clouds were present near Dayton, Ohio (KDAY) (see left panel of Figure 58). The V2 vertical profile could have been employed, starting with an over-the-top leg from NW to SE toward KDAY, followed by a missed approach through the clouds and drizzle at KDAY (V2, option "A"). After completing the missed approach, the climb could have been broken off at 5000 ft (V2, option "B") to start a stacked

lawnmower pattern (H2) at 5000 ft and 8000 ft to the northwest of KDAY (right panel Figure 58). The 5000 ft and 8000 ft levels would have captured data just above the freezing level and just below cloud top, respectively. The HRRR predicted supercooled DZ and LWC as high as 0.6 g/kg in this altitude range (center panel Figure 58). The V2 profile would have captured a vertical profile of the supercooled- and above-freezing liquid clouds and precipitation over KDAY, while the H2 lawnmower pattern would have captured the horizontal variability in satellite indicated drop-size, radar reflectivity, surface observations and model forecast microphysics fields over and near KDAY. An alternative vertical sequence would have the above-cloud run followed by lawnmower legs at 8000 ft, then 5000 ft, then a missed approach followed immediately by climb above cloud top. This is essentially the reverse of the sequence described above.

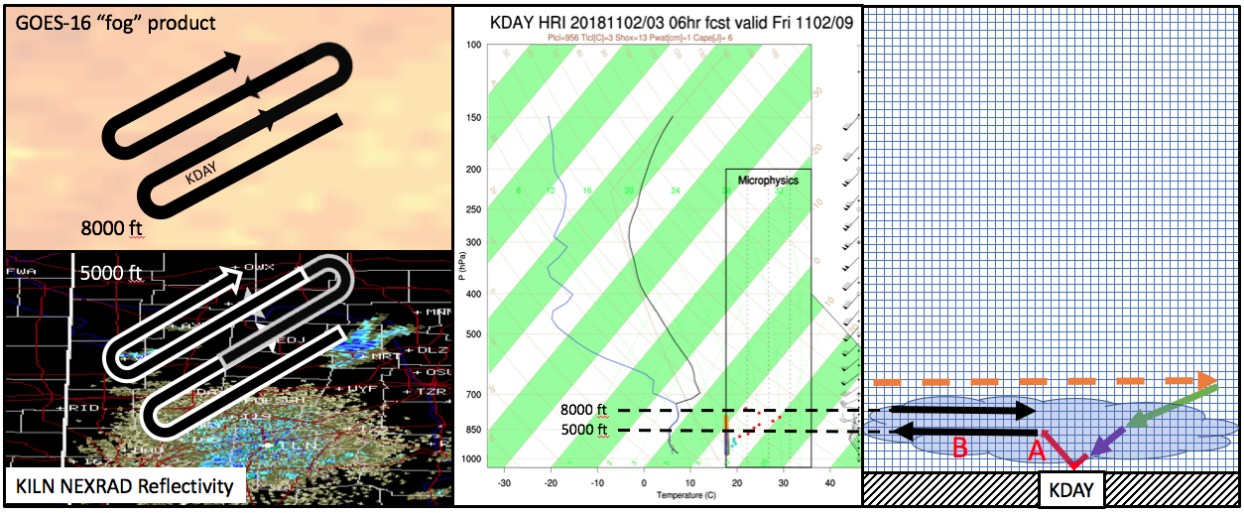

Figure 58. Combined H2, V2 sampling strategy that could have been executed in the drizzling clouds near KDAY.

7.4.2 November 1, 2018

A shallow, fairly uniform swath of stratocumulus clouds was present over the western Upper Peninsula of Michigan. These clouds streamed inland from Lake Superior, impacting Ironwood and Houghton (KIWD and KCMX) (see Figure 59). Slight variations in drop size and breaks in the clouds were evident in GOES-16 imagery, while minimal precipitation was evident on the Marquette, MI radar (KMQT) (see Figure 59, top). METARs indicated cloud bases near 3000 ft AGL (~4100 ft MSL) (see Figure 59, bottom). These clouds were candidates for porpoise sampling (V5) along a straight line cutting across the mild gradients described above, with the possibility of capturing clear air data below cloud base. A combination of H1 and V5 could have been employed, beginning with a pass over the cloud top for remote sensing followed by a

missed approach into KIWD (Option A), then a climb through the cloud to above cloud top (Option B), leading into the porpoise maneuver. Aerosol runs beneath cloud base could have also been made, if desired.

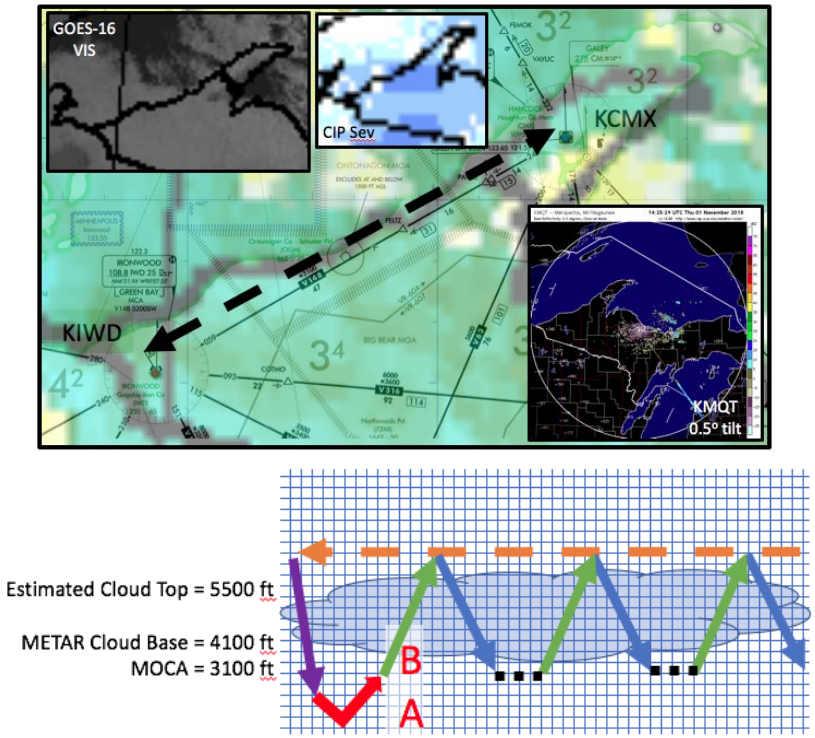

Figure 59. Combined H1, V5 sampling strategy that could have been executed through shallow, fairly uniform clouds between KIWD and KCMX. The top panel shows the orientation of the leg, crossing variations in the GOES-16 satellite imagery and the CIP severity field (upper left). The bottom chart shows the V5 porpoise profile in a vertical cross section along the flight path, including an over-the-top, downward looking leg (dashed orange line), missed approach ("A"), climb to above the cloud top ("B"), and porpoise maneuvers (green and blue arrows).

7.4.3 October 31, 2018

A highly complex, rapidly evolving situation was unfolding between Pontiac and Champaign, Illinois (KPNT and KCMI, respectively) (see Figure 60). The HRRR predicted a strong transition between mostly glaciated clouds near KPNT to water-dominated clouds with large amounts of supercooled cloud water (>0.8 g/kg) and drizzle (>0.4 g/kg) over KCMI (Figure 60, top left and top right panels). Cloud tops varied significantly in the liquid-dominated region, as demonstrated by changes in cloud top temperature across the KCMI area (Figure 60, bottom panel). Deeper, colder-topped clouds were present to the NW, including over KPNT. The tops of the deep, precipitating clouds present could have first been passed over during a NNW to SSE

leg oriented toward KCMI, gaining a top-down look at them using radar and lidar, before they would be sampled via a straight-line H1 pattern, combined with either the V1 or V4 vertical profiles. V1 (stacked black arrows) could have used a series of stacked, level flight legs from just below cloud top down to the freezing level. V4 (angled, green arrows) could have used gradual descents, cutting through the same altitudes. Both could have been followed by a missed approach into KCMI, followed by a climb to altitudes above cloud top (options "A" and "B") (see top-center panel of Figure 60).

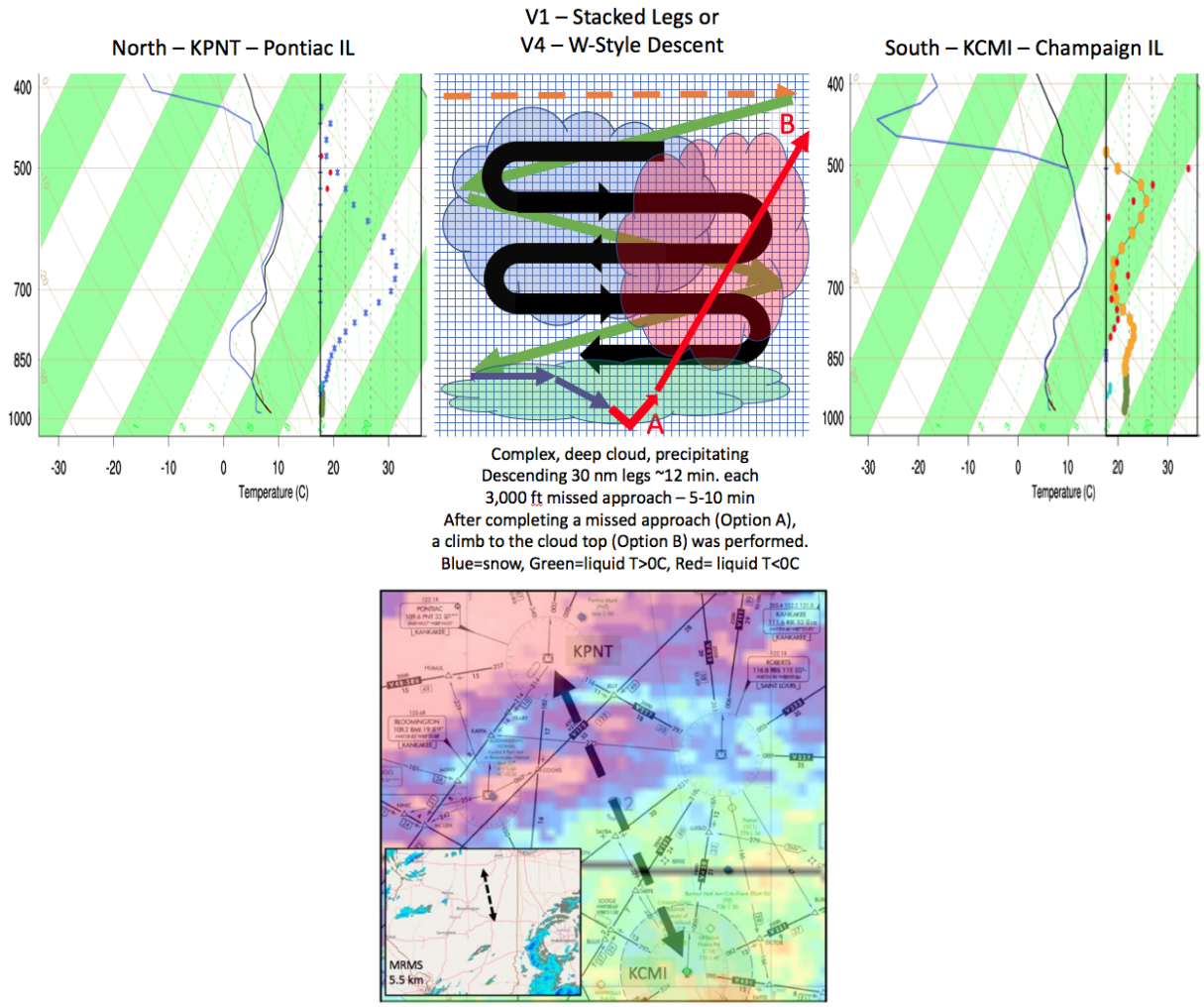

Figure 60. Combined H1, V1/V4 (black/green arrows in top-center panel) sampling strategy that could have been executed through the 31 Oct highly-variable, deep precipitating clouds near KCMI. The top panels show vertical profiles of HRRR output (left and right), and the strategies considered (center). The bottom panel shows the H1 pattern overlaid on the low-altitude IFR chart, satellite data, and the MRMS 5.5-km radar reflectivity pattern (lower-left).

7.5 Application to weather tools

It is important to consider the example application of the sampling strategies described above in the context of the spatial and temporal aspects of some of the weather tools that are being validated after ICICLE. For example, the operational RAP model and CIP and FIP have horizontal spacing of 13 km (~7 nm) every hour, while GOES-16 nominally provide infrared and visible images at 1-km (~0.54 nm) and 0.5 km (~0.27 nm) spacing, respectively, every 5 min.

For the discussion below, a 28-nm flight leg is used for simplicity. Considering horizontal grid spacing alone, an H1 sample using a 28-nm level flight leg would cover ~4 CIP grid points, but ~52 infrared and ~104 visible GOES-16 pixels. The flight leg would take ~12 min to complete, matching roughly one valid time for CIP, and two or three for GOES-16 (see Table 11).

An H2 lawnmower pattern using a series of four 28-nm level flight legs, separated by 21 nm would take roughly one hour (62 min) to complete. It would cover ~25 CIP grid points (16 along the legs [=4 points x 4 legs] plus nine more during transitions [=3 points x 3 lateral moves from one flight leg to the next]). The data from this H2 pattern could be matched to 1-2 CIP hourly diagnosis grids, depending on the timing of the sample. For GOES-16 infrared, such a sample would match ~325 pixels (208 along the legs [= 52 pixels x 4 legs] plus 117 during transitions [=39 pixels x 3 lateral moves]) over ~12 valid times. Table 11 summarizes such data matching using nominal values for grid spacing and timing for several icing tools.

Table 11. Rough comparison of how the spatial and temporal data from several weather tools compares to basic examples of the H1 and H2 flight patterns. Some values are approximate.

		Nominal			Data Points and Valid Times Covered (approx)				
Tool	Field	X/Y-spacing (km)	Z-spacing (ft)	Frequency (min)	H1: 28 nm leg	H1 Time = 17 min	H2: four 28 nm legs, 21 nm apart	H2 Time = 61 min	Notes
CIP/FIP (operational)	All	13	500	60	4	1	25	1	Experimental versions using HRRR have finer resolution
RAP	All	13	Variable / 25 mb	60	4	1	25	1	
HRRR (operational)	All	3	Variable / 25 mb	60	17	1	106	1	
HRRR TLE	All	3	Variable / 25 mb	60	17	1	106	1	
GOES-16	Infrared, all but visible	1	N/A	5	52	3	325	12	
GOES-16	Visible	0.5	N/A	5	104	3	650	12	
NEXRAD	Reflectivity, Dual-Pol	1	Variable	6	52	3	325	10	Frequency: 4-10 min/set of sweeps. Range resolution of 1 km taken from NCDC level-II data description for reflectivity. Dual-pol values are assumed to match. Z-spacing depends on distance and scan strategy. X/Y-spacing also depends on distance, but a value of 1 km is used here.
MRMS	All	1	820	2	52	9	325	31	Frequency: updates at each location depends upon updates from each NEXRAD. Z spacing: 0.25km = 820 ft

7.6 Application to ICICLE weather conditions

It was expected that, when practical, the sampling patterns described above would have been applied for each of the desired weather conditions for ICICLE, numbered 1 through 10 (see Table 5). Suggested strategies for each condition are provided below.

7.6.1 Conditions 1, 2, 6, and 8

CONDITION 1 –FZDZ aloft down to the surface

CONDITION 2 –FZDZ aloft only

CONDITION 6 – Shallow stratocumulus

CONDITION 8 – Typical Appendix C

- In some cases, conditions may be coincident (e.g., conditions 6 & 8; App. C in shallow stratocumulus)
- For conditions 1, 2, 6 and 8, any combination of H1-H3 and V1-V5 could be used.

- Cloud tops tend to be on the order of 3,000-10,000 ft MSL, making them easy to reach.
- When cloud tops are below MEAs (e.g., 2,600-3,000 ft MSL near KAZO), it may only be possible to sample them via missed approaches.
- Cloud bases are commonly between 200 and 1,000 ft AGL.
- This often places the cloud bases below MEA. See notes for cloud tops above.
- Sub-cloud, level flight legs are possible when ceiling heights are sufficiently high to allow for safe visual flight rules (VFR) flight.
- When sub-cloud flight legs are possible, they could be used for condition 1 (FZDZ aloft to the surface) and conditions 2, 6 (icing aloft only, not reaching the ground).
- When sub-cloud, level flight legs are not possible, the sub-cloud region can only be sampled via missed approaches.
- When multiple cloud layers are present, sampling strategies will be adjusted accordingly.

7.6.2 Condition 3

CONDITION 3 – FZDZ Seeder-Feeder

- This is generally a multi-layer icing situation, where the upper layer produces snow that falls into a lower layer that contains FZDZ.
- The approach is similar to that described above, but additional flight legs and greater vertical profile depths may be required to document both the snow-producing, upper cloud layer and the lower, drizzle-laden layer. Note that the snowing, upper cloud layer could also contain SLW, especially near cloud top, even when cloud tops are relatively cold (Rauber and Tokay 1991).
- It is important to document the top of the upper cloud layer and the cloud-free region between the cloud layers.
- Any combination of the H1-H3 and V1-V5 can be applied.

7.6.3 Condition 7

CONDITION 7 – High liquid water content (LWC) and/or Median Volumetric Diameter (MVD)

- These are defined in terms of the Appendix C envelope (see Figure 61).
- High LWC cases are near or above the highest values in the envelope (y-axis).
- High MVD cases are near or just to the right of the envelope (x-axis).
- In some cases, these environments may have some similarities to Conditions 1, 2, 6, and 8, such as horizontal and vertical extent, altitude.
- High MVD clouds often occur in low-droplet concentration situations, where cloud layers develop above the boundary layer. In these situations, the entire cloud may be located

above the MEA, which could allow for sampling of the sub-cloud layer. Sampling aerosols at more than one level, capturing vertical variation, such as above and below stable layers, may be desirable in some cases.

- High MVD clouds can be embedded between cloud layers or occur in narrow seams, both of which could be difficult to find and sample consistently. On-board remote sensors could be particularly useful when seeking and sampling these clouds effectively.
- High LWC clouds are known to occur in unstable environments, with relatively warm cloud bases (high mixing ratios) and sufficient depth to realize the significant LWC. Cloud tops are often warm enough that liquid water is expected to dominate, or phase changes had not yet commenced when cloud tops have cooled into a range where ice crystals are expected to develop. Such clouds often have relatively small areal extent and are highly variable in both space and time, such as a field of deep, broken cumulus (see Figure 62). On some occasions, widespread areas of deep stratocumulus can feature high LWC (e.g., Bernstein et al 2006a, 2011).
- For high MVD and especially high LWC cases, sampling strategies H1-H3 and V1-V5 can be applied, but hit-or-miss conditions are likely.

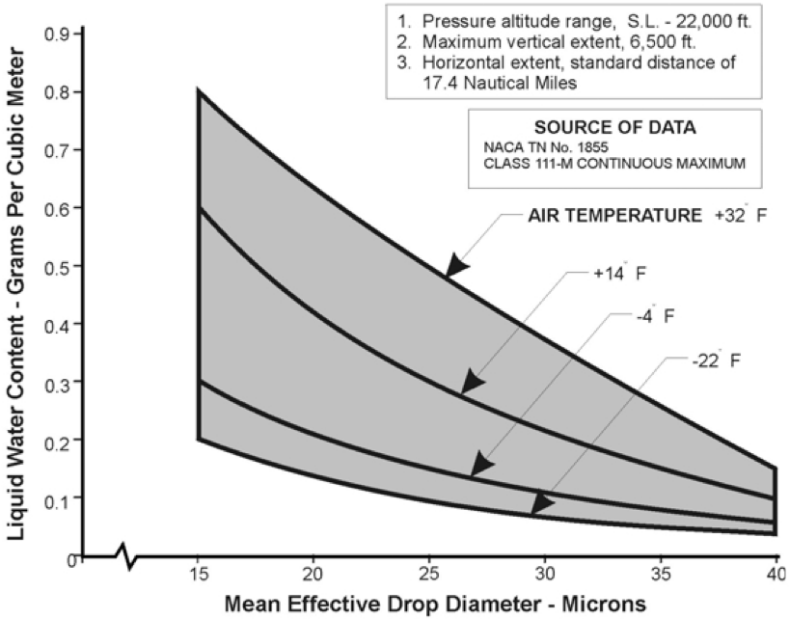

Figure 61. FAR 1419, Part 25 Appendix C stratiform icing envelope

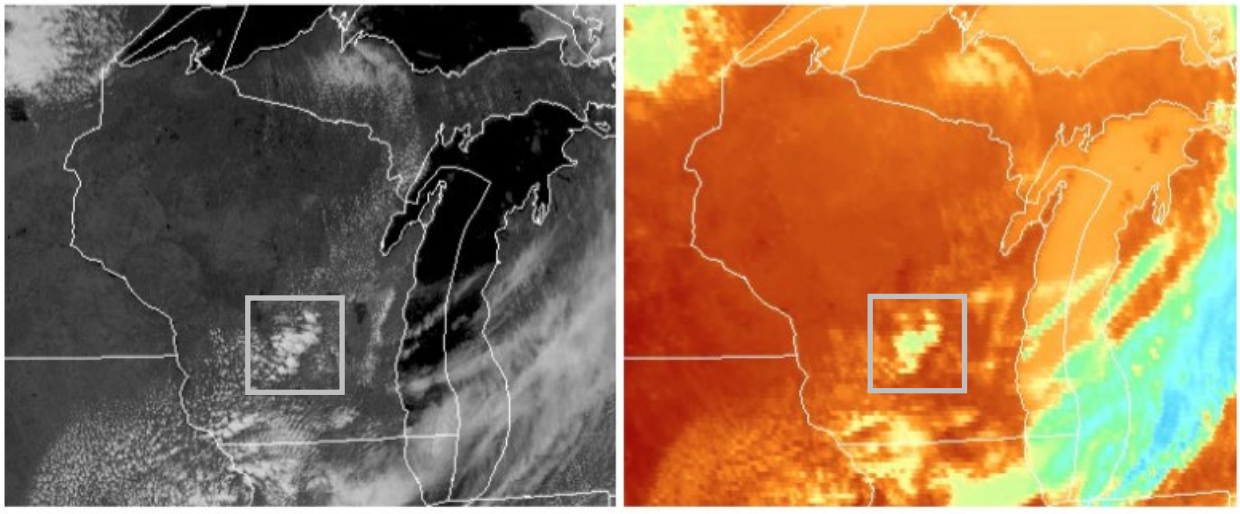

Figure 62. Example visible (left) and longwave IR (right) imagery for a small area of high LWC (relative to App. C) cumulus over south-central Wisconsin.

7.6.4 Conditions 4 and 5

CONDITION 4 –FZRA

CONDITION 5 – Classical ice pellets (PL)

- Classical FZRA and PL situations are unique, commonly associated with overrunning, and often feature marked transitions in precipitation type at the limits of the "warm nose" (T>0C layer) and the "cold wedge" (lower sub-freezing layer) (see Figure 2 and Figure 63).
- Cloud top altitudes can be too high to be practical to reach.
- Snow production ranges of most interest include the dendritic and aggregation zones.
- The warm nose, where snow melts to form rain, generally narrows toward the colder side of the transition zone, while the cold wedge (a.k.a. lower sub-freezing zone), where the RA becomes supercooled to form FZRA, is expected to become deeper.
- Where the warm nose narrows to the point where melting becomes incomplete, PL is expected to form within the cold wedge.
- Further into the colder part of the transition zone, melting would no longer occur and SN would typically reach the ground.
- The height of the upper and lower 0ºC isotherms can change significantly across the transition zone.
- FZRA cases tend to be shallow (see Figure 31 and Figure 63), so MEAs are sometimes near the top of the cold wedge, making sampling of the FZRA layer difficult or impossible using level flight legs. In such cases, a missed approach (Option A) or spiral

descent (V3) can sometimes be the most effective way to sample the FZRA and/or PL zones.

- If cold wedge and warm nose are located above MEA, then patterns H1-H3 can be particularly useful, especially with flight legs oriented across the temperature gradient and precipitation type transition zones.
- When practical, flight legs could be made above and within the dendritic zone, the aggregation zone, in addition to the warm nose and the cold wedge.
- According to NRC, clearing of FZRA ice accretions from the aircraft are typically done via climb into the snow above the warm nose. Melting of FZRA ice accretions can also be accomplished within the warm nose.
- Significant fluctuations in air temperature, cloud-water and rain-water content are sometimes found in the lower sub-freezing zone (Jeck 2011).
- It is possible for SLW and SLD to develop within the upper subfreezing layer if snow production is inefficient or non-existent, typically with relatively warm cloud tops, and sometimes in elevated convection (Rauber et al. 2000, 2001; Bernstein et al. 2019; Figure 64).

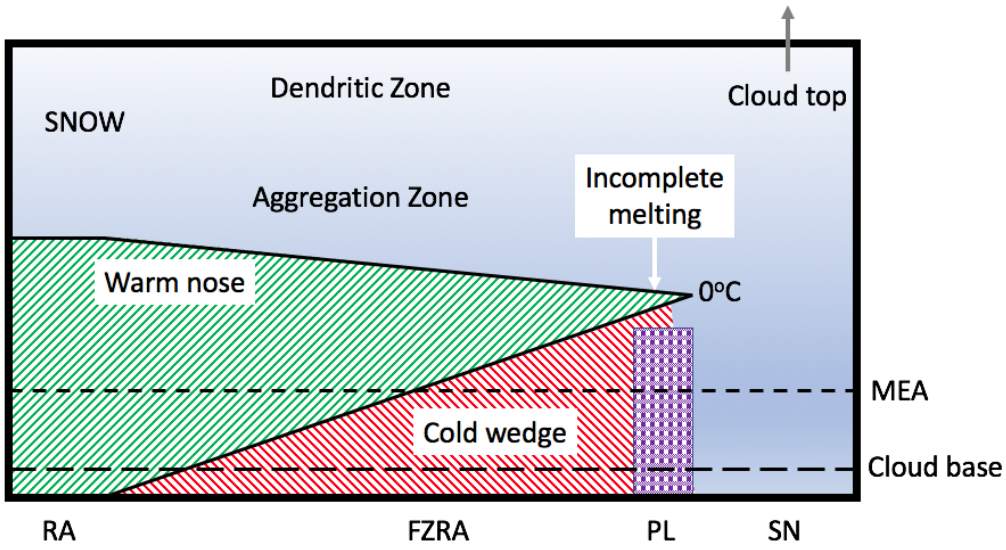

Figure 63. Conceptual model of classical FZRA cross-section

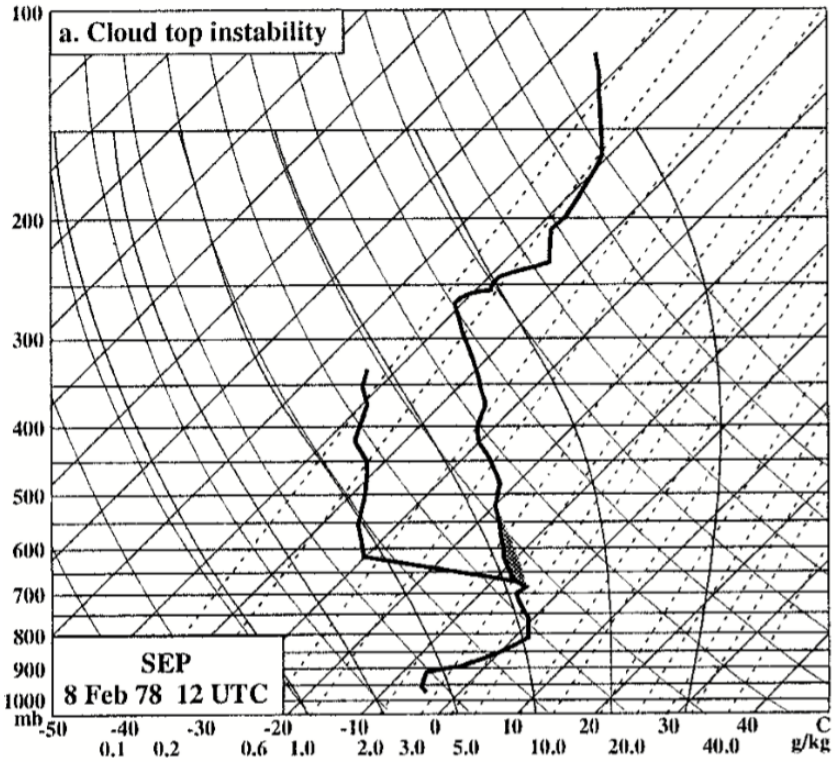

Figure 64. Example of warm cloud tops and (highly suspect) potential instability above a classical warm nose structure (Rauber et al. 2001).

7.6.5 Conditions 9 and 10

CONDITION 9 – Deep Glaciated

CONDITION 10 – Clear Air

- Specific sampling strategies are not required for these conditions, which are generally captured when seeking other conditions and during ferry flights.
- Capturing transitions from liquid to glaciated environments is of great value.
- Snow production ranges of most interest include the dendritic zone, aggregation zone and those favorable for secondary ice production (Hallett and Mossop 1974).
- Clear air samples are desirable in the immediate vicinity of icing clouds, such as near cloud base, cloud top, and cloud edges.
- Clear air samples are also desired to capture aerosol data above and beneath, as well as upstream of icing clouds and precipitation of interest, such as in clear air upstream of a warm front. Capturing clear air samples in areas where clouds are expected to form in the coming hours may also be of value.
- Sampling patterns designed to adequately sample aerosols at altitudes of interest are desired. One possibility is a repeated series of vertical stacks (see V6 in Figure 57). Other

possibilities include porpoise maneuvers (a clear air version of V5 in Figure 57) or upward and downward staircase patterns (not shown).

8 Operations support requirements

This section describes several aspects of operational support, including the daily schedule, and the roles and responsibilities for personnel and certain teams, including the Executive Steering Committee, Operations Director, Forecasters, Data and Product Support, Field Catalog production and data. Descriptions of roles are provided in Appendix A.

The daily schedule is built from a combination of the climatological timing of conditions of interest and the NRC/ECCC daily flowchart (see Figure 65).

Adjustments to the template daily schedules can be made the day before the planned mission, allowing for the possibility of a pre-dawn mission or delaying for a late morning or afternoon mission (moving things up or back by several hours).

8.1 Daily schedule templates

8.1.1 Single-flight day

- 0130 : *Forecaster A shift begins* / Sounding launch(es), if possible
- 0300 : Weather briefing
- 0330 : Message to pilots go/delay/no-go [pilot duty starts]
- 0330 : Operations planning meeting (Operations director, forecaster, others as needed)
- 0430 : Operations decision for the day; pilots arrive
- 0430-0500 : Brief pilots on plans
- 0630 : Takeoff
- 0630-0715: [FLIGHT] Transit to sampling location
- 0715-0945 : [FLIGHT] Sampling
- 0800 : Forecaster B shift begins
- 0945-1030: [FLIGHT] Transit back to KRFD
- 1030 : Landing [4hr flight]
- 1100 : Debrief morning flight (get pilots perspective first, project objectives second, then cover instrumentation, check data)
- 1130 : Forecaster A shift ends
- 1130 : Weather outlook for tomorrow (1-3 day); Provide estimated Takeoff Time and Number of flights (1 or 2) for tomorrow

- 1200 – pilot duty ends **[8.5 hours duty]**
- 1330 : Forecaster B weather outlook (long range; 1-7 day outlook - Operations Director and Forecaster B required, others as needed)
- 1400 : Send out email with times for tomorrow; END OF DAY

8.1.2 Two-flight day

- 0130 : Forecaster A shift begins / Sounding launch(es), if possible
- 0300 : Weather briefing
- 0330 : Message to pilots go/delay/no-go [pilot duty starts]
- 0330 : Operations planning meeting (Operations director, forecaster, others as needed)
- 0430 : Operations decision for the day; pilots arrive
- 0430-0500 : Brief pilots on plans
- 0630 : Takeoff
- 0630-0715: [FLIGHT] Transit to sampling location
- 0715-0945 : [FLIGHT] Sampling
- 0800 : Forecaster B shift begins
- 0945-1030: [FLIGHT] Transit back to KRFD
- 1030 : Landing [4hr flight]
- 1100 : Debrief morning flight, Forecaster B 2nd flight weather briefing
- 1130 : Forecaster A shift ends
- 1230 : Take off
- 1230-1300: [FLIGHT] Transit to sampling location
- 1300-1500 : [FLIGHT] Sampling
- 1500-1530: [FLIGHT] Transit back to KRFD
- 1530 : Landing [3hr flight]
- 1600 : Debrief afternoon flight, Forecaster B weather outlook (1-7 day outlook)
- 1630 : Pilot duty ends [13 hour duty]
- 1630 : Send out email with times for tomorrow; END OF DAY

NOTE 1: *Length and timing of flight, transit time, etc. varies from day to day.*

NOTE 2: *Pilots need a minimum of 10 hours before next "duty" can start.*

NOTE 3: *2-Flight Day could be performed up to 3 days in a row. After this, pilots were required to have off for at least 36 hours.*

NOTE 4: *Soundings could be launched at any time, including before early briefings.*

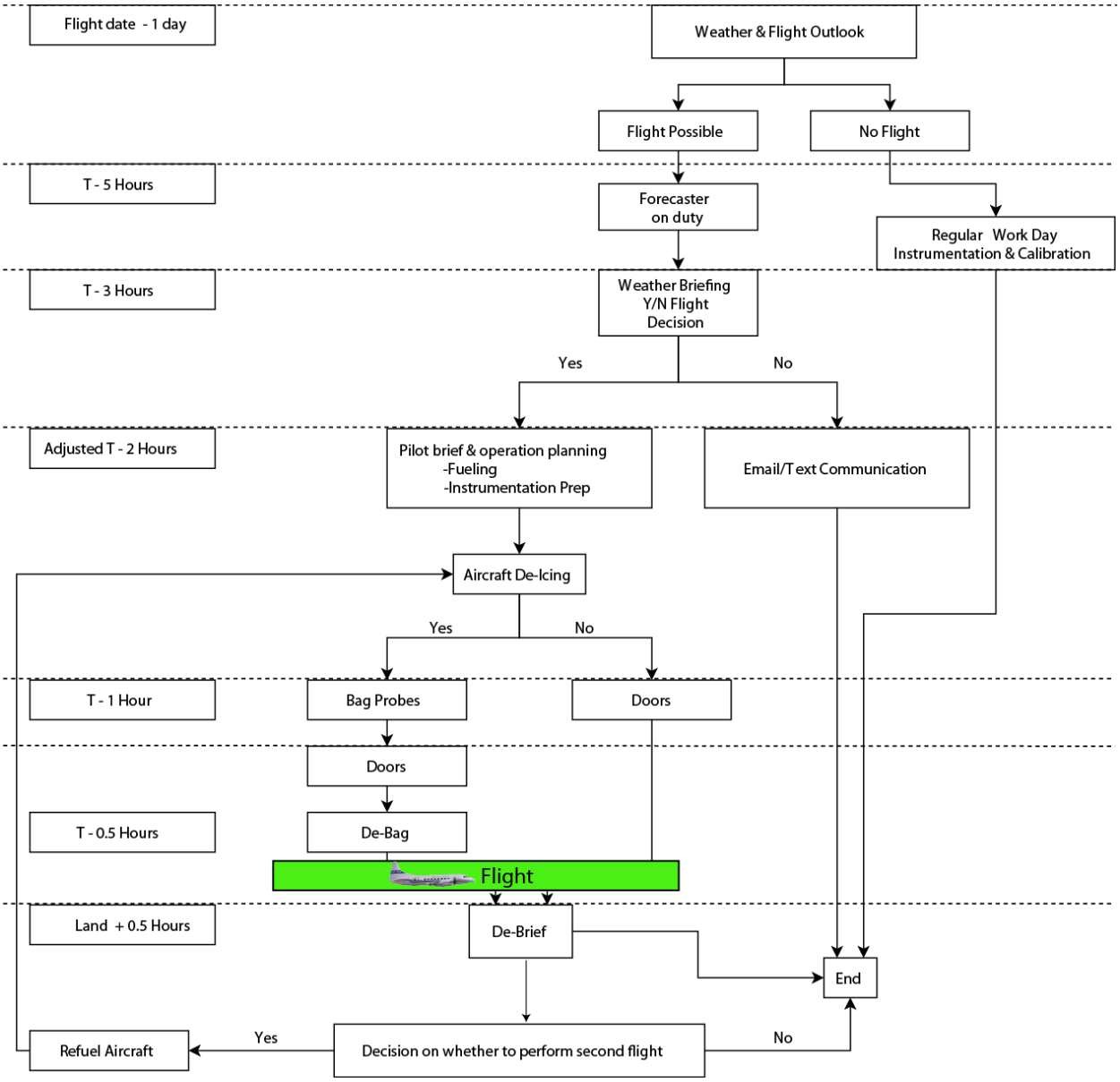

Figure 65. Daily Operations flow chart from NRC.

8.2 Forecasting services

Each day, forecasters are needed to examine the weather and make critical assessments of the complex environments associated with icing conditions within the ICICLE domain. This could include, but is not limited to, assessments of cloud phase, LWC, drop size, cloud top and base heights, layering, consistency, location, timing, movement, and the reliability of expected conditions. Such elements can be critical to relating potential targets to program priorities, determining their quality, value and accessibility, as well as which sampling strategies to employ.

Meteorologists from NCAR, DRI, and SAFIRE/Meteo France provided forecasting services. Primary tasks for the forecasters are described in Appendix A.

8.3 Experimental and operational product support requirements

It is crucial to the assessment and validation of icing tools to have them, and supporting data from other sources, available in real time and properly archived. A list of experimental and operational products available and requiring support is given in Table 10. The list covers many, but not all products of interest. Flight support scientists and ground support scientists address these product support requirements. The respective responsibilities are described in Appendix A.

8.4 Field Catalog and data management

NCAR's Earth Observing Laboratory (EOL) provides Field Catalog and Data Management services for the program. The Field Catalog serves as a repository and data access tool during the program for real-time, quick-look data products, mission summaries, forecast summaries, instrument status reports, and more (see Figure 66). It also provides a geographic information system (GIS) capability for overlaying flight tracks on various fields for real-time monitoring of research flights. Data management and post-project archival services ensures that the ICICLE data set, which includes aircraft data, will be maintained and accessible for as long as the data remain of interest to researchers.

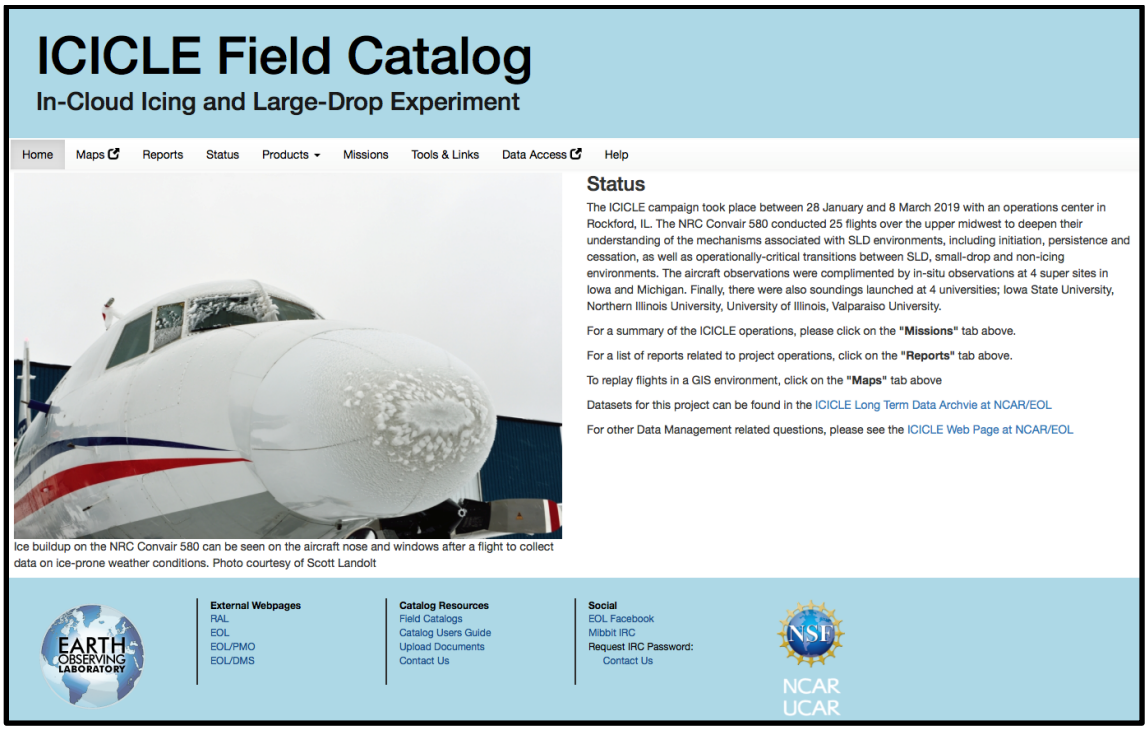

Figure 66. Snapshot of the main page of the ICICLE Field Catalog

8.5 Project personnel, roles and responsibilities

A list of primary project personnel, and their roles and responsibilities is provided in Table 12. This list covered most team members that were on-site or participated remotely on a regular basis, but it is not considered to be comprehensive.

Table 12. Primary project personnel, parent organization, roles and responsibilities.

Person	**Organization**	**Role(s)**	**Primary Program Responsibilities**
Bass, R.	FAA	AWD Weather Research Branch (ANG C-61) Manager	Oversight; Ensure flight program is meeting goals of AWD/AWRP mission. Provide approval for project plans.
Bauman, W.	FAA	Aviation Weather Division (AWD; ANG-C6) Manager	Oversight; Ensure flight program is meeting goals of AWD/AWRP mission. Provide final approval for project plans.
Bond, T. *(retired)*	FAA	Aircraft Icing Chief Scientific and Technical Advisor	Oversight; Provide guidance on flight program and meeting expectations of sponsors in Aircraft Certification Services.
DiVito, S.	FAA	Overall ICICLE program lead	Manage field program, tasking and coordination
		TAIWIN Project Lead	Oversight; Ensure flight program is meeting goals of TAIWIN.

Person	Organization	Role(s)	Primary Program Responsibilities
		Executive Steering Committee	Participate in daily flight-ops go/no-go decision-making meetings.
Dumont, C.	FAA	Contracting Officer's Representative for FAA-NRC and FAA-ECCC Appendices	Generate, negotiate agreements, route through approval. Establish data sharing protocol.
Riley, J. *(retired)*	FAA	Aviation Research Division (ARD) Aircraft Icing Program Manager	Oversight; Ensure flight program is meeting goals of TAIWIN and ARD Aircraft Icing mission. Support decision-making.
Sims, D.	FAA	IFI Project Lead	Oversight; Ensure flight program is meeting goals of IFI and AWD mission.
		Executive Steering Committee	Participate in daily flight-ops go/no-go decision-making meetings.
Bernstein, B.	LEA	Overall ICICLE Science lead	Develop Science Plan. Coordinate and identify operational needs, strategies, etc. between all participating parties.
		Primary Operations Director	Develop Operations Plan. Coordinate daily operations during the program, both on the ground and in-flight, with NRC, ECCC, NCAR and forecasters.
		Executive Steering Committee	Participate in daily flight-ops go/no-go decision-making meetings.
Bastian, M. *(retired)*	NRC	Flight Test & Software Engineer	Convair crew, communications with Operations Directors and pilots
Bliankinshtein, N.	NRC	Data Scientist	GVR and Lidar sensors
Brown, A.	NRC	Pilot	Convair crew
Carrothers, B.	NRC	Co-pilot	Convair crew
Ingram, S.	NRC	Crew Chief, Aircraft Maintenance Engineer (AME)	Convair crew
MacDonald, D.	NRC	Instrumentation	Convair crew, Instrumentation
Millett, J.	NRC	AME	Avionics AME
Nichman, L.	NRC	Data Scientist	Convair research crew, cloud microphysics sensors
Nguyen, C.	NRC	Data Scientist	Convair research crew, airborne radars
Roux, E.	NRC	Instrumentation Lead	Convair crew, Instrumentation Lead
Robichaud, S.	Contractor	Co-pilot	Convair crew
Van Westerop, T.	NRC	Aircraft Maintenance Engineer (AME)	Convair crew
Wolde, M.	NRC	NRC Overall Lead	Convair-580 management & prep, NRC airborne sensors operations and management
		Executive Steering Committee	Participate in daily flight-ops go/no-go decision-making meetings.
Yawo-Daniel, H.	NRC	AME	Avionics AME

Person	Organization	Role(s)	Primary Program Responsibilities
Korolev, A.	ECCC	ECCC Overall Lead	Airborne instrumentation, cloud microphysics data collection and management
		Executive Steering Committee	Participate in daily flight-ops go/no-go decision-making meetings.
Harwood, M.	ECCC	Maintenance Manager	Airborne instrumentation maintenance & operation
Heckman, I	ECCC	Data Scientist	Aircraft data quality control
Iwachow, J.	ECCC	Maintenance Manager	Airborne instrumentation maintenance & operation
Milbrandt, J.	ECCC	Support Scientist	Numerical models
Adriaansen, D.	NCAR	Forecast Team Coordinator	Point of contact (POC) for Forecast Team related activities
		Forecaster	Provide forecasting services during field program.
		Support Scientist – IFI	Monitor data in field in conjunction with scientific objectives and prepare data summary for field catalog, advise steering committee, provide preliminary data quality control (QC)
Costanza, C.	NCAR	NCAR Field Catalog Support	POC for Field Catalog requests and support users of the Field Catalog; (On-site) Support during ICICLE campaign
Cunning, G.	NCAR	NCAR IFI Experimental Product Lead	Prepare IFI experimental product runs/output/graphics
Echo-Hawk, L.	NCAR	Data Archive	Create the data archive and collect all project datasets
Gaydos, A.	NCAR	TAIWIN Lead Software Engineer	Prepare TAIWIN tools/output/graphics
Haggerty, J.	NCAR	NCAR IFI Lead	Manage IFI participation; coordinate with TAIWIN lead
		Executive Steering Committee	Participate in daily flight-ops go/no-go decision-making meetings.
		NCAR ICICLE Data Manager	Manage the data archive in coordination with UCAR EOL team.
		Operations Director	Coordinate daily operations during the field program, both on the ground and in-flight, with NRC, ECCC, NCAR and forecasters.
		Support Scientist – IFI	Monitor data in field in conjunction with scientific objectives and prepare data summary for field catalog, advise steering committee, provide preliminary data QC
Jacobson, D.	NCAR	Support Scientist – TAIWIN	Monitor data in field in conjunction with scientific objectives and prepare data summary for field catalog, advise

Person	Organization	Role(s)	Primary Program Responsibilities
			steering committee, provide preliminary data QC
		Ground Suite Team	Support ground suite deployment, monitoring, and removal.
Landolt, S.	NCAR	NCAR TAIWIN Lead	Manage NCAR TAIWIN participation, Freezing Precipitation Algorithm; coordinate with IFI lead
		Executive Steering Committee	Participate in daily flight-ops go/no-go decision-making meetings.
		Ground Suite & External (domestic) Collaboration Lead	Manage external domestic collaborations and ground suite/site deployment and operation
		Forecaster	Provide forecasting services during field program.
		Operations Director	Coordinate daily operations during the field program, both on the ground and in-flight, with NRC, ECCC, NCAR and forecasters.
		Support Scientist – TAIWIN	Monitor data in field in conjunction with scientific objectives and prepare data summary for field catalog, advise steering committee, provide preliminary data QC
Lave, J.	NCAR	Support Scientist – TAIWIN	Monitor data in field in conjunction with scientific objectives and prepare data summary for field catalog, advise steering committee, provide preliminary data QC
		Forecaster	Provide forecasting services during field program.
Lentz, J.	NCAR	Support Scientist – TAIWIN	Monitor data in field in conjunction with scientific objectives and prepare data summary for field catalog, advise steering committee, provide preliminary data QC
		Ground Suite Team	Support ground suite deployment, monitoring, and removal.
Loehrer, S.	NCAR	NCAR Field Catalog Support	POC for Field Catalog requests and support users of the Field Catalog; Support ICICLE Dry-Run Exercise
McCabe, G.	NCAR	Experimental Product Support -- IFI (Remote)	Remote support for IFI software/products
Prestopnik, P.	NCAR	Experimental Product Support -- IFI	Remote support for IFI software/products
Rugg, A.	NCAR	Support Scientist – IFI	Monitor data in field in conjunction with scientific objectives and prepare data summary for field catalog, advise

Person	Organization	Role(s)	Primary Program Responsibilities
			steering committee, provide preliminary data QC
Serke, D.	NCAR	NCAR IFI Radar Lead	Prepare and evaluate RadIA
		Forecaster	Provide forecasting services during field program.
		Support Scientist – IFI	Monitor data in field in conjunction with scientific objectives and prepare data summary for field catalog, advise steering committee, provide preliminary data QC
Stossmeister, G.	NCAR	Data Services Lead	Manage field catalog and Data Archive services and staff
		NCAR Data Archive Lead	Create the data archive.
Tessendorf, S.	NCAR	Support Scientist – IFI	Monitor data in field in conjunction with scientific objectives and prepare data summary for field catalog, advise steering committee, provide preliminary data QC
Thompson, G.	NCAR	NCAR TAIWIN Model Lead	Experimental model product (TLE, PC) preparation, graphics.
		Forecaster	Provide forecasting services during field program.
		Support Scientist – TAIWIN	Monitor data in field in conjunction with scientific objectives and prepare data summary for field catalog, advise steering committee, provide preliminary data QC
Wolff, C.	NCAR	Forecaster	Provide forecasting services during field program.
Xu, M.	NCAR	Support Scientist – TAIWIN (remote)	Remote support for TAIWIN modeling products
McDonough, F.	DRI	Forecaster	Provide forecasting services during field program
Brown, J.	NOAA GSL	Support Scientist	HRRR/WRF models; 1-km HRRR
Weygandt, S.	NOAA GSL	Support Scientist	HRRR/WRF models; 1-km HRRR
Smith, W.	NASA	Support Scientist	NASA-Langley satellite icing products
Kalinka, F.	Deutscher Wetterdienst	Collaborator – Support Scientist	DWD models and icing products
Desbios, J-P.	Meteo France	Forecaster	Provide forecasting services during field program
Vie, B.	Meteo France (MF)	Collaborator – Support Scientist	MF Numerical models
Bennett, K.	UK Met Office	Collaborator – Support Scientist	UKMO models and icing products

9 Data processing, availability and sharing protocol

Data processing, availability and protocol have been expressed in written agreements between the FAA and participating organizations. In general, it is expected that datasets will start to become available to outside researchers three and a half (3.5) years after the conclusion of the flight program, except as specified in the written agreements between the FAA and participant organizations. Attributes of the many available datasets may differ based on the type of data and the source. Because flight data is of particular interest to many program participants and collaborators, a description of that dataset is provided below. Regardless of what is stated herein with respect to flight data availability, all ICICLE datasets are subject to the agreements and terms described above. When appropriate, the various ICICLE datasets will be made available via the ICICLE Data Archive, a web-based archive that will be password protected and maintained by NCAR under the sponsorship of the FAA.

Convair-580 data: In-situ and remote sensing data collected during ICICLE has been processed by NRC and ECCC. ECCC and NRC data scientists perform data processing after each flight. Both NRC and ECCC data scientists are assigned to perform post-flight data quality control checks and provide feedback on the performance of the flight data. The cloud microphysics data are analyzed with the help of ECCC's D2G software package. This software handles and processes particle scattering and imaging probes, as well as bulk cloud microphysics.

The following is a non-exclusive list of the cloud microphysical data output being provided by ECCC using the ECCC D2G software:

- Size distribution of liquid droplets
- Size distribution of ice particles
- Number concentration of droplets
- Number concentration of ice
- LWC
- IWC
- Extinction coefficient
- Integral size of liquid droplets
- Integral size of ice particles
- Radar reflectivity of liquid
- Radar reflectivity of ice
- Liquid droplet MVD, MMD, D_{max}
- Ice particle MVD, MMD, D_{max}

- Habit recognition analysis for D>100um: fraction of spheres, dendrites, needles, irregulars

The following is the non-exclusive list of in situ and remote sensing data output being provided by NRC:

- Aircraft state parameters
- Atmospheric state parameters
- Size distribution of aerosol particles
- Number concentration of aerosol particles
- W-band reflectivity and Doppler profiles
- Lidar backscatter and depolarization

Some important additional information regarding the Convair-580 dataset is provided below.

1. The Convair-580 is instrumented by both NRC and ECCC. It carries some identical sensors such as CDP and Nevzorov, designated primary and backup sensors based on flight test results. During the course of the project, primary and backup sensors may have been swapped if there were probe issues.
2. Data are recorded by the NRC and/or ECCC Data Acquisition Systems during flight irrespective of who runs and owns the sensors.
3. NRC broadcasts real-time processed atmospheric and aircraft state data to the ECCC system included some key parameters such as true airspeed that are needed for imaging probes.
4. There are two 2DS sensors. One is maintained and its data is recorded on NRC system, while the other is maintained and recorded by ECCC.
5. All of the atmospheric state measurements, with the exception one temperature sensor, belong to NRC. NRC is responsible for processing of all the aircraft and atmospheric state parameters for the project. These data are given to ECCC and to be included in the dataset that will be submitted to FAA.
6. Aerosol sensors from the ECCC air quality group are included in the sensor suite. NRC data scientist, Dr. Leonid Nichman, is responsible for the data collection and processing. He is the instrumentation mentor, who leads the integration, calibration and initial data processing of the aerosol sensors on the Convair-580 for ICICLE. Dr. Nichman will work with ECCC team, NCAR, the FAA, and other participating organizations during the flight operations, data processing, and publication phases.

10 Summary

The In-Cloud Icing and Large-drop Experiment was conducted from 27 January to 8 March 2019 in an effort to:

1. Further advance the understanding of meteorological processes related to the production and depletion of supercooled liquid water, with an emphasis on supercooled large drops; and
2. Evaluate and refine icing tools that can be used to diagnose, forecast, and differentiate between icing and non-icing conditions.

Highly impactful data was collected by the NRC Convair-580 research aircraft and was complemented by icing-relevant information from operational sources, including numerical weather model forecasts and observations from GOES satellites, individual NEXRADs and mosaics thereof, surface stations including ASOS and AWOS, and the NWS sounding network, plus operational icing tools such as CIP, FIP, AIRMETs and PIREPs. Highly-valuable, supplemental information was also collected by several suites of ground-based instrumentation and four sounding sites across the primary ICICLE domain.

The development and execution of ICICLE required extensive background research, an understanding of the basic and applied science of aircraft icing weather research, formulation of objectives and associated data requirements as well as sampling strategies, and comprehensive planning. In the aggregate, these activities resulted in several rich datasets that will be used for in-depth analysis of icing and non-icing events and thorough examination of the ability of operational and developmental icing tools to properly observe, diagnose, and forecast those events.

11 References

Adriaansen, D., C. Wolff, and M. Politovich, 2012: Performance Analysis of the Current Icing Product (CIP) Algorithm under Variations in Icing Relevant Observational Datasets. AIAA 2012-3235. 4th AIAA Atmospheric and Space Environments Conference, 25-28 June, New Orleans. https://doi.org/10.2514/6.2012-3235.

Adriaansen, D., G. Thompson, C. Wolff, and M. Politovich, 2014: Improving diagnoses of in-flight icing conditions in regions of sparsely distributed surface observations. AIAA 2014-2069. 6th AIAA Atmospheric and Space Environments Conf. Atlanta, 16-20 June. https://doi.org/10.2514/6.2014-2069.

Adriaansen, D., P. Prestopnik, G. McCabe, and M. Politovich, 2015: Advancements in Combining Datasets for In-Flight Icing Diagnoses, SAE Technical Paper 2015-01-2137, 2015 SAE International Conference on Icing of Aircraft, Engines and Structures, Prague. https://www.sae.org/publications/technical-papers/content/2015-01-2137.

Adriaansen. D., A. Rugg, J. Haggerty, S. Tessendorf, G. McCabe, P. Prestopnik and G. Cunning, 2019: Toward a version of the Forecast Icing Product algorithm for use with the High-Resolution Rapid Refresh numerical weather prediction model. Presented at SAE International Icing Conference, Minneapolis, 17-21 June.

Air Weather Service 1980: Forecasters' guide on aircraft icing. Air Weather Service Rep. AWS/TR-80/001, 58 pp. U.S. Air Force, Scott AFB, IL 62225. https://apps.dtic.mil/sti/pdfs/ADA085490.pdf.

Appleman, H., 1954: Design of a cloud-phase chart. Bull. Amer. Meteor. Soc., 35, 223–225.

Austin, E., P. Williams, S. Goates, and A. Austin, 2011: "Severe Icing: Urgent PIREP!" Severe icing across the United States from 2002-2010: Relationship to icing type, terrain, altitude, aircraft type and climate. Presented at 15th Conf. on Aviation, Range and Aerospace Meteorology, Los Angeles CA, 1-4 August, Amer. Meteor. Soc., Boston. https://ams.confex.com/ams/14Meso15ARAM/webprogram/Paper190887.html.

Battaglia, A., E. Rustemeier, A. Tokay, U. Blahak, and C. Simmer, 2010: PARSIVEL Snow Observations: A Critical Assessment. J. Atmos. Oceanic Technol., 27, 333–344, https://doi.org/10.1175/2009JTECHA1332.1.

Beckwith, W. B., 1965: Supercooled fog dispersal for airport operations. Bull. Amer. Meteor. Soc., 46, 323–327, https://doi.org/10.1175/1520-0477-46.6.323.

Benjamin, S.G. and Coauthors, 1998: The operational RUC-2. Preprints, 16th Conf. on Wea. Analysis and Forecasting, Pheonix, AZ, 249-252.

Benjamin, S.G. and Coauthors, 2004: An hourly assimilation-forecast cycle: The RUC. Mon. Wea. Rev., 132, 495-518. https://doi.org/10.1175/1520-0493(2004)132<0495:AHACTR>2.0.CO;2.

Benjamin, S., J. Brown and T. Smirnova, 2016a: Explicit precipitation-type diagnosis from a model using a mixed-phase bulk cloud-precipitation microphysics parameterization. Wea. Fore., 31, 609-619. https://doi.org/10.1175/WAF-D-15-0136.1

Benjamin, S. G., and Coauthors, 2016b: A North American hourly assimilation and model forecast cycle: The Rapid Refresh. Mon. Wea. Rev., 144, 1669–1694. https://doi.org/10.1175/MWR-D-15-0242.1.

Bennett, I., 1959: Glaze: Its meteorology and climatology, geographical distribution, and economic effects. Environmental Protection Research Division Tech. Rep. EP-105, Headquarters, U.S. Army Quartermaster, Research and Engineering Command, Natick, MA, 217 pp. NTIS AD-216668.

Bernstein, B. C., 1996: A new technique for identifying locations where supercooled large droplets are likely to exist: The stovepipe algorithm. Proc., FAA Int. Conf. on In-Flight Aircraft Icing, Springfield, VA, Department of Transportation, Federal Aviation Administration, 353-364. http://www.tc.faa.gov/its/worldpac/techrpt/ar96-81-2.pdf.

Bernstein, B.C., 2000a: Regional and local influences on freezing drizzle, freezing rain and ice pellet events. Wea. Fore., 15, 485-508. https://doi.org/10.1175/1520-0434(2000)015%3c0485:RALIOF%3e2.0.CO;2

Bernstein, B.C., 2000b: Analysis of the meteorology associated with the 1998 NASA Glenn Twin Otter flights. NASA CR-2000-209413. https://ntrs.nasa.gov/citations/20120002773.

Bernstein, B.C., T.A. Omeron, F. McDonough and M.K. Politovich, 1997: The relationship between aircraft icing and synoptic scale weather conditions. Wea. Fore., 12, 742-762. https://doi.org/10.1175/1520-0434(1997)012<0742:TRBAIA>2.0.CO;2.

Bernstein, B.C., F. McDonough, M.K. Politovich, and B.G. Brown, 2000: A research aircraft verification of the Integrated Icing Diagnostic Algorithm (IIDA). 9th Conference on Aviation, Range and Aerospace Meteorology, Orlando, 11-15 Sep. 2000. https://ams.confex.com/ams/Sept2000/techprogram/paper_15920.htm.

Bernstein, B.C., F. McDonough, M.K. Politovich, B.G. Brown, T.P. Ratvasky, D.R. Miller, C.A. Wolff and G. Cunning, 2005: Current Icing Potential (CIP): Algorithm Description and Comparison with Aircraft Observations. J. Appl. Meteor., 44, 969-986. https://doi.org/10.1175/JAM2246.1.

Bernstein, B.C., W. Campo, L. Algodoal, F. Bottino, L. Lilie and A. Henriques, 2006a: The Embraer-170 and -190 Natural Icing Flight Campaigns: Keys to Success. 2006-264, Amer. Inst. of Aeronautics and Astronautics, Reno NV, 21 pp. https://doi.org/10.2514/6.2006-264.

Bernstein, B.C., F. McDonough, C. A. Wolff, M. K. Politovich, G. Cunning, S. Mueller, and S. Zednik, 2006b: The new CIP icing severity product. 12th Conf. on Aviation, Range and Aerospace Mete- orology, Atlanta, GA, Amer. Meteor. Soc., P9.5, https://ams.confex.com/ams/Annual2006/webprogram/Paper102273.html.

Bernstein, B.C., C. A. Wolff, and F. McDonough, 2007: An inferred climatology of icing conditions aloft, including supercooled large drops. Part I: Canada and the continental United States. J. Appl. Meteor. Climatol., 46, 1857–1878, https://doi.org/10.1175/2007JAMC1607.1.

Bernstein, B.C., F. McDonough, and C. A. Wolff, 2011: A regional comparison of icing conditions in boundary layer clouds. Int. Conf. on Aircraft and Engine Icing and Ground Deicing, Chicago, IL, SAE, 2011-38-0021, http://papers.sae.org/2011-38-0021.

Bernstein, B.C., R. Rasmussen, F. McDonough and C. Wolff, 2019: Differentiation of Large- and Small-Drop Icing Conditions Based on Liquid Water Content and Drop Concentration. J. Appl. Meteor. Climatol., 58, 1931-1953. https://doi.org/10.1175/JAMC-D-18-0038.1.

Bigg, E. K., 1953: The supercooling of water. Proc. Phys. Soc. London, 66B, 688–694. DOI:10.1088/0370-1301/66/8/309.

Bocchieri, J. R., 1980: The objective use of upper air soundings to specify precipitation type. Mon. Wea. Rev., 108, 596–603. https://doi.org/10.1175/1520-0493(1980)108<0596:TOUOUA>2.0.CO;2.

Braid, J., C. Wolff, A. Holmes, P. Boylan, and M. Politovich, 2006: Current Icing Potential (CIP) Algorithm with TAMDAR data – a verification analysis. 10th Symposium on Integrated Observing and Assimilation Systems for the Atmosphere, Oceans, and Land Surface, 30 Jan – 2 Feb, Amer. Met. Soc. https://ams.confex.com/ams/pdfpapers/104835.pdf.

Braid, J., P. Van Wie, and J. Rex, 2011: Using the TAMDAR sensor for in-flight ice detection and improved safety of flight. SAE 2011 International Conference on Aircraft and Engine Icing and Ground Deicing, Chicago, 13-17 June. https://www.sae.org/publications/technical-papers/content/2011-38-0051.

Brown, A., 2011: Aircraft Performance Degradation - the Effects of Inflight Icing upon Lift, Drag and Propulsive Efficiency, SAE Technical Paper 2011-38-0073, 2011. https://doi.org/10.4271/2011-38-0073.

Brown, B. G., 1996: Verification of in-flight icing forecasts: Methods and issues. Proc., FAA Int. Conf. on In-Flight Aircraft Icing, Springfield, VA, Department of Transportation, Federal Aviation Administration, 319-330. http://www.tc.faa.gov/its/worldpac/techrpt/ar96-81-2.pdf.

Brown, B. G., and G. S. Young, 2000: Verification of icing and turbulence forecasts: Why some verification statistics can't be computed using PIREPs. Preprints, Ninth Conf. on Aviation, Range, and Aerospace Meteorology, Orlando, FL, Amer. Meteor. Soc., 393–398. https://ams.confex.com/ams/Sept2000/techprogram/paper_16469.htm.

Brown, B.G. and B.C. Bernstein, 2006: An approach for calibration of probabilistic forecasts with limited observational data. Presented at 12th Conf. on Aviation, Range and Aerospace Meteorology, Atlanta GA, 29 Jan - 2 Feb, Amer. Meteor. Soc., Boston. https://ams.confex.com/ams/Annual2006/techprogram/paper_105378.htm. There is a more comprehensive NCAR/FAA Internal report available entitled "A Calibration Approach for CIP based on Forecast Performance Measures".

Brown, B. G., T. L. Fowler, B. C. Bernstein, and G. S. Forbes, 1993: Use of pilot reports for verification of aircraft icing diagnoses and forecasts. Preprints, Fifth Int. Conf. on Aviation Weather Systems, Vienna, VA, Amer. Meteor. Soc., 277-281.

Brown, B. G., G. Thompson, R. T. Bruintjes, R. Bullock, and T. Kane, 1997: Intercomparison of in-flight icing algorithms. Part II: Statistical verification results. Wea. Forecasting, 12, 890-914. https://doi.org/10.1175/1520-0434(1997)012<0890:IOIFIA>2.0.CO;2.

Cai, H., C. Kessinger, D. Ahijevych, J. Williams, N. Rehak, D. Megenhardt, M. Steiner, R. L. Bankert, J. Hawkins, M. F. Donovan and E. R. Williams, 2009: Nowcasting oceanic convection for aviation using random forest classification. 16th Conference on Satellite Meteorology and Oceanography, Amer. Meteo. Soc., Phoenix, AZ. https://ams.confex.com/ams/pdfpapers/150236.pdf.

Carriere, J., S. Alquier, C. Le Bot, and E. Moulin, 1997: Some results of a statistical evaluation of forecast icing risk algorithms. Meteor. Appl., 4, 115–130. https://doi.org/10.1017/S1350482797000443.

Chapman, M. and B.C. Bernstein, 2002: Analysis of problematic IIDA icing diagnoses in the Pacific Northwest. Preprints, 10th Conference on Aviation, Range and Aerospace Meteorology, Portland OR, 13-17 May, Amer. Meteor. Soc., Boston, 315-318. https://ams.confex.com/ams/pdfpapers/38401.pdf.

Chapman, M.B., C.A. Wolff, R.E. Bateman and B.C. Bernstein, 2004: An evaluation of the performance of the Current Icing Potential at high altitudes. 11th Conference on Aviation, Range and Aerospace Meteorology, Hyannis MA, 11-14 October, Amer. Meteor. Soc. https://ams.confex.com/ams/pdfpapers/81809.pdf.

Chapman, M., A. Holmes, and C. Wolff, 2006: Verification of aviation icing algorithms from the second Alliance Icing Research Study. 12th Conf. on Aviation, Range and Aerospace Meteorology, Atlanta, GA, 30 Jan - 2 Feb. https://ams.confex.com/ams/pdfpapers/104158.pdf.

Cober, S. and G. Isaac, 2012: Characterization of Aircraft Icing Environments with Supercooled Large Drops for Application to Commercial Aircraft Certification, J. Appl. Meteor., 51, 265-284. https://doi.org/10.1175/JAMC-D-11-022.1.

Cober, S.G., J.W. Strapp, and G.A. Isaac, 1996: An example of supercooled drizzle drops formed through a collision-coalescence process. J. Appl. Meteor., 35, 2250-2260. https://doi.org/10.1175/1520-0450(1996)035<2250:AEOSDD>2.0.CO;2.

Cober, S.G., G.A. Isaac, and J.W. Strapp, 2001: Characterizations of aircraft icing environments that include supercooled large drops. J. Appl. Meteor., 40, 1984–2002. https://doi.org/10.1175/1520-0450(2001)040<1984:COAIET>2.0.CO;2.

Cober, S., B. Bernstein, R. Jeck, E. Hill, G. Isaac, J. Riley and A. Shah, 2009: Data and Analysis for the Development of an Engineering Standard for Supercooled Large Drop Conditions. DOT/FAA/AR-09/10. Air Traffic Organization Operations Planning, Office of Aviation Research and Development Washington, DC 20591. http://www.tc.faa.gov/its/worldpac/techrpt/ar0910.pdf.

Cooper, W.A., W.R. Sand, M.K. Politovich, and D.L. Veal, 1984: Effects of icing on performance of a research aircraft. J. Aircraft, 21, 708-715. https://doi.org/10.2514/3.45018.

Cortinas, J. V., Jr., B. C. Bernstein, C. C. Robbins, and J. W. Strapp, 2004: An analysis of freezing rain, freezing drizzle, and ice pellets across the United States and Canada: 1976–90. Wea. Forecasting, 19, 377–390. https://doi.org/10.1175/1520-0434(2004)019<0377:AAOFRF>2.0.CO;2.

Curry, J. A., and G. Liu, 1992: Assessment of aircraft icing potential using satellite data. J. Appl. Meteor., 31, 605–621. https://doi.org/10.1175/1520-0450(1992)031<0605:AOAIPU>2.0.CO;2.

Curry, J. A., and Coauthors, 2000: FIRE Arctic Clouds Experiment. Bull. Amer. Meteor. Soc., 81, 5–29. https://doi.org/10.1175/1520-0477(2000)081<0005:FACE>2.3.CO;2.

Czys, R., R. Scott, K. Tang, R. Przybylinski, and M. Sabones, 1996: A physically based, nondimensional parameter for discriminating between locations of freezing rain and ice pellets. Wea. Forecasting, 11, 591–598. https://doi.org/10.1175/1520-0434(1996)011<0591:APBNPF>2.0.CO;2.

Davis, C.A., B.G. Brown, R. Bullock and J. Halley-Gotway, 2009: The Method for Object-Based Diagnostic Evaluation (MODE) Applied to Numerical Forecasts from the 2005 NSSL/SPC Spring Program. Wea. Fore., 24, 1252-1267. https://doi.org/10.1175/2009WAF2222241.1.

DeLaura, R.A., Y-H. Lin, R.K. Jordan, J.C. Venuti, and J.E. Evans, 2011: Evaluation of Consolidated Storm Prediction for Aviation (CoSPA) 0–8 Hour Convective Weather Forecast Using the Airspace Flow Program Blockage-based Capacity Forecast ("The Matrix"). MIT-LL Project Report ATC-385, 70 pp. https://www.ll.mit.edu/sites/default/files/publication/doc/2018-12/DeLaura_2001_ATC-385_WW-23618.pdf.

DiVito, S., and J. T. Riley, 2017: An overview of the Federal Aviation Administration (FAA) Terminal Area Icing Weather Information for NextGen (TAIWIN) Project. 18th Conf. on Aviation, Range and Aerospace, Seattle, WA, Amer. Meteor. Soc., https://ams.confex.com/ams/97Annual/webprogram/Paper314380.html.

DiVito, S., B. Bernstein, J. Riley, D. Sims, S. Landolt, J. Haggerty, M. Wolde, and A. Korolev, 2019: In-Cloud ICing and Large-drop Experiment – Program Overview. Presented at SAE International Icing Conference, Minneapolis, 17-21 June.

Ellis, S., D. Serke, J. Hubbert, D. Albo, A. Weekley, M. Politovich, A. Gaydos, D. Adriaansen, E. Williams, D. Smalley, and M. Donovan, 2012: Toward the detection of aircraft icing conditions using Dual-Polarimetric Radar,7th European Conference on Radar in Meteorology and Hydrology, June 24-29, Toulouse, FR. https://archive.ll.mit.edu/mission/aviation/publications/publication-files/ms-papers/Ellis_2012_ERAD_MS-65365_WW-26438.pdf.

Ellrod, G. and A. Bailey, 2007: Assessment of aircraft icing potential and maximum icing altitude from geostationary meteorological satellite data. Wea. Forecasting, 22, 160-174. https://doi.org/10.1175/WAF984.1.

Elmore, K. L., Z. L. Flamig, V. Lakshmanan, B. T. Kaney, V. Farmer, H. D. Reeves, and L. P. Rothfusz, 2014: mPING: Crowd-sourcing weather reports for research. Bull. Amer. Meteor. Soc., 95, 1335–1342, https://doi.org/10.1175/BAMS-D-13-00014.1.

Elmore, K. L., H. M. Grams, D. Apps, and H. D. Reeves, 2015: Verifying forecast precipitation type with mPING. Wea. Forecasting, 30, 656–667. https://doi.org/10.1175/WAF-D-14-00068.1.

Etherton, B., M. Wandishin, J. Hart, G. Layne, M. Leon, and M. Petty, 2014: Assessment of the Current Icing Product (CIP) and Forecast Icing Product (FIP). Version 1.1. NOAA Technical Memorandum OAR GSD-52. https://doi.org/10.7289/V5/TM-OAR-GSD-52.

Federal Aviation Administration, 1999: U.S. Code of Federal Regulations, Title 14 (Aeronautics and Space), Part 25 (Airworthiness Standard: Transport Category Airplanes), App. C. National Archives and Records Administration, U.S. Gov't Printing Office, Washington, DC. https://www.ecfr.gov/current/title-14/part-25/appendix-Appendix%20C%20to%20Part%2025.

Federal Aviation Administration, 2015: U.S. Code of Federal Regulations, Title 14 (Aeronautics and Space), Parts 25 and 33 (Airplane and Engine Certification Requirements in Supercooled Large Drop, Mixed Phase and Ice Crystal Icing Conditions; Final Rule). National Archives and Records Administration, U.S. Gov't Printing Office, Washington, DC. https://www.govinfo.gov/content/pkg/FR-2014-11-04/pdf/2014-25789.pdf.

Federal Aviation Administration, 2017: Automated Weather Observing Systems (AWOS) for non-Federal applications. Advisory Circular AC-150/5220-16E. https://www.faa.gov/documentLibrary/media/Advisory_Circular/AC_150_5220-16E.pdf.

Fenton, K., M. Wandishin, and M. Petty, 2017: Analysis of RAP and HRRR variables related to icing. NOAA/ESRL/GSD Quality Assessment Product Development Team report. 22 pp.

Fleishauer, R., V. Larson, and T. VonderHaar, 2002: Observed microphysical structure of midlevel, mixed-phase clouds. J. Atmos. Sci., 59, 1779-1804. https://doi.org/10.1175/1520-0469(2002)059<1779:OMSOMM>2.0.CO;2.

Forbes, G.S., Y. Hu, B.G. Brown, B.C. Bernstein and M.K. Politovich, 1993: Examination of soundings in the proximity of pilot reports of aircraft icing during STORM-FEST. Preprints, 5th Conf. on Aviation Weather Systems, Vienna, VA, 2-6 August. Amer. Meteor. Soc., Boston, 282-286.

Fowler, T. L., M. Crandell, and B. G. Brown, 2002: An inferred icing climatology - Part III: Icing AIRMETs and IIDA. Preprints, 10th Conf. on Aviation, Range, and Aerospace Meteorology, Portland, OR, Amer. Meteor. Soc., J25– J28. https://ams.confex.com/ams/pdfpapers/38757.pdf.

Fowler, T., J. Wolff, J. Halley Gotway, and M. Harrold, 2017: Final report on neighborhood evaluation of ice accretion. NCAR technical report completed under FAA AWRP Contract: DTFAWA-16-D-00036/0005, Task Order Number 21108/TAIWIN.

Geresdi, I., R. Rasmussen, W. Grabowski, and B. Bernstein, 2005: Sensitivity of freezing drizzle formation in stably stratified clouds to ice processes. Meteor. Atmos. Phys., 88, 91–105. https://doi.org/10.1007/s00703-003-0048-5.

Green, S. D., 2006: A study of U.S. inflight icing accidents and incidents, 1978 to 2002. 44th AIAA Aerospace Sciences Meeting and Exhibit, AIAA 2006-82, Reno, NV, AIAA, 26 pp. https://doi.org/10.2514/6.2006-82.

Green, S. D., 2015: The icemaster database and an analysis of aircraft aerodynamic icing accidents and incidents. DOT/FAA/TC-14/44, 135 pp. http://www.tc.faa.gov/its/worldpac/techrpt/tc14-44.pdf.

Grelson, E. F., 1997: A climatology of conditions known to lead to in-flight aircraft icing across North America. M.S. thesis, Dept. of Geosciences, University of Nebraska at Lincoln, 131 pp. See also https://ams.confex.com/ams/older/99annual/abstracts/1267.htm.

Guan, H., S.G. Cober, and G.A. Isaac, A. Tremblay and A. Methot, 2002: Comparison of three cloud forecast schemes with in- situ aircraft measurements. Wea. Fore., 17, 1226-1235. https://doi.org/10.1175/1520-0434(2002)017%3C1226:COTCFS%3E2.0.CO;2.

Gyakum, J. R., and P. J. Roebber, 2001: The 1998 ice storm - Analysis of a planetary-scale event. Mon. Wea. Rev., 129, 2983–2997. https://doi.org/10.1175/1520-0493(2001)129%3C2983:TISAOA%3E2.0.CO;2.

Haggerty, J.A., F. McDonough, J. Black, S. Landolt, C. Wolff, S. Mueller, P. Minnis, and W. Smith, Jr., 2008: Integration of Satellite-derived Cloud Phase, Cloud Top Height, and Liquid Water Path into an Operational Aircraft Icing Nowcasting System. Proc. 13th Conference on Aviation, Range and Aerospace Meteorology, New Orleans, Louisiana, USA, 20-24 January. https://ntrs.nasa.gov/citations/20080008470.

Hallett, J., and S. C. Mossop, 1974: Production of secondary ice particles during the riming process. Nature, 249, 26–28. https://www.nature.com/articles/249026a0.

Hanesiak, J. M., and R. E. Stewart, 1995: The mesoscale and microscale structure of a severe ice pellet storm. Mon. Wea. Rev., 123, 3144–3162. https://doi.org/10.1175/1520-0493(1995)123%3C3144:TMAMSO%3E2.0.CO;2.

Harbaugh, B.J., 2007: Freezing fog formation in a supercooled boundary layer solving the winter fog forecasting challenge for Elmendorf Air Force Base, Alaska. M.S. Thesis, Naval Postgraduate School Monterey, CA 93943-5000. https://apps.dtic.mil/sti/citations/ADA467247

Hardy, J.K., 1944: Measurement of free water in cloud under conditions of icing. National Advisory Committee for Aeronautics (NACA) Wartime Advanced Restricted Report (ARR) 4I11. https://ntrs.nasa.gov/api/citations/19930093553/downloads/19930093553.pdf.

Hauf, T., and F. Schroeder, 2006: Aircraft icing research flights in embedded convection. Meteor. Atmos. Phys., 91, 247–265, https://doi.org/10.1007/s00703-004-0082-y.

Heath, E. D., and L. M. Cantrell, 1972: Aircraft icing climatology for the Northern Hemisphere. Air Weather Service Tech. Rep. 220, 76 pp. Available from Environmental Technical Applications Center (ETAC), USAF, Bldg. 159, Navy Yard Annex, Washington, DC 20333.

Hocke, K., F. Navas-Guzmán, L. Moreira, L. Bernet, and C. Mätzler, 2017: Diurnal Cycle in Atmospheric Water over Switzerland. Remote Sens., 9, 909, 16 pp. https://doi.org/10.3390/rs9090909.

Horn, S., M. Asselin, and D. Baumgardner, 2007: Observations of ice ridge formation on the SJ30-2 leading edge slat in freezing drizzle conditions. SAE International Icing Conference. https://www.sae.org/publications/technical-papers/content/2007-01-3365.

Hudson, J. G., and S. S. Yum, 2001: Maritime–continental drizzle contrasts in small cumuli. J. Atmos. Sci., 58, 915–926. https://doi.org/10.1175/1520-0469(2001)058%3C0915:MCDCIS%3E2.0.CO;2.

Huffman, G. J., and G. A. Norman Jr., 1988: The supercooled warm rain process and the specification of freezing precipitation. Mon. Wea. Rev., 116, 2172–2182. https://doi.org/10.1175/1520-0493(1988)116%3C2172:TSWRPA%3E2.0.CO;2.

Ikeda, K., R. M. Rasmussen, W. D. Hall, and G. Thompson, 2007: Observations of freezing drizzle in extratropical cyclonic storms during IMPROVE-2. J. Atmos. Sci., 64, 3016–3043. https://doi.org/10.1175/JAS3999.1.

Ikeda, K., R. M. Rasmussen, E. Brandes, and F. McDonough, 2009: Freezing drizzle detection with WSR-88D radars. J. Appl. Meteor. Climatol., 48, 41–60. https://doi.org/10.1175/2008JAMC1939.1.

Ikeda, K., M. Steiner, J. Pinto, and C. Alexander, 2013: Evaluation of cold-season precipitation forecasts generated by the hourly updating high-resolution rapid refresh model. Wea. Forecasting, 28, 921–939. https://doi.org/10.1175/WAF-D-12-00085.1.

Isaac, G. A., S. G. Cober, J. W. Strapp, D. Hudak, T. P. Ratvasky, D. L. Marcotte, and F. Fabry, 2001a: Preliminary results from the Alliance Icing Research Study (AIRS). Proc. AIAA 39th Aerospace Science Mtg. and Exh., Reno, NV, AIAA, AIAA 2001-0393, 12 pp. https://www.researchgate.net/publication/44084782_Preliminary_Results_from_the_Alliance_Icing_Research_Study.

Isaac, G.A., S.G. Cober, J.W. Strapp, A.V. Korolev, A. Tremblay and D.L. Marcotte, 2001b: Recent Canadian research on in-flight aircraft icing. Canadian Aeronautics and Space Journal, 47, 1-9. https://www.researchgate.net/publication/257240101_Recent_Canadian_Research_on_Aircraft_In-Flight_Icing.

Isaac, G.A. and co-authors, 2005: First Results from the Alliance Icing Research Study II. AIAA-2005-0252. 43rd Aerospace Science Meeting and Exhibit, Reno, NV, 10-13 January. Amererican Institute of Aeronautics and Astronautics, Washington, D.C., 18pp. https://doi.org/10.2514/6.2005-252.

Jeck, R., 2008: Advances in the characterization of supercooled clouds for aircraft icing applications. FAA Tech. Rep. DOT/FAA/AR-07/4, 54 pp. http://www.tc.faa.gov/its/worldpac/techrpt/ar074.pdf.

Jeck, R., 2010: Models and characteristics of freezing rain and freezing drizzle for aircraft icing applications. FAA Tech. Rep. DOT/ FAA/AR-09/45, 32 pp. http://www.tc.faa.gov/its/worldpac/techrpt/ar0945.pdf.

Jeck, R., 2011: Spatial and Microphysical Characteristics of Low-Ceiling, Temperature-Inverted Clouds in Warm Overrunning and Freezing-Rain Conditions: A Case Study. J. Appl. Meteor., 50, 2062-2072. https://doi.org/10.1175/2011JAMC2448.1.

Jones, A.R. and W. Lewis, 1949: Recommended values of meteorological factors to be considered in the design of aircraft. NACA Tech. Note 1855, 14 pp. https://ntrs.nasa.gov/archive/nasa/casi.ntrs.nasa.gov/19930082528.pdf.

Kalinka, F., K. Roloff, J. Tendel, and T. Hauf, 2017: The in-flight icing warning system ADWICE for European airspace - Current structure, recent improvements and verification results. Meteor. Z., 26, 441–455. https://doi.org/10.1127/metz/2017/0756.

Katz, L. G., 1967: Climatological probability of aircraft icing. Air Weather Service Tech. Rep. 194, 28 pp. Available from Environmental Technical Applications Center (ETAC), USAF, Bldg. 159, Navy Yard Annex, Washington, DC 20333.

Kelsch, M., and L. Wharton, 1996: Comparing PIREPs with NAWAU turbulence and icing forecasts: Issues and results. Wea. Forecasting, 11, 385–390. https://doi.org/10.1175/1520-0434(1996)011%3C0385:CPWNTA%3E2.0.CO;2.

Korolev, A.V. and I. Heckman, 2019: Improved analysis of images of spherical droplets in 2D particle probes for characterization of supercooled sprays. Presented at SAE International Icing Conference, Minneapolis, 17-21 June.

Korolev, A. V., and G. A. Isaac, 2000: Drop growth due to high supersaturation caused by isobaric mixing. J. Atmos. Sci., 57, 1675–1685. https://doi.org/10.1175/1520-0469(2000)057%3C1675:DGDTHS%3E2.0.CO;2.

Korolev, A.V., G.A. Isaac, S.G. Cober, J.W. Strapp, and J. Hallett, 2003: Microphysical characterization of mixed-phase clouds. Q. J. R. Meteorol. Soc. 129: 39–65. https://doi.org/10.1256/qj.01.204.

Korolev, A.V., Isaac, G.A. and Strapp, J.W., 2006: Aircraft escape strategy from supercooled clouds. 44th Aerospace Science Meeting and Exhibit, Reno, NV, 9-12 January. American Institute of Aeronautics and Astronautics, Washington, D.C. AIAA 2006-265. https://doi.org/10.2514/6.2006-265.

Kristovich, D.A.R. and R.A. Steve III, 1995: A satellite study of cloud band frequencies over the Great Lakes. J. Appl. Meteor., 34, 2083-2090. https://doi.org/10.1175/1520-0450(1995)034%3c2083:ASSOCB%3e2.0.CO;2

Kucera, P. A., Brown, B. G., and Holmes, A., 2007: Calibration of the Forecast Icing Product (FIP) – Icing Potential, AWTT- TRB Report, NCAR, Boulder, CO, 2007.

Kunkel, K. E., and J. R. Angel, 1999: Relationship of ENSO to snowfall and related cyclone activity in the contiguous United States. J. Geophys. Res., 104, 19 425–19 434. https://doi.org/10.1029/1999JD900010.

Landolt, S.D., A.J. Schwartz, A. Gaydos and S. DiVito, 2017: Impacts of the implementation of the Automated Surface Observing System (ASOS) on the reports of precipitation type in airport terminal areas around the United States. 18th Conference on Aviation Range and Aerospace Meteorology, American Meteorological Society, Seattle WA, 23-26 Jan. https://ams.confex.com/ams/97Annual/webprogram/Paper313277.html.

Landolt, S.D., J.S. Lave, D. Jacobson, A. Gaydos, S. DiVito, and D. Porter, 2019 – The Impacts of Automation on Present Weather–Type Observing Capabilities across the Conterminous United States. J. Appl. Meteor. and Clim., 58, 2699-2715. https://doi.org/10.1175/JAMC-D-19-0170.1.

Landolt, S.D., A. Gaydos, D. Porter, S. DiVito, D. Jacobson, A. Schwartz, G. Thompson, and J. Lave, 2020: Inferring the presence of freezing drizzle using archived data from the Automated Surface Observing System (ASOS). J. Appl. Meteor. and Clim., 37, 2239-2250. https://doi.org/10.1175/JTECH-D-20-0098.1.

Le Bot, C., 2003: "SIGMA: System of Icing Geographic identification in Meteorology for Aviation," SAE Technical Paper 2003-01-2085, https://doi.org/10.4271/2003-01-2085.

Le Bot, C., and P. Lassegues, 2004: Climatology of icing areas derived from ERA40 analysis. Preprints, 11th Conf. on Aviation, Range, and Aerospace, Hyannis, MA, Amer. Meteor. Soc., P6.12. https://ams.confex.com/ams/pdfpapers/81706.pdf.

Le Bot, C., C. Pagé, and A. Drouin, 2008: "SIGMA: Diagnosis and nowcasting of in-flight icing supporting aircrew and ATM decision making process", AMS, 13th ARAM, 24-28 Jan, New Orleans. https://ams.confex.com/ams/pdfpapers/133706.pdf.

Lee, T. F., F. J. Turk, and K. Richardson, 1997: Stratus and fog products using GOES-8–9 3.9-m data. Wea. Forecasting, 12, 664–677. https://doi.org/10.1175/1520-0434(1997)012%3C0664:SAFPUG%3E2.0.CO;2.

Lentz, J., S. Landolt, S. DiVito and A. Gaydos, 2019: Investigating the variability of winter precipitation rates across an airport terminal area. 19th Conf. on Aviation, Range, and Aerospace Meteorology, Phoenix, 6-10 Jan. https://ams.confex.com/ams/2019Annual/webprogram/Paper351933.html.

Leone, D., R. Endlich, J. Petričeks, R. Collis and J. Porter, 1989: Meteorological considerations used in planning the NEXRAD network. Bull. Amer. Met. Soc., 70, 4-13. https://doi.org/10.1175/1520-0477(1989)070%3C0004:MCUIPT%3E2.0.CO;2.

Löffler-Mang, M. and J. Joss, 2000: An optical disdrometer for measuring size and velocity of hydrometeors. J. Atmos. Oceanic Technol., 17, 130-139. https://doi.org/10.1175/1520-0426(2000)017%3C0130:AODFMS%3E2.0.CO;2.

Majewski, A. and J.R. French, 2019: Supercooled Drizzle Development in Response to Semi-Coherent Vertical Velocity Fluctuations Within an Orographic Layer Cloud. Atmospheric Chemistry and Physics, European Geosciences Union. https://acp.copernicus.org/articles/20/5035/2020/acp-20-5035-2020.pdf.

Manning, K.W. and C.A. Davis, 1997: Verification and sensitivity experiments for the WISP94 MM5 forecasts. Wea. Fore., 12, 719-735. https://doi.org/10.1175/1520-0434(1997)012%3C0719:VASEFT%3E2.0.CO;2.

Martner, B. E., R. M. Rauber, R. M. Rasmussen, E. T. Prater, and M. K. Ramamurthy, 1992: Impacts of a destructive and well-observed cross-country winter storm. Bull. Amer. Meteor. Soc., 73, 169 –172. https://doi.org/10.1175/1520-0477(1992)073%3C0169:IOADAW%3E2.0.CO;2.

Marwitz, J.D., M.K. Politovich, B.C. Bernstein, F.M. Ralph, P.J. Neiman, R. Ashenden and J. Bresch, 1997: Meteorological conditions associated with the ATR-72 aircraft accident near Roselawn, Indiana on 31 October 1994. Bull. Amer. Mer. Soc., 78, 41-52. https://doi.org/10.1175/1520-0477(1997)078%3C0041:MCAWTA%3E2.0.CO;2.

McCray, C., E. Atallah, and J. Gyakum, 2019: Long-duration freezing rain events over North America: Regional climatology and thermodynamic evolution. Wea. Fore., 34, 665-681. https://doi.org/10.1175/WAF-D-18-0154.1.

McDonough, F. and B.C. Bernstein, 1999: Combining satellite, radar, and surface observations with model data to create a better aircraft icing diagnosis. Preprints, 8th Conference on Aviation, Range and Aerospace Meteorology, Dallas TX, 10-15 Jan. Amer. Meteor. Soc., Boston, 467-471. https://ams.confex.com/ams/99annual/abstracts/850.htm.

McDonough, F. and B.C. Bernstein, 2004: Case study of a Great Lakes supercooled large drop icing cloud. 11th Conf. on Aviation, Range and Aerospace, Hyannis, MA, Amer. Meteor. Soc., CD-ROM, P6.15. https://www.researchgate.net/publication/242223051_A_case_study_of_a_Great_Lakes_supercooled_large_drop_icing_cloud.

McDonough, F., D. Adriaansen, K. Shourd and K. Texeira, 2017: Anomalously cold icing conditions within atmospheric river winter storms along the West Coast of North

America. 18th Conf. on Aviation, Range, and Aerospace Meteorology, 23-26 Jan, Seattle, American Meteorological Society. https://ams.confex.com/ams/97Annual/webprogram/Paper314795.html.

McDonough, F., B.C. Bernstein, M.K. Politovich and C.A. Wolff, 2004: The Forecast Icing Potential algorithm. AIAA-2004-0232. 42nd Aerospace Science Meeting and Exhibit, Reno, NV, 5-8 Jan. American Institute of Aeronautics and Astronautics, Washington, D.C., 7pp. https://doi.org/10.2514/6.2004-231.

McDonough, F., J. Haggerty, J. Black, S. Landolt, C. Wolff, S. Mueller, P. Minnis and W. Smith, 2008a: Diagnosing icing severity and supercooled large drop regions with an operational aircraft nowcast system using advanced satellite products. AMS https://ams.confex.com/ams/pdfpapers/163904.pdf.

McDonough F, C.A. Wolff, and M.K. Politovich., 2008b. Forecasting supercooled large drop icing conditions. In 13th Conference on Aviation, Range and Aerospace Meteorology, New Orleans, LA, 11–15 Jan., American Meteorological Society. https://ams.confex.com/ams/pdfpapers/134167.pdf.

Mecikalski, J. R., and Coauthors, 2007: Aviation applications for satellite-based observations of cloud properties, convection initiation, in-flight icing, turbulence and volcanic ash. Bulletin of the American Meteorological Society, 88, 1589-1607, https://doi.org/10.1175/BAMS-88-10-1589.

Milbrandt, J.A., S. Bélair, M. Faucher, M. Vallée, M.L. Carrera and A. Glazer, 2016: The pan-Canadian high resolution (2.5 km) deterministic prediction system. Wea. Fore., 31, 1791-1816. https://doi.org/10.1175/WAF-D-16-0035.1

Miller, D., T. Ratvasky, B. Bernstein, F. McDonough and J.W. Strapp, 1998: NASA/ FAA/NCAR supercooled large droplet icing flight research: summary of winter 96-97 flight operations. 36th Aerospace Science Meeting and Exhibit, AIAA 98-0557, Reno NV, American Institute of Aeronautics and Astronautics, 20 pp. https://ntrs.nasa.gov/api/citations/19980016705/downloads/19980016705.pdf.

Minnis, P., W.L. Smith, L. Nguyen, J.J. Murray, P.W. Heck, and M.M. Khaiyer, 2003: Near-real-time satellite cloud products for icing detection and aviation weather over the USA. Proceedings, FAA In-flight icing/ground de-icing international conference, Chicago, 16-20 June. 2003-01-2097, 6 pp. https://ntrs.nasa.gov/api/citations/20040001075/downloads/20040001075.pdf.

Minnis, P., and Coauthors, 2011: CERES edition-2 cloud property retrievals using TRMM VIRS and Terra and Aqua MODIS data, Part I: Algorithms. IEEE Trans. Geosci. Remote Sens., 49, 4374–4400. https://www-pm.larc.nasa.gov/ceres/pub/journals/Minnis.CERES.Part.Io.pdf.

Mittermaier, M.P., 2014: A strategy for verifying near-convection-resolving forecasts at observing sites. Wea. Forecasting. 29(2), 185-204. https://doi.org/10.1175/WAF-D-12-00075.1.

Moninger, W.R., S. G. Benjamin, B. D. Jamison, T. W. Schlatter, T. L. Smith, and E. J. Szoke, 2008: New TAMDAR fleets and their impact on Rapid Update Cycle (RUC) forecasts. 13th Conference on Aviation, Range and Aerospace Meteorology, New Orleans, LA, 11–15 Jan., American Meteorological Society. https://amdar.noaa.gov/docs/Moninger_13_ARAM.pdf.

Montroy, D.L., M. Richman and P. Lamb, 1998: Observed nonlinearities of monthly teleconnections between tropical Pacific sea surface temperature anomalies and central and eastern North American precipitation. J. Clim., 11, 1812–35. https://doi.org/10.1175/1520-0442(1998)011%3C1812:ONOMTB%3E2.0.CO;2.

Morcrette, C., K. Brown, R. Bowyer, P. Gill, and D. Suri, 2019: Development and evaluation of in-flight icing index forecast for aviation. Wea. Fore., 34, 731-750. https://doi.org/10.1175/WAF-D-18-0177.1.

Mueller, C., T. Saxen, R. Roberts, J. Wilson, T. Betancourt, S. Dettling, N. Oien, and J. Yee, 2003: NCAR Auto-Nowcast System. Wea. Fore., 18, 545-561. https://doi.org/10.1175/1520-0434(2003)018%3C0545:NAS%3E2.0.CO;2.

Nakajima, T., M. D. King, J. D. Spinhirne, and L. F. Radke, 1991: Determination of the optical thickness and effective particle radius of clouds from reflected solar radiation measurements. Part II: Marine stratocumulus observations. J. Atmos. Sci., 48, 728-750. https://doi.org/10.1175/1520-0469(1991)048%3C0728:DOTOTA%3E2.0.CO;2.

NOAA, 1998: Automated Surface Observing System (ASOS) User Guide. https://www.weather.gov/media/asos/aum-toc.pdf.

NOAA, 2011: https://www.roc.noaa.gov/WSR88D/PublicDocs/WSR-88DCONUSCoverage2011.pdf.

NOAA, 2017: https://www.noaa.gov/media-release/noaa-s-newest-geostationary-satellite-will-be-positioned-as-goes-east-fall.

NOAA, 2018: GOES-16 Band Reference Guide. https://www.weather.gov/media/crp/GOES_16_Guides_FINALBIS.pdf. Note: the date of this reference is approximate.

NTSB, 1996: Aircraft accident report: In-flight icing encounter and loss of control, Simmons Airlines, d.b.a. American Eagle flight 4184, Avions de Transport Regional (ATR) Model 72- 212, N401MA, Roselawn, Indiana, October 31 1994. Safety Board Rep. NTSB/AAR-96/01, PB96-910401, DCA95MA001, Vol. 1, 341 pp. https://libraryonline.erau.edu/online-full-text/ntsb/aircraft-accident-reports/AAR96-02.pdf.

NTSB, 1998: Aircraft accident report: In-flight icing encounter and uncontrolled collision with terrain, COMAIR flight 3272, Embraer EMB-120RT, N265 CA, Monroe MI, January 9, 1997. Safety Board Rep. NTSB/AAR-98/04, PB08-910404, DCA97MA017, 348 pp. https://webharvest.gov/peth04/20041108013047/http://www.ntsb.gov/publictn/1998/AAR9804.pdf.

NTSB, 2001: Aviation accident final report. Accident number DCA01MA031. Embraer EMB-120. https://reports.aviation-safety.net/2001/20010319-0_E120_N266CA.pdf.

NTSB, 2006: Incident number LAX06IA076. Aviation Incident Data Summary, https://aircrafticing.grc.nasa.gov/documents/2006_SF340B_Santa_Maria_CA_Incident_Summary.pdf.

NTSB, 2007: Crash during approach to Landing, Circuit City Stores, Inc. Cessna Citation 560, N500AT, Pueblo, Colorado, February 16, 2005. Aircraft Accident Rep. NTSB/AAR-07/02, 86 pp., https://reports.aviation-safety.net/2005/20050216-0_C560_N500AT.pdf.

Ohtake, T., 1963: Hemispheric investigations of warm rain by radiosonde data. J. Appl. Meteor., 2, 594–607. https://doi.org/10.1175/1520-0450(1963)002%3C0594:HIOWRB%3E2.0.CO;2.

Olofsson, B., E. Olsson, S. Andersson, T. Mårtensson & E. Mårtensson, 2003: A new algorithm to estimate aircraft icing in the HIRLAM model. Meteorol. Appl., 10, 111-114. https://rmets.onlinelibrary.wiley.com/doi/pdfdirect/10.1017/S1350482703002020.

Petty, K. R., and C. D. J. Floyd, 2004: A statistical review of aviation airframe icing accidents in the U.S. Preprints, 11th Conf. on Aviation, Range and Aerospace, Hyannis, MA, Amer. Meteor. Soc. https://ams.confex.com/ams/pdfpapers/81425.pdf.

Pilewskie, P. and S. Twomey, 1987: Cloud phase discrimination by reflectance measurements near 1.6 and 2.2 microns. J. Atmos. Sci., 44, 3419-3420. https://doi.org/10.1175/1520-0469(1987)044%3C3419:CPDBRM%3E2.0.CO;2.

Plummer, D. A., S. Goke, R. M. Rauber, and L. Di Girolamo, 2010: Discrimination of mixed-phase versus ice-phase clouds using dual-polarization radar with application to detection of aircraft icing regions. J. Appl. Meteor. Climatol., 49, 920–936. https://doi.org/10.1175/2009JAMC2267.1.

Pobanz, B.M., J.D. Marwitz, and M.K. Politovich, 1994: Conditions associated with large-drop regions. J. Appl. Meteor., 33, 1366-1372. https://doi.org/10.1175/1520-0450(1994)033%3C1366:CAWLDR%3E2.0.CO;2.

Politovich, M.K., 1989: Aircraft icing caused by large supercooled droplets. J. Appl. Meteor., 28, 856-868. https://doi.org/10.1175/1520-0450(1989)028%3C0856:AICBLS%3E2.0.CO;2.

Politovich, M.K., 1996: Response of research aircraft to icing and evaluation of a severity index. J. Aircraft, 33, 291–297. https://arc.aiaa.org/doi/10.2514/3.46936.

Politovich, M.K. and B.C. Bernstein, 1995: Production and depletion of supercooled liquid water in a Colorado winter storm. J. Appl. Meteor., 34, 2631-2648. https://doi.org/10.1175/1520-0450(1995)034%3C2631:PADOSL%3E2.0.CO;2.

Politovich, M.K. and B.C. Bernstein, 2006: Recent success stories from the In-Flight Icing PDT. 12th Conf. on Aviation, Range and Aerospace Meteorology, Atlanta GA, 29 Jan - 2 Feb, Amer. Meteor. Soc., Boston. https://ams.confex.com/ams/pdfpapers/100728.pdf.

Politovich, M.K., B.C. Bernstein, J. Hopewell, T. Lindholm, L. Gauerke, C. Knable, D. Hazen and B. Martner, 2002: An Unusual Icing Case: 20 March 2000, Denver, Colorado. Preprints, 10th Conference on Aviation, Range and Aerospace Meteorology, Portland OR, 13-17 May, Amer. Meteor. Soc., Boston, 37-40. https://ams.confex.com/ams/pdfpapers/39170.pdf.

Politovich, M.K., C. Wolff, B.C. Bernstein, and F. McDonough, 2006: CIP Severity Scientific and Technical Document. Prepared for the FAA Aviation Weather Technology Transfer Board, June 2006.

Ramsay, A., 1999: A multi-sensor freezing drizzle algorithm for the automated surface observing system. Preprints, 15th Int. Conf. on Interactive Information and Processing Systems for Meteorology, Oceanography, and Hydrology, Dallas, TX, Amer. Meteor. Soc., 193–196. https://ams.confex.com/ams/older/99annual/abstracts/30.htm.

Rasmussen, R., and Coauthors, 1992: Winter Icing and Storms Project (WISP). Bull. Amer. Meteor. Soc., 73, 951–974. https://doi.org/10.1175/1520-0477(1992)073%3C0951:WIASP%3E2.0.CO;2.

Rasmussen, R.M., B.C. Bernstein, M. Murakami, G. Stossmeister, J. Reisner and B. Stankov, 1995: The 1990 Valentine's Day arctic outbreak, Part I: Mesoscale and microscale structure and evolution of a Colorado front range shallow upslope cloud. J. Appl. Meteor., 34, 1481-151. https://journals.ametsoc.org/view/journals/apme/34/7/1520-0450-34_7_1481.xml?rskey=cL8NqT&result=10.

Rasmussen, R., and Coauthors, 2001: Weather Support to Deicing Decision Making (WSDDM): A winter weather nowcasting system. Bull. Amer. Meteor. Soc., 82, 579–595. https://doi.org/10.1175/1520-0477(2001)082%3C0579:WSTDDM%3E2.3.CO;2.

Rasmussen, R.M., I. Geresdi, G. Thompson, K. Manning, and E. Karplus, 2002: Freezing drizzle formation in stably stratified layer clouds: The role of radiative cooling of cloud droplets, cloud condensation nuclei, and ice initiation. J. Atmos. Sci., 59, 837-860. https://doi.org/10.1175/1520-0469(2002)059%3C0837:FDFISS%3E2.0.CO;2.

Ratvasky, T.P., B.P. Barnhart, and S. Lee, 2010: Current methods for modeling and simulating icing effects on aircraft performance, stability and control. J. Aircraft, 47, 201-211. https://arc.aiaa.org/doi/abs/10.2514/1.44650.

Rauber, R. M. and A. Tokay, 1991: An explanation for the existence of supercooled liquid water at the top of cold clouds. J. Atmos. Sci., 48, 1005-1023. https://doi.org/10.1175/1520-0469(1991)048%3C1005:AEFTEO%3E2.0.CO;2.

Rauber, R. M., M. K. Ramamurthy, and A. Tokay, 1994: Synoptic and mesoscale structure of a severe freezing rain event: The St. Valentine's Day ice storm. Wea. Fore., 9, 183–208. https://doi.org/10.1175/1520-0434(1994)009%3C0183:SAMSOA%3E2.0.CO;2.

Rauber, R. M., L. Olthoff, M. Ramamurthy, and K. Kunkel, 2000: The relative importance of warm rain and melting processes in freezing precipitation events. J. Appl. Meteor., 39, 1185–1195. https://doi.org/10.1175/1520-0450(2000)039%3C1185:TRIOWR%3E2.0.CO;2.

Rauber, R. M., L. Olthoff, M. Ramamurthy, and D. Miller, 2001: Synoptic weather pattern and sounding-based climatology of freezing precipitation in the United States east of the Rocky Mountains. J. Appl. Meteor., 40, 1724-1747. https://doi.org/10.1175/1520-0450(2001)040%3C1724:ASWPAS%3E2.0.CO;2.

Rauber, R.M., D.M. Plummer, M.K. Macomber, A.A. Rosenow, G.M. McFarquhar, B.F. Jewett, D. Leon, N. Owens, and J. Keeler, 2015: The role of cloud-top generating cells and boundary layer circulations in the fine-scale radar structure of a winter cyclone over the Great Lakes. Mon. Wea. Rev., 143, 2291-2318. https://doi.org/10.1175/MWR-D-14-00350.1.

Reehorst, A., D. Brinker, M. Politovich, D. Serke, C. Ryerson, A. Pazmany, and F. Solheim, 2009: Progress towards the remote sensing of aircraft icing hazards. NASA/TM-2009-215828, 15 pp. https://ntrs.nasa.gov/api/citations/20100001322/downloads/20100001322.pdf.

Reeves, H.D. H. and K. Howard, 2017: Multi-radar/Multi-sensor tools for aviation. 18th Conf. on Aviation, Range, and Aerospace Meteorology, 23-26 Jan., Seattle, American Met. Society. https://ams.confex.com/ams/97Annual/webprogram/Paper306773.html.

Reeves. H.D. and J. Waters, 2019: Dual-polarized radar coverage in terminal airspaces and its effect on interpretation of winter weather signatures: current capability and future recommendations. J. Appl. Meteor. and Clim., 58, 165-183. https://doi.org/10.1175/JAMC-D-18-0123.1.

Reeves, H. D., K. L. Elmore, A. Ryzhkov, T. Schuur, and J. Krause, 2014: Sources of uncertainty in precipitation-type forecasting. Wea. Forecasting, 29, 936–953. https://doi.org/10.1175/WAF-D-14-00007.1.

Reeves, H. D., A. V. Ryzhkov, J. Krause, 2016: Discrimination between winter precipitation types based on spectral-bin microphysical modeling. J. Appl. Meteor. Climatol., 55, 1747-1761. https://doi.org/10.1175/JAMC-D-16-0044.1.

Regan, M., 1998: Canadian ice storm 1998. WMO Bull., 47, 250– 256.

Reges, H., N. Doesken, J. Turner, N. Newman, A. Bergantino, and Z. Schwalbe, 2016: CoCoRAHS: The evolution and accomplishments of a volunteer rain gauge network. Bull. Amer. Met. Soc., 97, 1831-1846. https://doi.org/10.1175/BAMS-D-14-00213.1.

Reinking, R.F., S.Y. Matrosov, B.E. Martner, and R.A. Kropfli 1997: Dual-polarization radar to identify drizzle, with applications to aircraft icing avoidance. J. Aircraft, 34, 778-784. https://doi.org/10.2514/2.2243.

Reisner, J., R. M. Rasmussen, and R. T. Bruintjes, 1998: Explicit forecasting of supercooled liquid water in winter storms using the MM5 mesoscale model. Quart. J. Roy. Meteor.

Soc., 124, 1071–1107. https://rmets.onlinelibrary.wiley.com/doi/abs/10.1002/qj.49712454804.

Roach, W. T., D. A. Forrester, M. E. Crewe, and K. F. Watt, 1984: An icing climatology for helicopters. Royal Meteorological Office Special Investigations Memo. 112, 41 pp.

Roberts N. M. and H. W. Lean: Scale-selective verification of rainfall accumulations from high-resolution forecasts of convective events. Mon. Wea. Rev., 136, 78–97, 2008. https://doi.org/10.1175/2007MWR2123.1.

Rosenfeld, D., and W. L. Woodley, 2000: Deep convective clouds with sustained supercooled liquid water down to -37.5°C. Nature, 405, 440–442. https://www.nature.com/articles/35013030.

Rosenfeld, D. and co-authors, 2013: The common occurrence of highly supercooled drizzle and rain near the coastal regions of the western United States. J. Geoph. Res.: Atmospheres, 118, 9819-9833. https://agupubs.onlinelibrary.wiley.com/doi/pdf/10.1002/jgrd.50529.

Rugg, A., S. Tessendorf, D.R. Adriaansen and J.A. Haggerty, 2019: Development of new icing products for supercooled large drop conditions. 19th Conf. on Aviation, Range, and Aerospace Meteorology, Phoenix, 6-10 Jan. https://ams.confex.com/ams/2019Annual/webprogram/Paper352349.html.

Ryerson, C. C., 1988: Atmospheric icing climatologies of two New England mountains. J. Appl. Meteor., 27, 1261–1281. https://doi.org/10.1175/1520-0450(1988)027%3C1261:AICOTN%3E2.0.CO;2.

Ryerson, C. and A. Ramsay, 2007: Quantitative Ice Accretion Information from the Automated Surface Observing System. J. Appl. Meteor., 46, 1423-1437. https://doi.org/10.1175/JAM2535.1.

Ryerson, C., G. Koenig, C. Scott, and E. Phetteplace, 2006: Supercooled cloud scale length and correlative relationships. 12th Conf. on Aviation, Range, and Aerospace Meteorology, 30 Jan - 2 Feb, Atlanta, GA, American Met. Society. https://ams.confex.com/ams/pdfpapers/105184.pdf.

Ryerson, C., M. Politovich, K. Rancourt, G. Koenig, R. Reinking, and D. Miller, 2000: Overview of Mount Washington Icing Sensors Project. AIAA-2000-0488. 38th Aerospace Sciences Meeting and Exhibit, 10-13 Jan, Reno. https://ntrs.nasa.gov/api/citations/20030068142/downloads/20030068142.pdf.

Sand, W.R., and C. Biter, 1997: Pilot response to icing: It depends. Preprints, 7th Conf. on Aviation, Range, and Aerospace Meteorology, 2-7 February, Long Beach, CA, American Meteorological Society, 116-119.

Sand, W., W. Cooper, M. Politovich, and D. Veal, 1984: Icing conditions encountered by a research aircraft. J. Climate Appl. Meteor., 23, 1427–1440. https://journals.ametsoc.org/view/journals/apme/23/10/0733-3021-23_10_1427.xml.

Sanders, K. J., C. M. Gravelle, J. P. Gagan, and C. E. Graves, 2013: Characteristics of major ice storms in the central United States. J. Oper. Meteor., 1 (10), 100□113. http://nwafiles.nwas.org/jom/articles/2013/2013-JOM10/2013-JOM10.pdf.

Schmit, T., M. Gunshor, W.P. Menzel, J. Gurka, J. Li and A.S. Bachmeier, 2005: Introducing the next-generation advanced baseline imager on GOES-R. Bull. Amer. Met. Soc., 86, 1079-1096. https://doi.org/10.1175/BAMS-86-8-1079.

Schneider, T.L., R.F. Reinking, W.C. Campbell, K.A. Clark, J.S. Gibson, D.A. Hazen, S.Y. Matrosov, K.P. Moran, and M.J. Post, 2002: NOAA/ETL's polarization radar-microwave radiometer system for detecting in-flight icing conditions: progress in the design and development of GRIDS. Proceedings of the 10th Conference on Aviation, Range and Meteorology, Portland, OR, May 2002. https://ams.confex.com/ams/pdfpapers/39117.pdf.

Schultz, P., and M. K. Politovich, 1992: Toward the improvement of aircraft-icing forecasts for the continental United States. Wea. Forecasting, 7, 491–500. https://doi.org/10.1175/1520-0434(1992)007%3C0491:TTIOAI%3E2.0.CO;2.

Schwartz, A., S. Landolt, J. Cyccone, A. Jachcik, A. Gaydos, R. K. Goodrich, and S. DiVito, 2017: Meso-Gamma and Microscale Variability of Snowfall Rate Across an Airport Terminal Area. 18th Conference on Aviation Range and Aerospace Meteorology, American Meteorological Society, Seattle WA, 23-26 January. https://ams.confex.com/ams/97Annual/webprogram/Paper313304.html.

Serke, D., G. Zhang, J. Vivekanandan, T.L. Schneider, P. Minnis, and M. Poellot, 2005: Verification of S-Polka Ka-band radar/radiometer LWC and RES retrievals with GRIDS retrievals and aircraft measurements and comparison to GOES icing products for the WISP04 10-11 March event. 32nd Conf. on Radar Met., 24-29 Oct. https://ams.confex.com/ams/pdfpapers/95741.pdf.

Serke, D. J., F. McDonough, and M. K. Politovich, 2008: Analysis of 3-D NEXRAD Mosaic reflectivity data co-located with research aircraft and satellite data: Implications on in-flight icing. 13th Conference on Aviation, Range and Aerospace Meteorology, American Meteorological Society, New Orleans, LA, US. https://ams.confex.com/ams/pdfpapers/128224.pdf.

Serke, D., S. Ellis, A. Reehorst, J. Hubbert, D. Albo, A. Weekley, D. Adriaansen, C. Johnston, and M. Politovich, 2012. Progress toward a volumetric in-flight icing hazard system for airports which incorporates operational dual-polarization S-band radars, 7th European Conference on Radar in Meteorology and Hydrology, June 24-29, Toulouse, FR, 2012. http://www.meteo.fr/cic/meetings/2012/ERAD/presentations/tuesday/4B-6.pdf.

Serke, D., M. King, and A. Reehorst, 2015: Initial Results from Radiometer and Polarimetric Radar-based Icing Algorithms Compared to In-situ Data. 2015-01-2153, 2015 SAE International Conference on Icing of Aircraft, Engines and Structures, Prague. https://www.sae.org/publications/technical-papers/content/2015-01-2153.

Serke, D., M. King, R. Hansen, and A. Reehorst, 2016: Analysis of 2015 Winter In-flight Icing Case Studies with Ground-based Remote Sensing Systems Compared to In-situ SLW-sondes, NASA/TM-2016-219130, October, 2016. https://ntrs.nasa.gov/api/citations/20160013219/downloads/20160013219.pdf.

Serke, D. and co-authors, 2017: Initial performance evaluation of a radar-based super-cooled water detection algorithm during the SNOWIE Field Campaign, AMS 38th Conference on Radar Meteorology, Aug 28-Sep 1, Chicago. https://ams.confex.com/ams/38RADAR/webprogram/Paper320660.html.

Serke, D., S. Tessendorf, A. Korolev, I. Heckman, J. French, A. Rugg, J. Haggerty, and D. Albo, 2019: Performance evaluation of a radar-based super-cooled water detection algorithm during the SNOWIE Field Campaign, American Meteorological Society, 39th Intl Conference on Radar Meteorology, Nara, Japan, 16-20 September 2019. https://www.researchgate.net/publication/335868094_Performance_evaluation_of_a_radar-based_super-cooled_water_detection_algorithm_during_the_SNOWIE_Field_Campaign.

Sims, D. and T. Carty, 2000: Integrated Icing Diagnostic Algorithm (IIDA) assessment at regional airlines - Final report. DOT/FAA/CT-TN00/18. https://apps.dtic.mil/sti/pdfs/ADA384904.pdf.

Sims, D., J. Haggerty and B. Pettigrew, 2019: Federal Aviation Administration Aviation Weather Research Program Plans for Enhanced In-Flight Icing Diagnosis and Forecast Capabilities. Presented at SAE International Icing Conference, Minneapolis. 18-21 June.

Smalley, D.J. and co-authors, 2017: BAIRS-II: The Second Buffalo Area Icing and Radar Study. 38th Conference on Radar Meteorology, Amer. Met. Soc., Zurich. https://ams.confex.com/ams/38RADAR/webprogram/Paper320331.html.

Smith, W., P. Minnis, C. Fleeger, and D. Spangenberg, 2015: Diagnosing aircraft icing potential from satellite cloud retrievals. 2015-01-0103, 2015 SAE International Conference on Icing of Aircraft, Engines and Structures, Prague.

Smith, W., C. Wang, and D. Spangenberg, 2019: Satellite cloud and icing analyses: challenges and progress addressing them. Presented at the FAA Icing Weather Tools Review, Boulder, Oct. 2019.

Spangenberg, D.A., P. Minnis, W.L. Smith, and F. Chang, 2011: Nowcasting aircraft icing conditions in the presence of multi-layered clouds using meteorological satellite data. 2011-38-0041, 2011 SAE International Conference on Icing of Aircraft, Engines and Structures, Minneapolis. https://ntrs.nasa.gov/citations/20110013244.

Stoelinga, M.T. and co-authors, 2003: Improvement of microphysical parameterization through observational verification experiments (IMPROVE) Bull. Amer. Meteor. Soc., 84, 1807–1826. https://doi.org/10.1175/BAMS-84-12-1807.

Strapp, J., R. Stewart, and G. Isaac, 1996: A Canadian climatology of freezing precipitation and a detailed study using data from St. John's, NF. Proc. FAA Int. Conf. on Aircraft Inflight Icing, Vol. 2, Springfield VA, FAA, DOT/FAA/AR-96/81, 45-56. https://www.researchgate.net/publication/309616506_A_CANADIAN_CLIMATOLOGY_OF_FREEZING_PRECIPITATION_AND_A_DETAILED_STUDY_USING_DATA_FROM_ST_JOHN'S_NEWFOUNDLAND.

Tafferner, A., T. Hauf, C. Leifeld, T. Hafner, H. Leykauf, and U. Voigt, 2003: ADWICE: Advanced Diagnosis and Warning System for Aircraft Icing Environments. Wea. Fore., 18, 184–203. https://doi.org/10.1175/1520-0434(2003)018%3C0184:AADAWS%3E2.0.CO;2.

Tessendorf, S.A., and co-authors, 2017a: Developing improved products to forecast and diagnose aircraft icing conditions based upon drop size. 2017 AIAA Aviation Forum, Denver, CO. https://arc.aiaa.org/doi/10.2514/6.2017-4473.

Tessendorf, S.A. and co-authors, 2017b: An evaluation of model-based icing forecasts of a supercooled large drop icing event using detailed in situ measurements. 18th Conf. on Aviation, Range, and Aerospace Meteorology, 23-26 January, Seattle, WA, American Meteorological Society. https://ams.confex.com/ams/97Annual/webprogram/Paper308095.html.

Tessendorf, S., D. Serke, K. Ikeda, 2017c: Dual-polarization radar analysis of orographic wintertime clouds with freezing drizzle. 38th Conf. Radar Meteorology, American Meteorological Society, Chicago, IL. https://ams.confex.com/ams/38RADAR/webprogram/Paper321123.html.

Tessendorf, S., and coauthors, 2017d: Final Report on Idaho Power Cloud Seeding Phase Six Study. Submitted to Idaho Power Company, 94 pp.

Tessendorf, S. A., and co-authors, 2019a: A transformational approach to winter orographic weather modification research: The SNOWIE Project, Bull. Amer. Meteor. Soc., https://doi.org/10.1175/BAMS-D-17-0152.1.

Tessendorf, S.A., A. Rugg, D. Jacobson, D. Serke, D. Adriaansen, J. Haggerty, and A. Korolev, 2019b: Predicting drop size for aircraft icing products. Presented at SAE International Icing Conference, Minneapolis, 17-21 June.

Thompson, G., 2019: High Resolution Numerical Weather Model Forecasts of Icing at the Ground and in the Air. International Workshop on Atmospheric Icing of Structures 2019. https://iwais2019.is/images/Papers/042_iwais_thompson.pdf.

Thompson, G. and T. Eidhammer, 2014: A study of aerosol impacts on clouds and precipitation development in a large winter cyclone. J. Atmos. Sci., 71, 3636–3658. https://doi.org/10.1175/JAS-D-13-0305.1.

Thompson, G., R. Bruintjes, B.G Brown, and F. Hage, 1997a: Intercomparison of In-Flight Icing Algorithms. Part I: WISP94 Real-Time Icing Prediction and Evaluation Program. Wea. Fore., 12, 878-889. https://doi.org/10.1175/1520-0434(1997)012%3C0878:IOIFIA%3E2.0.CO;2.

Thompson, G., R. Bullock, and T. F. Lee, 1997b: Using satellite data to reduce spatial extent of diagnosed icing. Wea. Forecasting, 12, 185–190. https://doi.org/10.1175/1520-0434(1997)012%3C0185:USDTRS%3E2.0.CO;2.

Thompson, G., R. M. Rasmussen, and K. Manning, 2004: Explicit forecasts of winter precipitation using an improved bulk microphysics scheme. Part I: Description and

sensitivity analysis. Mon. Wea. Rev., 132, 519–542. https://doi.org/10.1175/1520-0493(2004)132%3C0519:EFOWPU%3E2.0.CO;2.

Thompson, G., P. R. Field, R. M. Rasmussen, and W. D. Hall, 2008: Explicit forecasts of winter precipitation using an improved bulk microphysics scheme. Part II: Implementation of a new snow parameterization. Mon. Wea. Rev., 136, 5095–5115, https://doi.org/10.1175/2008MWR2387.1.

Thompson, G., M. Politovich, and R. Rasmussen, 2017: A Numerical Weather Model's Ability to Predict Characteristics of Aircraft Icing Environments. Wea. Fore., 32, 207-221. https://doi.org/10.1175/WAF-D-16-0125.1.

Tuttle, J. D., and G. B. Foote, 1990: Determination of the boundary layer airflow from a single Doppler radar. J. Atmos. Ocean. Tech., 7, 218-232. https://doi.org/10.1175/1520-0426(1990)007%3C0218:DOTBLA%3E2.0.CO;2.

USAF, 1986: Climatic atlas of icing potential over North America. Rep. USAFETAC/DS-86/001, U.S. Air Force, 129 pp. Environmental Technical Applications Center (ETAC), Scott Air Force Base, IL 62225–5458. https://apps.dtic.mil/dtic/tr/fulltext/u2/a174260.pdf.

Van Den Broeke, M.S., D.M. Tobin, and M.R. Kumjian, 2016: Polarimetric radar observations of precipitation type and rate from the 2-3 March 2014 winter storm in Oklahoma and Arkansas. Wea. Fore., 31, 1179-1196. https://doi.org/10.1175/WAF-D-16-0011.1.

van 't Hoff, S., Lammers, K., Hwang, Y., Kim, J. et al., 2020 "Korean Utility Helicopter KUH-1 Icing Certification Program," SAE Int. J. Adv. & Curr. Prac. in Mobility 2(1): 205-215. https://doi.org/10.4271/2019-01-1989.

Vivekanandan, J., D. S. Zrnic, S.M. Ellis, R. Oye, A. V. Ryzhkov and J. Straka, 1999: Cloud Microphysics Retrieval Using S-band Dual-Polarization Radar Measurements. Bull. Amer. Meteor. Soc., 80, 381-388. https://doi.org/10.1175/1520-0477(1999)080%3C0381:CMRUSB%3E2.0.CO;2.

Vivekanandan, J., Zhang, G., and Politovich, M., 2001: An Assessment of Droplet Size and Liquid Water Content Derived From Dual-Wavelength Radar Measurements to the Application of Aircraft Icing Detection. J. Atmos. Ocean. Tech., 18, 1787–1798. https://doi.org/10.1175/1520-0426(2001)018%3C1787:AAODSA%3E2.0.CO;2.

Wade, C. G., 2003: A multisensory approach to detecting drizzle on ASOS. J. Atmos. Oceanic Technol., 20, 820–832. https://doi.org/10.1175/1520-0426(2003)020%3C0820:AMATDD%3E2.0.CO;2.

Weener, E., 2011a: Lessons from icing accidents and incidents. Presented to the Experimental Aircraft Association.

Weener, E., 2011b: Icing: Accident Driven Actions and Inactions. Keynote presentation at SAE 2011 International Conf. on Aircraft and Engine Icing and Ground Deicing, Chicago, 13-17 June.

Weinrich, J., 2020: JPSS Aviation Initiative. 20th Conference on Aviation Range and Aerospace Meteorology. Amer. Met. Soc., Boston. https://ams.confex.com/ams/2020Annual/webprogram/Paper369145.html.

Weygandt, S. and Coauthors, 2016: Improvements in forecasting regions of aviation hazard impact from advances in the HRRR and RAP models. 5th Aviation, Range, and Aerospace Special Symposium, 11-13 January, New Orleans, American Meteorological Society. https://ams.confex.com/ams/96Annual/webprogram/Paper289712.html.

Weygandt, S. and Coauthors, 2017: Rap and HRRR Model/Assimilation System Improvements for Aviation Weather Applications: Latest Upgrades and Ongoing Work. 18th Conf. on Aviation, Range, and Aerospace Meteorology, 23-26 Jan, Seattle, American Meteorological Society. https://ams.confex.com/ams/97Annual/webprogram/Paper313324.html.

Williams, E. and Coauthors, 2011: Dual-polarization radar winter storm studies supporting development of NEXRAD-based aviation hazard products. 35th Conf. on Radar Meteorology, Amer. Met. Soc., Boston. https://ams.confex.com/ams/35Radar/webprogram/Paper191770.html.

Williams, E. and Coauthors, 2015a: Measurements of Differential Reflectivity in Snowstorms and Warm Season Stratiform Systems, J. Appl. Meteor., 54, 573-595. https://doi.org/10.1175/JAMC-D-14-0020.1.

Williams, E. and Coauthors, 2015b: Aircraft In Situ Validation of Hydrometeors and Icing Conditions Inferred by Ground-based NEXRAD Polarimetric Radar. 2015-01-2152, 2015 SAE International Conference on Icing of Aircraft, Engines and Structures, Prague. https://www.sae.org/publications/technical-papers/content/2015-01-2152.

Williams, J. K., 2014: Using random forests to diagnose aviation turbulence. Machine Learning, 95, 51–70. https://link.springer.com/article/10.1007%2Fs10994-013-5346-7.

Wilson, J.W., N.A. Crook, C.K. Mueller, J. Sun and M. Dixon, 1998: Nowcasting thunderstorms: a status report. Bull. Amer. Met. Soc., 79, 2079-2099. https://doi.org/10.1175/1520-0477(1998)079%3C2079:NTASR%3E2.0.CO;2.

Wolde, M. and D. Marcotte, 2008: NRC Convair-580 atmospheric remote sensing capabilities and recent research activities. https://www.arm.gov/news-events/docs/aaf/workshop2008/1015/1100to1115Wolde.pdf.

Wolde, M., D. Hudak and A. Pazmany, 2012: Characterization of supercooled and mixed phase clouds using airborne dual-frequency radar and G-band radiometer. ERAD 2012, 7th Conf. on Radar in Meteorology and Hydrology. Toulouse, 24-29 June. http://www.meteo.fr/cic/meetings/2012/ERAD/extended_abs/MIC_408_ext_abs.pdf.

Wolde, M. and co-authors, 2020: In-Cloud Icing and Large-Drop Experiment (ICICLE). Part II: Airborne Measurements. https://ams.confex.com/ams/2020Annual/meetingapp.cgi/Paper/369166.

Wolff, C.A. and B.C. Bernstein, 2004: Scales of aircraft icing: A comparison of icing PIREPs to liquid water measurements from research aircraft. 11th Conference on Aviation, Range and Aerospace Meteorology, Hyannis MA, 11-14 October, Amer. Meteor. Soc., Boston. https://ams.confex.com/ams/pdfpapers/81297.pdf.

Wolff, C.A. and F. McDonough, 2010: A Comparison of the WRF Rapid Refresh and Rapid Update Cycle Numerical Models to Aircraft Icing Conditions. AMS 14th Conference on Aviation Range and Aerospace Meteorology, Atlanta GA, 17-21 January 2010. https://ams.confex.com/ams/90annual/webprogram/Paper160083.html.

Wolff, C.A., F. McDonough, M.K. Politovich, B. C. Bernstein and G.M. Cunning, 2007: FIP Severity Technical Document. Created for the FAA Aviation Weather Technology Transfer Board.

Wolff, C.A., F. McDonough, M.K. Politovich, and G.M. Cunning, 2009: Forecast Icing Product: Recent upgrades and improvements. AIAA 2009-3531. 1st AIAA Atmospheric and Space Environments Conference. San Antonio, 22-25 June. https://arc.aiaa.org/doi/abs/10.2514/6.2009-3531.

Wolff, J.K., M. Harrold, T. Hertneky, K. Ikeda, J. Halley Gotway, and T.L. Folwer, 2017: Using Precipitation Type Weather Reports to Assess Select Operational Numerical Weather

Prediction Models for Terminal Area Icing Weather Information for Nextgen (TAIWIN). https://ams.confex.com/ams/97Annual/webprogram/Paper312090.html.

Xu, M., G. Thompson, D. Adriaansen, and S. Landolt, 2019: On the value of time-lag-ensemble averaging to improve numerical model predictions of aircraft icing conditions. Wea. Fore., 34, 507-519. https://doi.org/10.1175/WAF-D-18-0087.1.

Young, G. S., B. G. Brown, and F. McDonough, 2002: An inferred icing climatology - Part I: Estimation from pilot reports and surface conditions. Preprints, 10th Conf. on Aviation, Range, and Aerospace Meteorology, Portland, OR, Amer. Meteor. Soc. https://ams.confex.com/ams/pdfpapers/38737.pdf.

Yu, J. and Y. Zou, 2013: The enhanced drying effect of Central-Pacific El Niño on US winter. Environmental Research Letters 8, 014019. https://iopscience.iop.org/article/10.1088/1748-9326/8/1/014019/pdf.

Yuter, S.E., D.E. Kingsmill, L.B. Nance, M. Löffler-Mang, 2006: Observations of precipitations size and fall speed characteristics within coexisting rain and wet snow. J. Appl. Meteor. Clim., 45, 1450-1464. https://doi.org/10.1175/JAM2406.1.

Zhang, J. and co-authors, 2011: National Mosaic and Multi-Sensor QPE (NMQ) System: Description, results, and future plans. Bull. Amer. Meteor. Soc., 92, 1321–1338. https://doi.org/10.1175/2011BAMS-D-11-00047.1.

Zhang, G. and co-authors, 2019: Current Status and Future Challenges of Weather Radar Polarimetry: Bridging the Gap between Radar Meteorology/Hydrology/Engineering and Numerical Weather Prediction. Adv. Atmos. Sci. 36, 571-588. https://link.springer.com/article/10.1007/s00376-019-8172-4.

Zishka, K. M., and P. J. Smith, 1980: The climatology of cyclones and anticyclones over North America and surrounding ocean environs for January and July, 1950–77. Mon. Wea. Rev., 108, 387–401. https://doi.org/10.1175/1520-0493(1980)108%3C0387:TCOCAA%3E2.0.CO;2.

Zrnic, D., N. Balakrishnan, C. Ziegler, V. Bringi, K. Aydin and T. Matejka, 1993: Polarimetric signatures in the stratiform region of a Mesoscale Convective System. J. Appl. Meteor., 32, 678-693. https://doi.org/10.1175/1520-0450(1993)032%3C0678:PSITSR%3E2.0.CO;2.

A Appendix A - Daily reporting and forecaster briefing requirements

This section describes the expectations for daily reporting during the program.

1) OPERATIONS DIRECTOR

The **Operations Director** has the following daily reporting requirements:

- Submit Operations Plan of the Day to the Field Catalog (http://catalog.eol.ucar.edu/icicle) within 30 min after Executive Committee Meeting is complete. This should be short and indicate the plan for the next flight and the day, including whether the flight is a go or no-go, planned departure timing, location of flight and objectives. Note specific requests for supplemental soundings, high-resolution GOES-16 satellite data and any other needs, including their timing. Contact parties responsible for supplemental sounding launches and satellite data to make requests. Ideally, such requests are made well in advance.
- If a flight is planned, submit a description of the Flight Plan to the Field Catalog within 45 min after the Executive Committee Meeting is complete. This should include details on the planned timing, location, altitude, sampling strategy, and how objectives are to be met.
- After a flight has been completed, submit a Mission Summary to the Field Catalog, preferably within 12 hours after the flight. Include a thorough description of the flight, what was observed, and what was accomplished, including the relation to ICICLE objectives. Relevant details and graphics from the event should be included. Note any significant issues or events that are pertinent to the program, such as communications issues, aircraft maintenance issues, crew duty schedule limits, problems with key data sources, etc.

2) FORECASTER

Forecaster "A" (morning forecaster) has the following daily reporting requirements:

- Submit AM Forecast Summary to the Field Catalog by end of shift. When submitting to the Field Catalog, the time of the submission should be set to the time the briefing was delivered during the shift (e.g., 0300). Note that this time could change depending on

adjustments to the standard daily schedule due to weather or personnel requirements. Include relevant imagery, descriptions and annotation.

Forecaster "B" (afternoon forecaster) has the following daily reporting requirements:

- Submit PM Forecast Summary to the Field Catalog by end of shift. When submitting to the Field Catalog, the time of the submission should be set to the time the briefing was delivered during the shift (often 1130 or 1600 depending on the number of flights that day). Note that these times could change depending on adjustments to the daily schedule due to weather or personnel requirements. Include relevant imagery, descriptions and annotation.

Briefings will be given in-person, when possible, to personnel at the Operations Center and on WebEx for remote participants. The format of the briefing is up to the forecaster. Power Point is not required for the briefing. However, the Forecaster will use the provided Power Point templates to create formatted, organized reports for submission to the Field Catalog following the briefing (see below for reports requirements).

Both Forecasters A and B will communicate regularly with the Operations Director, and will upload forecast summaries and relevant graphics to the Field Catalog.

The forecaster on duty should be prepared with the following information, although the briefing will realistically only contain a subset of it:

- Icing and other features of interest for the day.
- Synoptic pattern, including:
    - Relevant features at the surface and aloft.
    - Event spatial and temporal features.
        - Evolution, motion, depth, strength, consistency.
        - Most interesting times of the day.
        - Coverage and duration.
        - Orientation of features that should be considered for sampling.
- Locations of the most favorable targets.
    - Distance from the Operations Base (e.g., KRFD).
    - Traffic density in the target area.
    - Potential landing site in that area if needed for refueling or an emergency.
    - Military or restricted areas that may be present in/near the area of interest.
- Type(s) of conditions expected – relate to ICICLE Priorities.
    - Expected ranges of T, LWC, drop size (MVD, D_{max}), hydrometeor type(s).

        - In App. C, App. O (subsets thereof) or something else.
        - Expected profiles of these parameters.
        - Identify expected vertical and horizontal transition zones.
        - Expected changes over time.
- Number of cloud layers likely to be present.
- Altitudes of the target(s) of interest and related features.
- Cloud top and base height.
- Freezing level height.
- Relation to terrain height, minimum flight altitudes, traffic altitudes.
- Determine whether sub-cloud sampling is possible for aerosols.
- Identify escape routes and their reliability.
- Source air characteristics.
- Note stability, upstream features (lakes, fronts), snow cover.
- Presence of clear air upstream or below cloud base for aerosol sampling.
- Significant hazards near the target area and between Ops Base and the target.
- Now and throughout the period of flight.
- Examples: Lightning, hail, turbulence. Include SIGMETs.
- Present and expected weather at operations base and any projected remote landing sites.
- Precipitation intensity and type, especially snow and/or freezing precipitation for deicing purposes
- Ceiling height and visibility
- Obscurations to visibility, such as fog (FG) and blowing snow (BLSN)
- Wind direction and speed. Note potential crosswind issues.
- Provide TAFs, and both current & recent observations.
- Other notable features and aspects of this event.
- Expectations for tomorrow and the coming days.
- Chances for icing on those days, location, types of conditions might exist.
- In context to ICICLE Priorities – especially ones that are rare or difficult to find.
- Potentially impactful weather at the operations base.
- Any major change in the pattern coming in the next few days? Next week?
- Consider potential need to use alternative operations bases or do sorties.
- Confidence in the forecast? HIGH, MED, LOW
- For today, tomorrow and at longer ranges.

<u>Requirements for briefings for possible flight:</u>

- Current and forecast synoptic charts (surface and upper-air)

- Soundings
- Satellite imagery (visible, infrared, etc.)
- Radar imagery
- Surface observations and TAFs at Ops Base and in target area
- Target locations, timing, movement, evolution
- Conditions expected within targets
- Escape route locations
- Presence of hazards
- Confidence in the forecast

Requirements for outlook briefings (no flight expected immediately afterward):

- Forecast synoptic charts (surface and upper-air)
- Forecast soundings, if applicable
- Predicted weather at Ops Base and potential target areas
- Possible target locations, timing, movement, evolution
- Conditions expected within targets
- Confidence in the forecast
- Potential need for supplemental soundings

3) FLIGHT SUPPORT SCIENTIST

Flight Support Scientists have the following daily reporting requirements:

- Monitor observations in-flight (especially those not regularly transmitted to ground). In coordination with Operations Director and NRC Air Crew, ensure that the specified flight plan is executed and advise on modifications that may be necessary to achieve goals. After a flight has been completed, submit a "Mission Scientist Summary" to the Field Catalog, preferably within 12 hours after the flight. Describe the following:
    - In-flight observations (e.g., cloud/precipitation structure, ranges for outside air temperature [OAT], LWC, drop size, particle type, crystal habit).
    - Features from instruments (e.g., structure evident on w-band radar, patterns in LWC when crossing meteorological features, transition zones).
    - Any relevant events (e.g., ice accretions on the wing or other parts of the aircraft, including their size, type, location, side window ice).
    - Instrumentation issues.
    - Features of note from icing tools.

4) GROUND SUPPORT SCIENTIST

Ground Support Scientists have the following daily reporting requirements:

- Monitor the status of ground-based instruments, tools and data sources for which they are responsible. Monitor experimental and operational product performance in conjunction with surface and aircraft observations. Report any outages or expected outages. Prepare and submit a "Product Performance Summary" to the Field Catalog, preferably within 12 hours after the flight or by the end of the calendar day.

B Appendix B - Locations of key sites

Table 13 contains a list of the latitude, longitude and elevation of several key sites within the ICICLE domain. All locations should be verified prior to using them for analysis. Information is from the following sources: A (AIRNAV, http://airnav.com/airports) and B (NCAR/Research Applications Laboratory, http://weather.rap.ucar.edu/surface/stations.txt). Locations and elevations listed for the supplemental sounding sites are for the nearest airports, which may be slightly different for the actual sounding sites.

Table 13. Approximate locations of several key sites for the ICICLE program.

Site ID	City	State	Latitude	Longitude	Elevation (m)	Description	Notes/Source
KRFD	Rockford	IL	42.20	-89.10	226	Primary Operations Base	A
KAZO	Kalamazoo	MI	42.23	-85.55	266	Super-Site	A
KLWA	South Haven	MI	42.35	-86.26	203	Sub-Site	A
KCID	Cedar Rapids	IA	41.88	-91.71	265	Super-Site	A
KDEH	Decorah	IA	43.28	-91.74	353	Sub-Site	A
KSQI	Sterling	IL	41.74	-89.68	197	Sub-Site	A
KSBN	South Bend	IN	41.71	-86.32	243	Alternate Landing Site - KAZO domain	A
CYOW	Ottawa	ON	45.32	-75.67	114	NRC Base	A
KBXM	Brunswick	ME	43.89	-69.94	23	Alternate Operations Base	A
KRIC	Richmond	VA	37.51	-77.32	51	Alternate Operations Base	A
KCMH	Columbus	OH	40.00	-82.89	248	Alternate Operations Base	A
KMQY	Smyrna	TN	36.01	-86.52	166	Alternate Operations Base	A
KFOE	Topeka/Forbes Field	KS	38.95	-95.66	329	Alternate Operations Base	A
KXNA	Fayetteville	AR	36.28	-94.31	393	Alternate Operations Base	A
KRAP	Rapid City	SD	44.05	-103.06	976	Alternate Operations Base	A
KLOT	Lockport/Romeoville	IL	41.60	-88.10	205	NEXRAD	B
KILX	Lincoln	IL	40.15	-89.33	177	NEXRAD & NWS Sounding	B
KMKX	Milwaukee/Dousman	WI	42.97	-88.55	292	NEXRAD	B
KGRB	Green Bay	WI	44.48	-88.13	208	NEXRAD & NWS Sounding	B
KARX	LaCrosse	WI	43.82	-91.18	389	NEXRAD	B
KDVN	Davenport	IA	41.62	-90.58	230	NEXRAD & NWS Sounding	B
KDMX	Des Moines	IA	41.73	-93.72	299	NEXRAD	B
KIND	Indianapolis	IN	39.72	-86.30	241	NEXRAD	B
KIWX	North Webster	IN	41.37	-85.70	293	NEXRAD	B
KGRR	Grand Rapids	MI	42.88	-85.52	237	NEXRAD	B
KDTX	Detroit	MI	42.70	-83.47	327	NEXRAD & NWS Sounding	B
KAPX	Gaylord/Alpena	MI	44.90	-84.72	446	NEXRAD & NWS Sounding	B
KMPX	Chanhassen/Minneapolis	MN	44.85	-93.57	288	NEXRAD & NWS Sounding	B
ISU	Ames	IA	41.98	-93.62	279	Supplemental Sounding Site	B* - KAMW
NIU	DeKalb	IL	41.93	-88.70	279	Supplemental Sounding Site	B* - KDKB
UIUC	Urbana-Champaign	IL	40.03	-88.27	228	Supplemental Sounding Site	B* - KCMI
Valpo	Valparaiso	IN	41.45	-87.00	231	Supplemental Sounding Site	B* - KVPZ
Valpo/KBEH	Benton Harbor	MI	42.13	-86.42	191	Supplemental Sounding Site	B* - KBEH